Methods in Molecular Biology 1691

Springer Protocols

Chris Hawes
Verena Kriechbaumer *Editors*

The Plant Endoplasmic Reticulum

Methods and Protocols

Humana Press

METHODS IN MOLECULAR BIOLOGY

Series Editor
John M. Walker
School of Life and Medical Sciences
University of Hertfordshire
Hatfield, Hertfordshire, AL10 9AB, UK

For further volumes:
http://www.springer.com/series/7651

The Plant Endoplasmic Reticulum

Methods and Protocols

Edited by

Chris Hawes and Verena Kriechbaumer

Department of Biological and Medical Sciences, Oxford Brookes University, Oxford, UK

Humana Press

Editors
Chris Hawes
Department of Biological
and Medical Sciences
Oxford Brookes University
Oxford, UK

Verena Kriechbaumer
Department of Biological and Medical Sciences
Oxford Brookes University
Oxford, UK

ISSN 1064-3745 ISSN 1940-6029 (electronic)
Methods in Molecular Biology
ISBN 978-1-4939-7388-0 ISBN 978-1-4939-7389-7 (eBook)
DOI 10.1007/978-1-4939-7389-7

Library of Congress Control Number: 2017954356

Printed on acid-free paper

This Humana Press imprint is published by Springer Nature
The registered company is Springer Science+Business Media LLC
The registered company address is: 233 Spring Street, New York, NY 10013, U.S.A.

Preface

The endoplasmic reticulum (ER) is a truly multifunctional organelle, displaying a wide range of structural, biosynthetic and metabolic functions. The network of tubules and sheets (cisternae) bounded by a single membrane effectively bisects the cytosol into two phases, a reducing cytosol and oxidative ER lumen, and the ER itself thus has two membrane surfaces and its lumen with which to support its biosynthetic capabilities.

As the first organelle of the secretory pathway, the ER is perhaps best known for its role in the co- and post-translational glycosylation and folding of proteins destined for post-Golgi secretion and the associated quality control of the cargo prior to export to the *cis*-Golgi [1, 2]. The list of the other functions of the ER is far too long to discuss in detail but includes: lipid biogenesis [3], the biogenesis of storage protein bodies in cereal seeds [4, 5], the biogenesis of oil bodies [6], immunity [7], biogenesis of peroxisomes [8, 9] and calcium homeostasis [10]. More recently, the ER has been linked to autophagy and the generation of the phagophore membrane [11, 12]. The cytosolic membrane surface also supports a range of enzymic activities including hosting enzymes involved in the biosynthesis of hormones such as auxin [13], which are perhaps organised into biosynthetic complexes known as metabolons.

Besides the extensively studied ER–Golgi interactions, it is now becoming clear that the ER interacts and may indeed form direct connections with other cellular organelles, although the study of the function of these is still in its infancy. For instance, there is an ungated connection with the outer nuclear envelope [14], transport of key plastid enzymes possibly via a close association of chloroplast stromules (tubular membrane extensions from the plastid surface) with the ER [1] and recently characterised contact sites with the plasma membrane which could facilitate exchange of lipids and signalling molecules as well as stabilising the ER network [15].

In this volume, we present a range of different techniques that have been used to characterise the structure and function of the higher plant ER. These include the application of modern microscopy techniques by fluorescence and electron microscopy, new protocols for analysing ER network structure, methods to purify and analyse ER membrane structure and to study protein glycosylation, protocols to study the unfolded protein response and the role of the ER in autophagy.

Oxford, UK

Chris Hawes
Verena Kriechbaumer

References

1. Stefano G, Hawes C, Brandizzi F (2014) ER—the key to the highway. Curr Opin Plant Biol 22:30–38
2. Hawes C, Kiviniemi, P, Kriechbaumer V (2015) The endoplasmic reticulum: A dynamic and well-connected organelle. J Integrative Plant Biol 57:50–62
3. Bessoule J-J, Moreau, P (2003) Phospholipid synthesis and dynamics in plant cells. In Lipid Metabolism and Membrane Biogenesis. Topics in Current Genetics 6:89–124
4. Galili G, Altschuler Y, Levanony H (1993) Assembly and transport of seed storage proteins. Trends Cell Biol 3:437–442

5. Herman EM (2008) Endoplasmic reticulum bodies: Solving the insoluble. Curr Opin Plant Biol 11:672–679
6. Huang AH (1996) Oleosins and oil bodies in seeds and other organs. Plant Physiol 110:1055–1061
7. Nakano RT, Yamada K, Bednarek P, Nishimura M, Hara-Nishimura I (2014) ER bodies in plants of the *Brassicales* order; biogenesis and association with innate immunity. Frontiers in Plant Science 10(5):73
8. Sparkes IA, Frigerio L, Tolley N, Hawes C (2009) The plant endoplasmic reticulum: a cell-wide web. Biochem J 423:145–155
9. Barton K, Mathur N, Mathur J (2013) Simultaneous live cell imaging of peroxisomes and the ER in plant cells suggests contiguity but no luminal connectivity between the two organelles. Frontiers in Physiology 24;4:196
10. Hong B, Ichida A, Wang Y, Gens JS, Pickard BG, Harper JF (1999) Identification of a calmodulin-regulated Ca^{2+}-ATPase in the endoplasmic reticulum. Plant Physiol 119:1165–1175
11. Le Bars, R., Marion, J., Le Borgne R, Satiat-Jeunemaitre B, Bianchi MW (2014) ATG5 defines a phagophore domain connected to the endoplasmic reticulum during autophagosome formation in plants. Nat Comms 5:4121
12. Wang P, Richardson C, Hawes C, Hussey P (2016) *Arabidopsis* NAP1 regulates the formation of autophagosomes. Current Biology 26:1–10
13. Kriechbaumer V, Botchway SW, Hawes C (2016) Localization and interactions between Arabidopsis auxin biosynthetic enzymes in the TAA/YUC-dependent pathway. Journal of Experimental Botany 67:4195–4207
14. Brandizzi F, Hanton S, DaSilva P, Boevink P, Evans D, Oparka K, Denecke J, Hawes C (2003) ER quality control can lead to retrograde transport from the ER lumen to the cytoplasm and the nucleoplasm I plant cells. The Plant Journal 34:269–281
15. Wang P, Hawkins TJ, Cummins I, Deeks MJ, Richardson C, Sparkes I, Hawes C, Hussey PJ (2014) The plant cytoskeleton mediates the link between the plasma membrane and endoplasmic reticulum through NET3C and VAP 27. Curr Biol 24:1–9

Contents

Preface . . . . . *v*
Contributors . . . . . *ix*

1 Labeling the ER for Light and Fluorescence Microscopy 1
Chris Hawes, Pengwei Wang, and Verena Kriechbaumer

2 3D Electron Microscopy of the ER 15
Maike Kittelmann

3 Characterization of Proteins Localized to Plant ER-PM Contact Sites 23
Pengwei Wang, Chris Hawes, Christine Richardson, and Patrick J. Hussey

4 Preparation and Imaging of Specialized ER Using Super-Resolution and TEM Techniques 33
Karen Bell, Karl Oparka, and Kirsten Knox

5 Quantitation of ER Structure and Function 43
Mark Fricker, Luke Heaton, Nick Jones, Boguslaw Obara, Stefanie J. Müller, and Andreas J. Meyer

6 Long-Term Imaging of Endoplasmic Reticulum Morphology in Embryos During Seed Germination 67
Natasha Dzimitrowicz, Emily Breeze, and Lorenzo Frigerio

7 Dancing with the Stars: Using Image Analysis to Study the Choreography of the Endoplasmic Reticulum and Its Partners and of Movement Within Its Tubules 75
Lawrence R. Griffing

8 Preparation of Highly Enriched ER Membranes Using Free-Flow Electrophoresis 103
Harriet T. Parsons

9 ER Microsome Preparation in *Arabidopsis thaliana* 117
Verena Kriechbaumer

10 ER Membrane Lipid Composition and Metabolism: Lipidomic Analysis 125
Laetitia Fouillen, Lilly Maneta-Peyret, and Patrick Moreau

11 2in1 Vectors Improve In Planta BiFC and FRET Analyses 139
Dietmar G. Mehlhorn, Niklas Wallmeroth, Kenneth W. Berendzen, and Christopher Grefen

12 Metabolons on the Plant ER 159
Verena Kriechbaumer and Stanley W. Botchway

13 Using Optical Tweezers Combined with Total Internal Reflection Microscopy to Study Interactions Between the ER and Golgi in Plant Cells 167
Imogen Sparkes, Rhiannon R. White, Benjamin Coles, Stanley W. Botchway, and Andy Ward

14 Protein Biosynthesis and Maturation in the ER 179
Emanuela Pedrazzini and Alessandro Vitale

15 ER Membrane Protein Interactions Using the Split-Ubiquitin System (SUS) 191
Lisa Yasmin Asseck, Niklas Wallmeroth, and Christopher Grefen

16 Analysis of Protein Glycosylation in the ER 205
Jennifer Schoberer, Yun-Ji Shin, Ulrike Vavra, Christiane Veit, and Richard Strasser

17 The Unfolded Protein Response 223
Kazuki Tabara, Yuji Iwata, and Nozomu Koizumi

18 Unfolded Protein Response in Arabidopsis 231
Cristina Ruberti and Federica Brandizzi

19 Fluorescence Imaging of Autophagy-Mediated ER-to-Vacuole Trafficking in Plants 239
Hadas Peled-Zehavi and Gad Galili

20 Imaging the ER and Endomembrane System in Cereal Endosperm 251
Verena Ibl, Jenny Peters, Eva Stöger, and Elsa Arcalís

Index *263*

Contributors

Elsa Arcalís • *Department of Applied Genetics and Cell Biology, University of Natural Resources and Life Sciences, Vienna, Austria*

Lisa Yasmin Asseck • *Centre for Plant Molecular Biology, Developmental Genetics, University of Tübingen, Tübingen, Germany*

Karen Bell • *Institute of Molecular Plant Sciences, School of Biological Sciences, University of Edinburgh, Edinburgh, UK*

Kenneth W. Berendzen • *Centre for Plant Molecular Biology, University of Tübingen, Tübingen, Germany*

Stanley W. Botchway • *Central Laser Facility, Science and Technology Facilities Council, Didcot, Oxon, UK*

Federica Brandizzi • *MSU-DOE Plant Research Lab and Plant Biology Department, Michigan State University, East Lansing, MI, USA*

Emily Breeze • *School of Life Sciences, University of Warwick, Coventry, UK*

Benjamin Coles • *Central Laser Facility, Science and Technology Facilities Council, Didcot, Oxon, UK*

Natasha Dzimitrowicz • *School of Life Sciences, University of Warwick, Coventry, UK*

Laetitia Fouillen • *CNRS-University of Bordeaux, UMR 5200 Membrane Biogenesis Laboratory, INRA Bordeaux Aquitaine, Villenave d'Ornon, France; MetaboHub-Metabolome Facility of Bordeaux, Functional Genomics Center, Bordeaux, France*

Mark Fricker • *Department of Plant Sciences, University of Oxford, Oxford, UK*

Lorenzo Frigerio • *School of Life Sciences, University of Warwick, Coventry, UK*

Gad Galili • *Department of Plant and Environmental Sciences, Weizmann Institute of Science, Rehovot, Israel*

Christopher Grefen • *Centre for Plant Molecular Biology, University of Tübingen, Tübingen, Germany*

Lawrence R. Griffing • *Biology Department, Texas A&M University, College Station, TX, USA*

Chris Hawes • *Department of Biological and Medical Sciences, Oxford Brookes University, Oxford, UK*

Luke Heaton • *Department of Plant Sciences, University of Oxford, Oxford, UK; Mathematics Department, Imperial College, London, UK*

Patrick J. Hussey • *Department of Biosciences, Durham University, Durham, UK*

Verena Ibl • *Department of Applied Genetics and Cell Biology, University of Natural Resources and Life Sciences, Vienna, Austria; Molecular Systems Biology, Faculty of Life Sciences, University of Vienna, Vienna, Austria*

Yuji Iwata • *Graduate School of Life and Environmental Sciences, Osaka Prefecture University, Sakai, Osaka, Japan*

Nick Jones • *Mathematics Department, Imperial College, London, UK*

Maike Kittelmann • *Plant Cell Biology, Biological and Medical Sciences, Oxford Brookes University, Oxford, UK*

Kirsten Knox • *Institute of Molecular Plant Sciences, School of Biological Sciences, University of Edinburgh, Edinburgh, UK*

Nozomu Koizumi • *Graduate School of Life and Environmental Sciences, Osaka Prefecture University, Sakai, Osaka, Japan*
Verena Kriechbaumer • *Department of Biological and Medical Sciences, Oxford Brookes University, Oxford, UK*
Stefanie J. Müller • *INRES-Chemical Signalling, Universität Bonn, Bonn, Germany*
Lilly Maneta-Peyret • *CNRS-University of Bordeaux, UMR 5200 Membrane Biogenesis Laboratory, INRA Bordeaux Aquitaine, Villenave d'Ornon, France*
Dietmar G. Mehlhorn • *Centre for Plant Molecular Biology, University of Tübingen, Tübingen, Germany*
Andreas J. Meyer • *INRES-Chemical Signalling, Universität Bonn, Bonn, Germany*
Patrick Moreau • *CNRS-University of Bordeaux, UMR 5200 Membrane Biogenesis Laboratory, INRA Bordeaux Aquitaine, Villenave d'Ornon, France; Bordeaux Imaging Center, UMS 3420 CNRS, US004 INSERM, University of Bordeaux, Bordeaux, France*
Boguslaw Obara • *School of Engineering and Computing Sciences, University of Durham, Durham, UK*
Karl Oparka • *Institute of Molecular Plant Sciences, School of Biological Sciences, University of Edinburgh, Edinburgh, UK*
Harriet T. Parsons • *Biochemistry Department, Cambridge University, Cambridge, UK*
Emanuela Pedrazzini • *Istituto di Biologia e Biotecnologia Agraria, Consiglio Nazionale delle Ricerche, Milan, Italy*
Hadas Peled-Zehavi • *Department of Plant and Environmental Sciences, Weizmann Institute of Science, Rehovot, Israel*
Jenny Peters • *Department of Applied Genetics and Cell Biology, University of Natural Resources and Life Sciences, Vienna, Austria*
Christine Richardson • *Department of Biosciences, Durham University, Durham, UK*
Cristina Ruberti • *MSU-DOE Plant Research Lab and Plant Biology Department, Michigan State University, East Lansing, MI, USA*
Jennifer Schoberer • *Department of Applied Genetics and Cell Biology, University of Natural Resources and Life Sciences, Vienna, Austria*
Yun-Ji Shin • *Department of Applied Genetics and Cell Biology, University of Natural Resources and Life Sciences, Vienna, Austria*
Imogen Sparkes • *School of Biological Sciences, University of Bristol, Bristol, UK; Biosciences, University of Exeter, Exeter, UK*
Eva Stöger • *Department of Applied Genetics and Cell Biology, University of Natural Resources and Life Sciences, Vienna, Austria*
Richard Strasser • *Department of Applied Genetics and Cell Biology, University of Natural Resources and Life Sciences, Vienna, Austria*
Kazuki Tabara • *Graduate School of Life and Environmental Sciences, Osaka Prefecture University, Sakai, Osaka, Japan*
Ulrike Vavra • *Department of Applied Genetics and Cell Biology, University of Natural Resources and Life Sciences, Vienna, Austria*
Christiane Veit • *Department of Applied Genetics and Cell Biology, University of Natural Resources and Life Sciences, Vienna, Austria*
Alessandro Vitale • *Istituto di Biologia e Biotecnologia Agraria, Consiglio Nazionale delle Ricerche, Milan, Italy*
Niklas Wallmeroth • *Centre for Plant Molecular Biology, University of Tübingen, Tübingen, Germany*

Pengwei Wang • *Key Laboratory of Horticultural Plant Biology (MOE), College of Horticulture and Forestry Sciences, Huazhong Agricultural University, Wuhan, Hubei, PR China*
Andy Ward • *Central Laser Facility, Science and Technology Facilities Council, Didcot, Oxon, UK*
Rhiannon R. White • *Biosciences, University of Exeter, Exeter, UK*

Chapter 1

Labeling the ER for Light and Fluorescence Microscopy

Chris Hawes, Pengwei Wang, and Verena Kriechbaumer

Abstract

The ER is a highly dynamic network of tubules and membrane sheets. Hence imaging this organelle in its native and mobile state is of great importance. Here we describe methods of labeling the native ER using fluorescent proteins and lipid dyes as well as methods for immunolabeling on plant tissue.

Key words Endoplasmic reticulum, Labeling, Fluorescent protein, Stable expression, Transient expression, Immunofluorescence, Fluorescent dyes

1 Introduction

The endoplasmic reticulum (ER) forms a dynamic, continually changing network of tubules and membrane sheets or cisternae that ramify throughout the cytoplasm of cells. As such in order to appreciate its true nature, it is often necessary to image the organelle in its native state in living cells. For convenience it is often best to think of the ER as two interconnected populations of tubules and cisternae. Firstly, there is the geometrical cortical network, which overlies the cortical cytoskeleton and is connected to the plasma membrane at specific contact points [1]. Secondly, cytoplasmic ER often rapidly streams and also transverses the vacuolar lumen via transvacuolar strands.

Two strategies are available for imaging the ER in its native form. A number of different probes have been used to directly label the ER in living cells. Most of them are not 100% specific for the ER membrane and may label other organelles at varying concentrations and incubation times. Two probes with different emission wavelengths which are relatively easy to use on a range of plant tissues are the rhodamine B hexyl ester [2] and 3,3′-dihexylocarbocyanine iodide ($DiOC_6$, green emission) [3, 4]. Expression of fluorescent protein constructs which are targeted to the ER is another efficient strategy for in vivo labeling. It is possible to use labeled proteins or peptide sequences that are targeted to the ER membrane [5, 6];

Chris Hawes and Verena Kriechbaumer (eds.), *The Plant Endoplasmic Reticulum: Methods and Protocols*, Methods in Molecular Biology, vol. 1691, DOI 10.1007/978-1-4939-7389-7_1,

although on occasions these can perturb the membrane and alter the structure of the ER network [5, 7, 8]. Alternatively a simple construct comprising a signal sequence and fluorescent protein with a KDEL or HDEL retrieval motif spliced to the C terminus is sufficient to label the lumen of the ER and is often the construct of choice [10].

Immunocytochemistry is an important technique for locating native proteins and confirming the validity of the location of fluorescent protein constructs. Many different preparative techniques for the immunofluorescence labeling of plant proteins have been described over the years, including production of single cells by enzyme digestion (the root squash technique), cryo-sectioning, wax or resin embedding and sectioning [11]. Here we describe a modification of the root squash technique to permeabilize root tip cells and the freeze shatter technique developed by Wasteneys et al. [12] that permits the physical rupture of arabidopsis tissues and cells, permitting antibody penetration, and is particularly suitable for arabidopsis seedling tissues.

In this chapter, we describe the following methods:

(a) Agrobacterium-mediated transient protein expression in tobacco epidermal leaf cells.

(b) Stable protein expression in tobacco.

(c) Stable protein expression in arabidopsis.

(d) Immunofluorescence in arabidopsis roots.

(e) Freeze-shattering and immunofluorescence.

(f) The use of lipid dyes Rhodamine B hexyl ester or $DiOC_6$.

2 Materials

2.1 Solutions and Equipment

2.1.1 For Agrobacterium-Mediated Transient Protein Expression in Tobacco Epidermal Leaf Cells

1. YEB medium: 5 g/l of beef extract, 1 g/l of yeast extract, 5 g/l of sucrose, 0.5 g/l of $MgSO_4 \cdot 7H_2O$.
2. Infiltration buffer: 50 mM MES, 2 mM $Na_3PO_4 \cdot 12H_2O$, 0.1 mM acetosyringone and 5 mg/ml glucose.
3. Water bath.
4. Nanodrop spectrophotometer (or equivalent) to determine optical density of bacterial culture.

2.1.2 For Stable Protein Expression in Tobacco

1. Sterilization solution: 1:1 hypochlorite solution: dH_2O, 0.01% (v/v) Tween 20.
2. Plates with shooting medium: 2.15 g/l Murashige and Skoog salts, pH 5.2 (without IAA, kinetin or sucrose; MP Biomedicals Inc.), 0.8% (w/v) agar, 3.0% (w/v) sucrose, 0.1 mg/l indole butyric acid (1.0 mg/ml stock), 0.8 mg/l 6-benzylaminopurine (1.0 mg/ml stock), 0.1 mg/l carbenicillin,

0.2 mg/l Ticarcillin/Clavulanic acid (Ducheva) and suitable selection for the binary vector carrying your FP fusion construct. Dissolve Murashige and Skoog salts and sucrose in ultrapure deionized water. Add stock solutions of plant growth regulators. Adjust the pH to 5.2 and autoclave. When the medium has cooled to 50 °C, add filter-sterilized antibiotics and pour into Petri dishes. Plates are kept at 4 °C in the dark.

3. Plates with rooting medium: 2.15 g/l Murashige and Skoog salts, 0.8% (w/v) agar, 3.0% (w/v) sucrose, 0.5 mg/l indole butyric acid (1 mg/ml stock), 0.1 mg/l carbenicillin, 0.2 mg/l Ticarcillin/Clavulanic acid (Ducheva).

2.1.3 For Stable Protein Expression in Arabidopsis

1. LB broth: Tryptone 10 g/l, NaCl 10 g/l, Yeast extract 5 g/l.
2. Dipping buffer: 5% sucrose, 50 µl/l Silwet L-77 in dH_2O.

2.1.4 For Immunofluorescence in Arabidopsis Root Cells

1. MBS ester (m-maleimidobenzoyl-N-hydroxysuccinimide).
2. Fixative: paraformaldehyde (PFA) 4%, glutaraldehyde 0.5%, EGTA 5 mM (pH 8.0), PIPES 50 mM (pH 7.0), $MgSO_4$ 2 mM, 0.01% Triton X-100 0.01% (*see* **Note 1**).
3. PBS buffer (pH 7.4).
4. Blocking buffer: PBS supplemented with 2% BSA.
5. Permeable buffer: PBS supplemented with 0.1% Triton X-100.
6. Dricelase solution: Dricelase (2%) in PBS.
7. Proteinase inhibitors: PMSF, leupeptin, and pepstatin A.
8. Liquid nitrogen.
9. Metal block and a hammer.
10. Glass Microscope slide.
11. Plastic Sieves.
12. Vectashield.

2.1.5 For Freeze-Shattering and Immunofluorescence

1. MBS ester (m-maleimidobenzoyl-N-hydroxysuccinimide).
2. PBS buffer.
3. Blocking buffer: PBS supplemented with 2% BSA.
4. Permeable buffer: PBS supplemented with 0.1% Triton X-100.
5. Driselase solution: Driselase (2%) in PBS.
6. Proteinase inhibitors: PMSF, leupeptin, and pepstatin A.
7. Liquid nitrogen.
8. Metal block and a hammer.
9. Glass Microscope slide.
10. Plastic Sieves.
11. Vectashield or equivalent antifade mountant.

2.1.6 For Lipid Dyes Rhodamine B Hexyl Ester or $DiOC_6$

1. Rhodamine B hexyl ester solution: stock solution 1 mM in DMSO, working solution 1 μM in water.
2. $DiOC_6$ (Molecular Probes): working solution: 1.8 mM in water.
3. 2 ml Eppendorf tubes.

2.2 Antibodies for Immunofluorescence

Various suppliers are possible for both primary and secondary antibodies.

1. Polyclonal mouse antibody against VAP27-1 [13].
2. Polyclonal mouse antibody against NET3C [1].
3. Polyclonal Rabbit antibody against BIP2 (Agriserum).
4. Polyclonal Rabbit antibody against HDEL (Agriserum).
5. Goat anti-rabbit FITC-conjugated antibody (Immuno Jackson or other supplier).
6. Goat anti-mouse TRITC-conjugated antibody (Immuno Jackson or other supplier).

2.3 Microscopy

1. Upright or inverted laser scanning or spinning disc confocal microscope, TIRF microscope, super-resolution fluorescence microscope.

3 Methods

1. Agrobacterium-mediated transient expression in tobacco epidermal leaf cells.
2. Stable protein expression in tobacco.
3. Stable protein expression in arabidopsis.
4. Immunofluorescence in arabidopsis root.
5. Freeze-shattering and immunofluorescence.
6. Labeling of ER with lipid dyes.

3.1 Agrobacterium-Mediated Transient Expression in Tobacco Epidermal Leaf Cells

1. For agrobacterium-mediated transient expression, 5-week-old tobacco (*Nicotiana tabacum* SR1 cv Petit Havana) plants grown in the greenhouse are used. Transient expression is carried out according to Sparkes et al. [14]. Alternatively *N. benthamiana* plants are also suitable for transient expression experiments.
2. Construct a suitable expression vector using standard molecular biology techniques such as conventional cut&paste cloning [15] or gateway cloning [16] Table 1 lists examples for constructs that can be used for labeling the ER in epidermal cells.
3. Introduce the expression vector into agrobacterium strain GV3101 by heat shock.

Table 1
Some suggested constructs suitable for imaging the ER in epidermal cells

Construct	Comments	Reference
SS-FP-HDEL	Labels ER lumen	[10]
Reticulon-FP	Labels membrane of ER tubules and cisternal rims. Overexpression can constrict tubules	[5]
Calnexin-TMD-FP	Membrane marker—Can induce cisternae on high expression	[6]
Derlin-FP	Labels membrane of whole ER network	[17]

4. Inoculate transformants into 5 ml of YEB medium with the appropriate antibiotic for the bacterial vector used as well as 25 mg/l rifampicin.
5. After overnight shaking at 28 °C, pellet 1 ml of the bacterial culture by centrifugation at 2000 × *g* for 5 min at room temperature.
6. Wash the pellet twice with 1 ml of infiltration buffer and then resuspended in 1 ml of infiltration buffer.
7. Initially dilute the bacterial suspension to a final OD_{600} of 0.1. If expression is successful, then different OD_{600} values can be tested to improve the expression results, or to reduce expression levels, such as OD_{600} of 0.05 or 0.01.
8. Carefully press the suspension through the stomata on the lower epidermal surface using a 1 ml syringe (*see* **Note 2**). The surface infiltrated appears darker at this point and should be outlined with a thin black marker pen to aid removal of correct segments of leaf for microscopy (for details *see* Fig. 1).
9. Inoculated plants are then incubated under normal growth conditions for 48–72 h depending on the proteins expressed. This will have to be determined experimentally by checking the expression after e.g., 2, 3, and 4 days after infiltration.
10. Excised a 0.5 × 0.5 cm piece of the infiltrated leaf and mount in a drop of water and observed with a microscope (*see* **Note 3** and Subheading 3.7).
11. Images can be recorded, e.g., using a laser scanning confocal microscope with ×63 or ×100 high numerical aperture oil or water immersion objective lenses. For imaging of combinations of the green fluorescent (GFP) and red fluorescent protein (RFP), samples should be excited using 488- and 543-nm laser lines in multitrack mode preferably using line switching. Images can be analyzed with proprietary software from the confocal manufacturer, with commercial image analysis software or freeware such as Fiji Image J (Fig. 2).

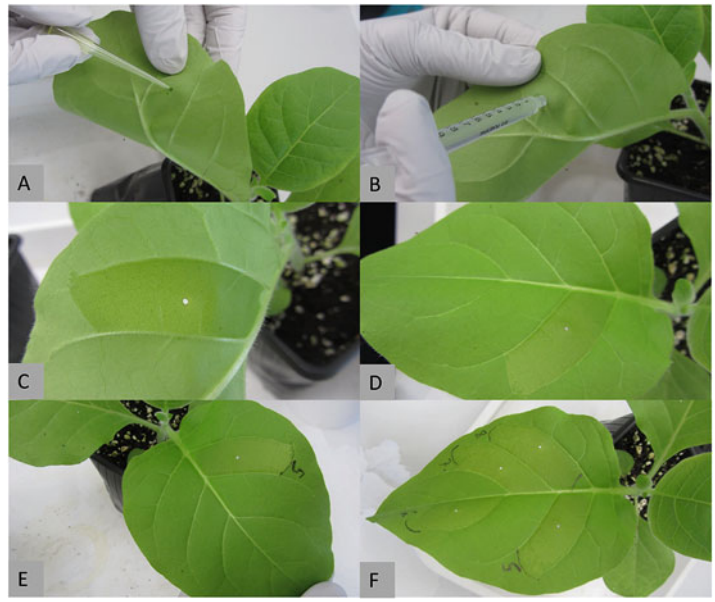

Fig. 1 Infiltration of tobacco epidermal leaf cells with *Agrobacterium tumefaciens*. (**a**) A hole is punched into a leaf section using a 100-μl pipette tip. (**b**) The bacterial suspension culture is carefully pressed into the leaf by covering the hole with a 1 ml syringe on the lower epidermal site and a finger on the upper side. (**c**) As much as possible of that leaf section is filled with the culture. (**d**) The infiltrated parts will show up darker now. (**e**) Mark the infiltrated area with a pen. (**f**) Infiltrate as many leaf sections as required for the constructs tested

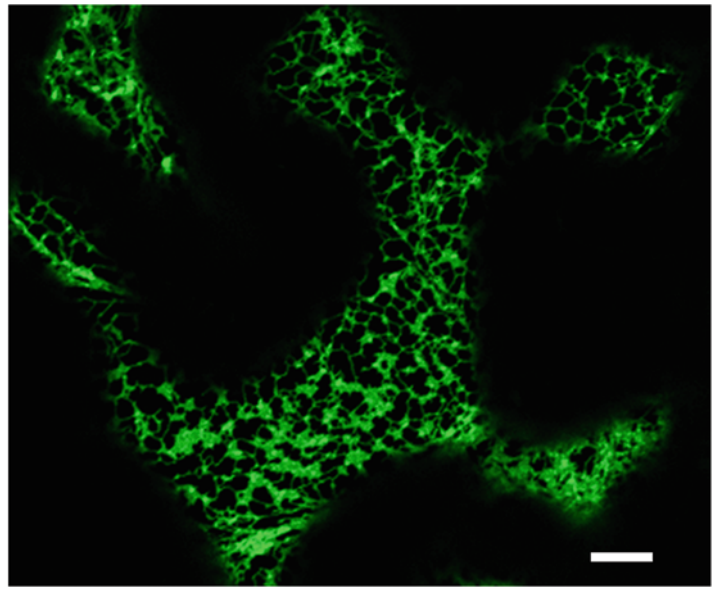

Fig. 2 GFP-labeled ER in tobacco leaf epidermal cells. The ER network is labeled with the ER membrane localized protein TAR2 [18] fused to GFP as a fluorophore and visualized using confocal microscopy. Scale bar = 10 μm

3.2 Stable Transformation of Tobacco from Transiently Expressing Tobacco Cells

1. Infiltrate at least two leaves on two different tobacco plants according to Subheading 3.1 and check the expression of the fusion protein by microscopy. If expression is low, then repeat infiltration until transformation levels are satisfactory and at least 70% of the cells in the field of view on the microscope are expressing the fusion protein.
2. Remove infiltrated leaves from the plant using scissors and immerse them completely into sterile 500 ml beakers containing sterilization solution to remove trace amounts of Agrobacterium and other microbes from the leaf surface.
3. Carefully agitate the leaves for 8 min and then rinse them in a series of three sterile beakers containing sterile water (*see* **Note 4**).
4. Using scissors cut the leaves into pieces approximately 2 × 2 cm avoiding the midrib (*see* **Note 5**).
5. Place the leaf squares onto agar plates of shooting medium plus the corresponding antibiotics for the transformation vector used and incubate at 25 °C, 16 h light, 8 h dark, until shoots appear. This will take between 3–4 weeks.
6. Check regularly for contamination and, if apparent, transfer uncontaminated pieces to plates of fresh shooting medium.
7. When shoots are present, transfer them from the tissue with sterile forceps to plates with rooting medium. Roots will appear within 7–10 days.
8. Check again with the microscope for expression as there may be many shoots to deal with.
9. If the plants are expressing well, transfer them to Phytatrays or other suitable growth containers containing 0.5% Murashige and Skoog agar to develop until they are large enough to be transferred to soil.

3.3 Transformation of Arabidopsis Using the Floral Dip Method

1. A 5 ml liquid pre-culture, inoculated from single colony of agrobacterium, carrying the appropriate binary vector, is grown with vigorous agitation (180 rpm) overnight at 28 °C with the appropriate antibiotics.
2. 100 ml of LB medium is inoculated with 1 ml of the pre-culture and shaken overnight at 28 °C and 180 rpm.
3. Decant culture into two 50 ml Falcon tubes.
4. Pellet the cells by centrifugation at 4 °C with 4000 rpm (1180 x *g*) for 10 min. Discard the supernatant and wash the resulting pellets by resuspension in 10 ml infiltration medium.
5. The pelleting step is repeated and the two pellets are combined into one Falcon tube in a total of 50 ml of dipping buffer.

6. Remove siliques from the inflorescence shoots from 2–4 plants of *Arabidopsis thaliana* (wild-type Col-0) so only unfertilized flowers remain.
7. Dip the shoots upside down into the Falcon tubes containing the Agrobacteria suspension and soaked for 30 s.
8. After dipping seal the plants with transparent plastic bags or cling film for the next 24 h, then remove the cover and return plants to their normal growing conditions (*see* **Note 6**).
9. After 2–3 weeks, the plants should not be watered anymore to allow the seeds to ripen. Plants with seeing heads should be bagged to stop loss of material or siliques grown through Aracon containers (Arasystem) to collect any loose seed.
10. Collect the seeds which are brown and dry (approximately after about 6 weeks).
11. Selection of transformed arabidopsis plants is carried out by germinating seeds collected from transformed plants on MS plates containing 1% sucrose and the appropriate antibiotics or herbicide depending on the vector used.

3.4 Immunofluorescence in Arabidopsis Roots

This protocol is designed for immunolabeling of root tips, a similar method and also be used for fixing cells from suspension culture (e.g., BY2 cells).

1. Arabidopsis seedlings are grown vertically in Petri dishes for 5–7 days before fixation. The tips region (about 1 cm) are collected and transferred into a plastic sieve (Fig. 3).
2. The fixative is prepared fresh each time. For making 10 ml, 0.4 g of PFA is added to 5 ml of ddH_2O in a falcon tube. The mixture is warmed to 65 °C in a water bath, and drops

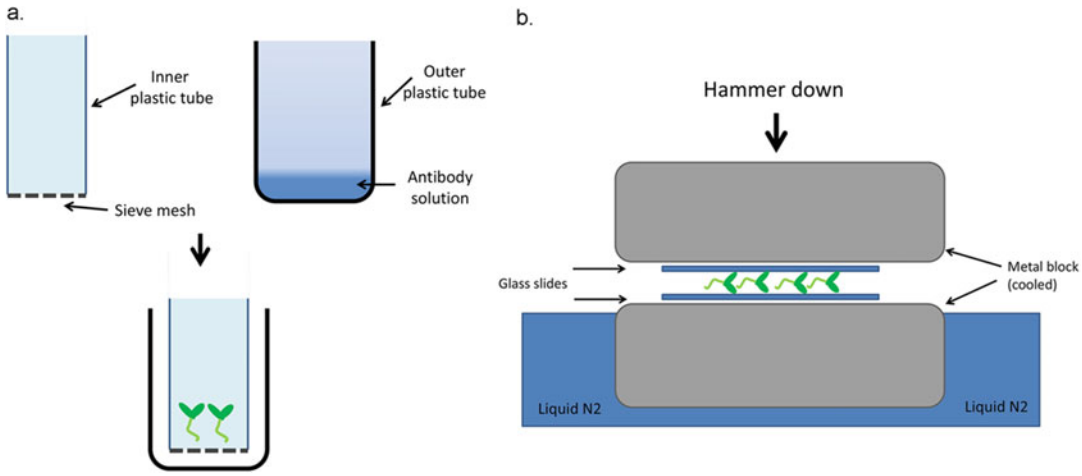

Fig. 3 Experiment setup for immune-labeling (**a**) and freeze-shattering (**b**)

(about 20 μl per 10 ml) of 0.1 M NaOH solution are added. The tube is agitated periodically until the PFA is dissolved. Cool the solution to room temperature, and add remaining buffer components. Bring the final volume to 10 ml with ddH_2O. Finally, add Triton X-100 to 0.01% v/v (*see* **Note 7**).

3. Fix roots for 90 min, and then wash in PBS buffer three times for 5 min each.
4. Incubate roots in a Driselase solution (2% w/v) for 7 min at room temperature. Driselase solution is stored at −20 °C. For each 1 ml solution, add 10 μl of PMSF (100 mM), 1 μl of leupeptin (10 mg/ml), and 1 μl of pepstatin A (1 mg/ml) immediately before use (*see* **Note 8**). The protease inhibitors are there to block proteinases in the driselase solution.
5. Quickly wash roots in PBS three times, and incubate them for 15 min in PBS containing 0.1% Triton X-100 to make cells permeable.
6. Quickly wash roots in PBS three times, and leave them in blocking buffer for 1 h.
7. Incubate roots in primary antibody (diluted in blocking buffer, *see* **Note 9**) for 3–6 h at room temperature or overnight at 4 °C.
8. Wash roots in PBS buffer three times for 30 min each, and incubate them in secondary antibody solution for 1–3 h. Antibodies (e.g., FITC or TRITC conjugated) with minimal cross activity should be used for dual labeling; this is especially important for using primary antibodies raised in two close related species (e.g., rat and mouse, *see* **Note 10**).
9. Wash roots in PBS buffer three times for 30 min each (*see* **Note 11**), and mount the slide using Vectashield. Samples are now ready for microscopy.
10. In most cases, ER bodies, a spindle-like ER-derived structure, can be seen in wild-type arabidopsis root cells. This can affect the visibility of the ER network (Fig. 3). To overcome this problem, an arabidopsis mutant without ER bodies (*nai1*, [19]) can be used (Fig. 3).
11. If plants expressing GFP-HDEL are used for immunocytochemistry, the GFP signal can withstand fixation; therefore it can be used as a marker to test the co-localization of any protein of interest. As an example arabidopsis (*nai1*) roots expressing GFP-HDEL were immuno-stained with anti-NET3C antibodies (an ER-PM contact site protein). The result indicates the endogenous NET3C localized to punctate structure that co-aligned with the ER (*see* **Note 12**).

3.5 Freeze-Shattering and Immunofluorescence

This protocol is designed for immunolabeling of whole plant tissue, ideally for leaf epidermal cells [11]. It is based around using physical pressure on frozen material, after fixation, to fracture the cuticles and cell walls, thus enabling the easy penetration of antibodies.

1. Whole arabidopsis plantlets or excised leaves (10 days old) grown in Petri dishes can be used; they are preincubated for 15 min in MBS ester (100 μM) solution. Transfer plants to fixative (supplemented with 100 μM MBS ester) as described in Subheading 3.4 for 1 h.
2. After incubation, wash samples twice in PBS to remove all fixative. Transfer seedlings onto a glass slide and dry them using tissue paper. Put another glass slide on top to make a "sandwich" (Fig. 3).
3. Rapidly freeze the "sandwich" by immersion in liquid nitrogen, and place it in-between two metal blocks that are also cooled in liquid nitrogen (Fig. 3). Knock the top metal block gently with a hammer; this will shatter the arabidopsis seedlings into small pieces (1 mm × 1 mm, *see* **Note 13**).
4. Use cold tweezers to transfer plant pieces to a plastic sieve (Fig. 3). Then follow the protocol in Subheading 3.4 (**steps 5–9**) for antibody incubation.
5. Mount the slide using Vectashield or Citifluor antifade mountants. Samples are now ready for microscopy (Fig. 4).

3.6 Lipophilic Dyes Rhodamine B Hexyl Ester or $DiOC_6$ for Live Imaging of the ER

1. Whole arabidopsis seedlings 7–10 days after germination are transferred to an Eppendorf tube containing the staining solution (Rhodamine B hexyl ester-1 μM or $DiOC_6$-1.8 mM) and incubated for 15 min for Rhodamine B or 10–30 min for $DiOC_6$ (*see* **Note 14**).
2. After incubation in the dye, transfer the seedlings to a fresh Eppendorf tube containing water to wash off excess staining solution.
3. Samples stained with Rhodamine B hexyl ester can be imaged with a 514-nm line of an argon ion laser using a 458/514 dichroic mirror, and the subsequent emission can be detected using 470- to 500-nm and 560- to 615-nm band-pass filters (Fig. 5).
4. Samples stained with $DiOC_6$ should be imaged with a 488-nm line of an argon ion laser and emission can be detected at 492–629 nm.

3.7 Microscopy

While it is perfectly feasible to image fluorescent endoplasmic reticulum with a conventional wide-field epifluorescence microscope, the use of a point scanning or spinning disc confocal is

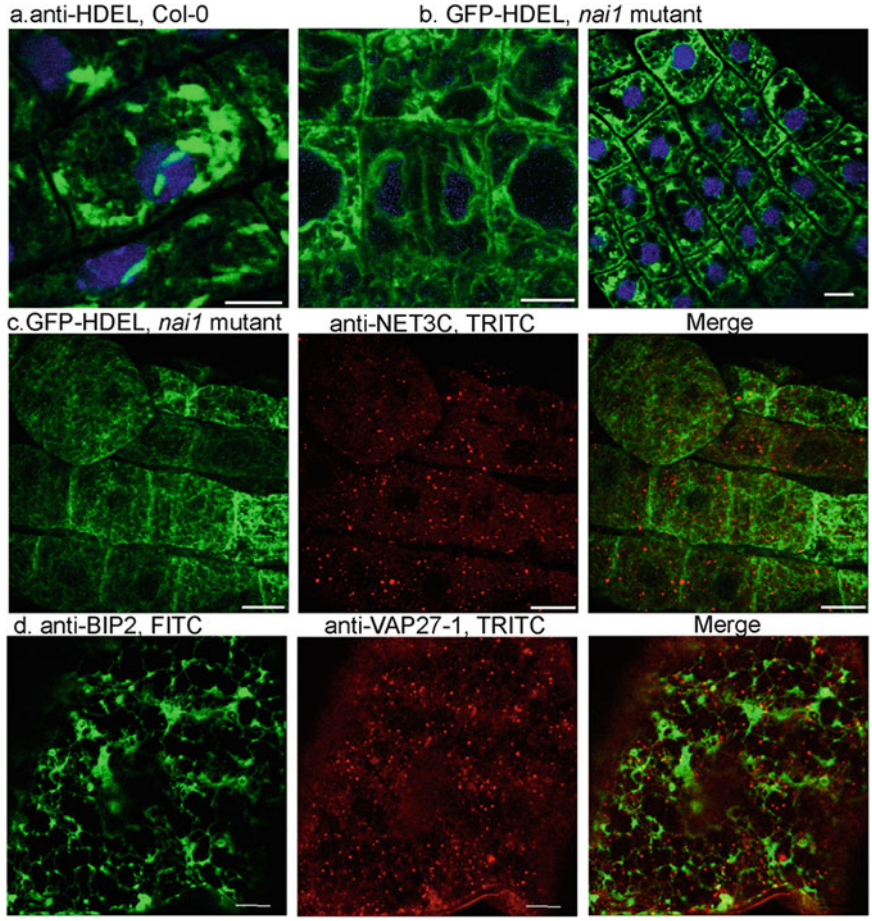

Fig. 4 Immunolabeling of the ER network from different cell types. (**a**) The ER network is labeled with anti-HDEL in combination with a FITC-conjugated secondary antibody; ER bodies can be identified throughout the cell. (**b**) Arabidopsis mutant (*nai 1*) transformed with GFP-HDEL does not produce ER bodies. The GFP-HDEL labeled ER network is still strong after fixation. The ER network from root meristem cells and a dividing cell at the anaphase is shown. For both (**a**) and (**b**), nuclei are stained with DAPI. (**c**) GFP-HDEL expressing root cells (*nai 1*) are fixed and stained with anti-NET3C in combination with a TRITC-conjugated secondary antibody. As demonstrated, NET3C-labeled punctate structures are localized to the ER network. (**d**) After freeze-shattering, arabidopsis leaf epidermal cells are stained with anti-BIP2 (ER) and anti-VAP27-1 (ER and ER-PM contact sites) antibodies. The ER structure is much clear and defined in leaf cells than in root tips

recommended. For cortical ER in epidermal cells of living tissue it is also possible to obtain excellent images with a TIRF (Total Internal Reflection Fluorescence microscopy).

4 Notes

1. Concentrated stock solution of PIPES, EGTA, and $MgSO_4$ can be made, aliquoted, and stored at −20 °C.

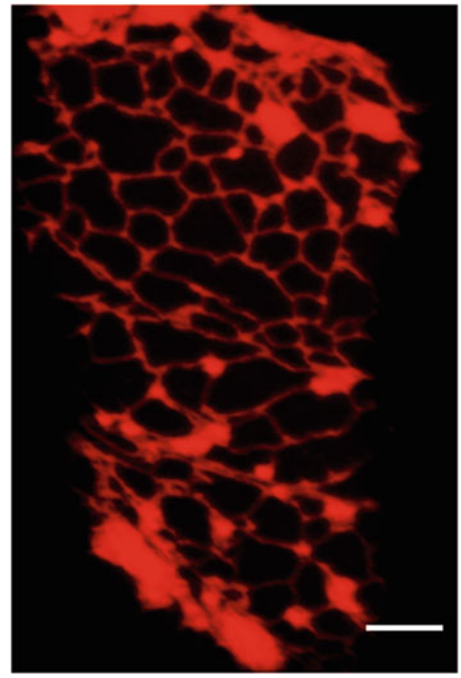

Fig. 5 Confocal image of arabidopsis *reticulon6* mutant dyed with Rhodamine B hexyl ester. The ER network is stained with the dye Rhodamine B hexyl ester and visualized using confocal microscopy. Scale bar = 5 μm

2. Try to avoid large veins. A small hole may be punched into the lower epidermis to aid infiltration.
3. For use with an inverted microscope it can be useful to stick coverslips to the slide with a tape such as electrical tape, in order to prevent movement of the coverslip and specimen during observation of the specimen.
4. Make sure the leaves are not damaged by hypochlorite and shorten the exposure time to a minimum of 5 min if necessary. Incubations longer than 8 min will be detrimental to the tissue, resulting in cell death.
5. From this step on throughout the following tissue culture steps proper sterile techniques need to be applied.
6. The same plants can be dipped again about 5–7 days after the first dipping, which can dramatically increase the transformation efficiency. Note: do not cut any siliques for the second dipping as they might already have been successfully transformed in the first round.
7. The concentration of Triton X-100 is critical here, especially for fixing fragile ER network. High levels of detergent can destroy the membrane structure and produce fragmented ER.

8. After enzyme treatment, handle the roots gently to avoid loss of tips.
9. Dilution factors vary for different antibody, 1:100–200 is recommended to start with. For the experiments described here, about 200–300 μl of antibody solution was sufficient to cover root in the plastic sieve.
10. For negative controls, omit the primary antibody and the secondary antibody only sample should not produce any signal. Likewise with anti-peptide antibodies, the antibody in the serum can be titrated out through addition of the peptide.
11. For nuclear staining, PBS supplemented with 10 ng/ml DAPI or Hoechst can be used after the second wash.
12. The ER network is cisternalized in cells from root tips, and these cells are small. Therefore, it can often be difficult to resolve the ER membrane from the cytoplasmic signals.
13. Only a gently tap with the hammer is required. Wear eye protection when handling liquid nitrogen.
14. Low concentrations of $DiOC_6$ will label mitochondria.

References

1. Wang P, Hawkins TJ, Richardson C, Cummins I, Deeks MJ, Sparkes I, Hawes C, Hussey PJ (2014) The plant cytoskeleton, NET3C, and VAP27 mediate the link between the plasma membrane and endoplasmic reticulum. Curr Biol 24:1397–1405
2. Boevink P, Santa Cruz S, Hawes C, Harris N, Oparka KJ (1996) Virus mediated delivery of the green fluorescent protein to the endoplasmic reticulum of plant cell. Plant J 10:35–941
3. Terasaki M, Song J, Wong JR, Weiss MJ, Chen LB (1984) Localization of endoplasmic reticulum in living and glutaraldehyde-fixed cells with fluorescent dyes. Cell 38:101–108
4. Quader H, Schnepf E (1986) Endoplasmic reticulum and cytoplasmic streaming: fluorescence microscopical observations in adaxial epidermis cells of onion bulb scales. Protoplasma 131:50–252
5. Sparkes I, Tolley N, Aller I, Svozil J, Osterrieder A, Botchway S, Mueller C, Frigerio L, Hawes C (2010) Five Arabidopsis reticulon isoforms share endoplasmic reticulum location, topology, and membrane-shaping properties. Plant Cell 22:1333–1343
6. Irons SL, Evans DE, Brandizzi F (2003) The first 238 amino acids of the human lamin B receptor are targeted to the nuclear envelope in plants. J Exp Bot 54:943–950
7. Ivanov S, Harrison MJ (2014) A set of fluorescent protein-based markers expressed from constitutive and arbuscular mycorrhiza-inducible promoters to label organelles, membranes and cytoskeletal elements in *Medicago truncatula*. Plant J 80:1151–1163
8. Lee H, Sparkes I, Gattolin S, Dzimitrowicz N, Roberts LM, Hawes C, Frigerio L (2013) An Arabidopsis reticulon and the atlastin homologue RHD3-like2 act together in shaping the tubular endoplasmic reticulum. New Phytol 197:481–419
9. Denecke J, De Rycke R, Botterman J (1992) Plant and mammalian sorting signals for protein retention in the endoplasmic reticulum contain a conserved epitope. EMBO J 11:2345–2355
10. Gomord V, Denmat LA, Fitchette-Lainé AC, Satiat-Jeunemaitre B, Hawes C, Faye L (1997) The C-terminal HDEL sequence is sufficient for retention of secretory proteins in the endoplasmic reticulum (ER) but promotes vacuolar targeting of proteins that escape the ER. Plant J 11:313–325
11. Satiat-Jeunemaitre B, Hawes C (2001) Immunocytochemistry for light microscopy. In: Hawes C, Satiat-Jeunemaitre B (eds) Plant cell biology: practical approach. O.U.P., New York, pp 207–233. (Chapter 10)

12. Wasteneys G (1997) Freeze shattering: a simple and effective method for permeabilizing higher plant cell walls. J Microsc 188:51–61
13. Wang P, Richardson C, Hawkins TJ, Sparkes I, Hawes C, Hussey PJ (2016) Plant VAP27 proteins: domain characterization, intracellular localization and role in plant development. New Phytol 210:1311–1326
14. Sparkes IA, Runions J, Kearns A, Hawes C (2006) Rapid, transient expression of fluorescent fusion proteins in tobacco plants and generation of stably transformed plants. Nat Protoc 1:2019–2025
15. Kriechbaumer V, Shaw R, Mukherjee J, Bowsher CG, Harrison AM, Abell BM (2009) Subcellular distribution of tail-anchored proteins in Arabidopsis. Traffic 10:1753–1764
16. Karimi M, De Meyer B, Hilson P (2005) Molecular cloning in plant cells. Trends Plant Sci 10:103–105
17. Lilley BN, Ploegh HL (2004) A membrane protein required for dislocation of misfolded proteins from the ER. Nature 24:834–840
18. Kriechbaumer V, Botchway SW, Slade SE, Knox K, Frigerio L, Oparka K, Hawes C (2015) Reticulomics: protein-protein interaction studies with two plasmodesmata-localized reticulon family proteins identify binding partners enriched at plasmodesmata, endoplasmic reticulum, and the plasma membrane. Plant Physiol 169:1933–1945
19. Matsushima R, Fukao Y, Nishimura M. Hara-Nishimura I (2004) NAI1 gene encodes a basic-helix-loop-helix-type putative transcription factor that regulates the formation of an endoplasmic reticulum-derived structure, the ER body. The Plant Cell 16:1536–1549

Chapter 2

3D Electron Microscopy of the ER

Maike Kittelmann

Abstract

The endoplasmic reticulum (ER) forms an extensive network in plant cells. In leaf cells and vacuolated root cells it is mainly restricted to the cortex whereas in the root meristem the cortical and cytoplasmic ER takes up a large volume throughout the entire cell. Only 3D electron microscopy provides sufficient resolution to understand the spatial organization of the ER in the root. However, high contrast staining and optimally ER specific staining is essential. Here we describe a protocol for selective ER staining that allows automated or semiautomated segmentation of the organelle in 3D datasets obtained from serial sections, Array Tomography, Serial Block Face Scanning Electron Microscopy (SBFSEM), or Focused Ion Beam (FIB) SEM.

Key words 3D EM, Serial Block Face SEM, Endoplasmic reticulum, ZIO, Automated segmentation

1 Introduction

The plant endoplasmic reticulum has a very distinct morphology of tubular and cisternal domains [1]. However, how they are generated and maintained and how alterations in ER morphology alter ER function remains to be fully understood in all eukaryotic cells. In plants, the physical nature of ER exit sites and their connection to the Golgi apparatus [2], ER function in cell plate formation during cell division [3], and the characterization of anchor points of the ER with the plasma membrane [4] are still under investigation and require high resolution imaging in 3D. Light microscope resolution is usually not sufficient to analyze these ultrastructural details, especially not in small arabidopsis root cells. Electron microscopy has therefore been the imaging technique of choice. For a long time, the 3D architecture of the ER in these cells could only be studied by serial sectioning, tomography, or high voltage electron microscopy of thick sections (Fig. 1). However, these techniques are either extremely laborious or would only depict a very small area of the ER.

Chris Hawes and Verena Kriechbaumer (eds.), *The Plant Endoplasmic Reticulum: Methods and Protocols*,
Methods in Molecular Biology, vol. 1691, DOI 10.1007/978-1-4939-7389-7_2,

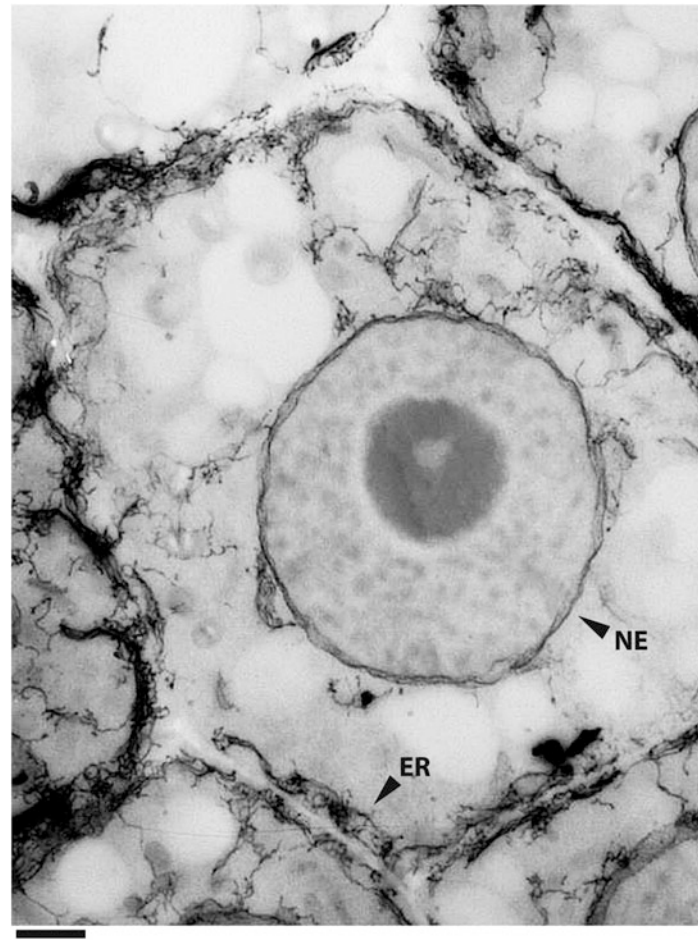

Fig. 1 High voltage electron micrograph of a 1 μm thick ZIO impregnated zea root tip meristem cell. The cortical ER and the nuclear envelop (NE) are heavily stained. Scale bar = 2 μm

Recent developments of automated 3D EM techniques now enable us to study the root ER of entire cells more easily and in more detail. FIBSEM, SBFSEM, and array tomography allow the acquisition of hundreds of images in the *Z* axis, of a fairly large area in an automated or semiautomated fashion. Especially SBFSEM has recently become more widely used for imaging of plant tissue [5]. FIBSEM and SBFSEM are both destructive techniques where the surface of the resin-embedded sample is scanned and then a layer is removed by either ion beam milling (removing a layer of few nanometers) or diamond knife sectioning (sections of at least 20 nm). Both techniques require strong pre-embedding staining to allow sufficient signal detection without the electron beam penetrating too far into the sample.

Array tomography involves the collection of serial sections which can now be automated with the ATUMtome (RMC) [6]. The sections are collected onto a moving tape and can then be post-stained for additional contrast, immunolabeled or otherwise post-processed and imaged repeatedly with desired settings and region of interest (ROI) in a high resolution field emission SEM.

To allow automated or semiautomated segmentation of the complex ER network in a 3D image stack, tissue or organelle specific staining is essential. Automated algorithms including thresholding, region growth, or watershed then allow unbiased 3D modeling [5].

There are two main ways to achieve selective staining of the ER: (1) Enzyme cytochemistry, based on heavy metals as osmium or lead salts reacting with enzyme substrates at the site of targeted enzyme activity. For example, the inosine 5′-diphosphatase (IDPase) shows specific dictyosome staining [7] in the green alga, *Gloeomonas kupfferi*. In animal cells, a horseradish peroxidase can be targeted to the ER by fusion with the KDEL retention signal [8]. A variety of other enzymes for plant enzyme cytochemistry were reviewed by Sexton and Hall already in 1991 [9]. More recently, miniSOG [10] and APEX [11] have been developed as genetically encoded tags allowing also correlative microscopy. However, their usefulness in plants still needs to be evaluated. (2) Endomembrane specific staining techniques where zinc-iodide or potassium ferryicyanide guide osmium reduction to the membrane and cisternae of the ER [12, 13] or a combination of uranyl acetate, copper and lead citrate that leads to selective membrane and polysaccharide contrast [14]. So far the zinc-iodide-osmium technique (ZIO) is the most reliable and selective method for the ER. After prefixation in aldehydes the tissue is incubated in a mixture of zinc-iodide and osmium and then embedded in resin. The ER membrane as well as ER lumen, Golgi bodies, and the nuclear envelop are heavily stained, whereas other organelles show no or only very little staining (Fig. 2).

ER network characteristics can then be quantified not only in 2D but also in 3D. Measurements of the surface area and volume are standard options in 3D rendering programs. Algorithms that are able to distinguish between sheets and tubules and allow the quantification of tubule lengths and sheet size have yet to be developed but will in the future allow the analysis of ER network composition and changes in mutant backgrounds.

2 Materials

1. Fixative: 1% paraformaldehyde (*see* **Note 1**), 1% glutaraldehyde, 2% sucrose, 50 mg calcium chloride, drop of Brij.35 surfactant (*see* **Note 2**) in 0.1 M sodium cacodylate buffer (NaCac, pH 6.9) (*see* **Note 3**).

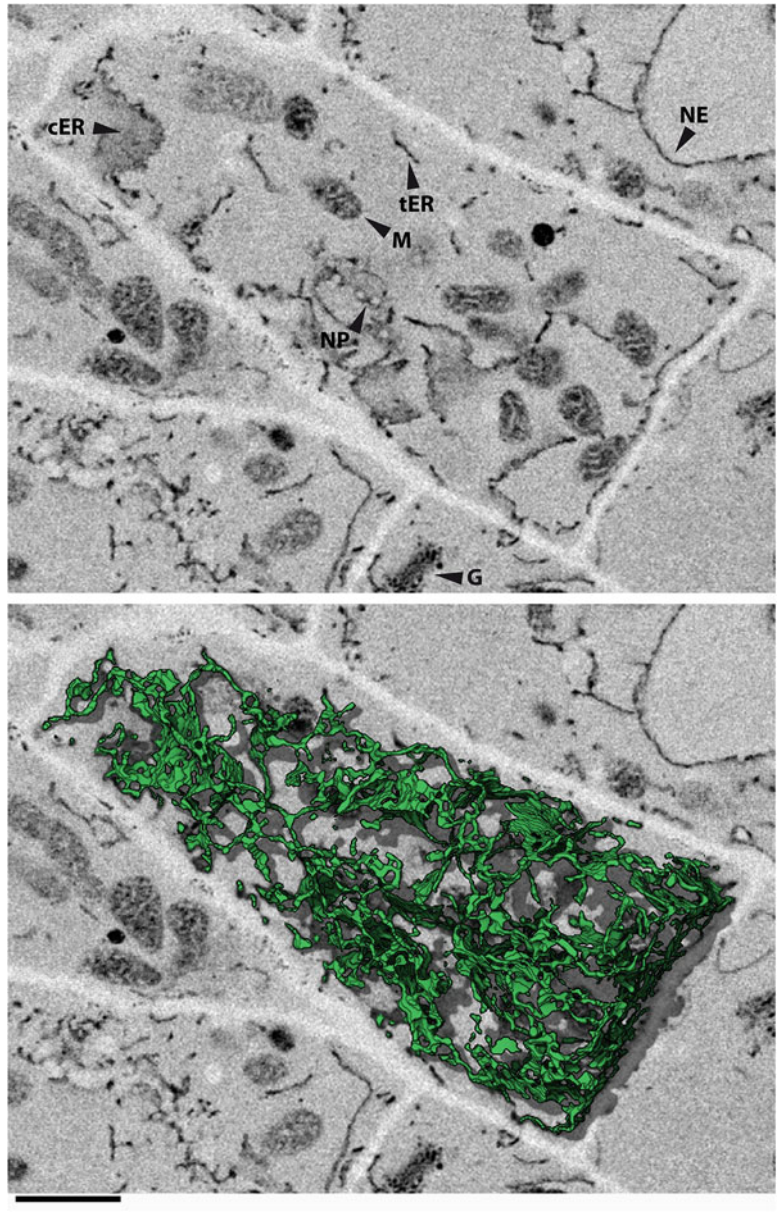

Fig. 2 Arabidopsis root meristem cell stained with the ZIO technique. The endomembrane system including the cisternal ER (cER), tubular ER (tER), nuclear envelop (NE) with clearly visible nuclear pores (NP) and Golgi bodies (G) is heavily stained (*top*). Mitochondria (M) show variable staining as well. This staining technique allows a semiautomated rendering of the ER network (*green*, *bottom*). Scale bar = 1 μm

2. Zinc-Iodide: Add 3 g zinc to 20 ml of deionized water, add 0.5 g of resublimed iodine (*see* **Note 4**), stir for 5 min, then filter through No. 1 filter paper.
3. Osmium: prepare 2% osmium tetroxide in deionized water (*see* **Note 5**). Mix 2% osmium and filtered zinc-iodide 1:1 just before adding to the sample.

4. EtOH dilution series and absolute EtOH dried over a molecular sieve.
5. Spurr resin, hard (*see* **Note 6**).

3 Methods

3.1 Fixation of Arabidopsis Seedling for 3D EM

1. Prepare fixative and zinc-iodide.
2. Place 1-week-old seedling or cut off root and leaves (*see* **Note 7**) into small glass vial with fixative and apply mild vacuum for 1 min by placing open vial into vacuum pump (*see* **Note 8**).
3. Close glass vials and leave on rocker for 1 h at room temperature to fix.
4. Wash seedlings 2× with 0.1 M NaCac buffer for 10 min, then 1× with deionized water for 10 min.
5. Mix zinc-iodide and 2% osmium tetroxide 1:1 to make an appropriate volume of ZIO depending on the number of samples and size of fixation vials. Remove water from samples and add ZIO mix.
6. Leave closed vials for incubation for 4 h for roots or at least 12 h for leaf tissue to obtain sufficient staining (*see* **Note 9**).
7. Wash quickly 3× with deionized water to remove precipitates and ZIO solution.
8. Wash 2× for 10 min with deionized water.
9. If seedlings are still intact, cut off roots to allow better dehydration and resin infiltration.
10. Dehydrate tissue in ethanol series for at least 15 min per dilution in 10%, 30%, 50%, 70%, 90%, and 100% EtOH. Dehydrate 2× 30 min in absolute EtOH.
11. Infiltrate with Spurr resin (*see* **Note 10**) for at least 1 h per dilution in 10%, 30% and at least 3 h in 50%, 70%, and 90% and 3× in 100% Spurr (*see* **Note 11**). Mix with fresh 100% Spurr resin and pour into flat embedding dishes or place samples into embedding molds and polymerize for 12 h at 70 °C (*see* **Note 12**).

4 Notes

1. 10% stock paraformaldehyde: mix 2 g of PFA in 20 ml deionized water and heat up to 70 °C while stirring. When reaching target temperature, slowly add drops of 1 M NaOH until PFA is completely dissolved. Store in fridge.

2. Brij.35 surfactant is used to enhance access of the fixative to the hydrophobic leaf surface. Other or no surfactant may be used and may result in similarly good fixation results.
3. 0.2 M stock sodium cacodylate buffer: Mix 400 ml of deionized water with 21.4 g sodium cacodylate, adjust pH with HCl and add deionized water to final volume of 500 ml. Dilute 1:1 with deionized water for 0.1 M buffer.
4. Resublimed iodine currently available from most companies seems to cause precipitates when used in the previously published ratio with zinc [15]. We reduced the iodine to 0.5 g per 3 g zinc and found that the precipitates disappeared almost completely and the ZIO solution after incubation showed significantly less precipitates.
5. If preparing osmium tetroxide solution from crystalline osmium tetroxide, leave overnight for the crystals to dissolve completely. Sonication speeds up the process if needed.
6. Depending on the country, Spurr resin is now available again with ERL 4221D instead of ERL 4206 or a similarly low viscosity resin is offered as a substitute.
7. For arabidopsis seedling roots, one can leave the seedlings intact for at least the initial fixation step to allow easier handling. For larger tissues and plants, cut off tissue of interest to allow quicker diffusion of fixative into the tissue.
8. Air is extruded from the intercellular space and thus allows the fixative to enter the leaves more easily for quicker fixation. If only the roots are of interest, this procedure is not necessary.
9. Depending on the tissue, those incubation times vary. It's a good idea to run an initial experiment with three different time points to determine the ideal incubation time to obtain enough staining but prevent cytoplasmic precipitates.
10. We prefer Spurr resin due to its low viscosity and thus quicker and better infiltration properties through the cell walls. Other resins might be similarly suitable but potentially require longer infiltration times.
11. Resin infiltration times can be shortened by mild centrifugation to about half an hour each step; however, the root tips are very delicate at this stage and damage may occur when trying to detach the roots from the tube wall.
12. To label the sample we print fixation date, strain, and other important information in Arial font size 3 and place the paper into the mold or embedding dish with the sample. Test if the ink is stable in Spurr resin before using the label. Color printed labels usually don't work, therefore use the black and white print option.

References

1. Friedman JR, Voeltz GK (2011) The ER in 3D: a multifunctional dynamic membrane network. Trends Cell Biol 12:709–717
2. Hawes C, Osterrieder A, Hummel E, Sparkes I (2008) The plant ER-Golgi interface. Traffic 10:1571–1580
3. Seguı-Simarro JM, Austin JR 2nd, White EA, Staehelin LA (2004) Electron tomographic analysis of somatic cell plate formation in meristematic cells of Arabidopsis preserved by high-pressure freezing. Plant Cell 16:836–856
4. Hamada T, Ueda H, Kawase T, Hara-Nishimura I (2014) Microtubules contribute to tubule elongation and anchoring of endoplasmic reticulum, resulting in high network complexity in Arabidopsis. Plant Physiol 166:1869–1876
5. Kittelmann M, Hawes C, Hughes L (2016) Serial block face scanning electron microscopy and the reconstruction of plant cell membrane systems. J Microsc 263:200–211
6. Hayworth KJ, Morgan JL, Schalek R, Berger DR, Hildebrand DG, Lichtman JW (2014) Imaging ATUM ultrathin section libraries with WaferMapper: a multi-scale approach to EM reconstruction of neural circuits. Front Neural Circuits 8:68
7. Domozych DS (1989) The endomembrane system and mechanism of membrane flow in the green alga, *Gloeomonas kupfferi* (*Volvocales, Chlorophyta*) II. A cytochemical analysis. Protoplasma 149:108–119
8. Puhka M, Vihinen H, Joensuu M, Jokitalo E (2007) Endoplasmic reticulum remains continuous and undergoes sheet-to-tubule transformation during cell division in mammalian cells. J Cell Biol 179:895–909
9. Sexton R, Hall JL (1991) Enzyme cytochemistry. In: Hawes C, Hall JL (eds) Electron microscopy of plant cells. Academic Press, London, pp 67–84
10. Shu X, Lev-Ram V, Deerinck TJ, Qi Y, Ramko EB, Davidson MW, Jin Y, Ellisman MH, Tsien RY (2011) A genetically encoded tag for correlated light and electron microscopy of intact cells, tissues, and organisms. PLoS Biol 4: e1001041
11. Martell JD, Deerinck TJ, Sancak Y, Poulos TL, Mootha VK, Sosinsky GE, Ellisman MH, Ting AY (2012) Engineered ascorbate peroxidase as a genetically encoded reporter for electron microscopy. Nat Biotechnol 11:1143–1148
12. Barlow PW, Hawes C, Horne JC (1984) Structure of amyloplasts and endoplasmic reticulum in the root caps of *Lepidium sativum* and *Zea mays* observed after selective membrane staining and by high-voltage electron microscopy. Planta 160:363–371
13. Hepler PK (1981) The structure of the endoplasmic reticulum revealed by osmium tetroxide-potassium ferricyanide staining. Eur J Cell Biol 26:102–111
14. Hawes CR, Horne JC (1983) Staining plant cells for thick sectioning: uranyl acetate, copper and lead citrate impregnation. Biol Cell 48:207–210
15. Hawes CR, Jumiper B, Horn JC (1981) Low and high voltage electron microscopy of mitosis and cytokinesis in maize. Planta 152:397–407

Chapter 3

Characterization of Proteins Localized to Plant ER-PM Contact Sites

Pengwei Wang, Chris Hawes, Christine Richardson, and Patrick J. Hussey

Abstract

Like in most eukaryotic cells, the plant endoplasmic reticulum (ER) network is physically linked to the plasma membrane (PM), forming ER-PM contact sites (EPCS). The protein complex required for maintaining the EPCS is composed of ER integral membrane proteins (e.g., VAP27, synaptotagmins), PM-associated proteins (e.g., NET3C), and the cytoskeleton. Here, we describe methods for identifying possible EPCS-associated proteins. These include GFP-tagged protein expression followed by image analysis, and immuno-gold labeling at the ultrastructural level. In combination, these methods can be used to identify the localization of putative EPCS proteins as well as used to postulate their subcellular function.

Key words Endoplasmic reticulum, ER-PM contact sites, *N. benthamiana*, Chi-square analysis, Immuno-gold TEM, VAP27 family, NET3C

1 Introduction

The cortical endoplasmic reticulum (ER) in plants forms a dynamic geometrical network, and these dynamics are controlled, in part, by the cortical actin network [1] and several members of the myosin XII family [2, 3]. Another interesting feature of the ER network is that it forms physical interactions with various membrane compartments and organelles [4, 5] and the most well characterized to date is the ER-PM contact/anchor site (EPCS, [6–9]). Contact sites can be identified using electron microscopy, but their function in plants is not fully understood, possibly due to the lack of molecular markers and the difficulty in resolving the EPCS structure using conventional microscopy.

Our understanding of plant EPCS at the molecular level has increased dramatically over the last few years. Various proteins have been reported to be associated with the EPCS [6–9], and this has allowed studies to be carried out on the function of plant EPCS (e.g., cargo transport, signal communication, and cytoskeleton

Chris Hawes and Verena Kriechbaumer (eds.), *The Plant Endoplasmic Reticulum: Methods and Protocols*, Methods in Molecular Biology, vol. 1691, DOI 10.1007/978-1-4939-7389-7_3,

reorganization). In this chapter, we present several methods that can be used to confirm the EPCS localization of candidate proteins. These include conventional light and electron microscopy approaches, as well as immunocytochemical studies.

Fluorescent protein fusions and transient protein expression in leaf epidermal cells (*N. benthamiana* or *N. tabacum*) are widely accepted for studying protein localization [10] and this is the most straightforward approach for studying putative EPCS localized proteins in plants. But due to the nature of light microcopy, EPCS structures can be difficult to resolve, and protein overexpression, in rare cases, can cause problems in ascertaining the endogenous localization. Therefore, additional confirmation is required, such as using electron microscopy and immuno-gold labeling.

ER-PM contact sites can be distinguished at the ultrastructural level. Morphologically, EPCS can be defined as a region where the two membranes are less than 10 nm apart and where ribosomes are excluded (as suggested our study [6], and studies conducted in yeast). At the EPCS, PM and ER membranes contact each other but are not fused (Fig. 1). We have found that overexpression of certain EPCS proteins (e.g., VAP27, or VAP27 and NET3C together) can enhance the ER-PM association and, as a consequence, the size of the EPCS appears enlarged [7]. Furthermore, immuno-gold labeling can also be used to characterize the sites, and we routinely use chi-square analysis to ensure that gold particles found at the EPCS are specifically localized and enriched. In summary, we suggest a few methods for studying EPCS in plants which can be used to test if a protein candidate is localized to the ER-PM contact site.

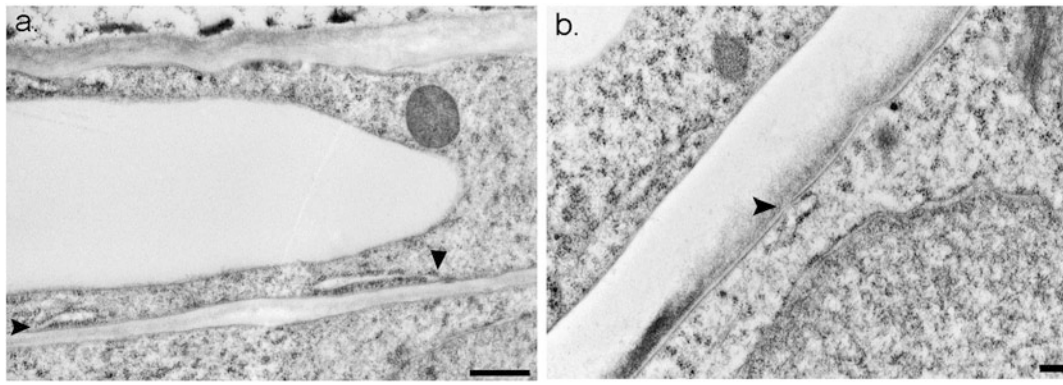

Fig. 1 Transmission electron microscopy image of a cell from arabidopsis hypocotyl (**a**) and a *N. benthamiana* leaf epidermal cells (**b**). The ER-PM contact site (*arrowhead*) can be observed. ER membrane and plasma membrane are connected but not fused to each other, the average space between the membranes is less than 10 nm (scale bar = 100 nm)

2 Materials

2.1 Plant and Microscopy Material

1. *N. benthamiana* or *N. tabacum* grown in plant growth rooms with a 16 h day length (25 °C) and 8 h dark (18 °C) regime. Plants around 5 weeks old are ideal for transient expression studies.
2. Arabidopsis (Col-0) wild type or genetically transformed can be grown either on compost or 1/2MS medium (1% Sucrose, 0.7% Plant Agar) in a growth chamber with a 16 h light (22 °C) and 8 h dark (18 °C) regime.
3. Low melting point agarose.
4. FM4-64 membrane dye.
5. Glass slides and coverslips.
6. Razor blade.

2.2 Plasmids and Agrobacterium Mediated Transformations

1. Endoplasmic reticulum markers: GFP/RFP-HDEL, Calnexin (TMD)-GFP [6].
2. ER-PM contact site markers: VAP27-1-YFP, GFP-NET3C, SYT1-GFP [6, 9, 11].
3. Suppressor of post-transcriptional gene silencing (PTGS): pCB301-p19 [12].
4. Agrobacterium strain: GV3101::pMP90.

2.3 Immuno-Gold Labeling

1. Monostep Lowicryl HM20 (Agar Scientific).
2. Mouse polyclonal antibody raised against NET3C, NAP1 [6, 13], or protein of interest.
3. 5 or 10 nm gold-conjugated goat anti-mouse antibody (British Biocell International, Cardiff, UK).
4. Blocking buffer: PBS supplemented with BAS, 1% w/v.
5. BSAc buffer: PBS buffer supplemented with acetylated BSA, 0.1% w/v.
6. Phosphate Buffered Saline (PBS).

2.4 Computer Programs Required

1. Image J.
2. Adobe Photoshop.

3 Methods

3.1 Live Cell Imaging and Quick Identification of Immobile ER-PM Contact Sites

The method described here can be used for a brief determination of putative EPCS localized proteins using fluorescence protein fusions and bacteria infiltration-mediated transient expression.

1. Follow the leaf infiltration protocol (*see* Chapter 1), infiltrate with Agrobacterium (GV3101) transformed with the relevant construct, e.g., VAP27-1-YFP (*see* **Notes 1** and **2**).
2. Normally 48–60 h after infiltration dissect a leaf segment (25–50 mm^2) and mount on a slide with coverslip. To avoid sample drifting during live imaging, low melting agarose can be used here instead of water for mounting (*see* **Note 3**) or tape can be used to stick coverslips to the slide.
3. Using a laser scanning confocal microscope, capture a time series over 3–5 min (frame size 512 × 512; two times line average; no time interval between every image).
4. Make sure samples do not drift during the image capture series, and choose three frames at different time points and assign them a different color. For example, use red for image at 0 s, green for 15 s, and cyan for 30 s (Fig. 2).
5. With Adobe Photoshop, overlay three images on top of each other and merge them into one picture. Any persistent sites over the time period should be colored magenta; and the color for each point should still be distinguished for mobile structures.
6. As shown in Fig. 2a, a time series of VAP27-YFP over 30 s, each image represents a time point and is pseudo-colored to represent the different time frames. A merged picture indicates that the ER-PM contact sites are persistent (magenta) while the rest of the ER network remodels. In contrast, when the same analysis is applied to moving Golgi bodies, no persistent structures can be identified (Fig. 2b).

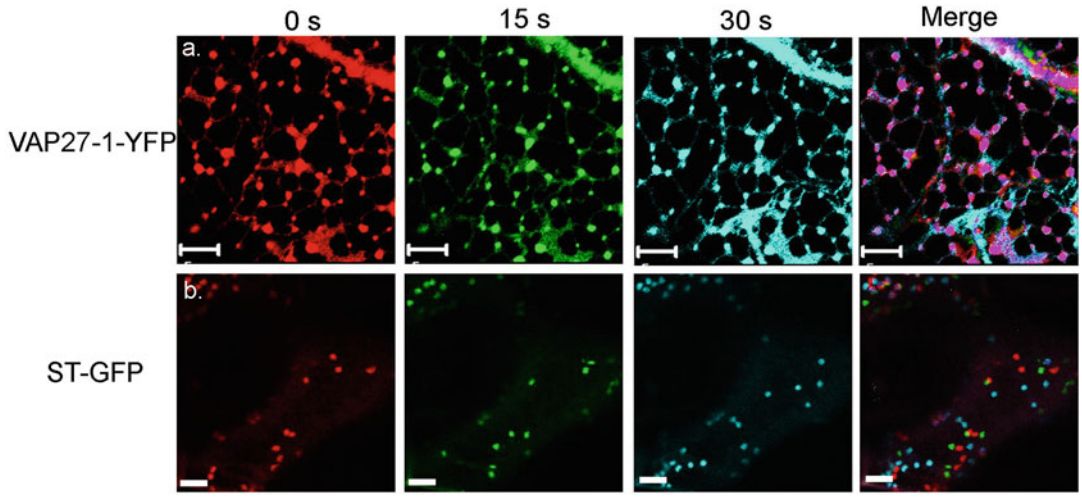

Fig. 2 Persistency analysis of VAP27-1-YFP labeled EPCS (**a**) and ST-GFP labeled Golgi bodies (**b**). Images representing time points (0, 15, and 30 s) are pseudo-colored, and structures colored magenta indicates they are persistent during the time frame, such as VAP27-1 labeled EPCS (**a**). In contrast, when the same analysis is applied to moving Golgi bodies (**b**), no persistent structures can be identified (scale bar = 5 μm)

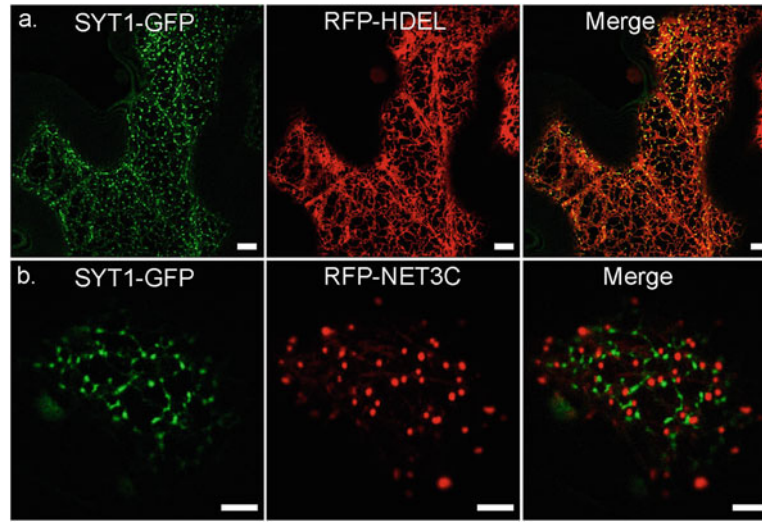

Fig. 3 *N. benthamiana* leaf epidermal cells expressing EPCS proteins. (**a**) SYT1-GFP is associated with ER-PM contact sites and the ER network labeled by RFP-HDEL. (**b**) SYT1 labeled EPCS do not co-localize with RFP-NET3C, another known EPCS protein. Most are closely attached, suggesting different populations of EPCS exist in plants (scale bar = 5 μm)

7. Persistent structures that appear to be localized to stable ER nodes are likely to be ER-PM contact site associated, and can be analyzed using the procedures detailed in Subheadings 3.2 and 3.3.
8. In addition, protein co-expression studies with EPCS markers (e.g., VAP27, NET3C) can be used to determine EPCS localization. But care should be taken, as our recent study suggested the EPCS in plants are likely to be represented by different protein complexes (e.g., SYT1), which do not necessarily overlap (Fig. 3).
9. Further determination of ER-PM contact sites is also recommended (Subheading 3.3 especially).

3.2 ImageJ Analysis for Signal Distribution

By definition, protein complexes of EPCS must localize in-between the ER and PM. Using fluorescent protein markers, we should be able to distinguish distribution of the signals from the ER, PM, and EPCS localized proteins.

1. Agrobacterium-mediated transformation and sample preparation are the same as in Subheading 3.1.
2. Dissect a leaf segment (5×5 mm^2) and incubate it in water solution containing FM4-64 (8 μM) for 10 min. This will stain the plasma membrane without the labeling of endocytotic vesicles.

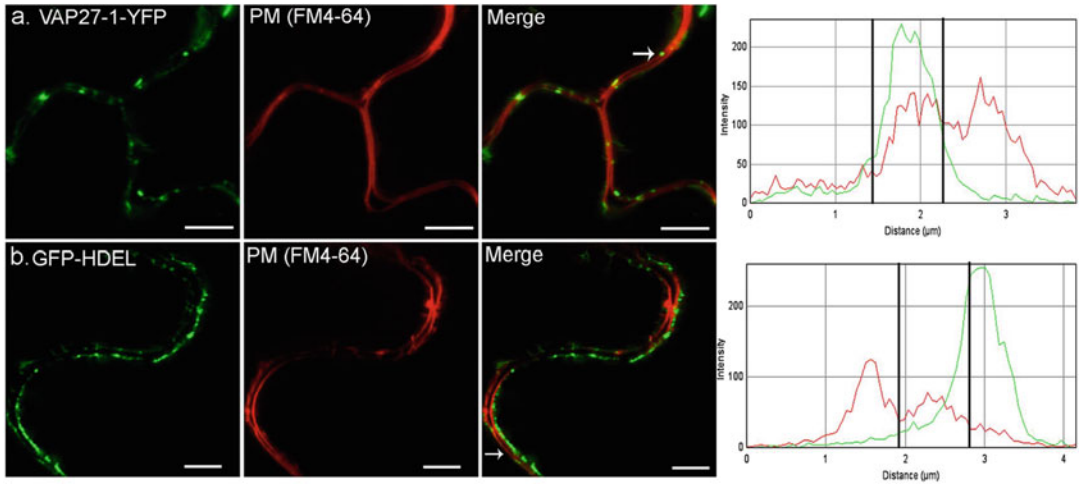

Fig. 4 Signal distribution of EPCS (**a**) and the ER network (**b**) in relation to the plasma membrane. A selected area (*arrow*) was analyzed and signal from VAP27-1 labeled EPCS (*green*) overlaps with PM (*red*); whereas signal from ER network (GFP-HDEL) is distinct from the PM (scale bar = 5 μm)

3. Set the focal plane in the middle of the cell, and take images of cell periphery, where cytoplasm, plasma membrane, and cell wall can be distinguished (*see* **Note 4**).
4. Open the merged picture using ImageJ, and draw a line where ER-PM contact sites can be identified (Fig. 4a, arrow).
5. In the Plugins option, go to Graphics and then choose RGB Profile Plot. An image that indicates signal distribution should appear. The signal from ER network, ER-PM contact sites, and plasma membrane should be identifiable. For example, the signal from EPCS structures and PM appear to be overlapped; while ER network/cytoplasmic labeling is separated from PM (Fig. 4b, arrow)
6. This only gives a rough idea of the signal distribution, and it largely depends on the quality of the image. Further analysis is required (*see* Subheading 3.3).

3.3 Immuno-Gold TEM and Chi-Square Analysis of Gold Particle Enrichment

Protein localization at the ultrastructural level can be achieved by immuno-gold labeling. This approach, in combination with Subheadings 3.1 and 3.2, can provide convincing results for determining the location of proteins and proteins of the ER-PM contact site.

1. Ideally, high pressure freezing with freeze-substitution should be used for this purpose. It faithfully preserves cell structure especially the plasma membrane which is important for correct location of EPCS.

2. The protocol is adapted from [14] with some modifications. Before high pressure freezing, the distal 1–2 mm tips of the Arabidopsis roots (7 days after germination) were excised with a razor blade in 20% BSA.
3. The samples were freeze-substituted in anhydrous acetone containing 0.25% (v/v) glutaraldehyde and 0.1% (w/v) uranyl acetate for 48 h at −80 °C, then the temperature was slowly raised to −50 °C over a 30 h period.
4. After several rinses in anhydrous acetone at −50 °C, infiltration continued at −50 °C into Monostep Lowicryl HM20 (Agar Scientific) by increasing the concentration of resin to acetone stepwise (12 h in 22%, 33%, and 66%, and then three times in 100% 96 h). Final embedding and UV polymerization was carried out at −50 °C for 48 h followed by a slow warming to 20 °C; the polymerization then continued for a further 24 h.
5. Ultrathin sections (50–70 nm) are prepared according to [11] and transferred onto Formvar-coated nickel grids.
6. Incubate sections for 20 min at room temperature in a PBS buffer supplemented with glycine (0.1% w/v), and then incubate for a further 30 min in a blocking buffer containing 1% BSA.
7. Wash the grids in BSAc buffer three times for 5 min.
8. In a humid chamber, incubate the sections for a further 30 min with primary antibody, which is diluted in blocking buffer (dilution from 1:50 to 1:200 depends on antibody, *see* **Note 5**).
9. After washing in BSAc buffer (3 × 5 min), incubate the sections in 5–10 nm gold labeled goat anti-mouse antibody diluted in blocking buffer (1:20) for 30 min (*see* **Note 6**).
10. With the TEM, the structure of ER-PM contact sites can be identified (Fig. 5). The closely associated gold particle indicates that the protein that the primary antibody recognizes is localized to these sites.
11. Next, a chi-square test can be used to test if the gold particle labeling is enriched at the selected region is genuine or random.
12. For ER-PM contact sites, count the number of gold particles in an area 50 nm either side of the plasma membrane. Similarly, count the number of gold particles at the EPCS (Fig. 5).
13. From these measurements, the area of EPCS in proportion to the PM, the density of gold particle in EPCS, and the expected number for a random distribution (total gold number × the proportion of EPCS area) can be calculated (Fig. 5).
14. Finally, the p value can be calculated based on the real distribution of gold particles compared to the expected number from a

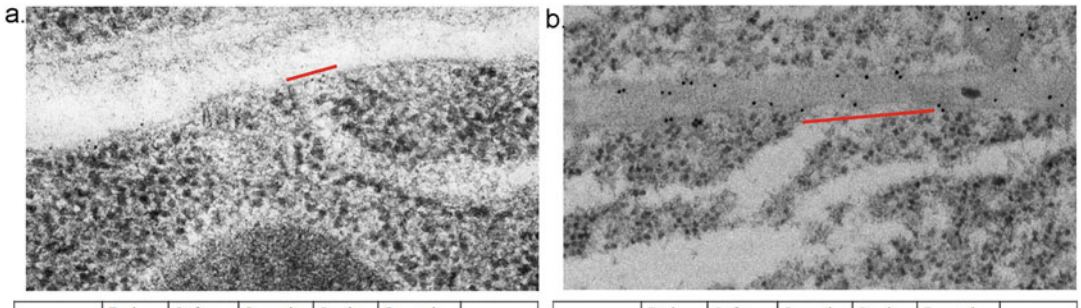

	Total Numbers	Surface area (μm2)	Proportion to total area	Density (per μm2)	Expected for random distribution	P-Value
PM associated	4	0.076	9.2%	92	6.36	P = 0.002*
ER-PM contact sites associated	3	0.007	90.8%	428.6	0.36	

	Total Numbers	Surface area (μm2)	Proportion to total area	Density (per μm2)	Expected for random distribution	P-Value
PM associated	12	0.064	26.6%	265.6	12.5	P = 0.783*
ER-PM contact sites associated	5	0.017	73.4%	294.1	4.5	

Fig. 5 Immuno-gold labeling of Arabidopsis root tips. (**a**) With an NET3C antibody gold particles are located at the ER-PM contact sites and the PM. The region of ER-PM contact sites is highlighted in *red*. The *p* value of 0.002 from chi-square analysis indicates that the labeling of NET3C positive gold is enriched at the EPCS compared to the PM. (**b**) When a NAP1 (actin binding protein) antibody is used as a control, it is evenly distributed on the PM. The calculated *p* value is much larger than 0.05, indicating that any association with EPCS is a random event. The chi-square calculation for PM and EPCS is shown in a table (scale bar = 100 nm)

random distribution. This can be achieved using the online program http://graphpad.com/quickcalcs/chisquared1.cfm.

15. As shown in Fig. 5, the real association (Fig. 5a) and random association (Fig. 5b) can be distinguished based on their p values, and a number below 0.05 indicates the enrichment of gold particles in the selected area.

4 Notes

1. When infiltrating the leaf epidermis of *N. benthamiana*, the viral p19 suppressor [12] can be used to increase protein expression and signal intensity. But it cannot be applied to *N. tabacum* due to lethality.
2. The ideal optical density of GV3101 (OD_{600}) used in infiltration depends on the construct that has been transformed. Normally OD_{600} around 0.05–0.2 are used; the principle is to use the lowest OD that can result in a useable level of protein expression.
3. Prolonged imaging on the same leaf segment should be avoided; the mechanical pressure from coverslips can induce cellular stress. Normally samples should be changed at least every 20 min.
4. Such procedures can also be carried out on most proprietary confocal and image analysis programs.

5. For each grid, approximately 10 μl of antibody solution can be applied.
6. Negative controls are required; to do this the secondary antibody can be applied directly without primary antibody incubation.

References

1. Boevink P, Oparka K, Santa Cruz S et al (1998) Stacks on tracks: the plant Golgi apparatus traffics on an actin/ER network. Plant J 15:441–447
2. Sparkes I, Runions J, Hawes C et al (2009) Movement and remodeling of the endoplasmic reticulum in nondividing cells of tobacco leaves. Plant Cell 21:3937–3949
3. Avisar D, Abu-Abied M, Belausov E et al (2009) A comparative study of the involvement of 17 Arabidopsis myosin family members on the motility of Golgi and other organelles. Plant Physiol 150:700–709
4. Gao H, Metz J, Teanby NA et al (2016) In vivo quantification of peroxisome tethering to chloroplasts in tobacco epidermal cells using optical tweezers. Plant Physiol 170:263–272
5. Stefano G, Hawes C, Brandizzi F (2014) ER – the key to the highway. Curr Opin Plant Biol 22:30–38
6. Wang P, Hawkins TJ, Richardson C et al (2014) The plant cytoskeleton, NET3C, and VAP27 mediate the link between the plasma membrane and endoplasmic reticulum. Curr Biol 24:1397–1405
7. Wang P, Richardson C, Hawkins TJ et al (2016) Plant VAP27 proteins: domain characterization, intracellular localization and role in plant development. New Phytol 210:1311–1326
8. Levy A, Zheng JY, Lazarowitz SG (2015) Synaptotagmin SYTA forms ER-plasma membrane junctions that are recruited to plasmodesmata for plant virus movement. Curr Biol 25:2018–2025
9. Siao W, Wang P, Voigt B et al (2016) Arabidopsis SYT1 M maintains stability of cortical ER networks and VAP27-1 enriched ER-PM contact sites. J Exp Bot 67:6161–6171
10. Sparkes I, Runions J, Kearns A et al (2006) Rapid, transient expression of fluorescent fusion proteins in tobacco plants and generation of stably transformed plants. Nat Protoc 1:2019–2025
11. Deeks MJ, Calcutt JR, Ingle EK et al (2012) A superfamily of actin-binding proteins at the actin-membrane nexus of higher plants. Curr Biol 22:1595–1600
12. Voinnet O, Rivas S, Mestre P et al (2003) An enhanced transient expression system in plants based on suppression of gene silencing by the p19 protein of tomato bushy stunt virus. Plant J 33:949–956
13. Wang P, Richardson C, Hawes C et al (2016) Arabidopsis NAP1 regulates the formation of autophagosomes. Curr Biol 26:2060–2069
14. Fiserova J, Goldberg MW (2011) Immunoelectron microscopy of cryofixed freeze-substituted *Saccharomyces cerevisiae*. Methods Mol Biol 657:191–204

Chapter 4

Preparation and Imaging of Specialized ER Using Super-Resolution and TEM Techniques

Karen Bell, Karl Oparka, and Kirsten Knox

Abstract

The plant endoplasmic reticulum (ER) forms several specialized structures. These include the sieve element reticulum (SER) and the desmotubule formed as the ER passes through plasmodesmata. Imaging both of these structures has been inhibited by the resolution limits of light microscopy and their relatively inaccessible locations, combined with the fragile nature of the ER. Here we describe methods to view desmotubules in live cells under 3D-structured illumination microscopy (3D-SIM) and methods to fix and prepare phloem tissue for both 3D-SIM and transmission electron microscopy (TEM) which preserve the fragile structure and allow the detailed imaging of the SER.

Key words 3D-SIM, BY2, Endoplasmic reticulum, Desmotubule, Sieve element reticulum, Imaging, OMX, ZIO

1 Introduction

The limit of lateral resolution in light microscopy was determined more than 100 years ago [1]. The diffraction limit of light means that objects closer together than 200 nm cannot be fully resolved, instead appearing blurred. This limit remained largely unchallenged, despite the development of confocal laser scanning microscopy (CLSM). Theoretically, CLSM can produce images below the diffraction limit, but this is not generally seen with biological samples, principally as the pinhole needs to be smaller than the Airy pattern [2]. This results in most of the superfluous out-of-focus light being discarded, but also has the unwanted consequence of losing a significant portion of the in-focus emission. With biological specimens the fluorescence is often too weak, or labile, to sustain a detectable signal when emission light is discarded. Therefore, in practice, the pinhole is used at an aperture larger than the Airy pattern, and as such any chance of significantly increased lateral resolution is lost.

Chris Hawes and Verena Kriechbaumer (eds.), *The Plant Endoplasmic Reticulum: Methods and Protocols*, Methods in Molecular Biology, vol. 1691, DOI 10.1007/978-1-4939-7389-7_4,

Structured Illumination Microscopy (SIM) offers an alternative method to gain greater resolution while avoiding discarding the desired emitted light [3]. Optimally conducted, SIM can increase the lateral resolution to 100 nm and the axial resolution to 200 nm [4]. The technique relies on using spatially patterned excitation light. By introducing structure to the excitation light, and subtracting that known value from the emitted light pattern, it is possible to gain new information about the unknown sample. Exciting a fluorescently labeled sample with such structured light results in a Moiré interference fringe, created by the two different fine patterns being superimposed. As the illumination pattern is predetermined, the Moiré Fringe will describe the unknown structure of the sample, thus accessing super-resolution data otherwise unobtainable [3].

Due to the directionality of the light, and to gain a complete image, it is necessary to shift the phase of the light through five patterns, and then the orientation angle, which is usually shifted three times by at least 60° [5]. Post-imaging processing then produces the final image from 15 raw images from each *z*-plane.

The 3D-SIM imaging system was developed commercially by Applied Precision Inc. (Washington, USA) and the platform was named Optical Microscope eXperimental (OMX). The OMX is designed to maximize physical stability and photon budget with the aim of producing a platform suited to both rapid live-cell imaging and super-resolution of fixed material [5–7]. The basic components of the OMX system are described in [5] and the current Deltavision OMX Blaze model specification is available on the GE Healthcare website (http://www.gelifesciences.com).

In this chapter, we present protocols that describe methods of preparing fixed and live plant cells in order to visualize specialized ER components. Each protocol presents its own challenges concerning image optimization. Elements of these protocols have been described elsewhere [8–10] but here we describe methods optimized for the imaging of specialized ER structures.

Acquiring high-resolution 3D-SIM images from fixed tissue requires that the samples are labeled with a probe that is specific, highly photostable and with a high quantum yield. The tissue must be carefully fixed in order to preserve as much of the fine morphological structure as possible.

Imaging live cells requires a highly stable fluorophore for labeling structures that will not move during the timescale required to capture an image. During live-cell imaging, speed is of the essence in order to avoid any blur caused by components streaming within the cells. In this regard, the OMX system offers several advantages; simultaneous recording of up to four separate channels, or in cases where there may be some emission overlap between fluorophores, sequential imaging combined with rapid shuttering and fast, stable focusing resulting in delays of less than 1–2 ms. This means that together with its fully integrated electronic control, fast and precise

3D high-resolution image capture is possible [5, 6]. Despite this, many live cells will suffer bleaching during the image capture so it is important to optimize the setup to minimize bleaching, although this may come at the cost of losing some of the resolution.

The sieve element reticulum (SER) is a specialized ER system in the phloem of higher plants [11] and has long posed difficulties when imaging, as the sieve elements are located deep within tissues, beyond the working distance of most objectives. Fixation and sectioning is therefore a good way to visualize this structure (Fig. 1e and f). However, extreme care must be taken that the fixation method chosen does not disrupt the delicate structure.

In addition, tobacco-derived BY2 cell lines make good model systems as they are readily transformable, both transiently and stably with fluorescent reporters and often divide in long chains along one plane, allowing single cell layers to be imaged [12]. Close to the cell wall the ER is tightly appressed as it passes through the plasmodesmata, forming a desmotubule [13]. At just 15 nm wide this structure is well beyond the resolution limit of a standard confocal, but 3D-SIM allows greater resolution [14] (Fig. 1b and c).

Although super-resolution imaging can resolve structures beyond the diffraction limit, it cannot compete with transmission

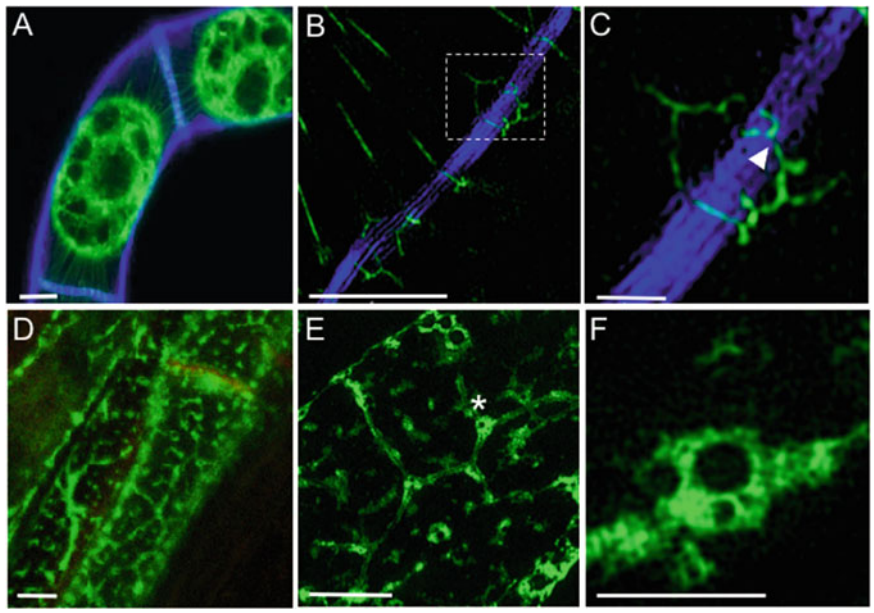

Fig. 1 (**a**) Confocal image of plasmolyzed BY2 cells, showing ER labeled by RTN6-GFP (*green*) and the cell wall labeled with Calcofluor White (*blue*); scale 10 μm. (**b**) 3D-SIM image of the cross wall between two BY2 cells; scale 5 μm. (**c**) Detailed view of the *boxed area* in (**b**), showing the narrowing of the ER as it forms the desmotubule (*arrow*, scale 1 μm). (**d**) Confocal image of sieve elements showing the SER labeled by pSEO2: GFP-HDEL; scale 5 μm. (**e**) 3D-SIM image showing structural details of the reticulum not resolved by the confocal scale 5 μm. (**f**) Detailed view of a region of SER similar to the region marked (*asterisk*) in (**e**); scale 2 μm

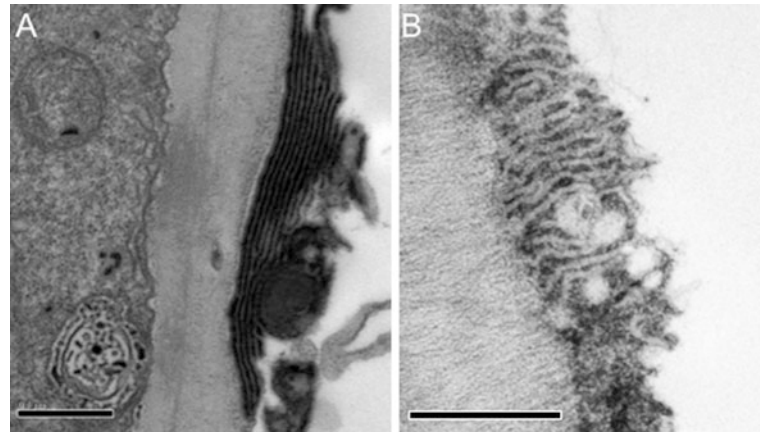

Fig. 2 TEM images taken at the sieve element and companion cell walls of tobacco petioles, stained with ZIO. (**a**) The SER adjacent to the cell wall has strongly labeled showing detailed structure of the SER cisternae. (**b**) An alternate angle section of the SER, with ZIO clearly enhancing the contrast between the lumen and the membranes. Scale 0.5 μm

electron microscopy (TEM) for the magnification of fine structures. To observe such fine structures requires contrast enhancement and this is usually achieved by using specific electron dense heavy-metal based stains. In this chapter, we describe a protocol for zinc-iodide osmium tetroxide (ZIO) staining of the SER (*see* Fig. 2 for representative images). The impregnation of tissue with ZIO was initially used to stain autonomic nerve fibers for visualization using light microscopy and subsequently TEM [15]. Notable for forming electron dense accumulations between double-membraned structures, it was soon adopted for the study of the ER in general [16], and by our group for imaging the SER.

2 Materials

2.1 Preparation of Phloem Tissue for 3D-SIM

1. Fixative: 50 mM 1,4-piperazinediethanesulfonic acid (PIPES) pH 6.9, 2 mM EGTA, 1% (w/v) bovine serum albumin (BSA) in dH_2O. Add 4% (v/v) formaldehyde and 0.25% glutaraldehyde (*see* **Note 1**).
2. Stabilizing solution: 5% (w/v) Phytoagar in ddH_2O (*see* **Note 2**).
3. Wash Buffer: 2 mM EGTA, 1% BSA, 50 mM PIPES, pH 6.9 in ddH_2O.
4. PBS: Phosphate buffered saline, 1 mM KH_2PO_4, 155 mM NaCl and 10 mM Na_2HPO_4 in ddH_2O, pH 7.4.
5. Calcofluor White solution: 10 μg/ml in dH_2O.

2.2 Growth and Preparation of BY2 Cells for Live Imaging

1. BY2 growth media: 0.43% MS Basal Salts media, 3% sucrose, 2 μg/ml 2,4-Dichlorophenoxyacetic acid in ddH_2O. Sterilize by autoclaving.
2. 1 M Mannitol: dissolved in dH_2O.
3. 170 μg/ml Calcofluor White Stock Solution: dissolved in ethanol. Stored in the dark at −20 °C.
4. 100 mM $DiOC_6$ (3,3′-dihexyloxacarbocyanine iodide) stock solution: dissolved in DMSO. Stored in the dark at −20 °C.

2.3 ZIO Staining

1. Fixative: 3% (v/v) glutaraldehyde in 0.1 M sodium cacodylate (*see* **Note 3**).
2. 0.2 M sodium cacodylate: In a fume cupboard, add 21.4 g sodium cacodylate to 400 ml dH_2O. Mix well and add dH_2O to a final volume of 500 ml. Add 0.1 M HCl dropwise until the solution reaches pH 7.3. For wash buffer dilute 1:1 with dH_2O.
3. 1% Osmium tetroxide in 0.1 M sodium cacodylate: Add a 0.25 g glass vial of osmium tetroxide to a glass duran bottle and screw lid on. Shake to break vial and then add 12.5 ml dH_2O, mix gently on a rocking platform. Mix equal volumes of osmium tetroxide and sodium cacodylate buffer
4. Zinc iodide: 3 g zinc powder and 1 g resublimed iodine to 20 ml dH_2O, stir for 5 min and then filter. Leave to mature in flow hood for 4 h (*see* **Note 4**).
5. ZIO: Combine equal volumes of zinc iodide with 2% osmium tetroxide in a small aliquot, mix and use immediately.
6. Epon812.
7. 1:1 ratio of Epon812:propylene oxide.
8. 2:1 ratio of Epon812:propylene oxide.

3 Methods

3.1 Preparation of Phloem Tissue

1. Cut the stem or petiole of a 35–55-day-old tobacco plant expressing the desired fluorescent reporter (in this case pSEO2.GFP-HDEL [17]) and transfer immediately to a glass beaker containing the fixative solution and submerge the cut end. Trim approximately 5 mm from the end of the stem to avoid air blocks. Allow to transpire in an illuminated fume hood for 1 h (*see* **Note 5**).
2. Trim the tissue and add to molten stabilizer cooled to 40 °C. Submerge sample fully by gently pressing with a blunt instrument. Remove any air bubbles and carefully orient the tissue to allow for the desired angle of sectioning, e.g., positioned at 90° to the surface for transverse sections or at 180° for longitudinal sections.

3. When set, trim around the sample to form a block and then section using a vibrating microtome on a medium-fast setting to obtain sections of 100 μm.
4. Place sections into wash buffer contained in a 5 ml petri dish. Wash by replacing the buffer three times, 10 min for each wash.
5. Rinse with PBS and stain with Calcofluor White (at 10 μg/ml) for 1 min at room temperature. Rinse sections well with dH_2O.
6. Mount sections directly on a number 1.5 coverslip with a drop of Citifluor AF1 antifade medium. Apply gentle pressure to spread the mountant and remove air bubbles before sealing with nail varnish.

3.2 Preparing BY2 Cells for Live 3D-SIM Imaging

1. In advance, culture BY2 cell lines in 50 ml Erlenmeyer flasks with sterile Murashige and Skoog Basal Salts media supplemented with 3% (w/v) sucrose and 2μg/ml 2,4-Dichlorophenoxyacetic acid (*see* **Note 6**).
2. Aliquot 1 ml of cell suspension to an Eppendorf tube and stain cell walls with Calcofluor White at a final concentration of 3.5 μg/ml. Stain for 5 min at room temperature before rinsing cells twice with fresh media. Optional: if imaging wild-type cells, use $DiOC_6$ to stain the ER at a final concentration of 50 μM (*see* **Note 7**). Incubate for 10 min and then rinse twice with fresh media.
3. Induce plasmolysis by pipetting off 450 μl of media and adding 450 μl 1 M mannitol. Incubate for 10 min at room temperature before gently inverting the tube to resuspend the cells (*see* **Note 8**).
4. Pipette 40 μl of cells onto a very clean microscope slide before carefully placing the coverslip. Using a folded paper towel apply gentle, even pressure to remove excess media from the slide (*see* **Note 9**). Carefully wipe all edges, making sure the coverslip does not become smudged. Seal with nail varnish.

3.3 3D-SIM Imaging with an OMX Deltavision Blaze

1. Locate ideal cells on the auxiliary microscope (PersonalDV Deltavision) which has stage coordinates synchronized with the OMX. Use the lowest level brightfield possible to view candidate cells and mark their position on the slide using the point visiting tool. Expose all candidate cells briefly to check that both the Calcofluor White stain and the GFP reporter (or $DIOC_6$) are sufficiently bright (*see* **Note 10**).
2. Transfer the slide to the OMX and apply immersion oil (*see* **Note 11**). Using the Point List, find the marked cells and then center the cell in the image using the Spiral Mosaic function.
3. Empirically determine the lowest laser power required to achieve optimal intensities of between 1000 and 3000 counts in a raw image acquired by a 15-bit dynamic range Edge sCMOS camera.

Also optimize the shortest exposure times for each channel, typically between 100 and 200 ms (*see* **Note 12**).

4. Following optimization, acquire image stacks of appropriate cells. Set the start and end positions for a minimal z-stack quickly to avoid excess light exposure.
5. Using the SoftWorx 6.0 alignment tool, adjust the images from the separate channels and then reconstruct 3D super-resolution image stacks using SoftWorx 6.0 with channel specific OTFs and Wiener filter settings of 0.002 (*see* **Note 13**).

3.4 ZIO Staining of the SER

1. Cut the stem or petiole of a 35–55-day-old tobacco plant expressing the desired fluorescent marker (in this case pSEO2.GFP-HDEL [17]) and transfer immediately to the fixative solution and submerge the cut end. Trim approximately 5 mm from the end of the stem to avoid air blocks. Allow to transpire in an illuminated fume hood for 1 h (*see* **Note 5**).
2. Remove the leaf and chop the petiole into 5 mm by 5 mm sections.
3. Wash twice in 0.1 M Sodium Cacodylate for 10 min each wash.
4. Wash twice in dH_2O for 10 min each wash.
5. Incubate in ZIO solution at room temperature for 4 h in a sealed vial with gentle agitation on a rotating wheel.
6. Wash twice in dH_2O for 10 min each wash.
7. Dehydrate tissue in an ethanol series: submerge for 15 min per solution in 50%, 70%, and 95% ethanol before two 15 min incubations in 100% ethanol.
8. Infiltrate dehydrated tissue with a 1:1 ratio of Epon812 and propylene oxide at room temperature for 2 h.
9. Continue infiltration overnight in a 2:1 ratio of Epon812: propylene oxide at 58 °C.
10. Incubate in 100% Epon812 at room temperature for 1 h. Replace the Epon812 and incubate for one further hour.
11. Embed in flat bed molds, for 48 h at 58 °C.
12. Check orientation and quality of the tissue by cutting semi-thin sections (0.5–1 μm) using a glass knife. Stain sections briefly with Toluidine blue for accurate visualization on a bright field microscope.
13. Following identification of an appropriate area of a block, cut ultrathin sections (60 nm) with a diamond knife and float onto dH_2O. Mount sections on an EM grid by touching the dull face of the grid to the middle of a section without breaking the surface tension of the water. The sections will readily adhere to a clean grid.

14. Stain sections with uranyl acetate and lead citrate by first wetting the grids in dH_2O (*see* **Note 14**) and then float section side down for 45 min on a drop of uranyl acetate (*see* **Note 15**). Wash by dipping in dH_2O, manipulating the grid by its edge using fine forceps for 1 min and repeat the wash in fresh dH_2O. Invert the grid onto a drop of lead citrate for counter staining, for 10 min. Wash again in dH_2O for 1 min and then repeat for a further 1 min in fresh dH_2O.
15. Air dry before imaging with the TEM.

4 Notes

1. The fixative solution should be prepared freshly on the day of use. However, the PIPES, EGTA, and BSA stock solutions may be prepared in advance and stored on the bench following autoclave sterilization. Glutaraldehyde should be EM-grade and formaldehyde from a methanol free solution. Fixatives provided in single-use glass ampules provide the best source and any unused can be decanted into a glass bottle and sorted for up to 1 month, glutaraldehyde at 4 °C and formaldehyde at room temperature.
2. Phytoagar is a specialist agar used for plant tissue culture. With a high gel strength at a 5% solution this matches the mechanical properties of petiole tissue and thus supports the tissue well during sectioning. The concentration may require optimization when used as a stabilizer for other tissues types to avoid the agar pulling away from the tissue or disintegrating.
3. To preserve the fine ultrastructure of the cell in ultrathin TEM sections, it is necessary to increase the glutaraldehyde content of the fixative to 3%.
4. The solution should turn a light straw color during the maturation process.
5. Due to transpiration the fixative is drawn up into the xylem, from where it moves laterally to the phloem and other tissues, providing a gentle delivery system which avoids mechanical damage of the phloem cells.
6. Incubate liquid BY2 cell cultures at 28 °C, in the dark, shaking at 140 rpm. Sub-culture cells weekly using a 1:40 dilution. If the cells are stably transformed with a fluorescent marker for the ER such as RTN6-GFP, ensure that the signal is strong and relatively homogenous in the line of choice. Best results are usually obtained with cells which were subbed 3–4 days prior to imaging.
7. $DiOC_6$ will stain the ER, mitochondria, and vesicle membranes. It is, however, extremely phototoxic so the cells must

be kept in the dark once stained and illumination minimized to reduce ER damage.

8. Plasmolysis allows clearer imaging of the desmotubules as the membrane is retracted away from the cell wall, and the Hechtian strands can be clearly labeled either by RTN6-GFP or $DiOC_6$.
9. To achieve optimal imaging, the cells need to be as close to the coverslip as possible.
10. It is vital to keep all light exposure as brief as possible prior to the SIM imaging so as to minimize any pre-imaging photobleaching or phototoxicity from $DiOC_6$.
11. The type of immersion oil should be matched as closely as possible to the refractive index of the sample to minimize spherical aberrations. To achieve the best combination, in theory the cells should be mounted in a high concentration of glycerol/antifade mountant, but this was found to affect the ER structure, so cells were mounted in media.
12. It is advisable to carry out the optimization on a sacrificial cell—by the time the process is complete, the GFP is likely to have bleached sufficiently to prohibit good image capture during the 3D-SIM process.
13. The microscope must be routinely calibrated by measuring channel specific optical transfer functions (OTFs) to optimize both lateral and axial image resolution. Alignment tools should also be regularly calibrated based on alignment parameters obtained from calibration measurements with 100 nm-diameter TetraSpeck beads.
14. Pre-wetting the EM grids minimizes potential artifacts by reducing air–stain contact [18].
15. Spot stain on to a plastic petri dish and keep covered to reduce contamination or artifacts from dust, evaporation, and CO_2 (particularly important for lead citrate).

References

1. Abbe E (1873) Beiträge zur Theorie des Mikroskops und der mikroskopischen Wahrnehmung. Arkiv Mikroskop Anat 9:413–468
2. Wilson T (1995) The role of the pinhole in confocal imaging system. In: Pawley JB (ed) Biological confocal microscopy. Plenum Press, New York, pp 167–182
3. Gustafson MGL (2000) Surpassing the lateral resolution limit by a factor of two using structured illumination microscopy. J Microsc 198:82–87
4. Schermelleh L, Carlton PM, Haase S et al (2008) Subdiffraction multicolour imaging of the nuclear peripheray with 3D structured illumination microscopy. Science 320:1332–1336
5. Dobbie I, King E, Partion RM et al (2011) OMX: a new platform for multimodal, multichannel wide-field imaging. Cold Spring Harb Protoc 8:899–909
6. Kner P, Chhun BB, Griffis ER et al (2009) Super-resolution video microscopy of live cells by structured illumination. Nat Methods 6:339–342
7. Fitzgibbon J, Bell K, King E, Oparka K (2010) Super-resolution imaging of plasmodesmata

using 3-dimensional structured illumination microscopy. Plant Physiol 153:1453–1463

8. Bell K, Mitchell S, Paultre D, Posch M, Oparka K (2013) Correlative imaging of fluorescent proteins in resin-embedded plant material. Plant Physiol 161:1595–1603
9. Bell K, Oparka K (2015) Preparative methods for imaging plasmodesmata at super-resolution. Methods Mol Biol 1217:67–79
10. Bell K, Oparka K, Knox K (2016) Super-resolution imaging of live BY2 cells using 3D-structured illumination microscopy. Bio-protocol 6(1):e1697
11. Evert RF (1990) Dicotyledons. In: Behnke H-D, Sjolund RD (eds) Sieve elements: comparative structure, induction and development. Springer-Verlag, Berlin, pp 103–137
12. Nagata T, Nemoto Y, Hasezawa S (1992) Tobacco BY-2 cell line as the "HeLa" cell in the cell biology of higher plants. Int Rev Cytol 132:1–30
13. Overall RL, Blackman LM (1996) A model of the macro-molecular structure of plasmodesmata. Trends Plant Sci 1:307–331
14. Knox K, Wang P, Kriechbaumer V, Tilsner J, Frigerio L, Sparkes I, Hawes C, Oparka K (2015) Putting the squeeze on plasmodesmata: a role for reticulons in primary plasmodesmata formation. Plant Physiol 168:1563–1572
15. Maillet M (1968) Etude critique des fixations au tétraoxyde d'osmium-iodure. Bull Assoc Anat 79:233–394
16. Barlow PW, Hawes C, Horne JC (1984) Structure of amyloplasts and endoplasmic reticulum in the root caps of *Lepidium sativum* and *Zea mays* observed after selective membrane staining and by high-voltage electron microscopy. Planta 160:363–371
17. Knoblauch M, Peters WS (2010) Münch, morphology, microfluidics: our structural problem with the phloem. Plant Cell Environ 33:1439–1452
18. Hayat MA (1968) The principles and techniques of electron microscopy, vol 1. Van Nostt and Reinold Company, New York, NY

Chapter 5

Quantitation of ER Structure and Function

Mark Fricker, Luke Heaton, Nick Jones, Boguslaw Obara, Stefanie J. Müller, and Andreas J. Meyer

Abstract

The plant endoplasmic reticulum forms a network of tubules connected by three-way junctions or sheet-like cisternae. Although the network is three-dimensional, in many plant cells, it is constrained to a thin volume sandwiched between the vacuole and plasma membrane, effectively restricting it to a 2-D planar network. The structure of the network, and the morphology of the tubules and cisternae can be automatically extracted following intensity-independent edge-enhancement and various segmentation techniques to give an initial pixel-based skeleton, which is then converted to a graph representation. Collectively, this approach yields a wealth of quantitative metrics for ER structure and can be used to describe the effects of pharmacological treatments or genetic manipulation. The software is publicly available.

Key words Confocal imaging, Endoplasmic reticulum, Network analysis, Phase congruency, Reticulon, ER tubule morphology, ER cisternae

1 Introduction

The endoplasmic reticulum (ER) forms a complex and dynamic network of tubules and sheet-like cisternae that ramify throughout the cytoplasm [1]. In this chapter, we describe an ER network analysis program that is designed to quantify:

1. The length, width, and morphology of the ER tubules (Fig. 1a and b).
2. The topological organization of the network (Fig. 1c).
3. The size and shape of the ER cisternae (Fig. 1d).
4. The size and shape of the polygonal regions enclosed by the network (Fig. 1a).

The programs were originally designed to quantify ER organization in plant epidermal cells, where the ER is confined to a very thin layer of cytoplasm appressed to the periclinal cell wall as a

Chris Hawes and Verena Kriechbaumer (eds.), *The Plant Endoplasmic Reticulum: Methods and Protocols*, Methods in Molecular Biology, vol. 1691, DOI 10.1007/978-1-4939-7389-7_5,

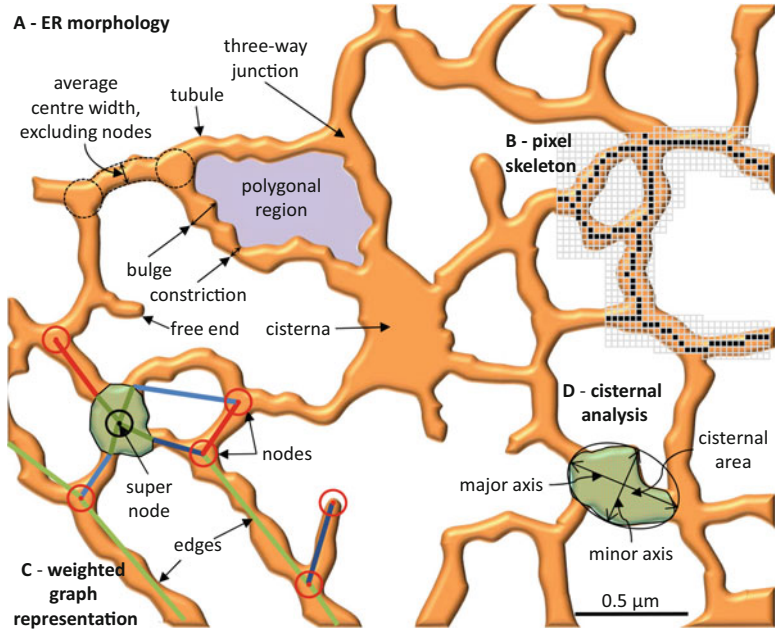

Fig. 1 Schematic outline of the terminology used to describe the ER morphology. (**a**) Representation of the main features of the ER including tubules, cisternae, enclosed polygonal regions, three-way junctions, and free ends. Measurements of the tubule width may average over the "centre" region, excluding the junctions, or involve more detailed analysis of local bulges and constrictions. (**b**) The image of the network is converted to a single-pixel wide skeleton following automated ridge enhancement and segmentation. (**c**) Elements within the pixel skeleton are classified as nodes (junctions and free ends) connected by edges that inherit the length and width of the underlying tubules. Cisternae are represented as a super-node that is connected to each tubule incident on the boundary. (**d**) The cisternae (and polygonal regions) are analyzed separately to determine their area and various shape metrics such as the major and minor axis of a bounding ellipse

planar, 2-D network. The input image typically comprises single plane (x,y) confocal fluorescence images of ER-targeted fluorescent proteins.

The simplest method to identify the ER automatically would be an intensity-based segmentation of the fluorescence image to give a binary image, with ones representing the ER structure and zeros for the background. However, the resultant binary image is critically dependent on the value for the threshold used, and it is rare that a single threshold provides adequate segmentation without either losing dimmer structures if it is set too high, or artificially expanding and fusing adjacent regions if it is set too low [2]. Thus the approach adopted here exploits additional intensity-independent information over a range of scales and orientations to enhance the network structure, prior to segmentation as a single-pixel wide skeleton. The skeleton is then used as a template to interrogate the image locally to provide an estimate of the relative amount of fluorescent probe present and to provide an indication of the tubule width.

The expected width of the ER tubule is 50–70 nm [1], which is below the resolution of the confocal microscope, but can just be resolved with super-resolution techniques, such as stimulated emission depletion microscopy (STED [3]), although this is extremely challenging for dynamic imaging. For most laboratories, access to super-resolution techniques may be limited, necessitating the development of approaches that can be used on a routine basis with existing systems. Nevertheless, with additional assumptions about the distribution of the fluorescent lumenal marker and the point spread function (psf) of the microscope, the approximate width of the ER can be estimated, even if this is below the resolution limit of the microscope system [4]. In this approach, the skeleton is used as a template to interrogate the image locally to provide an estimate of the relative amount of fluorescent probe present, and the width is inferred from the integrated intensity signal from estimates of the profile of intensity with distance normal to the skeleton. We describe some basic routines to estimate the relative tubule width (effectively convolved with the psf) and also introduce measures using the intensity values to infer the approximate sub-resolution tubule width.

Topological measures of the ER network structure can also be extracted following conversion of the pixel skeleton to a weighted, undirected graph, where nodes represent junction points and edges represent the tubules that connect them [2, 5, 6] (Fig. 1c). A wide range of metrics can be calculated using such a graph representation, such as betweenness centrality of nodes or edges, although it is not yet clear how these may relate to underlying mechanism or function. Nevertheless, unlike morphological measurements, the topology of the network is less sensitive to the resolution of the imaging system as it reflects the connectivity of the ER rather than the physical size of the components [2].

In addition to analysis of the ER structure and topology, a number of engineered fluorescent reporters have been developed to characterize dynamic physiological processes in living cells. In particular, fluorescent reporters, such as the roGFP family [7] or the tandem fusion proteins Grx1-roGFP2 [8] or roGFP2-Grx1 [9], respond to the glutathione redox potential and allow redox imaging in vivo. roGFP and its derivatives can be expressed in the cytoplasm or targeted to different organelles, such as the ER, giving fine control of measurements from subcellular compartments [7, 8, 10–13]. The redox potential of the ER is of particular interest as it influences the rate and fidelity of protein folding [14]. Measurements of physiological parameters in the ER, however, demand less reducing probes with midpoint potential tweaked to the redox potential in the ER. For this roGFPn-iX variants with midpoint potentials between −229 and −238 mV have been designed [15, 16]. Furthermore, potential potential artifacts due to formation of intramolecular disulfide bridges and probe dimerization [17] can

be minimized by the use of Grx1 fusion proteins, which also confer specificity for GSH redox potential and greatly increase the probe response kinetics [14]. The difference in redox potential between the cytoplasm and ER can also be harnessed to probe the topology of ER membrane proteins by introducing roGFP in predicted lumenal or cytoplasmic loops in a technique termed redox-based topology analysis (ReTA [18]). The relative ratio of the roGFP signal gives a macroscopic readout of whether the labeled loop is within the ER (more oxidized) or facing the cytoplasm (more reduced).

1.1 Outline of the Main Steps in the ER Analysis

The ER network analysis progresses through a number of parallel threads that are designed to extract different information from the underlying image to characterize the tubular network, cisternae, and enclosed polygonal regions of cytoplasm. A flow diagram of the overall sequence for morphological measurements is shown in Fig. 2 and is discussed in more depth in Subheading 3.1.

We also outline the steps required to make measurements of physiological parameters in the ER using roGFP as an example, although the same methods can be applied to any ratioable reporter [13, 19, 20]. The sequence of steps implemented for physiological measurements is shown in Fig. 5. A full description of the redox ratio analysis package is given in [20].

2 Materials

The ER network analysis and redox ratio analysis programs were written in MATLAB (The Mathworks, Nantick, MA) and are each packaged in a single compiled executable file for distribution as a stand-alone package, or as MATLAB apps that run within the MATLAB 2016a or later environment. In the case of the apps, the ER network analysis package requires the MATLAB image processing toolbox, while the redox ratio analysis package requires the MATLAB image processing toolbox and statistics toolbox. The programs, manuals, and tutorials can be downloaded from:

www.markfricker.org

The software has been tested on Windows10 and requires a minimum screen resolution of 1600 × 900. In addition, an appropriate version of the MATLAB Compiler Runtime (MCR) is required to install the set of shared libraries that enables execution of the compiled MATLAB application. The MCR should automatically be downloaded from MathWorks when the program is installed for the first time. Alternatively, the MCR can be downloaded from the MathWorks Website:

http://www.mathworks.com/products/compiler/mcr

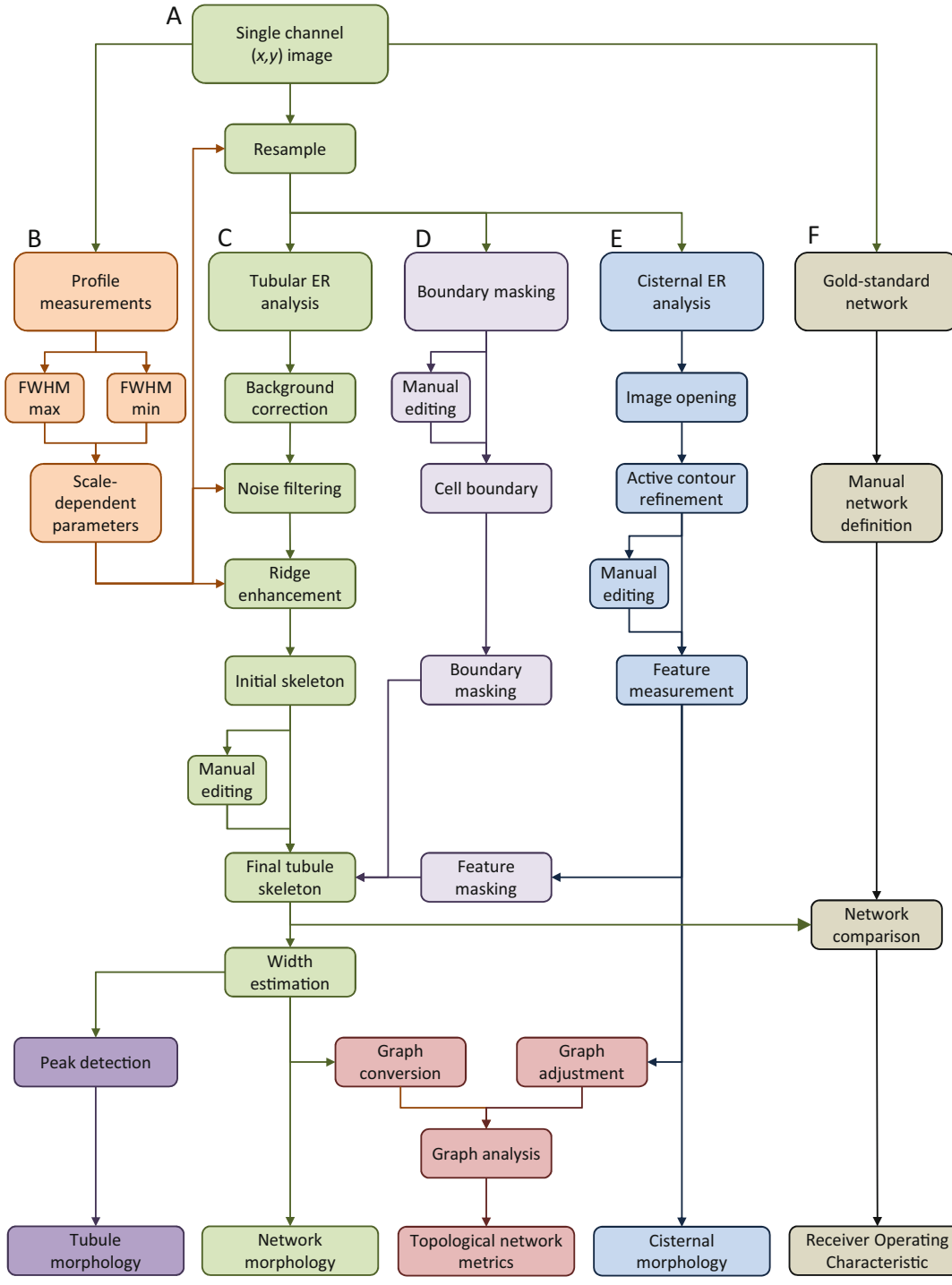

Fig. 2 Flow diagram showing the main steps in the morphological ER analysis. (**a**) The starting point is typically a single channel confocal fluorescence of the ER labeled with a fluorescent protein. (**b**) The minimum and maximum tubule diameters are estimated manually from line transects to resample the image and standardize all the subsequent processing parameters; (**c**) ER tubules are segmented following filtering and enhancement

A number of additional files needed to run the full suite of programs may also be installed at the same time as the main program. For example, the Bio-Formats package [21] has been designed to read in images from different microscope manufacturers and store them in a standardized format. Full details are available on the open microscopy website:

http://www.openmicroscopy.org/site/support/bio-formats4/

The bioformats_packages.jar program needs to be available on the search path or installation directory of the matlab programs. The bioformats_package.jar is available from:

http://downloads.openmicroscopy.org/bio-formats/5.6.0/

The latest version of Java needs to be installed and is available from:

http://www.java.com/en/

Output of images at full resolution uses *export_fig.m* originally written by Oliver Woodford (2008–2014) and now maintained by Yair Altman (2015-present). When exporting to vector format (PDF or EPS), this function requires Ghostscript which can be downloaded from:

http://www.ghostscript.com

When exporting images to eps, *export_fig* additionally requires pdftops, from the Xpdf suite of functions. This can be downloaded from:

http://www.foolabs.com/xpdf

3 Methods

3.1 Extraction of ER Network Structure

3.1.1 Setting the Scale Parameters

Images of the ER may have been collected at different pixel resolutions, depending on the microscope settings, and may span different width scales depending on the experimental treatment and genetic background. If estimates of the tubule width are required, the pixel size may need to be reduced below the optimal Nyquist sampling value (as low as ~20–30 nm) to reduce downstream discretization errors due to pixelation. To standardize all the

Fig. 2 (continued) steps to give a single-pixel wide skeleton. This provides basic morphological information on the length and width of the tubules and can be interrogated further to examine individual tubule morphology. (**d**) The analysis can be constrained to a particular cell or subcellular region by masking the image; (**e**) ER cisternae are detected independently using image opening followed by active contour refinement; (**f**) The performance of the automated segmentation approaches can be compared to a manually defined "gold-standard" pixel skeleton

subsequent processing steps, it is useful to define the expected minimum and maximum width of the tubular components manually using a transect drawn on the image.

1. Draw a two-point transect on the image across a tubule that, by eye, appears to be close to the smallest tubule diameter. A graph of the transect profile is automatically displayed, and the full width at half-maximum peak height (FWHM) calculated to give $FWHM_{min}$.
2. Repeat the transect profile across the largest diameter tubule present to give the maximum tubule diameter ($FWHM_{max}$).
3. Values for FWHM displayed in the interface are given in pixels, while the peak intensities are given in normalized units ranging from 0 to 1 (*see* **Note 1**).

3.1.2 Defining a Boundary Mask

In some instances, it may be appropriate to define a boundary mask to exclude regions that should not be analyzed, or to restrict the analysis to a specific region of the cell or tissue. Several approaches are available to segment the main fluorescent structures automatically or manually:

1. Automatic segmentation using a threshold determined by Otsu's method [22] that minimizes the intraclass variance of the foreground and background distributions.
2. Manual segmentation using a threshold determined from a region-of-interest (ROI) placed on the background. The threshold is calculated as mean + 2 × SD.
3. Manual delineation by drawing a boundary on the image. If this option is selected, a separate window opens to give access to a number of drawing tools. The edited binary image is automatically saved alongside the other parameters used for processing the image and can be reapplied or edited further every time the image is processed (*see* **Note 2**).

3.1.3 Background Measurement and Correction

Accurate measurements of the fluorescence signal from the ER typically require correction for the instrument dark current, amplifier offset, and background signal. A number of options to automatically or manually correct the background contribution are provided, including:

1. *Subtraction of a single measured value:* A constant value is measured from a ROI defined on the image and is subtracted. This is appropriate for removing instrument black-level offsets or very diffuse fluorescence.
2. *Image opening*: The image is processed with a grayscale opening function using a disk-shaped kernel with the radius set by $FWHM_{max}$ (i.e., twice the size of the largest tubular feature expected). This removes any features smaller than

$2 \times \text{FWHM}_{max}$ and provides an estimate of the local background around each pixel. The opened image is subtracted from the original to correct for the local background. This method may be useful if there is some out-of-focus blur in the image or an amount of signal from another compartment, such as the cytoplasm. However, it is less useful if there are sheet-like cisternal regions larger than FWHM_{max}, as these remain after the opening operation and are then subtracted from the image, distorting the pixel intensities in the neighboring regions.

3. *Subtraction of a surface fit to the local background:* The local minima across the image are detected and a smooth surface fit to points in the 10–90% interval of the local minimum distribution. The surface is converted to an image and subtracted from the original.
4. *Subtraction of a low pass filtered image:* The image is filtered using a Gaussian kernel with a large radius sufficient to remove all the high-frequency information in the image. The standard deviation for the Gaussian kernel is calculated as FWHM_{max}, or approximately twice the size of the largest tubule diameter. The low pass image is subtracted from the original and the image renormalized. This approach also suffers if there are cisternal regions present.

3.1.4 Filtering the Image to Improve Signal-to-Noise

Most simple noise reduction algorithms use isotropic kernels and smooth the noise in the image equally in all directions. This is not desirable when analyzing the ER, as the tubule boundaries will become blurred. Instead a number of adaptive anisotropic filters are provided that smooth within the tubular network structures, but do not spread across boundaries. In addition, the image intensities can subsequently be rescaled using local contrast-limited adaptive histogram equalization (CLAHE [23], *see* **Note 3**).

1. *Coherence filtering*: This applies an anisotropic diffusion filter written by Dirk-Jan Kroon [33] that smooths regions of low variance, but avoids blurring of object boundaries.
2. *Guided filtering:* This uses an edge-preserving smoothing filter that is "guided" by the structure of the underlying image [24] (*see* **Note 4**).

3.1.5 Enhancing the Tubular Elements

A number of options can be used to improve the relative contrast of tubular ER elements prior to segmentation, by using kernels designed to pick out "ridge" like features that are detected over a range of scales and angles. These include:

1. *Phase Congruency*: This uses the phase-congruency approach developed by Peter Kovesi [25, 26] which provides contrast-invariant ridge detection over a range of scales and angles. The

MATLAB implementation [26] provides a number of outputs, including the level of phase congruency as a measure of the edge strength, and also the "feature type," calculated as the weighted mean phase angle at every point in the image. A value for the feature type of pi/2 corresponds to a bright line, 0 corresponds to a step, and −pi/2 is a dark line. The feature type has proved to be one of the most robust and reliable outputs for subsequent segmentation, as all ridges irrespective of their original intensity are identified with almost equal strength in the feature type image.

2. *Frangi vesselness filter*: This calls the Matlab implementation of the classic Frangi "vesselness" filter [27] written by Marc Schrijver and Dirk-Jan Kroon and available from the MathWorks website (http://uk.mathworks.com/matlabcentral/fileexchange/24409-hessian-based-frangi-vesselness-filter). This gives a strong response for bright features where the second-order derivative of the intensity image (Hessian) shows a strong anisotropy. It can perform well for tubular elements across a range of scales, but leaves holes at the junctions, and only partially compensates for differences in intensity in the original image, which can lead to breaks in the skeleton during the subsequent segmentation step.
3. *Ridge enhancement*: Applies a version of the second-order anisotropic Gaussian kernel originally proposed by Meijering [28] as part of their "Neuriteness" detector. This uses a slightly flattened second-order Gaussian kernel at a range of scales and angles to give better discrimination of ridge-like structures, but does not include any additional information related to the anisotropy of the ridge.
4. *Anisotropic ridge enhancement*: This applies the multi-scale ridge detector developed by Lopez-Molina [29] that uses anisotropic second-order Gaussian kernels. These can be configured flexibly in terms of size, orientation, and anisotropy. This gives good ridge enhancement, but still retains the variation in local intensity along the tubules that can make subsequent segmentation more difficult (*see* **Notes 5** and **6**).

3.1.6 Skeletonization

The aim of the skeletonization step is to convert the enhanced image to a one-pixel wide skeleton along the centerline of the tubule ridges. Nevertheless, this is only an approximation to the true centerline due to pixel discretization errors. There are two main approaches that can be used, namely "*hysteresis thresholding*," that uses the intensity information and some degree of local pixel connectivity to provide an initial binary image that is then thinned to give a single pixel skeleton, and "watershed thresholding" which follows connected ridges, irrespective of their absolute intensity, and automatically generates a single-pixel skeleton.

1. *Hysteresis thresholding*: This starts with seed pixels above a user-defined upper threshold and then propagates the initial segmentation as long as pixels remain above a user-defined lower threshold. The resulting binary image is then thinned to give a single-pixel wide skeleton. The value of the lower threshold is critical—too high and the network becomes disconnected; too low and large blocks of the image are included in the resultant binary image that may fuse separate tubules into a single object. Consequently, when this block is thinned, the skeleton does not map onto the ridge centerlines. In addition, as the thinning process is not guided by the intensities in the enhanced image, the skeleton does not necessarily converge on the expected pattern at junction points. Using an *h-minimum* transform smooths out regions with low fluctuations in intensity, but then sets these regions as local minima to ensure that the surrounding ridges will be segmented individually and do not spread into the basin, even if the absolute values are above the lower hysteresis threshold.
2. *Watershed thresholding*: This applies a watershed segmentation and then extracts the watershed lines as the pixel skeleton. The watershed method is good at segmenting the centerline of the ridges and can handle variations in intensity well. However, it does not include any tubules that have a free end, and has a tendency to over-segment regions with noise. Over-segmentation can be avoided by including additional steps that suppress regions with small intensity fluctuations using an *h-minimum* transform. In addition, setting the local minima to zero ensures that adjacent structures are separated (*see* **Note 7**).

3.2 Estimation of ER Tubule Width

Once the pixel skeleton has been segmented satisfactorily, the first step in the analysis is to estimate the tubule width. Unfortunately, the average ER tubule diameter (50 nm) is below the theoretical resolution of most confocal microscopes and at the resolution of current live-cell super-resolution techniques such as STED [3], so direct physical estimates of the width are challenging. The methods described here typically return a value of the true width convolved with the point spread function (psf) of the microscope. In addition, the typical pixel spacing leads to significant digitization errors, even with over-sampling. A number of different approaches are available that all provide some information on the tubule diameter including:

1. *50% threshold distance*: This estimates the local FWHM from the original tubule image for each pixel in the skeleton. The peak height is estimated from the original intensity, while the distance is estimated from the distance transform of the pixel skeleton. The 50% threshold is estimated from where the pixel intensity

falls below half the peak intensity, assuming a local background of zero.

2. *Maximum-gradient granulometry*: The intensity image is subject to a series of image openings (erosion followed by dilation) that successively remove structures as the size of the opening kernel exceeds the underlying object. This results in an intermediate (*x,y,s*) image, where *s* increases with the size of the disk-shaped kernel to a maximum of $FWHM_{max}$. The intensity of each pixel initially decreases slowly with *s* as the kernel samples more of the object, but then reduces dramatically once the boundary of the object is reached, and the kernel only samples the background. The transition point for any pixel is determined from the maximum (negative) gradient of the granulometry curve. This approach constrains the width to integer pixels values and also suffers from the digital approximation of small kernels to a true disk shaped kernel.
3. *Integrated intensity granulometry*: This approach follows the same methodology as the maximum-gradient granulometry method, but rather than extract a specific size threshold, the integrated intensity under the granulometry curve is calculated. An additional option is available to use the $FWHM_{max} + 1$ kernel as a local background correction. The integrated intensity provides a more nuanced interrogation of the local ER structure, but cannot be directly related to the physical tubule width without additional assumptions about the relationship between fluorescence intensity and sampled volume, or full deconvolution with an experimentally measured psf. Nevertheless, this approach does help with estimation of relative tubule widths, even if they are sub-resolution objects, provided it is assumed that the fluorescent probe is evenly distributed throughout the ER, and the ER is within the sampling volume of the confocal defined by the psf (Fig. 3). A conversion factor can be estimated to convert relative fluorescence to width if it is possible to correlate the physical width, measured from transect profiles, with the intensity (*see* **Notes 8–9**).

The principle behind the integrated intensity measurements can be illustrated empirically using a simulated model of ER tubules with different widths (Fig. 3a and b) that are convolved with an excitation and emission psf, modeled as anisotropic 3-D Gaussian [30] blurring functions (Fig. 3c and d). The performance of the three different width estimators can be assessed by analysis of a single confocal plane to represent a single (*x,y*) image (Fig. 3e) and shows that all measures perform well above about twice the theoretical lateral FWHM of the psf (0.14 μm for the Zeiss AiryScan), but the 50% distance measure and the maximum-gradient granulometry measure both converge to a fixed value close to the psf for

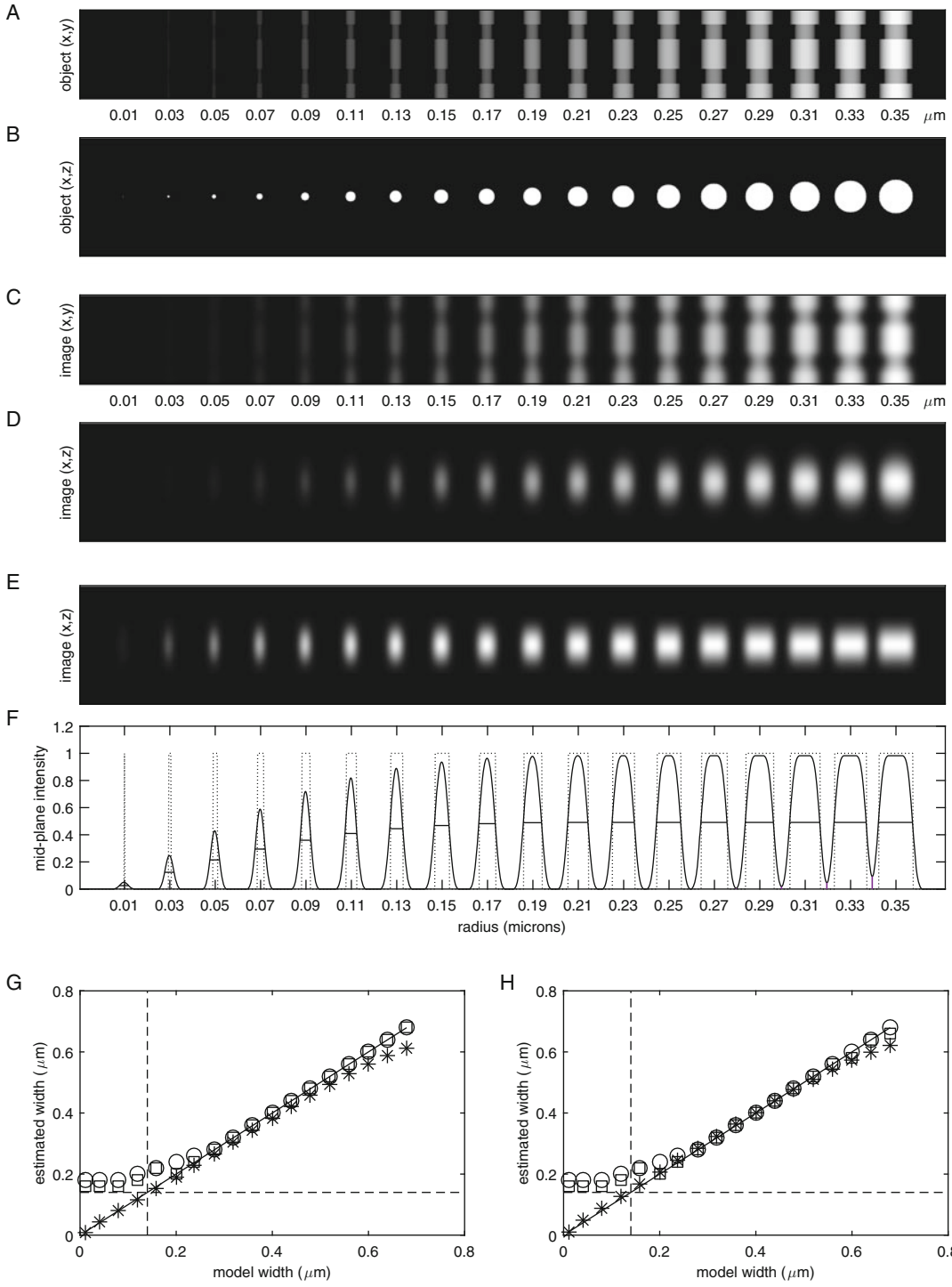

Fig. 3 Estimation of sub-resolution tubule widths. A set of ER tubules with increasing width were simulated as cylinders and viewed as an average (*x,y*) projection (**a**, **c**) or a single (*x,z*) section (**b**, **d**) before (**a**, **b**) and after (**c**, **d**) blurring with simulated anisotropic 3-D Gaussian excitation and emission point spread functions (FWHM

sub-resolution objects as expected (Fig. 3f). By contrast, the integrated intensity measure provides near linear performance even with sub-resolution objects (Fig. 3g).

3.3 Segmentation and Measurement of the Cisternal Regions

In addition to the tubular-reticulum, the ER may also include sheet-like regions called cisternae, or regions of closely appressed tubules that are difficult to separate. The methods used to segment the tubular ER do not work with the cisternae, so a different set of methods are available to segment these structures independently. These include:

1. *Automatic segmentation* using an intensity-based threshold to pick out the brightest structures. An automatic multi-threshold is used to partition pixel intensities into three bins, and the upper bin selected. This will extract the brightest objects, but it does not usually give a good unique segmentation of cisternae, as junctions or other bright features are also included.
2. *Image opening* calculates a modified image after grayscale opening to remove all objects smaller than $FWHM_{max}$ and then converts the resultant image to a binary mask using an automatic threshold. This is more effective at detecting larger sheet-like regions of the ER, but the resultant binary image tends to give blob-like features that extend beyond the original cisternal region.
3. *Active contour* performs the same image opening step as 2 above, but then "shrinks" the features detected down to match the underlying intensity profile using an active contour algorithm. This performs better than a simple opening operation and is set as the default.
4. If no satisfactory segmentation of the features can be achieved with the automatic settings, the cisternae can be defined manually. If this option is selected, the image editing window opens again to give access to the drawing tools. As with the boundary mask, the edited binary image is automatically saved and can be reapplied or edited further every time the image is processed.

Fig. 3 (continued) 0.14 μm × 0.14 μm × 0.42 μm in *x*, *y*, and *z*, respectively). The simulated result for scanning a single confocal section is illustrated in (**e**). The intensity profile across the midsection of the original tubules and after blurring is shown in (**f**). The reduction in intensity for sub-resolution tubules is apparent. (**g**) shows the performance of the three different estimates of tubule width. The 50% distance measure (*circle*) and the maximum-gradient granulometry (*square*) perform well above about twice the psf, but return a value close to the expected FWHM of the psf for sub-resolution objects. The integrated intensity measure (*asterisk*) gives a near linear response throughout the range of tubule widths examined unless the tubes overlap at large diameters. Similar results are obtained using a faster granulometry method that includes decomposition of the circular structuring element into linear approximations, along with an empirical correction of −1 pixel to compensate for over-sampling by rectangular kernels (**h**)

5. A number of morphological measurements of the cisternae are provided including the area, major and minor axis lengths, perimeter, and solidity.
6. The cisternal regions are punched out of the pixel skeleton so that they do not contribute to analysis of the tubular elements. During the subsequent analysis steps, each cisternal region is represented as a set of linear connections radiating out from the centroid of the cisterna to connect with the tubules incident on the boundary. This ensures the overall connectivity of the network is retained.

The results for the cisternal segmentation using image opening and active contour refinement are shown in Fig. 4c. The modification to the color-coded pixel skeleton is shown in Fig. 4d and the graph representation in Fig. 4e, where the cisternae are represented as a super-node connected to each of the tubules incident on the cisternal boundary.

3.4 Measurement of Enclosed Polygonal Regions

The polygons enclosed by the ER network are automatically extracted as the inverse of the pixel skeleton and various morphological measures calculated, including the area, major and minor axis, perimeter, and solidity in a similar manner to the cisternal measurements.

3.5 Analysis of ER Organization Using Graph-Theoretic Metrics

Topological measures of the ER structure are calculated by converting the pixel skeleton to a weighted graph representation. For the tubular regions of the skeleton, the nodes are defined at the junctions between the ER tubules, or the end-points of free tubules, which are connected by straight edges that preserve the topology of the network. If any ER cisternae have been identified, they are represented as a "super-node" positioned at the intensity-weighted centroid of the cisternae, which is connected to all the tubules that are incident on the feature boundary by edges that are given an arbitrary value equal to the average or maximum width value.

A number of metrics are associated with each edge including the Euclidean length of the underlying pixel skeleton, the average width for the entire tubule, calculated using each of the three methods above, and the average width of the tubule excluding the region around the nodes (termed the "centre width"—*see* Fig. 1), which provides a more accurate measure of the tubule diameter itself.

3.6 Measurement of Tubule Morphology

Under some conditions or in certain genetic backgrounds, such as overexpression of reticulons [31], the ER tubules show fluctuations in diameter along their length. The number, size, and distribution of these bulges and constrictions can be analyzed using the graph representation of the network to extract the intensity profile,

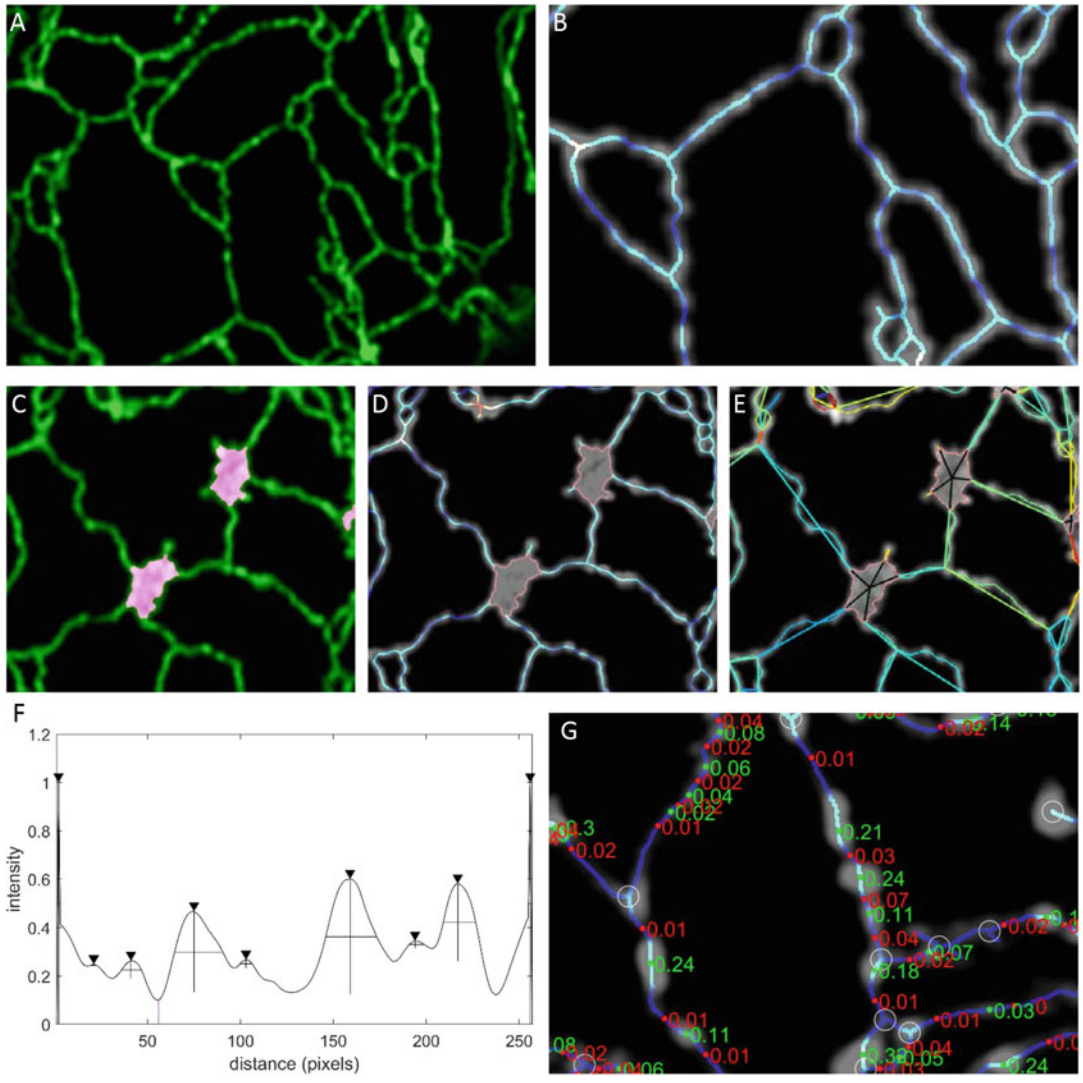

Fig. 4 Stages in the analysis of the ER morphology. (**a**) Original single (*x*, *y*) image of GFP-HDEL targeted to the ER and imaged with a Zeiss Airyscan confocal. (**b**) Pseudo-color coded representation of the tubule width ranging from blue ($FWHM_{min}$) to red ($FWHM_{max}$), superimposed on the filtered image to visually inspect the performance of the overall segmentation and width analysis method. (**c**) Automated segmentation of ER cisternae (*magenta*) using image opening and active contours. (**d**) Cisternae are removed from the pixel skeleton before graph conversion. (**e**) Conversion of the weighted pixel skeleton to a weighted graph. Junctions and free ends are represented as nodes linked by edges that have a vector of properties associated with them, including tubule width, length, and average intensity. Cisternae are represented as a "super-node" connected to all the incident tubules on the boundary. (**f**) Automated characterization of ER tubule morphology. The intensity profile along each ER tubule is scanned to detect peaks above a minimum intensity that are also a minimum height above their neighbors. In addition, peaks have to be greater than a minimum separation from each other, with the nodes set to one. (**g**) The location and width (in μm) for bulges (*green*) and constrictions (*red*) are shown superimposed on the merged pixel skeleton and intensity image

integrated normal to the tube axis, from each individual tubule, excluding the junctions. The method uses a peak-finding algorithm, initially to find the bulges (peaks) on the original intensity profile, and then the constrictions (troughs) on an inverted intensity profile (Fig. 4f). The process operates as follows:

1. Scan the pixel intensities along the length of each tubule starting at the nodes (which are set to 1). The position and intensity of each peak that is greater than a user-defined minimum peak height and minimum peak prominence is recorded. An additional minimum separation condition is imposed to prevent noisy adjacent pixels from being considered as separate peaks. This separation defaults to $FWHM_{min}$.
2. A similar scan is used on the inverted tubule profile to detect the "constrictions."
3. Once the location of the bulges and constrictions has been determined, the width parameters at each point are extracted along with the separation between the peaks.
4. The summary statistics for the bulges and constrictions for all tubules are output to Excel.

3.7 Measurement of the ER Environment Using Transgenic Reporters

Physiological measurements of the redox poise of the ER can be made with roGFP reporters targeted to the ER. While the original measurements used roGFP1 and roGFP2 [13, 19], newer variants have been developed that are better suited to the oxidizing environment within the ER [14]. The redox ratio analysis package [20] has a number of programs that are useful to quantify single (x,y) images, or 3-D (x,y,t) or 4-D (x,y,z,t) time series to capture ER dynamics [20]. Each program can also store or access the processing and calibration parameters used in a corresponding probe database, and have various output options to view animations of the data, or generate publication-ready figures. The Advanced Ratio Program covers 4-D (x,y,z,t) images with up to five fluorescence channels, and a parallel bright-field image, to allow correlation of changes in autofluorescence-corrected ratio images with up to two other parameters, and the (non-confocal) bright-field morphology. The ROI Time Series is designed to allow segmentation of objects, such as mitochondria, from a time-series image and analyze fluctuations in signal or ratio for each object individually. Results can be viewed for each object or as a population response with various statistical fits to the data. Only the Batch and Basic Ratio analysis are described here as these represent the minimum needed for ER redox measurements.

3.8 Ratiometric Analysis of ER Redox Potential

1. Import a 3-D (x,y,t) image, with two wavelength channels representing the protonated (oxidized) and deprotonated (reduced) forms of the roGFP chromophore, and an additional autofluorescence channel if there is significant autofluorescence

bleed-through into the protonated channel. The default is the Zeiss .lsm format, but it is possible to import files in a variety of formats using the Bio-Formats package.

2. As the relationship between the order each channel was collected and the physiological parameter of interest depends on the precise configuration of the microscope for each experiment, each of the three channels is assigned to the appropriate parameter. Thus the default order for a roGFP-based redox ratio experiment would be protonated (oxidized), deprotonated (reduced), and autofluorescence.
3. To improve the signal-to-noise ratio (S/N), the initial images are typically smoothed in (x,y) with a spatial averaging filter, using a 3×3 or 5×5 kernel, and/or a temporal filter.
4. Accurate visualization and quantitation require measurement and subtraction of the background signal for each channel. The background is measured from a user-defined ROI on the image.
5. Pixels with intensity values close to background (typically less than background $+2 \times$ SD) or near saturation (typically 90%) are also masked from the ratio image, as these give a misleading impression of the real ratio value. These pixels are also excluded from quantitative measurements.
6. The ratio is calculated on a pixel-by-pixel basis for all pixels that meet the criteria above.
7. For pseudo-color display to visualize spatial and temporal patterns of redox potential, the masked ratio is coded in HSV color-space by hue on a spectral color scale ranging from saturated blue (fully reduced) to saturated red (fully oxidized), with the limits set by an in situ calibration or extrapolated from an in vitro calibration. The intensity of the ratio image is calculated as the mean intensity for each pixel in the two channels. This effectively gives bright colors for regions with good signals that fade to background for regions of low signal.
8. As the signal contributing to each pixel in a ratio image is very noisy, it is preferable to make quantitative measurements from user-defined regions-of-interest (ROIs) that average the signals spatially or temporally from a larger number of pixels prior to calculation of the ratio.
9. While relative changes in ratio values can provide a reasonable amount of information for comparative studies, more precise calibration may be possible with experimental treatments that define the in vivo probe response. Thus perfusion with a reductant, such as 10 mM DTT (5 min), followed by an oxidant, such as H_2O_2 (10–100 mM, 5 min), can be used to drive the roGFP to a fully reduced or oxidized form, respectively. These calibration values can be stored and applied to other data sets collected under identical conditions.

10. The degree of oxidation (OxD) of the roGFP sensor is calculated from Eq. 1, according to [10]:

$$\mathrm{OxD}_{\mathrm{roGFP}} = \frac{R - R_{\mathrm{red}}}{\frac{I_{488\mathrm{ox}}}{I_{488\mathrm{red}}}(R_{\mathrm{ox}} - R) + (R - R_{\mathrm{red}})} \tag{1}$$

where R is the ratio of excitation at 405/488 nm after background subtraction and autofluorescence correction, R_{red} is the ratio of fully reduced form following perfusion with 10 mM DTT, R_{ox} is the ratio of the fully oxidized form following perfusion with 10–100 mM H_2O_2, and $I_{488\mathrm{ox}}$ and $I_{488\mathrm{red}}$ are the intensities at 488 nm for the fully oxidized and fully reduced forms, respectively.

11. The redox potential is then estimated from Eq. 2:

$$E' = E^{0'\mathrm{pH}}_{(\mathrm{roGFP})} - \frac{2.303\mathrm{RT}}{zF}\log_{10}\frac{1 - \mathrm{OxD}_{\mathrm{roGFP}}}{\mathrm{OxD}_{\mathrm{roGFP}}} \tag{2}$$

where R is the gas constant (8.315 J/K/mol), T is the absolute temperature (298.15 K), z is the number of transferred electrons (2), F is the Faraday constant (9.648×10^4 C/mol), and $E^{0'\mathrm{pH}}_{(\mathrm{roGFP})}$ is the midpoint redox potential based on the standard midpoint potential $E^{0'}$ at 30 °C and pH 7, adjusted for the estimated compartment pH and experimental temperature (20–25 °C) according to Eq. 3:

$$E'^{\,\mathrm{pH}}_{0(\mathrm{roGFP})} = E'_{0(\mathrm{roGFP})} - \frac{2.303\mathrm{RT}}{zF}(\mathrm{pH} - 7) \tag{3}$$

Prominent examples are the SEC61 translocon mediating protein import into the ER [32], the ethylene receptor ETR1 [34], SNARE proteins responsible for specific vesicle recognition by membranes along the secretory pathway [18], or reticulons that have been suggested to contribute to shaping the ER structure [31]. For their function all these proteins need to adopt a distinct topology which is often not predicted well by bioinformatics algorithms. As an alternative approach, the steep gradient in the glutathione redox potential (E_{GSH}) across the ER membrane enables simple and straightforward experimental analysis of membrane protein topology in living cells through ratiometric visualization of N- and C-terminal fusions with roGFP2 (Fig. 5e). After excitation at 405 and 488 nm, the resulting Redox-based Topology Analysis (ReTA) provides a binary readout with a four- to fivefold difference in the fluorescence ratio, depending on which side of the membrane the roGFP2 is located. With this large dynamic range the difference can be easily detected from merge images and the respective false-colored ratio image (Fig. 6).

ReTA is also applicable to the analysis of multi-spanning proteins. Successive deletion of predicted transmembrane domains

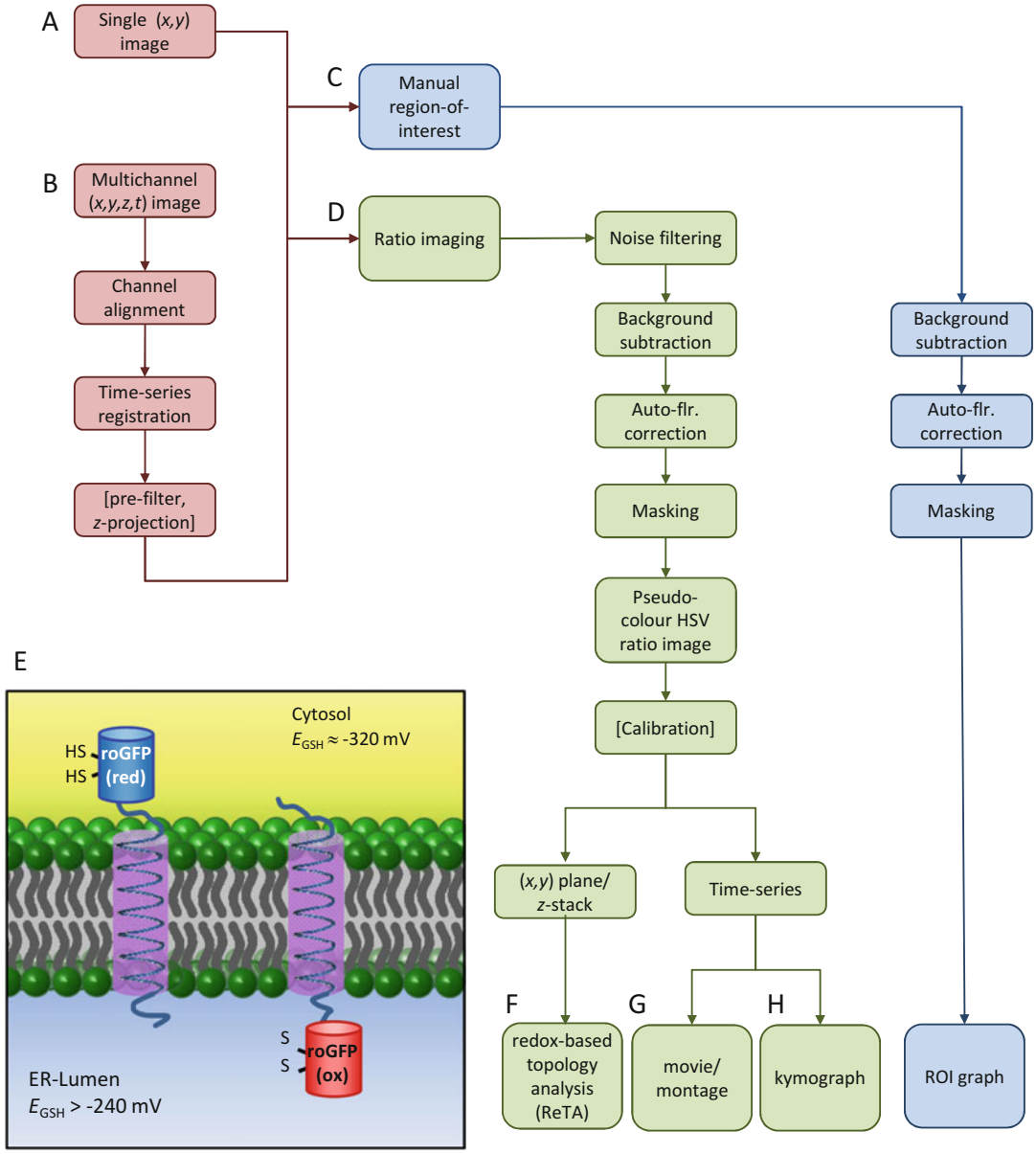

Fig. 5 Schematic diagram showing the main elements of the redox ratio analysis software. Single images (**a**) or multichannel, multidimensional images (**b**) are loaded into the software, aligned, filtered and, if appropriate, the dimensionality reduced using projection algorithms. Quantitative measurements of the redox potential in the ER are made using manually defined regions-of-interest (ROIs) (**c**). Alternatively, the redox potential can be visualized from pseudo-color coded ratio images, following background subtraction and autofluorescence correction (**d**). Redox-based Topology Analysis (ReTA) can be used to determine the topology of membrane proteins by exploiting the oxidizing environment within the lumen of the ER versus the reducing environment in the cytoplasm to alter the signal from roGFP fused to either the N- or the C-terminus (**e**, **f**). Alternatively, dynamics in ER redox potential can be visualized from movies (**g**) or kymograph analysis (**h**)

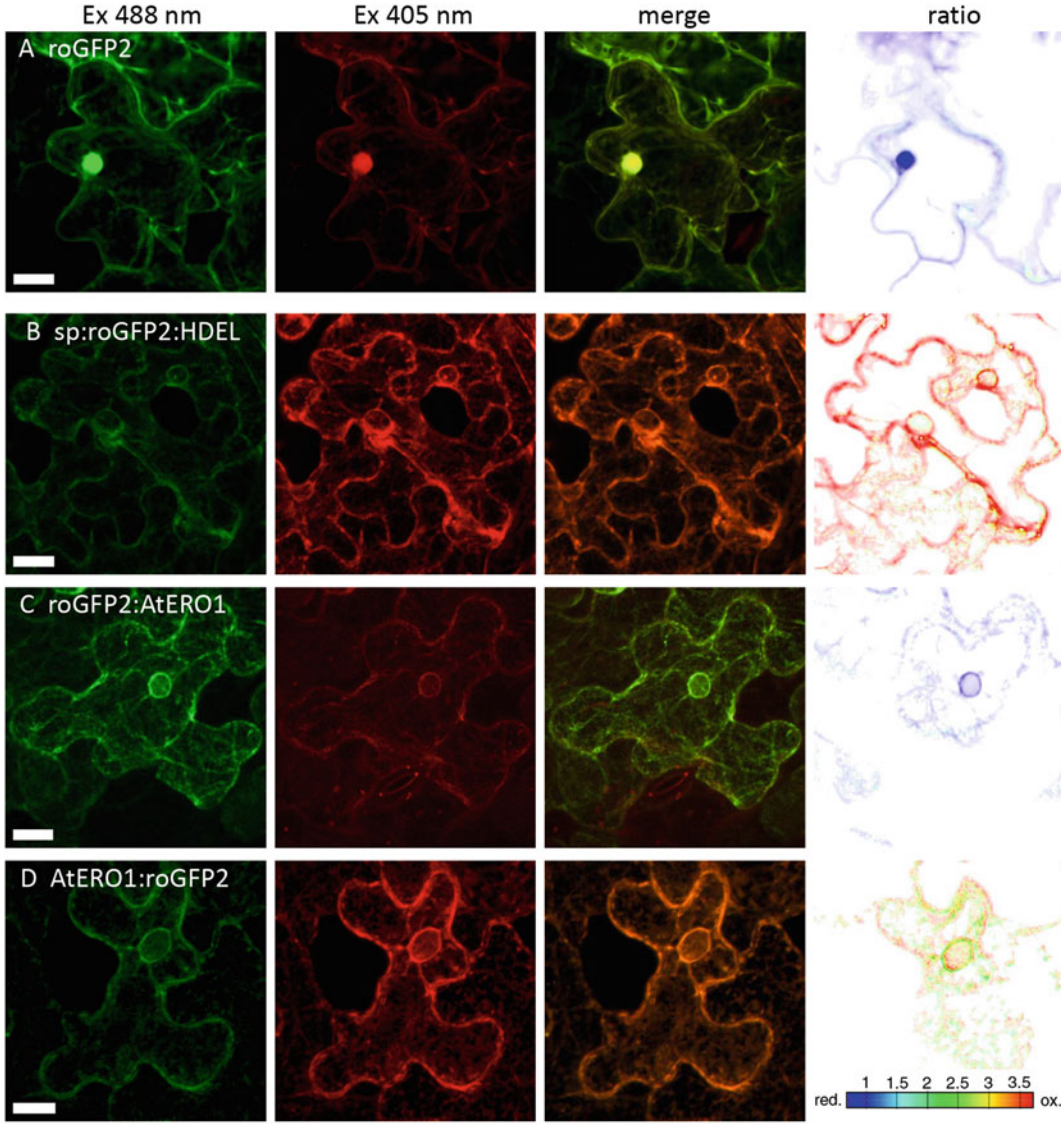

Fig. 6 Redox-based Topology Analysis (ReTA) of ERO1. Soluble roGFP2 in either the cytosol (**a**, roGFP2) or the ER lumen (**b**, sp::roGFP2:HDEL) provide reference values for the ratio values expected in each compartment. Fusion of roGFP2 to the N- and the C-terminus reports the ER thiol oxidase ERO1 as a type II protein with the N-terminus facing the cytosol (**c**) and the C-terminus being localized in the ER lumen (**d**). Images are shown as maximum intensity projections of *z*-stacks of epidermal cells of Agrobacterium-infiltrated tobacco leaves with excitation at 488 or 405 nm light and as a merged image. The pseudo-color coded ratio images were generated from single *z*-planes of the depicted cells using the ratio analysis software

from the C-terminus and fusion of roGFP2 to the new C-terminus enables alternate orientation of roGFP2 to either the cytosol or the ER lumen depending on the presence of even or uneven numbers of transmembrane domains remaining [18]. Severe truncations may prevent integration into the ER membrane. In this case,

internal tagging of the protein of interest by integrating roGFP2 into extramembrane loops may allow the visualization of these loops with respect to their orientation.

3.9 Plant Growth and Transient Transfection

Routine screening for membrane topology uses transient expression in tobacco leaf epidermis as a convenient experimental system. Transformation of tobacco leaf epidermal cells is performed by standard techniques [35] using *Agrobacterium tumefaciens* containing binary vectors with roGFP2 or roGFP2 fusion proteins. Epidermal cells from infected regions of the tobacco leaf epidermis are imaged by confocal laser scanning microscopy (CLSM) 2–4 days after inoculation.

3.10 Targeting of roGFP2 to the ER Lumen

1. PCR-amplify roGFP2 using the primers 5′-ACCATGGTGAGCAAGGGCGAGGAG-3′ (forward; NcoI site underlined) and 5′-TCTAGACTTGTACAGCTCGTCCAT-3′ (reverse; XbaI site underlined) to introduce appropriate restriction sites and remove the start and stop codons.
2. Blunt end-ligate the amplified product into pCAPS (Roche, http://www.roche.de).
3. Clone the NcoI/XbaI fragment into pWEN81 between the N-terminal chitinase ER-signal peptide and the HDEL retrieval signal.
4. Sub-clone the entire cassette consisting of roGFP2 with the N-terminal chitinase targeting signal and the C-terminal HDEL motif into the binary vector pWEN22 under the control of a strong constitutive CaMV 35S promoter using XhoI and SacI restriction sites.

3.11 Construction of roGFP2 Fusions with Transmembrane Proteins

The objective is to splice the roGFP2 cDNA sequence in-frame upstream or downstream of the N- or C-terminus, respectively, of the target protein or in-frame after each putative transmembrane domain (TMD) in truncated protein fragments. The orientation of the TMD is inferred from the degree of oxidation of the roGFP2, with the assumption that the addition of the roGFP2 moiety does not alter the native target protein structure.

1. Fusion proteins can be generated by assembly PCR, using appropriate primers, gateway cloning, or by replacement of elements within a full length construct. A full set of gateway compatible vectors for N- and C-terminal fusion of transmembrane proteins with roGFP2 plus control constructs are available from Addgene.
2. Constructs are introduced via *Agrobacterium*-mediated transformation as in Subheading 5.1 and imaged with CLSM [35].
3. Data are analyzed using the redox ratio software (*see* **Note 10**).

4 Notes

1. The values of $FWHM_{min}$ are used to calculate a resampling factor needed to ensure that the minimum apparent tubule width is at least 7 pixels wide to reduce pixelation errors later on. This is based on a pixel size of 20 nm and an estimated lateral FWHM for the Zeiss Airyscan psf of 140 nm. Likewise, $FWHM_{max}$ is used to determine the number of scales to use in the subsequent steps to ensure both that the largest tubules are correctly segmented and also that structures above this limit are identified as cisternae.
2. Care is needed with this step as the automatic thresholding operation may introduce breaks in some dim tubules, rendering those tubules unavailable for consideration in subsequent processing and analysis steps.
3. CLAHE visually helps the user see detail across the whole image, but is only needed if the subsequent segmentation step is dependent on image intensities rather than phase congruency.
4. The filtering and contrast adjustment are applied to aid segmentation of the pixel skeleton. Quantitative measurements always refer back to the original image intensities.
5. The result of the enhancement steps can also be smoothed using coherence or guided filtering.
6. In each case, the number of scales is initially set by the ratio of $FWHM_{max}/FWHM_{min}$ with a minimum bound of 3. However, this can be overridden by the user. This may be necessary to ensure that larger features are also processed prior to segmentation. The number of orientations is fixed at 6. In the case of the anisotropic Lopez-Molina filters, the anisotropy is set at 1.3.
7. If the automated methods to delineate the pixel skeleton are still incorrect, the skeleton can be edited manually.
8. An additional option is available to increase the speed of the granulometry by using decomposition of the disk-shaped structuring element into a set of linear elements. This requires an empirically determined correction of −1 pixel to the estimated width to compensate for the over-sampling with essentially square kernel approximations (see for example Fig. 3h).
9. We have found that the simplest way to estimate the empirical intensity calibration factor is to take the average intensity for a cisternal sheet (using the profile tool). Typically this is about 0.3–0.5 and represents the signal expected for a sheet-like structure completely filling the (x,y) plane of the psf with the same thickness as the tubules.

10. While roGFP2 in most fusions with membrane proteins will provide a four- to fivefold difference in the 405/488 mm fluorescence ratio depending on whether the probe faces the cytosolic or the lumenal side of the ER membrane, there may be cases in which roGFP2 thiols undergo formation of mixed disulfides with lumenal proteins or even thiol residues of the protein under investigation. Because the respective thiols of roGFP2 would then not be available for internal disulfide formation, this would effectively diminish the dynamic range of the reporter. Nevertheless, the difference in ratio will be large enough to get a binary readout (see for example Fig. 5f).

Acknowledgements

Funding is gratefully acknowledged from the DFG in the framework of the priority program SPP1710 (A.M.), The Human Frontier Science Program (RGP0053/2012, M.D.F., L.L.H., N.J.), and the Leverhulme Foundation (RPG-2015-437, M.D.F., L.L.H., N.J.).

References

1. Westrate LM, Lee JE, Prinz WA, Voeltz GK (2015) Form follows function: the importance of endoplasmic reticulum shape. Annu Rev Biochem 84:791–811
2. Bouchekhima AN, Frigerio L, Kirkilionis M (2009) Geometric quantification of the plant endoplasmic reticulum. J Microsc 234:158–172
3. Hein B, Willig KI, Hell SW (2008) Stimulated emission depletion (STED) nanoscopy of a fluorescent protein-labeled organelle inside a living cell. Proc Natl Acad Sci U S A 105:14271–14276
4. Streekstra GJ, van Pelt J (2002) Analysis of tubular structures in three-dimensional confocal images. Netw Comput Neural Syst 13:381–395
5. Lin CP, Zhang YW, Sparkes I, Ashwin P (2014) Structure and dynamics of ER: minimal networks and biophysical constraints. Biophys J 107:763–772
6. Sparkes I, Runions J, Hawes C, Griffing L (2009) Movement and remodeling of the endoplasmic reticulum in nondividing cells of tobacco leaves. Plant Cell 21:3937–3949
7. Hanson GT, Aggeler R, Oglesbee D, Cannon M, Capaldi RA, Tsien RY, Remington SJ (2004) Investigating mitochondrial redox potential with redox-sensitive green fluorescent protein indicators. J Biol Chem 279:13044–13053
8. Gutscher M, Pauleau AL, Marty L, Brach T, Wabnitz GH, Samstag Y, Meyer AJ, Dick TP (2008) Real-time imaging of the intracellular glutathione redox potential. Nat Methods 5:553–559
9. Albrecht SC, Sobotta MC, Bausewein D, Aller I, Hell R, Dick TP, Meyer AJ (2014) Redesign of genetically encoded biosensors for monitoring mitochondrial redox status in a broad range of model eukaryotes. J Biomol Screen 19:379–386
10. Meyer AJ, Brach T, Marty L, Kreye S, Rouhier N, Jacquot JP, Hell R (2007) Redox-sensitive GFP in Arabidopsis thaliana is a quantitative biosensor for the redox potential of the cellular glutathione redox buffer. Plant J 52:973–986
11. Meyer AJ, Dick TP (2010) Fluorescent protein-based redox probes. Antioxid Redox Signal 13:621–650
12. Schwarzlander M, Dick TP, Meyer AJ, Morgan B (2016) Dissecting redox biology using fluorescent protein sensors. Antioxid Redox Signal 24:680–712
13. Schwarzlander M, Fricker MD, Muller C, Marty L, Brach T, Novak J, Sweetlove LJ, Hell R, Meyer AJ (2008) Confocal imaging of glutathione redox potential in living plant cells. J Microsc 231:299–316
14. Birk J, Meyer M, Aller I, Hansen HG, Odermatt A, Dick TP, Meyer AJ, Appenzeller-Herzog C (2013) Endoplasmic reticulum:

reduced and oxidized glutathione revisited. J Cell Sci 126:1604–1617

15. Aller I, Rouhier N, Meyer AJ (2013) Development of roGFP2-derived redox probes for measurement of the glutathione redox potential in the cytosol of severely glutathione-deficient rml1 seedlings. Front Plant Sci 4:506
16. Lohman JR, Remington SJ (2008) Development of a family of redox-sensitive green fluorescent protein indicators for use in relatively oxidizing subcellular environments. Biochemistry 47:8678–8688
17. Sarkar DD, Edwards SK, Mauser JA, Suarez AM, Serowoky MA, Hudok NL, Hudok PL, Nuñez M, Weber CS, Lynch RM, Miyashita O, Tsao TS (2013) Increased redox-sensitive green fluorescent protein reduction potential in the endoplasmic reticulum following glutathione-mediated dimerization. Biochemistry 52:3332–3345
18. Brach T, Soyk S, Muller C, Hinz G, Hell R, Brandizzi F, Meyer AJ (2009) Non-invasive topology analysis of membrane proteins in the secretory pathway. Plant J 57:534–541
19. Au KKC, Perez-Gomez J, Neto H, Muller C, Meyer AJ, Fricker MD, Moore I (2012) A perturbation in glutathione biosynthesis disrupts endoplasmic reticulum morphology and secretory membrane traffic in Arabidopsis thaliana. Plant J 71:881–894
20. Fricker MD (2015) Quantitative redox imaging software. Antioxid Redox Signal 24:752–762
21. Linkert M, Rueden CT, Allan C, Burel JM, Moore W, Patterson A, Loranger B, Moore J, Neves C, Macdonald D, Tarkowska A, Sticco C, Hill E, Rossner M, Eliceiri KW, Swedlow JR (2010) Metadata matters: access to image data in the real world. J Cell Biol 189:777–782
22. Otsu N (1979) Threshold selection method from gray-level histograms. IEEE Trans Syst Man Cybern 9:62–66
23. Pizer SM, Amburn EP, Austin JD, Cromartie R, Geselowitz A, Greer T, ter Haar Romeny B, Zimmerman JB, Zuiderveld K (1987) Adaptive histogram equalization and its variations. Comput Vis Graphics Image Process 39:355–368
24. He KM, Sun J, Tang XO (2013) Guided image filtering. IEEE Trans Pattern Anal Mach Intell 35:1397–1409
25. Kovesi PD (1999) Image features from phase congruency. Videre 1:1–26
26. Kovesi PD (2000) MATLAB and octave functions for computer vision and image processing. http://www.csse.uwa.edu.au/~pk/research/matlabfns/
27. Frangi A, Niessen W, Vincken K, Viergever M (1998) Multiscale vessel enhancement filtering. In: Wells W, Colchester A, Delp S (eds) Medical image computing and computer-assisted intervention, vol 1496. Springer, Berlin/Heidelberg, pp 130–137
28. Meijering E, Jacob M, Sarria JCF, Steiner P, Hirling H, Unser M (2004) Design and validation of a tool for neurite tracing and analysis in fluorescence microscopy images. Cytometry 58:167–176
29. Lopez-Molina C, Vidal-Diez de Ulzurrun G, Baetens JM, Van den Bulcke J, De Baets B (2015) Unsupervised ridge detection using second order anisotropic Gaussian kernels. Signal Process 116:55–67
30. Zhang B, Zerubia J, Olivo-Marin J-C (2007) Gaussian approximations of fluorescence microscope point-spread function models. Appl Opt 46:1819–1829
31. Breeze E, Dzimitrowicz N, Kriechbaumer V, Brooks R, Botchway SW, Brady JP, Hawes C, Dixon AM, Schnell JR, Fricker MD, Frigerio L (2016) A C-terminal amphipathic helix is necessary for the in vivo tubule-shaping function of a plant reticulon. Proc Natl Acad Sci U S A 113:10902–10907
32. Zimmermann R, Eyrisch S, Ahmad M, Helms V (2011) Protein translocation across the ER membrane. Biochim Biophys Acta 1808:912–924
33. Kroon DJ, Slump CH, Maal TJ (2010) Optimized anisotropic rotational invariant diffusion scheme on cone-beam CT. Med Image Comput Comput Assist Interv 13:221–228
34. Merchante C, Alonso JM, Stepanova AN (2013) Ethylene signaling: simple ligand, complex regulation. Curr Opin Plant Biol 16:554–560
35. Sparkes IA, Runions J, Kearns A, Hawes C (2006) Rapid, transient expression of fluorescent fusion proteins in tobacco plants and generation of stably transformed plants. Nat Protoc 1:2019–2025

Chapter 6

Long-Term Imaging of Endoplasmic Reticulum Morphology in Embryos During Seed Germination

Natasha Dzimitrowicz, Emily Breeze, and Lorenzo Frigerio

Abstract

Imaging plant embryos at the cellular level over time is technically challenging, since the embryo, once its protective seed coat is removed, must be kept viable and unstressed on a microscope slide for the duration of the experiment. Here we describe a procedure and suitable apparatus for the visualization, over several days, of changes in endoplasmic reticulum (ER) morphology associated with the process of germination in *Arabidopsis thaliana* seeds. Moreover, we also present a user-friendly image analysis tool which enables subtle perturbations in the ER network to be measured.

Key words Confocal microscopy, Imaging chamber, Embryo, Germination

1 Introduction

Seed germination can be defined as the series of events occurring between the uptake of water by the dry seed (imbibition) and the elongation of the embryonic axis which, in Angiosperms, culminates in the emergence of the radicle through the seed coat [1, 2]. Upon imbibition the seed rapidly commences metabolic activities with a high concomitant demand for de novo protein and lipid biosynthesis, thus placing a considerable burden on the endoplasmic reticulum (ER), which continues throughout germination [1, 3]. Since the time taken for germination and post-germination growth can vary from hours to weeks, depending on the plant species and/or environmental conditions, imaging changes in cellular morphology associated with this process is challenging. Moreover, it is not possible to obtain confocal microscopy images through the seed coat which must, therefore, be removed prior to imaging. Here we describe a time series of ER morphology changes associated with the germination of *Arabidopsis thaliana* embryos over a period of 8 days, from seed imbibition through to fully emerged seedling. By first removing the seed coat and then immobilizing the embryos in sterile Murashige and Skoog (MS) media,

Chris Hawes and Verena Kriechbaumer (eds.), *The Plant Endoplasmic Reticulum: Methods and Protocols*, Methods in Molecular Biology, vol. 1691, DOI 10.1007/978-1-4939-7389-7_6,

containing appropriate antibiotics, in an imaging chamber, we were able to obtain live confocal images of cellular events occurring during germination. It is possible to embed several arabidopsis embryos in a single imaging chamber, enabling multiple replicates to be imaged under identical conditions; and also to apply the described methodology to other plant species, depending on the size of the embryos. We were further able to analyze the images post-acquisition in order to assess the subtle temporal differences in the ER network.

2 Materials

Prepare all solutions using sterile ultrapure water.

1. Murashige and Skoog (MS) medium: Weigh 0.44 g Murashige and Skoog basal salt mixture and 1 g bacteriological agar into a suitable, autoclavable container. Add water to a volume of 90 ml and mix. Adjust pH to 5.7 ± 0.1 with KOH or HCl. Add additional water to bring the total volume to 100 ml. Sterilize the medium by autoclaving. Use immediately or store at 65 °C. Appropriate antibiotics can be added immediately prior to use.
2. Arabidopsis seeds transformed with the desired fluorescent markers or fusion proteins. Here we used stable lines carrying the ER luminal marker GFP-HDEL [4].
3. CoverWell™ imaging chamber (1 × 20 mm) (supplier Grace Biolabs). A reusable press-to-seal silicone chamber which forms a removable enclosure designed to stabilize and support free-flowing samples (Fig. 1).

3 Methods

All procedures should be carried out at room temperature unless otherwise stated.

3.1 Preparation of Embryos for Imaging

1. Add 50–100 dry seeds to a 2 ml round-bottomed Eppendorf tube and carefully add 1 ml sterile water. Incubate tube at 4 °C for 1 h in the dark.
2. Using a wide bore pipette tip (or a cut yellow tip), transfer some of the seeds to a clean petri dish (*see* **Note 1**) and view under a stereomicroscope with appropriate lighting and magnification.
3. Hold an individual seed against its longitudinal axis with fine forceps. Carefully cut the seed coat (including testa and endosperm) along its length using a syringe needle (e.g., U100 insulin needle), starting at the end of the seed closest to where the cotyledons join the radicle.

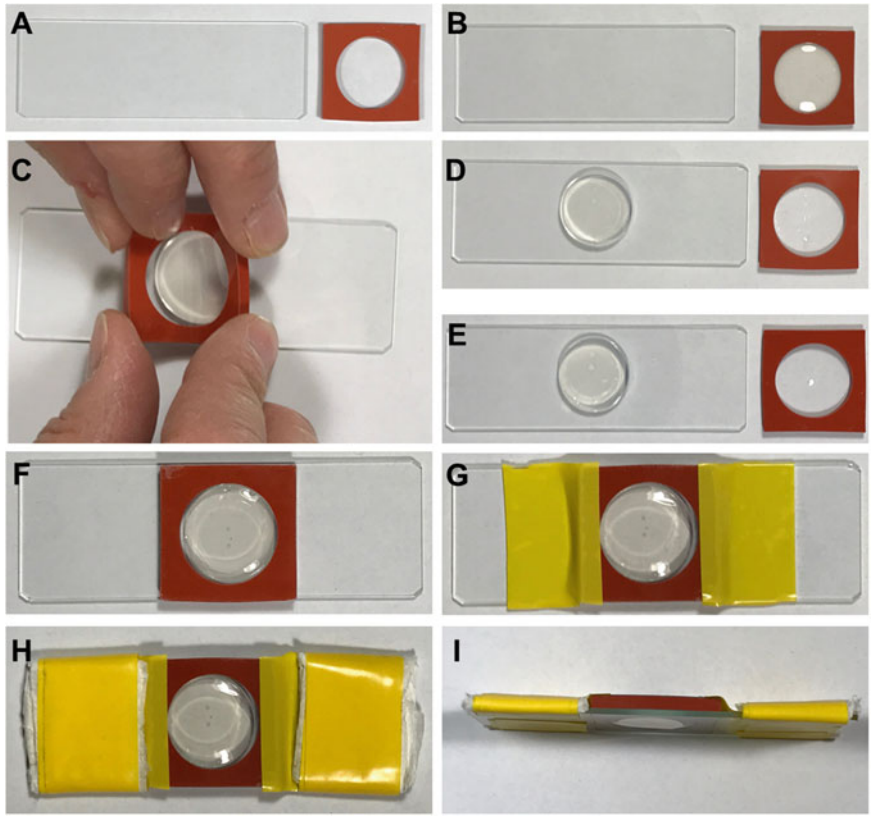

Fig. 1 Assembly of the imaging chamber. The clean imaging chamber (**a**) is filled with MS agar media containing appropriate antibiotics (**b**) and allowed to set before carefully being turned out onto a sterile microscope slide (**c**, **d**). Uncoated embryos, prepared previously and stored in water, are gently pipetted into the chamber (**e**) and covered with the agar disk (**f**), and the chamber securely taped to the slide (**g**). The height of the assembled apparatus is adjusted, as required with tissue and further tape (**h**, **i**). All steps should be performed under sterile conditions. *Arrow* indicates position of uncoated embryo

4. Using forceps, gently and smoothly squeeze the seed at the end furthest from the cut (i.e., closest to the tip of the cotyledons and radicles) to release the intact embryo out of the seed coat through the created opening (*see* **Note 2**).
5. Using a syringe needle, carefully transfer the uncoated embryo to a 2 ml round-bottomed Eppendorf tube and store in a minimal amount of sterile water while further embryos are collected, for up to a maximum of 60 min.

3.2 Preparation of Imaging Chamber

The following steps should be carried out inside a laminar flow hood cabinet. For all stages, *see* Fig. 1.

1. Prior to use, thoroughly clean the imaging chamber with 70% ethanol (Fig. 1a).

2. With a sterile pipette tip, add 900 μl MS agar at ~60 °C to a CoverWell™ imaging chamber (or equivalent) and allow to set (Fig. 1b).
3. Carefully transfer the disk of agar onto a clean, sterile, microscope slide (Fig. 1c, d) (*see* **Note 3**).
4. Using a sterile wide-bore pipette, transfer 3–4 uncoated embryos into the imaging chamber in a minimal amount of water (Fig. 1e) (*see* **Note 4**).
5. Carefully invert the imaging chamber and place it onto the agar disk on top of the embryos in the chamber (Fig. 1f) (*see* **Note 5**). Remove excess water with a tissue. Once mounted, the embryos should not move freely under the agar.
6. Fix the prepared imaging chamber to a clean microscope slide and secure with electrical insulation tape, or equivalent, ensuring that the embryos are clearly visible (Fig. 1g). Fold two suitably sized pieces of tissue paper and affix to the outer edges of the slide with additional tape, to equalize the thickness of the whole apparatus (Fig. 1g, h).
7. Place the assembled chamber into a growth cabinet under the desired environmental conditions. Remove the apparatus at the desired time points and image under a confocal microscope with the appropriate settings for the desired fluorophores. After imaging remove any residual immersion oil from the slide with ethanol. Between imaging sessions, return the chamber to the growth cabinet (Fig. 2).

3.3 Analysis

The following macro is designed to estimate the proportion of ER sheets to tubules from a confocal image (Fig. 3). The macro runs in the freely available ImageJ-based open-source processing package Fiji [5] using the Bio-Formats plugin [6] and so requires the latest version of this software to be installed prior to use. It also requires a representative image of the ER containing both sheets and tubules in order to train the segmentation classifier.

1. Open the relevant confocal image file in Fiji (*see* **Note 6**), and set the background of the binary image to black (Edit > Options > Colors...) (Fig. 3a).
2. Apply a median filter (radius 2 pixels) to reduce the salt and pepper noise (Process > Filters > Median) (Fig. 3b).
3. Normalize the image by setting the saturation levels to 0.5% (Process > Enhance > Contrast...) (Fig. 3c).
4. Segment the image to create a binary image of the total ER network by applying the Trainable Weka Classifier (v3.2.5) function (Plugins > Segmentation > Trainable Weka Segmentation) [7, 8] (Fig. 3d). Load a representative image of the ER containing both tubules and sheets. Use the "Freehand line"

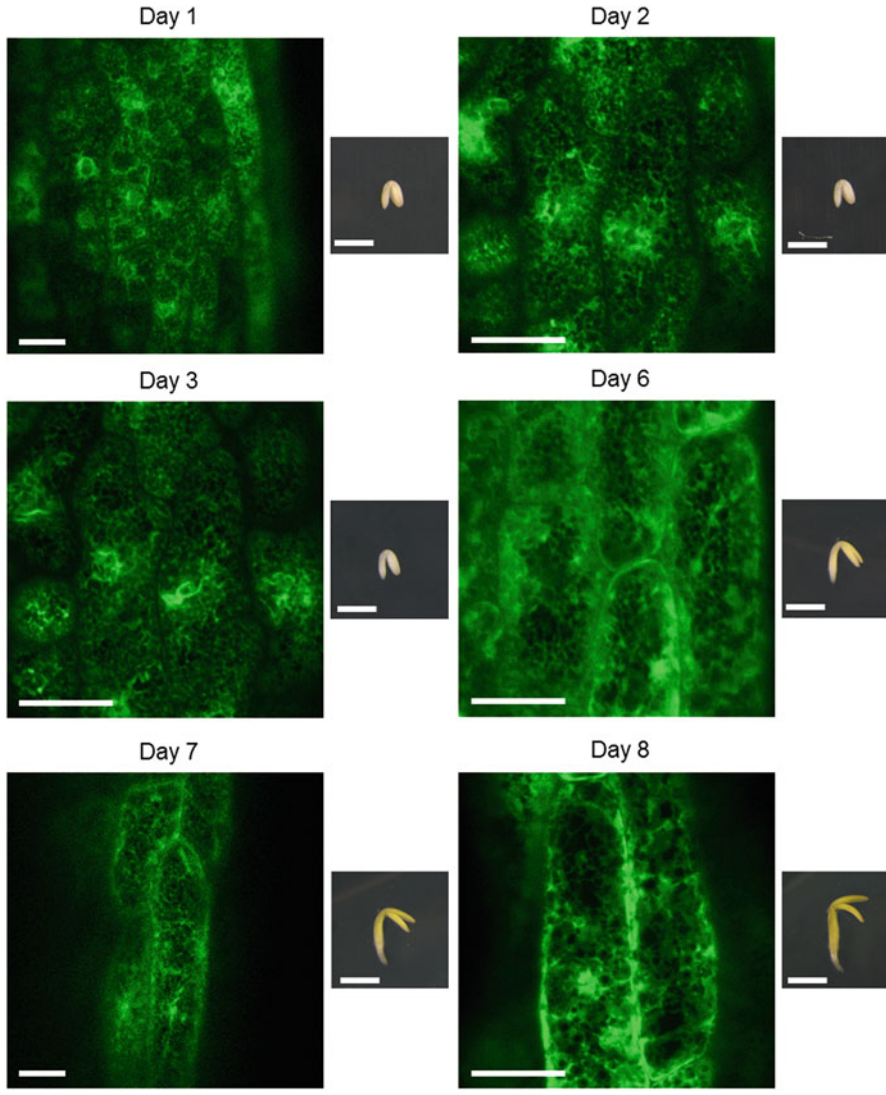

Fig. 2 Changes in ER morphology during germination. Confocal images of the ER, as labeled with the luminal marker GFP-HDEL, obtained from a single germinating embryo in an imaging chamber with images obtained daily for a total of 8 days, together with the corresponding images of the whole embryo. Confocal image scale bars = 10 μm. Whole embryo image scale bars = 0.5 mm

selection tool to identify areas of ER and background and assign them to either Class 1 (ER) or Class 2 (Background). Use a minimum of five selections for each class to train the classifier, and save as a ".model" file.

5. Load the classifier file and select Create Result to segment the image ("Classified Image"). Convert this image into a binary image (Process > Binary > Make Binary).

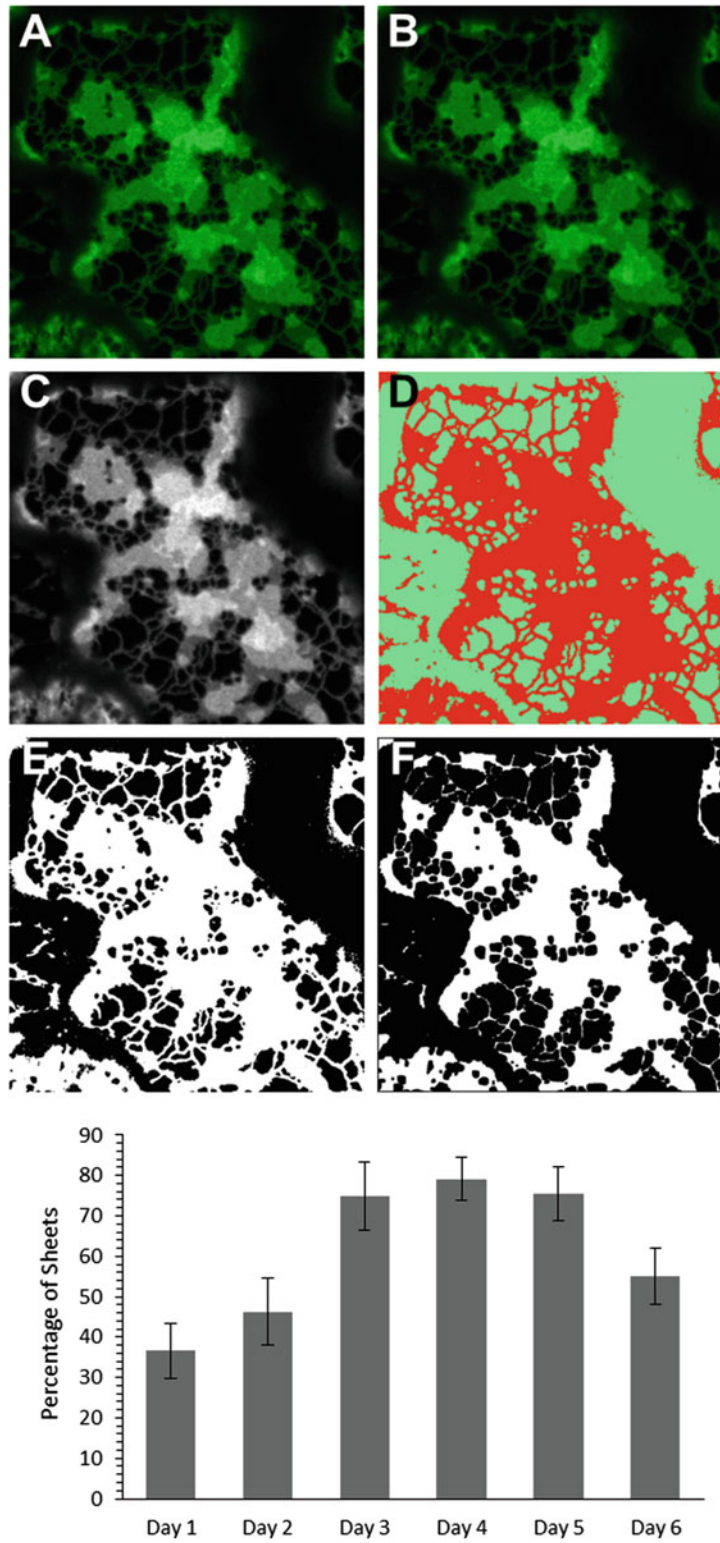

Fig. 3 A Fiji-based macro for the estimation of ER sheet abundance post-image acquisition. A confocal image of the ER network in a germinating embryo was analyzed by a macro written for the open-source platform Fiji

6. Duplicate the binary segmented image (a and b). Apply an erode function to ImageA (iterations = 3; count = 1) to remove thinner structures from the image such as tubules (Process > Binary > Erode). Save eroded image file (ER sheets only) (Fig. 3f) and unaltered binary image (total ER network) (Fig. 3e).
7. Color Pixel Counter plugin [9] (*see* **Note 7**). Convert both images to RGB Color (from 8-bit) (Image > Type > RGB Color). Run the Color Pixel Counter to count green pixels in the unaltered binary image (Fig. 3e) and red pixels in the eroded image file (Fig. 3f) (cells = 20; pixels = 0.2100; minimum = 30) (Plugins > Color Pixel Counter) (*see* **Note 7**).
8. The proportion of sheets in the image can be calculated from the ratio of pixels in the eroded image (Fig. 3f) to that in the total binary image (Fig. 3e) (*see* **Note 8**) (Fig. 3g).

4 Notes

1. It may help to have a small piece of Whatman filter paper or microscope lens cleaning tissue on the petri dish to absorb excess water and limit movement of the seed during uncoating.
2. Uncoating embryos, and ensuring that they remain intact and undamaged, is technically challenging and likely requires extensive practice. The use of two syringe needles, in addition to forceps, may help with both the manipulation of the seed and the application of pressure to ease the embryo out of the seed coat.
3. The imaging chamber is relatively flexible and so it is possible to bend it slightly to allow the agar disk to become dislodged.
4. When transferring the uncoated embryos to the imaging chamber, care should be taken to ensure that they don't become damaged. Once in the chamber it is beneficial to ensure that the embryos are well-spaced and not clumped together to allow them sufficient room to expand over the time course.
5. It is important to ensure that only a minimal amount of water is used to transfer the embryos to the imaging chamber so that when the chamber is inverted the surface tension of the water keeps the embryos on the coverslip.

Fig. 3 (continued) [5]. (**a**) Original (unmanipulated) confocal image. (**b**) Median-filtered image. (**c**) Contrast-enhanced image. (**d**) Trainable Weka Classified image. (**e**) Binary image (total). (**f**) Eroded binary image. (**g**) Proportion of the total ER network identified as sheets by our image analysis macro from day 1 to 6 of embryo germination

6. If the image file is a Z-stack, then it must be converted into single images, by either selecting an appropriate slide (Image > Stacks > Stack to Image) or converting the stack to a projection (Image > Stacks > Z-project. . ..).
7. The Color Pixel Counter plugin is not included in the standard Fiji package and so must be downloaded separately and saved to Program Files\Fiji.app\plugins (or equivalent location; NB the filename must be altered so that each word is capitalized). It is freely available from http://imagejdocu.tudor.lu/doku.php?id=plugin:color:color_pixel_counter:start.

   The choice of red or green pixels for the eroded and binary images, respectively, is arbitrary and simply allows the user to identify which results were obtained from which image since the Color Pixel Counter identifies the number of white pixels as colored pixels.
8. Be aware that the zoom level applied in the images will impact on the results obtained. This can be negated by converting the pixel count to an area (microns). First identify the resolution of the image (Image > Show Info. . .), and then calculate the square root of the number of green or red pixels, divided by the resolution. By squaring this result the area in microns can be calculated, and used to determine the proportion of ER sheets present in the image.

References

1. Bewley JD (1997) Seed germination and dormancy. Plant Cell 9:1055–1066
2. Finch-Savage WE, Leubner-Metzger G (2006) Seed dormancy and the control of germination. New Phytol 171:501–523
3. Holdsworth MJ, Bentsink L, Soppe WJJ (2008) Molecular networks regulating Arabidopsis seed maturation, after-ripening, dormancy and germination. New Phytol 179:33–54
4. Boevink P, Cruz S, Hawes C, Harris N (1996) Virus-mediated delivery of the green fluorescent protein to the endoplasmic reticulum of plant cells. Plant J 10:935–941
5. Schindelin J, Arganda-Carreras I, Frise E et al (2012) Fiji: an open-source platform for biological-image analysis. Nat Methods 9:676–682
6. Linkert M, Rueden CT, Allan C et al (2010) Metadata matters: access to image data in the real world. J Cell Biol 189:777–782
7. Arganda-Carreras I, Kaynig V, Rueden C et al (2017) Trainable Weka Segmentation: a machine learning tool for microscopy pixel classification. Bioinformatics. doi:10.1093/bioinformatics/btx180
8. Arganda-Carreras I, Kaynig V, Rueden C et al Trainable_Segmentation: release v3.1.2 [data set]. Zenodo. doi:10.5281/zenodo.59290
9. Pichette B (2012) Color pixel counter. Available at http://imagejdocu.tudor.lu/doku.php?id=plugin:color:color_pixel_counter:start

Chapter 7

Dancing with the Stars: Using Image Analysis to Study the Choreography of the Endoplasmic Reticulum and Its Partners and of Movement Within Its Tubules

Lawrence R. Griffing

Abstract

In this chapter, approaches to the image analysis of the choreography of the plant endoplasmic reticulum (ER) labeled with fluorescent fusion proteins ("stars," if you wish) are presented. The approaches include the analyses of those parts of the ER that are attached through membrane contact sites to moving or nonmoving partners (other "stars"). Image analysis is also used to understand the nature of the tubular polygonal network, the hallmark of this organelle, and how the polygons change over time due to tubule sliding or motion. Furthermore, the remodeling polygons of the ER interact with regions of fundamentally different topology, the ER cisternae, and image analysis can be used to separate the tubules from the cisternae. ER cisternae, like polygons and tubules, can be motile or stationary. To study which parts are attached to nonmoving partners, such as domains of the ER that form membrane contact sites with the plasma membrane/cell wall, an image analysis approach called persistency mapping has been used. To study the domains of the ER that are moving rapidly and streaming through the cell, the image analysis of optic flow has been used. However, optic flow approaches confuse the movement of the ER itself with the movement of proteins within the ER. As an overall measure of ER dynamics, optic flow approaches are of value, but their limitation as to what exactly is "flowing" needs to be specified. Finally, there are important imaging approaches that directly address the movement of fluorescent proteins within the ER lumen or in the membrane of the ER. Of these, fluorescence recovery after photobleaching (FRAP), inverse FRAP (iFRAP), and single particle tracking approaches are described.

Key words Endoplasmic reticulum, Network flow, Network movement, Persistency mapping, Membrane contact sites

1 Introduction

The endoplasmic reticulum (ER) is an extremely dynamic organelle that ramifies throughout the cytosol of plant cells [1, 2]. One might expect this, given that it is tethered to other dynamic organelles like the Golgi body, the peroxisome, and the mitochondrion. Remarkably, it is also tethered to less dynamic organelles such as the chloroplast, the nucleus, and the plasma membrane. How image analysis is currently used and could be used in the future to analyze

Chris Hawes and Verena Kriechbaumer (eds.), *The Plant Endoplasmic Reticulum: Methods and Protocols*, Methods in Molecular Biology, vol. 1691, DOI 10.1007/978-1-4939-7389-7_7,

the choreography of this dance with still, slow, and fast partners is the subject of the first part of this chapter. But there is another dance going on as well: the dance of the proteins, lipids, ions, and secondary metabolites in the endoplasmic reticulum itself. Sometimes these two dances are confused. As proteins move through the ER, they are sometimes considered as the movement of the ER itself. It is as if the movement of costume of the dancer were taken to be the movement of the dancer herself. Although this is an easy enough mistake to make, it is important to follow the movement of the dancer, the ER, and the costume, the surface or luminal markers of the ER, separately. It is important to keep in mind that both forms of movement involve the complicated physics of the small (the ER is about 60 nm in diameter) in a highly viscous, high Reynold's number, environment.

We approach this by deconstructing ER dynamics into two broad categories: *network movement*, the movement and remodeling of the tubules and cisternae, and *network flow*, the movement of protein and lipid (and ions) within the ER lumen and the ER membrane. Approaches to the analysis of network movement are first described. The ER is made of network of tubules and cisternae, and in special cases like brassicaceous plants, e.g., arabidopsis species, the lozenge-shaped ER body. One quantifiable characteristic of the network is the mesh size of the network (Sects. 3.3 and 3.4.2). Another quantifiable feature is the distribution of the tubules and the cisternae, which can be separated using morphological image processing routines on binary images (Sects. 3.4.3 and 3.4.6). The ends and junctions of tubules can be quantified (Sect. 3.4.5). These operations, when combined with image interval subtraction, can be used to create separate persistency maps for tubules and cisternae that identify the most and least persistent tubules over the time period of observation and interval of analysis (Sect. 3.4.7). Using persistency mapping, the movement and form of the ER was shown to be differentially sensitive to dominant-negative tail domain expression of the six (of 13 in arabidopsis) paralogs of myosin XI that are involved in the motility of spheroid organelles like peroxisomes, mitochondria, and Golgi [3–5]: XI-2 (Myo11B2), XI-C (Myo11C1), XI-E (Myo11C2), XI-K (Myo11E), XI-1 (Myo11F), and XI-I (Myo11G). Note that the new nomenclature for these genes [6, 7] follows their old nomenclature in parentheses. While XI-C (Myo11C1) and XI-E (Myo11C2) have their largest effects on ER tubulation, XI-K (Myo11E), XI-1 (Myo11F), and XI-I (Myo11G) have their largest effects on cisternalization. Of the latter, XI-I (Myo11G) localizes to the nuclear envelope and is involved in forming or maintaining tubules that are coextensive with the cisternal structure of the nuclear envelope [8].

In a separate study examining insertional mutants of XI-K (Myo11E), XI-1 (Myo11F), and XI-2 (Myo11B2) [9], XI-1

(Myo11F) mutation was only found to have an effect on ER dynamics if it was crossed with XI-2 (Myo11B2) or XI-K (Myo11E) mutations. This contrasts with the work [4], where XI-1 (Myo11F) tail domain expression alone caused an increase in cisternal and tubule persistency, while XI-2 (Myo11B2) tail domain expression alone shows no effect on tubule or cisternal persistency [4], but has been shown to slow streaming rates of spheroid organelles. However, the way that dynamics were measured in [9] was different from persistency analysis. LPX flow (originally called Kbi flow, [9]) uses an optic flow approach and is described below (Fig. 7). The reason for the difference between the two analyses is that optic flow approaches do not distinguish network movement from network flow and, using a mask, excludes the dynamics of the fainter, tethered, polygonal ER, where much of the remodeling occurs (Fig. 7).

The implementation of persistency mapping has identified persistent junctions in the ER at which it remains tethered to the plasma membrane (persistent cisternae less than 0.3 square μm in area [2]). Originally called anchor points, they are now considered ER/PM membrane contact sites (MCS) [5]. However, it is important to note that the cortical ER probably has more than one manner of tethering to the plasma membrane, with some tethers more persistent than others. To date, persistency mapping has only been used on cortical ER, but could be used for other organelles or features of them. For example, if organelles need to be anchored to the plasma membrane/cell cortex in order to divide, as occurs in with mitochondria in yeast [10], the population of those mitochondria becoming attached to the membrane/wall could be quantified in plants and related to those events which accompany division. It could map the choreography that leads to ER associating with the mitochondria and then tethers to the plasma membrane as mitochondrial division is completed.

Just as the movement of the dancer's costume is different from the movement of the dancer, so the flow of the proteins and, probably, lipids in the membrane and lumen of the ER network is different from the movement of the network itself. As mentioned above, optic flow approaches combine these two types of movement into one measurement [9]. However, there is a remarkable, directional network flow of membrane [3, 11] and luminal [12] protein in plants that is not found in animal cells where network flow in the ER is primarily by diffusion [13] and diffusional constraints imposed by glycosylation and the actin cytoskeleton [14]. When considering network flow in plants, the distinction is therefore made between advective flow (movement in a constant velocity field), active flow (movement in changing velocity fields), and flow by diffusion. The directional flow in the ER is dependent on the actinomyosin cytoskeleton, but whether it is advective or active is unknown. Directional flow of photoactivated GFP fused to the

cytoplasmic domain of truncated calnexin (CNX-paGFP [3, 11]) can be inhibited with latrunculin b treatment or tail domain expression of XI-K (Myo11E). Directional flow can also be shown with fluorescence recovery after photobleaching (FRAP) approaches (see below, sect. 3.5.1), where the movement of the photobleached GFP-HDEL can be studied. A similar kind of directional flow also occurs in the tubules arising from chloroplasts, the stromules, but it has been shown, using fluorescence correlation spectroscopy (FCS), to be active and dependent of cellular ATP levels [12]. While myosin XI and the actin cytoskeleton have been shown to associate with stromules and are involved in movement of stromules [15], evidence for cytoskeletal involvement in stromule directional flow is lacking.

Even though *flow directionality* in the plant ER is dependent on the actinomyosin cytoskeleton, how the cytoskeleton modulates *flow rate* is unknown. In fact, it is difficult to get consistent measurements of flow rates in plant epidermal cells. Half-times of fluorescence spread after photoactivation of CNX-paGFP vary by 50% in the same cell type, at the same developmental stage [3]. Half-times of fluorescence recovery after photobleaching (FRAP) of CNX-GFP vary less, but by 30% [3]. In the face of this high variability, no significant difference in the rate of flow has been detected between control (untreated) cells and those with latrunculin b treatment and XI-K (Myo11E) tail domain expression [3]. A major contributor to this variability may be the different, changing geometries of the 3D structure of the ER [16–20]. In animal cells, during diffusion-limited network flow, very different FRAP half-times of recovery can be completely attributed to different 3D geometries [16, 19]. In the last method in this chapter (see below, sect. 3.5.2), it is shown how particle tracking of ER aggregates in constitutively stressed cells in the mutant *ceh-1* [21] can be used to examine rates of flow in the ER after the cell, thereby overcoming the problems of calculating diffusion constants from fluorescence recovery rates and providing a means to examine rates in specific 3D domains.

2 Materials

1. Medium: Murashige and Skoog basal medium (Cat # MSPO1-1LT, Caisson Labs, Smithfield, UT, USA) with or without 0.25 (w/v) sucrose and 0.9% w/v agar (Plant cell culture tested, Cat # A8678, Sigma-Aldrich, St. Louis, MO, USA).
2. VALAP: a 1:1:1 mixture of VAsaline, LAnolin, and Parafin (or beeswax) [22].
3. 100 mM MES (Free Acid, Cat # 475893, Sigma-Aldrich, St. Louis, MO, USA) Buffer, titrated to pH 5.8 with 100 mM

KOH—as stock, diluted 1:10 for imaging and for treatment with different fluorescent dyes.

4. Fluorescent dyes (*see* **Note 1**): Cell walls (and nuclei of dead cells): Propidium iodide (Cat # P1470, Sigma, St. Louis, MO, USA) used at a final concentration of 1 μg/ml. DiOC6 stains the ER and mitochondria of the abaxial epidermis of onion scales adequately [23], but there are problems with the generation of reactive oxygen species with exposure to light [24]. $DiOC_6$ ($DiOC_6(3)$, 3,3′-Dihexyloxacarbocyanine Iodide, Cat # D273, ThermoFisher Scientific, Molecular Probes) 2 mM stock solution dissolved in 100% ethanol (or acetone) as a stock solution and used at 2 μM concentration (*see* **Note 2**). ER Tracker red and green dyes (ThermoFisher Scientific) are not recommended for arabidopsis, since the protein to which they bind through the glibenclamide adduct, AtMRD5/AtABCC5, the sulfonyl receptor portion of the ATP-sensitive potassium channel that transports phytate, is on the plasma membrane in guard cells [25] and the vacuole in other plant cell types [26].
5. Transgenic arabidopsis expressing GFP-HDEL [27], mCherry-HDEL, or YFP-HDEL (plasmids and/or seed is available through the arabidopsis Biological Resource Center, www.arabidopsis.org), and transgenic *Nicotiana benthamiana* expressing GFP-HDEL [28] or *Nicotiana tabacum* leaves transiently expressing the above fluorescent ER-labeling constructs [29] and the fluorescent tail domains of myosin XI [4]. A significant fraction of eGFP could be nonfluorescent and misfolded [30]. The relatively noninteractive mCherry-HDEL and superfolded (sf)GFP-HDEL are good passive markers of the ER lumen. mCherry constructs are reported to be "sticky" when labeling oligomeric or membrane proteins [24], so should probably only be used for studies on luminal proteins. sfGFP [31] has the advantages of being monomeric, lacking N-glycosylation sites, and being resistant to disulfide bond formation [24]. It should be fusion protein of choice for both luminal fusion proteins and membrane fusion proteins.
6. Laser Scanning Confocal Microscope with FRAP software. The ones used for these analyses are the Zeiss LSM510 and the Olympus Fluoview 1000.
7. In all of the following methods, implementation is described using ImageJ (https://imagej.nih.gov/ij/) version 1.45 or higher, and as it is used in the ImageJ version containing many useful plugins, FIJI (www.fiji.sc), version 2.0.0. Additional plugins not part of the FIJI package are listed below. For security reasons, it is recommended that Java version 1.8 jre or higher is used (*see* **Note 3**).

3 Methods

3.1 Microscopy of Living Plant Tissue

1. Select relatively planar surfaces for imaging 25 square mm or less (half a cm on a side or less) sections of mature tobacco leaves in buffer under a 22 × 22 mm coverslip sealed with VALAP.
2. Select relatively planar regions from epidermal cells of roots, shoots, or cotyledons from 6–7-day-old seedlings of arabidopsis, which fit entirely under a single coverslip (*see* **Notes 4 and 5**).

3.2 Using ImageJ Macros for Image Processing Pipelines

1. In order to provide the methods of several approaches in this chapter, an example imaging pipeline is included as a Macro file, available for download at http://griffing.tamu.edu.
2. Copying these files, or following the sequence given below while recording a Macro, saving them in ImageJ macro format (as an .ijm file in the Macro folder), and editing them so that they use file systems on the host computer of choice should provide an easily accessible way to implement the approaches described below.
3. Recording a Macro. ImageJ provides a useful Macro implementation that can be set up for processing pipelines using the command, Plugins>Macro>Record. Command sequences such as this one are described by the sequence of "pull down" sub-commands from the menu bar (Fig. 1) which appears

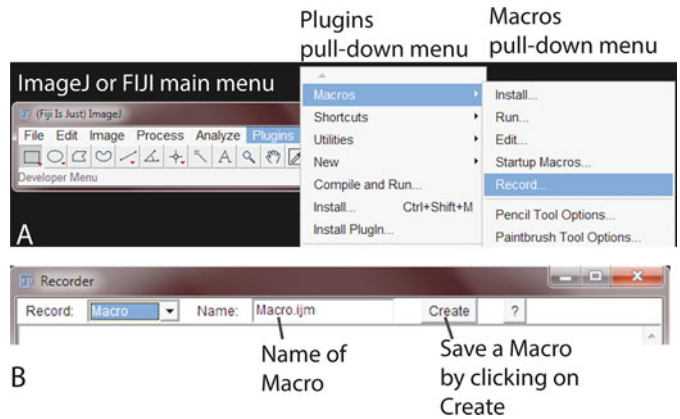

Fig. 1 ImageJ menu structure and accessing macro commands. (**a**) Top menu bar of ImageJ (or the FIJI version) with the Plugins command highlighted in *blue*. The Plugins>Macros command is shown in the plugins pull-down menu. The Plugins>Macros>Record command is shown in the macros pull-down menu. (**b**) Macro recorder window. The top of the window is shown. The name of the macro can be edited, but the recorder does not save the recorded actions until the Create button is clicked. Closing the recorder without clicking on create loses the macro

when ImageJ or FIJI is started. To record a Macro, click on (select) Plugin in the main menu bar. Select the top option Macro. Select the Record option. Besides being useful for processing image pipelines, the Macro feature can be used as an imaging "lab book" to record the steps by which an image is processed (*see* **Note 6**).

4. After recording the sequence of steps in the imaging pipeline, the Create command on the Macro dialog box (Fig. 1) has to be selected because just closing the Macro dialog box does not save the recorded Macro and it will be lost.
5. For ImageJ to "see" the Macro, the Macro file (written in the imagej macro or .ijm format) is saved or placed in the Macro folder in the ImageJ folder.

3.3 Installing, Running, and Editing Macros

1. To install a Macro, use the Plugins>Macro>Install command and the Macro comes up as a separate command in the Plugins>Macro bar. This is very useful for shortcuts and for making Macros that include other Macros.
2. To run a Macro, use the Plugins>Macro>Run command and select the .ijm file manually.
3. To edit a Macro, use the Plugins>Macro>Edit command and select the .ijm file for editing. This can then be text-edited in the Macro dialog screen.
4. Using image stacks for measurement after processing using a Macro:
   (a) The Macro saves a series of images for measurement under a common name for each sample in a group of replicates. For example, each replicate could have an image named AND.tif. These are transferred to a new folder sequentially and Windows automatically assigns them numbers if they have the same name (e.g., AND.tif, AND(2).tif, AND(3).tif). Measurements are assigned with the command, Analyze>Set Measurements.
   (b) The separate images can then be stacked in sequence with the command, Image>Stacks>Images to Stack.
   (c) The different replicates of one treatment can be measured in the stack with one Analyze>Analyze Particles command following selection with the Image>Adjust>Threshold command.

3.4 Network Movement

3.4.1 Removing the drift

1. Make a time series movie.
2. Check to see if reference points are moving, such as cell corners or other external wall features that can be seen after treatment with propidium iodide. This is done by mousing over the precise points in the first and last frame in an imaging sequence and noting if their coordinates have changed.

3. If reference points are moving, use the optic flow-based stabilization plugin by Kang Li using the Lucas–Kanade algorithm with the command Plugins>Image_Stabilizer.
4. Another plugin that has more options in terms of template matching and the implementation of cross-correlation is the "Align slices in stack" plugin by Qingzong Tseng (*see* **Note 7**).

3.4.2 Measuring average mesh size (Fig. 2)

1. Make a time series movie, usually 80 frames at about a second per frame for standard line-scanning confocal microscopes.
2. The in-focus region is selected for the entire time series (movie). This can be done manually (Fig. 2a) with the polygon tool. This

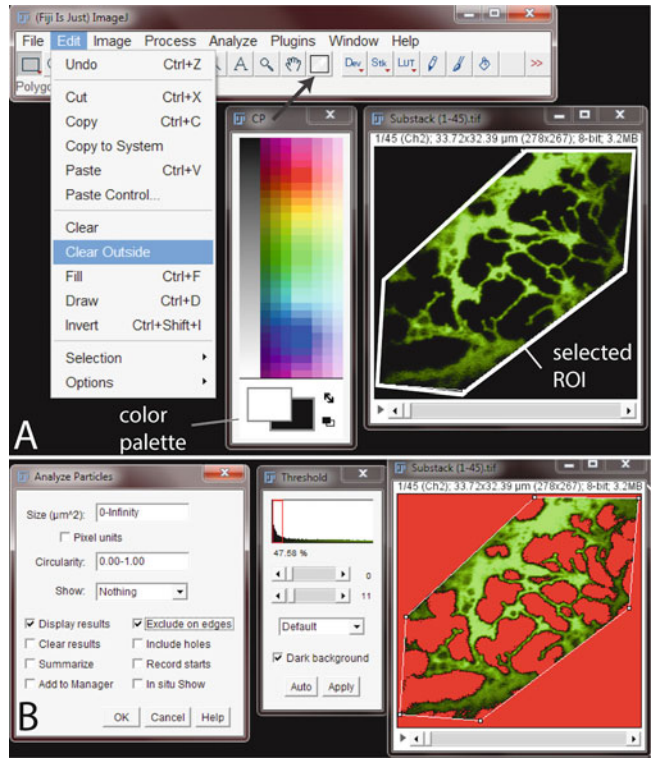

Fig. 2 ImageJ commands for ER mesh counting. (**a**) ImageJ top menu bar showing the Edit>Clear Outside command. This can be achieved after a region of interest (ROI) is selected with the polygon tool that excludes out-of-focus regions (*right-hand panel*). If the image has a black background, the out-of-focus regions can be excluded with the Clear Outside command once the background has been set to black using the color palette (*center panel*) accessed by double-clicking the eye-dropper icon (*arrow*). (**b**) Analyzing the mesh. The dialog box for the Analyze>Analyze Particles command is shown (*left panel*), with the "Exclude on edges" option checked. The Threshold dialog box (*center panel*) from the Image>Adjust>Threshold command is shown selecting the low intensity regions (mesh openings). During thresholding, the selected region is *red* (*right panel*)

region of interest is saved as infocus.roi using the File>SaveAs>Selection command. Those out-of-focus areas are cleared by the Edit>Clear Outside command after the color picker (CP) is set to white on a black background. The color picker is accessed by clicking twice on the "eye dropper" icon.

3. Those regions not occupied by membrane, i.e., the mesh spaces (low intensity values), are selected using manual or automatic gray scale thresholding. If the intensity differences between pixels with and without ER are large enough, many different automatic thresholding routines that isolate the low values from the majority of the high values could be used (e.g., Minimum, Otsu, or IsoData segmentation algorithms found in the Image>Adjust>Auto Threshold), but if not, then the image is thresholded manually with the Image>Adjust>Threshold command (Fig. 2b)—they turn red.
4. The low value regions in each frame are then counted and measured. The "Area" and the "Stack Position" are selected in the Analyze>Set Measurements dialog box. The area of the mesh spaces for each image in the stack is measured with the Analyze>Analyze Particles command. To avoid counting very small (single pixel) regions, a lower limit of mesh space is put in the Size variable in the Analyze Particles dialog box. Also, make sure to click the exclude edge regions (Fig. 1b) before clicking OK. This will produce a results table with Area and Slice values—this can be ported to a spreadsheet program, such as Microsoft Excel.
5. The mesh number (counted or calculated by average area per mesh space/total mesh space area measured) and the number and average area of mesh space per cubic μm (derived from the in-focus area imaged and the depth of field) of cytoplasm can then be calculated in a spreadsheet program, such as Microsoft Excel (using the Averageif command to specify that feature areas are averaged if they are in a certain frame), or with a simple separate script in Python or Matlab.

3.4.3 Identification of tubules vs. cisternae (Fig. 3)

1. Select the fluorescent membrane with a threshold command, Image>Adjust>Threshold, either on 8 or 16 bit images. The original bit depth (intensity range) of the acquired image should be maintained. In the example image (Fig. 3b), an 8 bit image is used.
2. The out-of-focus region can be cropped away using the instructions in **step 2(b)**. This will make the choice in the next step easier.
3. A manual threshold value is used that is a compromise between eliminating the out-of-focus low intensity blur and eliminating continuity between thin tubules. Once a manual threshold level

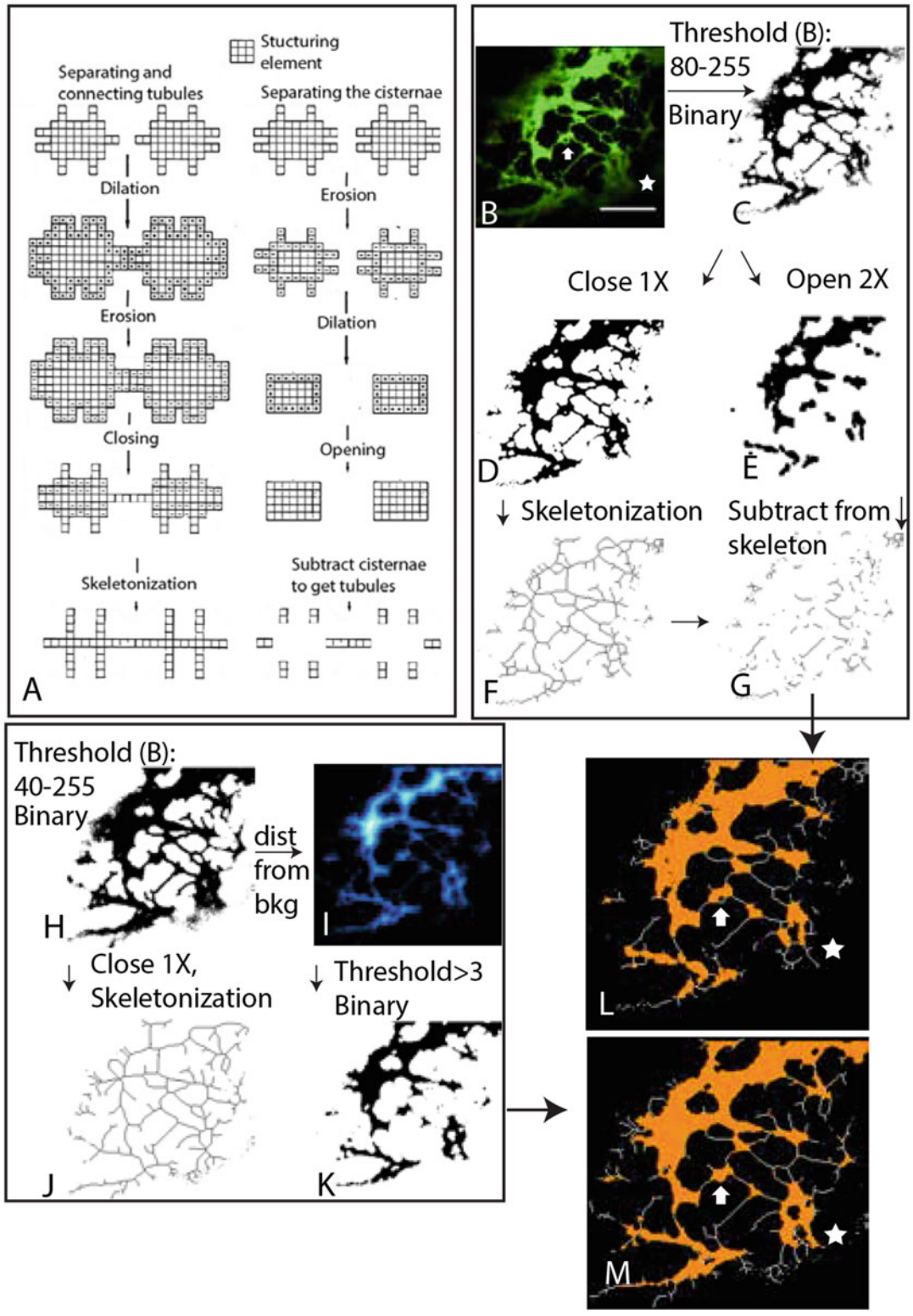

Fig. 3 Separating tubules from cisternae using 8 bit (Image>Type>8bit) morphological image processing. (**a**) Morphological procedures for binary images summarized using a 3 × 3 pixel structuring element. *Squares* represent neighboring pixels. *Squares with minus signs* produced during erosion or skeletonization mean that the pixel is removed. *Squares with plus signs* produced during dilation means the pixel is added. The center of

is set, it is generally not changed between samples of procedures. Two different threshold values are shown in Fig. 3. One is chosen to eliminate the out-of-focus low intensity values (80–255 Fig. 3c) while the lower intensity values are chosen (40–255 Fig. 3h) to preserve the continuity of tubules. Automatic thresholding based on the histogram can be used as in MorphoER (LPX plugin [32], Fig. 5) but in the current implementation of MorphoER the threshold is so low that much the out-of-focus image is included if smoothing is not used (compare Fig. 5b with Fig. 2m). Automatic minimum value thresholding algorithms such as the Minimum, Otsu, and IsoData (from the pull-down menu in the Image>Adjust>Threshold dialog box or from the Image>Adjust>Auto threshold dialog box) and WEKA trainable segmentation (Plugin>Segmentation>WEKA trainable segmentation) could be explored to make the initial threshold values less subjective.

4. Create a binary image with the Make Binary command, Process>Binary>Make Binary. Morphological image processing (Fig. 3a) takes a binary image (Fig. 3c and d).
5. Operate on the binary image with the Open command, Process>Binary>Open. Morphological processing can either add (dilation) or subtract (erosion) pixels from a binary object's periphery based on the shape of the structuring element. Opening is erosion followed by dilation. The number of iterations for opening (and closing, **step 1**) can be set in the Process>Binary>Options dialog box. In Fig. 3a, two side-by-side cisternal structures with emanating tubules are considered. The distance between them is two pixels. Opening eliminates the emanating tubules. After opening the cisternae are isolated, but remain the same area (Fig. 3a and e) [2, 4]. The areas of all of the cisternae in a frame can then be measured using the Analyze>Measure Particles command, described above in

Fig. 3 (continued) the structuring element is put over the target pixel and if any of the structuring element pixels don't cover a neighboring pixel, the pixels underlying the structuring element are added (dilation) or removed (erosion). (**b**) An image of the ER. Scale bar = 10 μm. (**c**) Result of thresholding at a gray level of 80 and using the Binary>Make Binary command. (**d**) One iteration of a Process>Binary>Close command. (**e**) The result of two iterations of the Process>Binary>Open command (number of iterations can be adjusted in the Binary>Options command). (**f**) Skeletonization of (**d**) using the Process>Binary>Skeleton command. (**g**) Subtracting the cisternal regions from the skeletons using the Process>Image Calculator command. (**h**) Binary image resulting from thresholding at a gray value of 40 using the Process>Binary>Make Binary command. (**i**) Euclidean distance map of (**h**) (pseudo-colored with the Cyan>Hot lookup table, LUT) using the Process>Binary>Distance Map command. (**j**) Skeletonization of (**h**) after one closing operation. (**k**) Result of thresholding (**i**) above a gray value of 3. (**l**) Result of combining (**e**) and (**g**), pseudocoloring (**e**) *orange* and (**g**) *white*. (**m**) Result of combining (**k**) and (**j**) (**k** can be subtracted from **j** for analysis), pseudocoloring (**k**) orange and (**j**) white. *Arrows* in (**l**) and (**m**) show a differently processed cisterna. *Stars* show region of low signal

mesh measurement. The results table is saved as an .xls file, opened in Excel, and converted to a worksheet format (.xlsx).

6. The Euclidean distance of each pixel from a background (0) value can be calculated and mapped as an intensity map or image (Fig. 3i) using the Process>Binary>Distance Map command. The image is adjusted so that the largest structures have the brightest values in their center using the Image>Adjust>Brightness and Contrast command. Fig. 3i also has a Cyan Hot lookup table applied using the command, Image>Look up tables>Cyan Hot. That image is then thresholded using the Image>Adjust>Threshold command to select only the cisternae; in the example in Fig. 3i, the tubules can be eliminated by selecting values that have intensity values of three or greater (i.e., are more than 3 pixels away from background). This operation on the Euclidean distance map removes all pixels a distance of three or less from the periphery of the cisternae, as well as the tubules, unlike the open operation that preserves the area of the cisternae, but creates object edges that are similar in shape to the structuring element. MorphoER addresses this by increasing the cisternal size with a manually applied Gaussian blur function (*see* below).
7. Operate separately on the binary image with the Close command, Process>Binary>Close. After closing (dilation followed by erosion), the tubules that are separated by two pixels become connected (Fig. 3a, d and h). This thresholding operation (either automatic or manual) is used to create the binary image that may exclude faint tubule pixels (undesirable) as well as faint noise pixels (desirable). If the condition, set by the size of the structuring element, is met that two disconnected tubules are separated by one or two pixels, then the closing operation connects them and they are counted as a continuous tubule. Faint noise is mostly eliminated with manual thresholding. The closing operation also fills in pixels between two side-by-side tubules that are separated by one or two pixels; hence, if clusters of tubules are being examined, then the pixel size should be at least twofold smaller than the diffraction limit (the Nyquist criterion).
8. For tubules, the closed image is skeletonized (Fig. 3f) using the Process>Binary>Skeletonize command. Skeletonize implements a 2D thinning algorithm [33].
9. Skeletonization is followed by subtraction of the regions that contain cisternae (Figs. 3a and g) using the Process>Image Calculator command. The 8 bit images need to be inverted first, with the Edit>Invert command. This turns the skeletons and cisternae to white on a black background instead of black on a white background. In the Image Calculator dialog box,

the upper image selection should be the skeletonized image and the lower image selection should be the opened cisternal image. When cisternae are skeletonized, they give rise to multiple radiating skeletons, and depending on the skeletonization algorithm these have diagnostic radiating or angular geometries (Fig. 3f and j). Consequently, to eliminate this artifactual data set from the tubule population, these regions are subtracted from the tubule population:

3.4.4 Measurement of cisternal areas and numbers

1. Set the Analyze>Set Measurement dialog box for area and stack location.
2. The opened binary image (Fig. 3e) or the thresholded Euclidean distance map (Fig. 3i) can be analyzed using the Analyze>Analyze Particles command.
3. The results table is saved as an .xls file.
4. The CountIf formula is used in Excel to count the number of cisternae in each slice of the stack (stack location).
5. The AverageIf formula is used to get the average size of cisternae.
6. These are normalized using the area of the membrane imaged, which is the area of the original binary thresholded object (Fig. 2c or h).

3.4.5 Measurement of tubule numbers, lengths, and junctions (Fig. 4)

1. The skeletonized region can be evaluated using the Analyze>Skeleton>Skeleton 2D/3D command (Fig. 4). This procedure provides a list of the length of all of the separate skeletonized tubules, with their number of junctions and the type of junction.

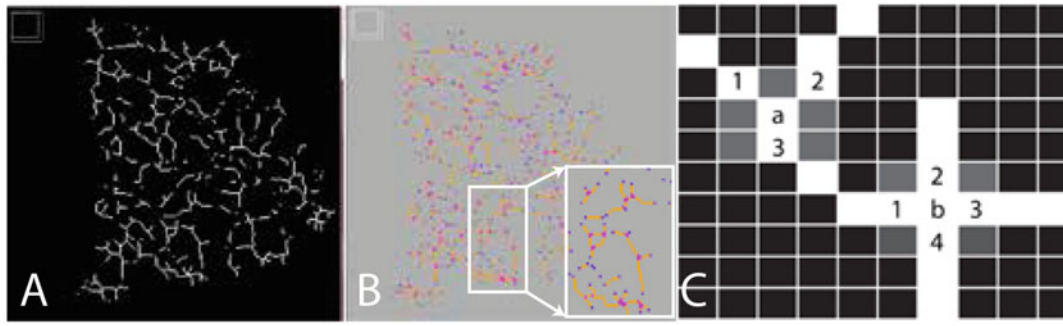

Fig. 4 Analysis of skeletons representing tubules. (**A**) Skeletonized region of ER from a time-lapse series with the cisternal component subtracted (*see* Fig. 6a for original image). (**B**) Result of the Analyze>Skeleton>Skeleton 2D/3D command in FIJI. Inset is blow-up of region showing the *blue* single and end pixels, *orange-yellow* slab pixels, and *pink/purple* junction pixels. (**C**) Identification of junctions as triple or quad junctions: (a) is a triple junction because it has three neighboring pixels that are occupied (*white*). (b) is a quad junction showing four neighboring pixels that are occupied. Gray pixels are unoccupied neighboring pixels

2. To analyze the skeletons, they need to be white on a black background (using the Edit>Invert command as above, if that has not already been done) (Fig. 4B; *see* **Note 8**).
3. There are several images and tables that are produced by this algorithm: A color-tagged skeleton image showing blind ends as blue, junctional regions purple-pink, and tubule lengths yellow-orange (Fig. 4B and inset); a gray-scale image (labeled skeletons, shown for clarity with a color table in Fig. 4D) has a different gray value for each identified skeleton; a results table that includes a list of all of the independent skeletons with the following: # branches, # junctions, # end-point voxels (blue in Fig. 4B—they have less than two pixel neighbors), # junction voxels (pink in Fig. 4B—they have more than 2 pixel neighbors), # slab voxels (yellow in Fig. 4B—if they have exactly 2 pixel neighbors), average branch length, # triple points (a in Fig. 4C), # quadruple points (b in Fig. 4C), and maximal branch length. This can be saved as an .xls file; a branch information table that includes the skeleton ID, the branch length, the coordinates of the start and end of the branches, and the Euclidean (straight line) distance between the start and the end of the branches. Branch length divided by the Euclidean distance is a measure of the complexity of the branch. This can be saved as an .xls file (*see* **Note 9**).

3.4.6 Using MorphoER for analysis of tubules and cisternae (Fig. 5)

MorphoER (*see* LPX plugins above), accessed through LPX plugin set with the command Plugin>LPX>LPX IjTool command (Fig. 5a), can be opened from the IjTool dialog box by selecting morphoER from the projects pull-down menu (Fig. 5c) once an image for analysis is open (Fig. 5b).

MorphoER uses automatic thresholding/segmentation as mentioned above, selecting as a threshold, the value which maximizes the distance between the histogram values to a line defined by the histogram peak value and histogram blackest value [34]. However, it also has several user-defined variables (Fig. 5d): Gaussian blur radius to reduce noise (σ_1), ER body minimum size (for arabidopsis ER body identification), the threshold value in the Euclidean distance map for the width of tubules (τ), and the Gaussian blur radius (σ_2) that enlarges the cisternae after the threshold operation on the Euclidean distance map. A tubule minimum length value (λ) can also be specified that removes small skeletonized isolated tubules from counting. In Fig. 5e–h, the cisternae are colored orange and red, while the tubules are identified as white.

1. Effect of setting σ_1: This blurs the initial image with a Gaussian function of the radius set by the user. It has a large influence on the region selected by automatic thresholding; compare Fig. 5e

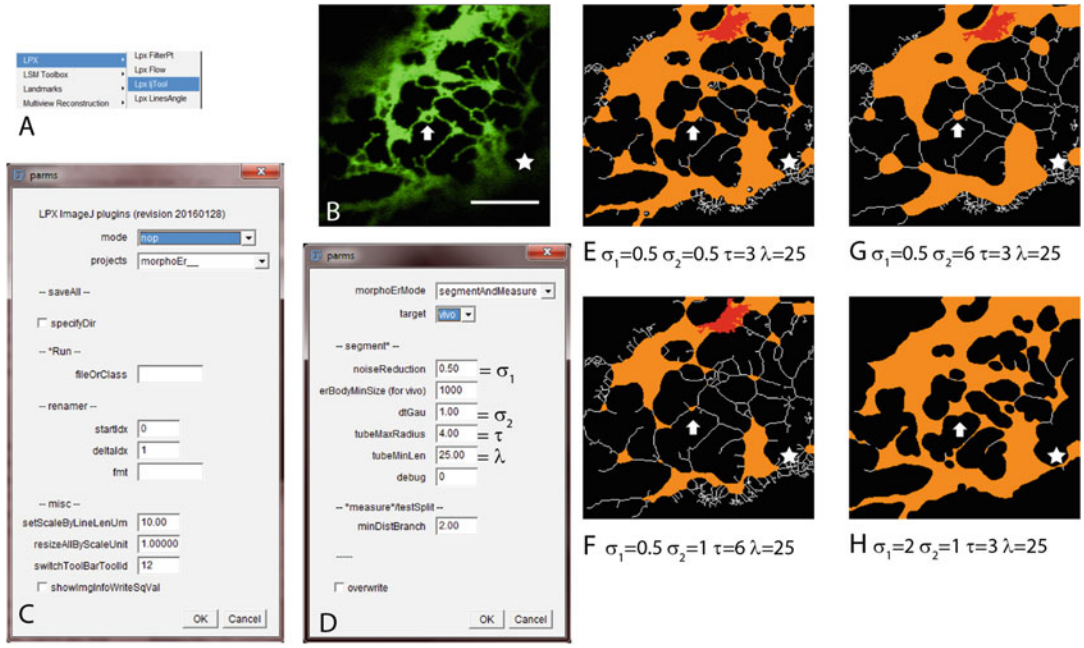

Fig. 5 Separation of ER tubules and cisternae using the morphoER plugin from LPX. (**a**) Pull-down plugin menu showing the LPX option and the LpxljTools option. (**b**) Dialog box brought up by LpxljTools. The nop "mode" should be selected. The morphoEr "projects" should be selected. Other options can be run using the default choices. (**c**) The first image in a time-lapse sequence of ER for analysis. Scale bar = 10 μm. (**d**) After clicking OK in (**c**), this dialog box comes up. The segmentAndMeasure option is shown. The target (in vivo as opposed to in vitro) is shown. In order to segment (select) the tubules vs the cisternae, there are several user variables that can be chosen. (**e**–**h**) show the results of different choices after clicking OK in (**d**). σ_1 is the radius of the Gaussian (blur filter) used to reduce noise. σ_2 is the radius of the Gaussian used to "fill in" the cisternae eroded by Euclidean distance subtraction. τ is the radius of the tubules in the image. λ is the minimum length of skeletons shown, in order to remove skeleton fragments resulting from noise. Tubules are generated by the same skeletonization as in Figs. 3j and f, but without binary closing. Cisternae are generated by the same Euclidean distance subtraction shown in Fig. 3k. Tubules are white and cisternae are *orange*, with saturating pixels *red*. *Arrows* show a cisterna that changes shape and area with different settings. All of the settings do not show the hole in this cisterna shown in Fig. 3l. *The stars* show regions of low signal and the consequent large proliferation artifactual skeletonization that occurs in these regions in (**e**)–(**g**) that is excluded with manual thresholding (Figs. 3l and m)

($\sigma_1 = 0.5$) and h ($\sigma_1 = 2.0$). As shown in Fig. 5h, it will thicken the tubules, changing the value needed for τ.

2. Effect of setting τ: This is the threshold of the Euclidean distance map. Larger values will threshold away the tubules, but with higher values, more of the cisternal area is lost (Fig. 5f).
3. Effect of setting σ_2: This is the radius of a Gaussian blur of the selected cisternae. Larger values produce cisternae with different areas and shapes (Fig. 5g).

4. Clicking OK in the second dialog box produces a final image that is a composite of three values, tubules with a value of 1 (white in Fig. 5e–h), cisternae with a value of 2 (orange in Fig. 5e–h), and saturated pixels with a value of 3 (red in Fig. 5e–h). These can be selected for measurement using a thresholding command. Note that the arrows in Fig. 5b and e–h show a cisterna with a fairly large hole or tubule loop. All of the settings remove the hole or loop. The tubule loop is preserved in Fig. 3l (arrow), which uses a higher threshold and opening instead of a Euclidean distance map (Fig. 3m). The stars in Fig. 5b and e–h are in regions of low or out-of-focus signal. These produce an array of tubules in the MorphoER program, Fig. 5e and f, but they do not exist. These are excluded in both thresholding approaches shown in Fig. 3 (stars in l and m). MorphoER produces a MorphoER results table that has several aspects of tubules and cisternae measured, but the nature of evaluation is not currently published or open source. It is apparently done in pixel number values, but the units are undefined in the software.

3.4.7 Persistency mapping (Fig. 6)

1. In order to identify the regions that are moving rapidly, one can subtract frames between defined intervals in an 80 s time series of 50 frames. In the original approach [3], every fifth frame subtracts an image taken 8 s earlier. This is done by making substacks using the Image>Stacks>Tools>Make Substack command twice; first to remove the first five in the stack leaving a Substack of 6–50, and the second to remove the last five, leaving a Substack of 1–45. Substack (6–50, Fig. 6b) subtracts Substack (1–45, Fig. 6a) using the Process>Image Calculator command and specifying the subtract option. Only those regions which are moving have a value, so this is the "moving" or SUB data set, (Fig. 6c; *see* **Note 10**).
2. The nonmoving data, or AND data set, is the result of a Boolean AND operation between every fifth frame of Substack (1–45, Fig. 6a), and Substack (6–50, Fig. 6d) using the Process>Image Calculator command and specifying the AND option. To generate the persistent data set, the moving data set is subtracted from the nonmoving data set (Fig. 6e) by using the Process>Image Calculator command and subtracting the SUB data set from the AND data set. These operations are done on 8 bit images and ImageJ truncates the results so that negative-valued pixels are set to zero.
3. The persistent data set is then thresholded by a value that includes the in-focus membrane (**step 3(c)**, Fig. 3c or h) using the Image>Adjust>Threshold command.
4. Total detected persistent membrane area can be measured at this stage using the Analyze>Analyze Particles command,

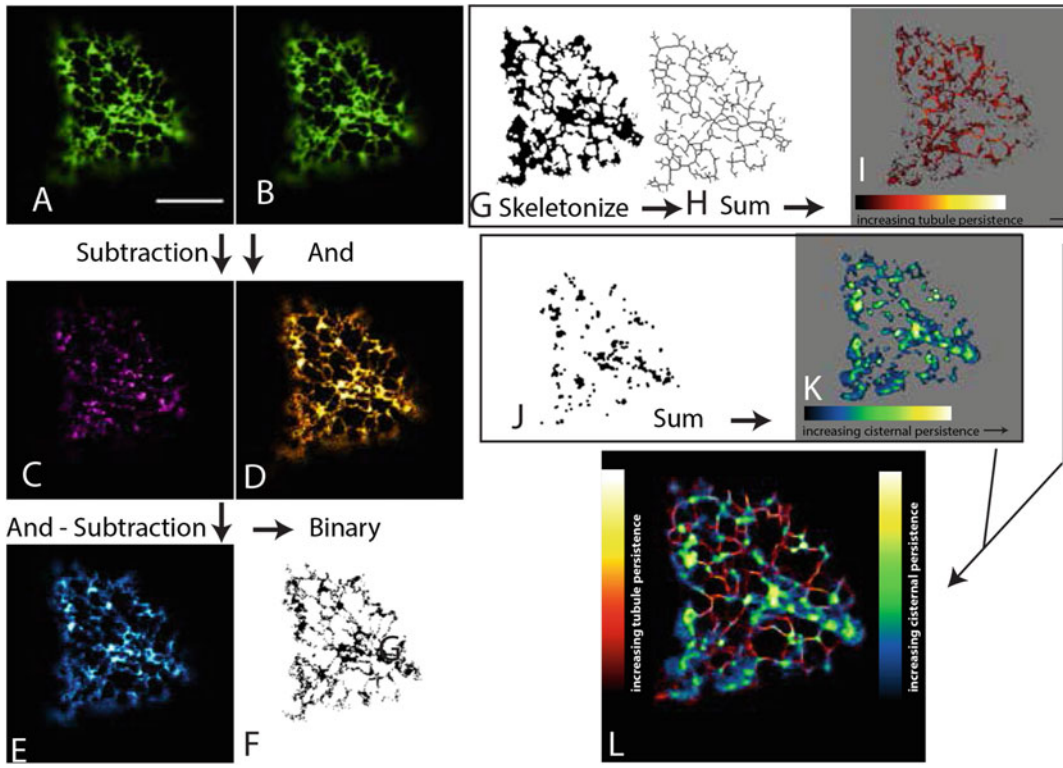

Fig. 6 Persistency mapping. (**a**) Image of ER taken at 0 s. Scale bar = 10 μm. (**b**) Image taken 8 s later than (**a**). (**c**) Result of subtracting image (**a**) from image (**b**) using the Analyze>Image Calculator command, pseudocolored magenta-hot. This is done on the entire stack of images as a stack. So all of the following images represent stacks of images every 8 s apart (0 and 8, 1 and 9, 2 and 10, etc.). (**d**) Result of the Boolean "And" operation between (**a**) and (**b**) using the Process>Image Calculator command, pseudocolored orange-hot. (**e**) Result of subtracting (**c**) from (**d**) using the Process. Image Calculator command, pseudocolored Cyan-hot. (**f**) Result of converting (**e**) to a binary image with the Process>Binary>Make Binary command. (**g**) Closed version of (**f**). (**h**) Skeletonized version of (**g**). (**i**) Tubule Persistency Map: The individual images in stack (**h**) are summed using the Images>Stack>Z Project>Sum Images command, following subtraction of the cisternae. Pseudocolored red-hot, with the lighter regions being the more persistent. (**j**) Opened version of (**f**). (**k**) Cisternal Persistency Map: The individual images in the stack (**j**) are summed using the Images>Stack>Z Project>Sum Images command. Pseudocolored Green-Fire-Blue, with the more persistent cisternae being *white-yellow*. (**l**) Composite image of (**i**) and (**j**) with the more persistent features being pseudocolored *white-yellow*

specifying stack location and area in the Analyze>Set Measurements dialog box. In the Analyze Particles dialog box, if the Masks option is taken, then a binary mask is generated that can then be used instead of the next step (Fig. 6f).

5. A binary image is generated from this thresholded image using the Process>Binary>Make Binary command (if a binary image mask has not been generated in the prior step). Use the default settings in the Make Binary dialog box—do NOT check the

option to have the threshold calculated for each image, or any of the options.

6. The binary image stack is separately converted into the persistent tubule stack using the closing (Fig. 6g) and skeletonization (Fig. 6h) commands (**steps 3(g)** and **(h)**), followed by inverting (Edit>Invert), subtracting the (inverted) persistent cisterna stack and summing them, using the Image>Stacks>ZProject command, specifying the Sum Slices option, Fig. 6i.
7. The binary image stack is then converted into the persistent cisternae stack using either the opening operation (**step 3(d)**), Fig. 6j, or the Euclidean distance operation followed by thresholding (**step 3(e)**), inverted (Edit>Invert) and summed as above (Fig. 6k).
8. The Tubule Persistency Map (Fig. 6i) is the sum of all of the skeletons and only those that persist the longest are the brightest. A colored ramp is made as above, but for tubules (Image>Lookup Table>Red Hot). Because of the variation in skeletonization that occurs with cisternae as they are changing shape, this image can also be thresholded to eliminate these skeletons, without subtracting the cisternae from tubules.
9. The Cisternal Persistency Map (Fig. 6k) is the sum of all of the opened binary images, and has as its lowest value objects, the least persistent cisternae, and as its highest value objects, the most persistent cisternae (Fig. 6k). A colored ramp is made with the Image>New>Ramp command and given the same color table as the cisternae (Image>Lookup Table>GreenFireBlue).
10. Both Cisternal Persistency Maps and Tubule Persistency Maps are color coded to show the most and least persistent values (Fig. 6l). Those that persist (are added together) in the same position for 32 s (the first 8 s difference interval and then 24 s thereafter, or 15 of the 45 difference frames) can be thresholded, measured, and counted.

3.4.8 Analysis of network movement using optical flow with LPX flow (Fig. 7)

1. LPX flow (Plugin>LPX>LPXflow) starts by subtracting the temporally averaged image from the data set. This is done by checking the subtAvgT box in the first dialog box that comes up (Fig. 7a). The temporally averaged image includes several of the persistent features in the data set. This differentiates it from the persistency map above and emphasizes the fact that it is the change between frames that is being measured.
2. It then implements a cross-correlation function based on spatiotemporal image correlation spectroscopy (STICA [35, 36]). The motion is examined by the cross-correlation of pixel blocks. The position of peaks produced by the cross-correlation

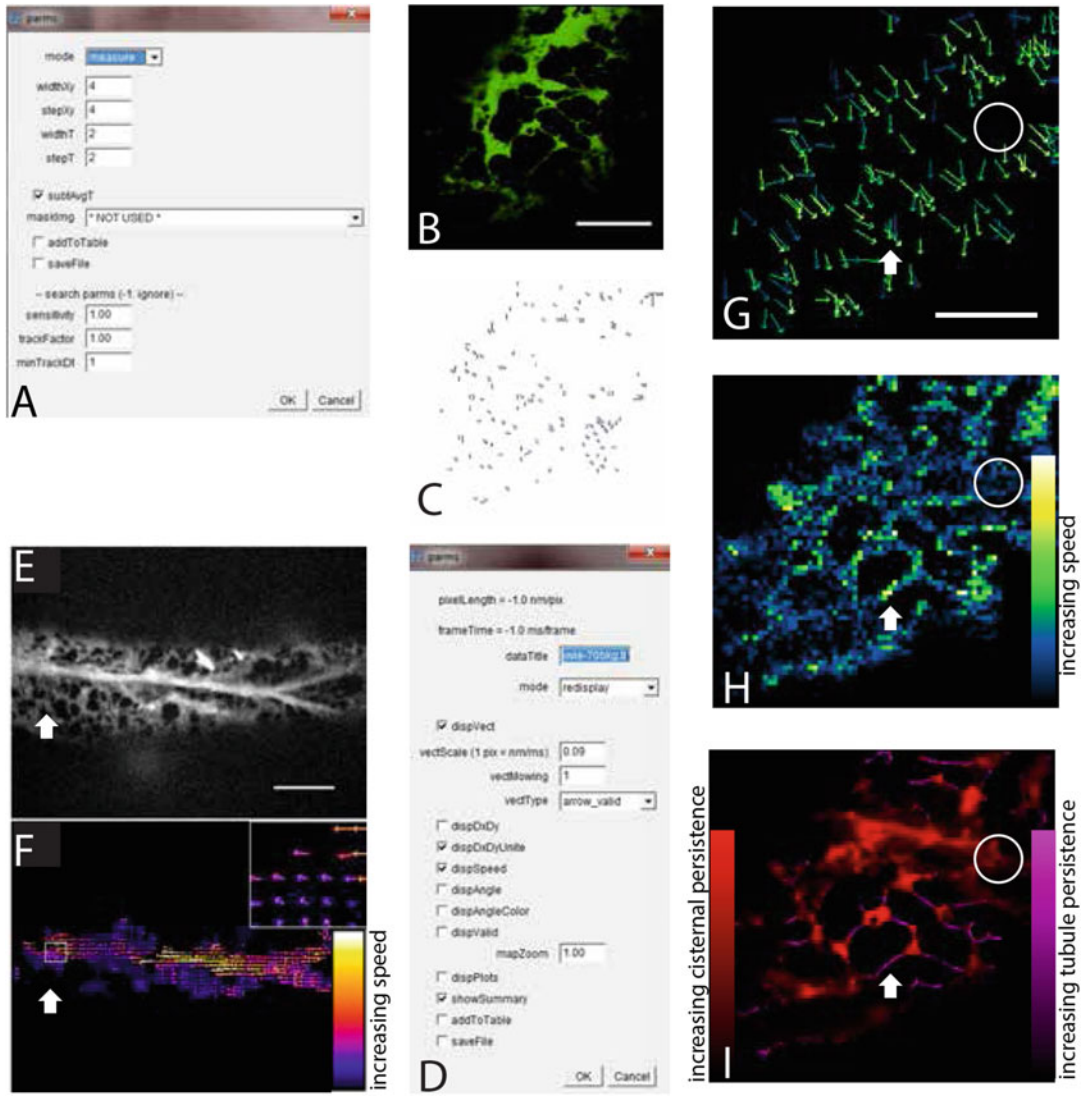

Fig. 7 Optic flow analysis of movement in ER using LpxFlow. (**a**) The dialog box that comes up with the Plugins>LPX>LPXflow command. The settings are set so that there is 4 × 4 matrix being analyzed using spatiotemporal image correlation over an interval of every two frames. Subtracting the average intensity over time is selected. The mask option is not available. (**b**) Image of first frame of time series with background subtracted. Scale bar = 10 μm. (**c**) First image of image stack resulting from clicking OK in (**a**) showing the position of vectors having various directions and different colors representing different magnitudes. (**d**) Second dialog box that comes after the Plugins>LPX>LPXflow command is re-entered with the image stack (**c**) open. DispVector (display vector) is checked. The vector scale is derived by dividing pixel size in nm by the frame interval in milliseconds. Vector type is chosen as arrows. (**e**) Image 2S from [9] supplementary data showing fluorescence of the ER network in the petiole tissue from arabidopsis. Scale bar = 10 μm. (**f**) The *arrow* vectors shown from one frame from a 16 × 16 pixel matrix, pseudocolored to show speed. *Arrows* in (**e**) and (**f**) show masked region where polygonal network is excluded. (**g**) *Arrow vector* display from (**c**). Bar = 10 μm. (**h**) Summed speed values from network from checking the DispSpeed output setting in (**d**). (**i**) Persistency Map of same region showing more persistent tubules (*magenta*) and more persistent cisternae (*red*). Note that in areas of high tubule persistence, the optic flow program shows high speed (*arrows* **g**, **h**, and **i**). Also note that areas of low cisternal persistence are areas of low speed (*circles* in **g**–**i**)

is a measure of how well the two blocks in subsequent frames match. These peaks, therefore, represent the amount and direction (a vector) by which the second image block has to be moved in time and space in order to best match the first image block. The variables defined by the user and the system are:

- The spatial lag variables in the x and y direction, respectively, ξ and η.
- The temporal lag variable, τ, or the time difference between frames.

3. The above variables are entered in the interface (Fig. 7a) and the space block and time difference (frame difference) over which the optic flow operates is defined. In the case of the example data set (Fig. 7b, also used in Figs. 3 and 5), the time is 1.6 s per frame and the pixel size is 121 nm. In the analysis between every second frame is chosen (widthT and step T = 2). A pixel block size of 4 pixels is chosen (widthXy and step Xy = 4). The output from clicking OK in the first dialog box is shown in Fig. 7c. This shows the displacement or flow vector calculated on all pairs of correlated time-successive 4 × 4 blocks.
4. Once Fig. 7c is generated, other image plots of the data can be produced by using the Plugin>LPX>LPXflow command while this image is open. This second reiteration of the command produces the dialog box in Fig. 7d. Figure 7e and f show part of Supplemental Fig. S2 from [9], which has an image of the cortical cytoplasm of petiolar tissue from arabidopsis labeled with GFP-HDEL (Fig. 7e) and a flow map of the region in Fig. 7f. Figure 7f has, however, been masked using the MaskImg pull-down from the first LPXflow dialog box (Fig. 7a). The mask applied to Fig. 7e is generated to remove the regions containing "Error vectors." These are regions which exclude the relatively static polygonal regions of the ER, leaving areas that include the fast flow rates of ER motion (Fig. 7f and inset). As shown by the large white arrows in Fig. 7e and f, much of the labeled network is removed from the image, but the region containing bundles of dynamic ER remain has been rendered using the vectType pull-down in Fig. 7d using the arrow_valid choice. Figure 7g shows an arrow vector map of one of the sequences in the data set starting with image Fig. 7b but with no masking. Note that when the mask is not included in the approach, the flow velocities do not correlate with persistency mapping. Comparing circled regions in Fig. 7h (sum of speed maps shown when dispSpeed is checked in Fig. 7d with i; persistency map like that shown in Fig. 6i, but with different color tables), it can be seen that areas of low persistency (circled

region, Fig. 7i, high degree of remodeling) can show low flow velocities (circled region, Fig. 7h), whereas in the persistent tubule region indicated by the arrow in Fig. 7i, there can be high flow velocities (arrow in Fig. 7h). This lack of correlation is because *network movement* of the ER is not the same as *network flow* within the ER. However, optic flow approaches do not distinguish between these two types of network dynamics. To assess network flow, the two following approaches are described.

3.5 Network flow

3.5.1 Measurement of directional vs. nondirectional (diffusive) flow in tubules using FRAP and iFRAP (Fig. 8)

1. FRAP investigations on directional network flow can be carried out on tubular branch networks that are persistent for about 30 s using persistency mapping. The example used has two separate junctions, one on each side of the main branch (Fig. 8a). Movement of tubules into or out of the region that is being FRAP'ed will invalidate the results, so it is difficult to measure the movement in regions of fast flow, where there are many tubules moving as well as movement of materials within the tubules.
2. The recovery of the region of interest (FRAP ROI—main branch) exposed to the FRAP (Fig. 8b) is monitored using a time window (in this case 150 ms per frame) that allows the exponential curve to be drawn by the software in the FRAP profile plugin (the plugin source is in methods). This time can be entered into the FRAP plugin dialog box (Fig. 8c).
3. To distinguish between directional and nondirectional movement of the photobleached GFP, similar ROIs (Fig. 8b) in adjacent branches are monitored. This is a form of inverse FRAP or iFRAP, so these are iFRAP ROIs (lower branch, upper branch 1 and upper branch 2). These can be monitored using the same FRAP profile plugin.
4. The FRAP profile plugin can compensate for the general bleaching that occurs in the region outside the region containing the FRAP ROI before and after the photobleaching. Because the iFRAP ROIs are also, in part, monitoring the drop in fluorescence outside of the FRAP ROI, it is important to use a region well outside of the FRAP influence, the background ROI (Fig. 8b).
5. The measurement of iFRAP with this technique gives a time of maximal bleaching, followed by options for one or two exponent exponential fit to the data.
6. This approach can identify gated or directional flow, as evidenced by the differential movement of photobleached GFP out of the FRAP ROI (main branch) and into the iFRAP ROIs, with very little going into the lower branch, which recovers very quickly, and with a definite lag in the appearance of maximal

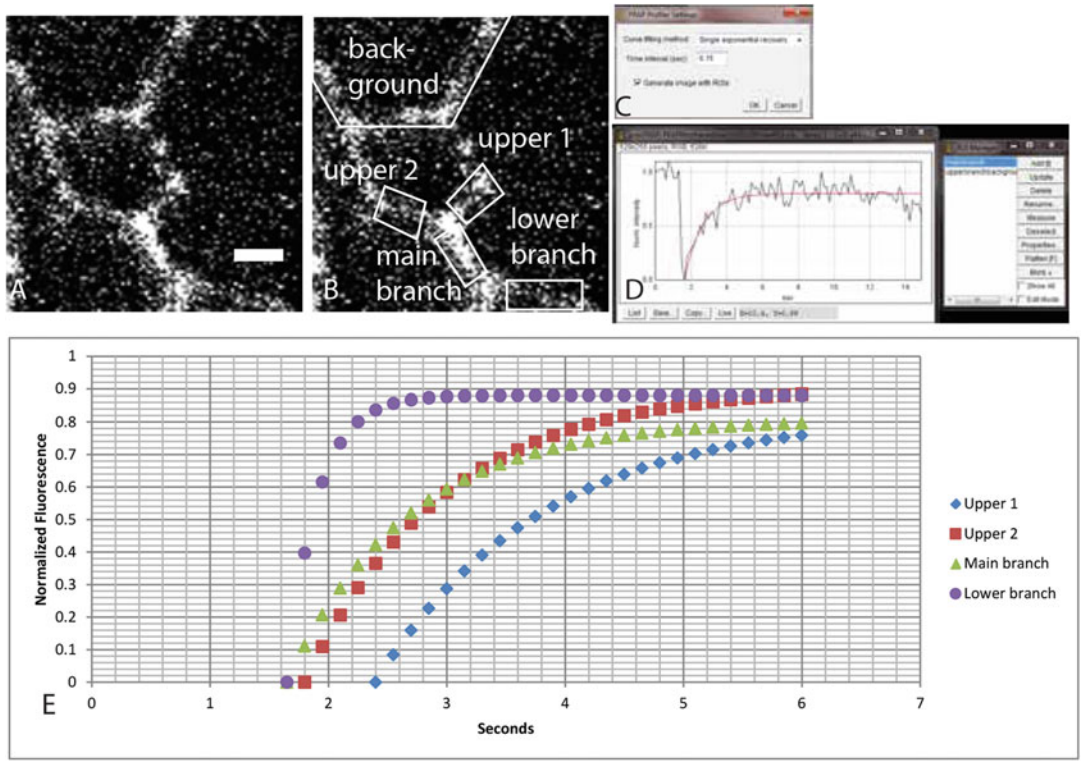

Fig. 8 Analysis of movement of photobleached GFP in ER tubules using FRAP and iFRAP (inverse FRAP). (**a**) Persistent tubule network in the cortical cytoplasm of a cell. Scale bar = 2 μm. (**b**) Regions used for FRAP and iFRAP. FRAP is conducted on the main branch which contained the region of photobleaching (smaller than ROI shown). iFRAP is conducted on two upper branches, 1 and 2, and a lower branch. The background ROI is used to normalize the data and account for any overall photobleaching that results from viewing. (**c**) FRAP Profile dialog box from the Plugins>—FRAP profile command, with the frame time interval entered and a single exponential used to model the data. (**d**) Normalized raw data output from main branch, showing the drawn FRAP curve that is replotted in (**e**). Note that only the main branch and background ROIs are used in this analysis, as shown in the ROI manager in the left-hand panel. (**e**) FRAP for main branch and iFRAP for peripheral branches. Note the time lag in the appearance of upper branch 1, indicating slower movement of the photobleached GFP into that tubule, compared with upper branch 2 and lower branch. The very fast recovery in the lower branch is probably due to the small amount of photobleached GFP entering that branch, indicating the GFP is flowing away from this branch into the upper branches via the main branch

photobleached GFP going into upper branch 1 and upper branch 2. The role of the 3D organization of the ER network in this differential flow [16, 18] has yet to be determined (*see* **Note 11**).

3.5.2 Analysis of advective and active flow of aggregated YFP in constitutively stressed ER within the lumen of the ER using the particle tracking plugin, TrackMate (Fig. 9)

When the ER is constitutively stressed (*ceh1* mutants [21]), aggregates appear in the tubules (Fig. 9a). However, in regions of the cortex with polygonal networks, these aggregates are usually at the vertices of polygons that can be seen when all of the sequences are summed (Fig. 9b). Other tubule aggregates are very dynamic and move by active flow. This can be measured with TrackMate.

1. TrackMate uses a temporal optimization algorithm based on a mathematical framework called the Linear Assignment Problem (LAP) that calculates the cost matrices for certain linkages of the identified particles in frame 1 to frame 2 to etc. [37] and the merging and splitting of particles (simple LAP ignores merging and splitting).
2. The spatial and time characteristics of the image sequence need to be carefully calibrated and entered. It is often best to do this in the Image>Properties command which then defines the metadata used for the TrackMate program (Fig. 9c).
3. The program uses a variety of filters to identify the particles, including particle size, intensity thresholding, Laplacian of Gaussian or Difference of Gaussian filters, and a median filter to reduce noise (Fig. 9d). The spots can be previewed by clicking the Preview button in the spot detector dialog box (Fig. 9d). When the particles or spots are identified, they can be displayed by intensity and confidence level. The confidence level of particle assignment can then be used to further refine the selection of particles.
4. The maximal distance between particles that are to be linked and the maximal number of frames in which the particle disappears are entered manually as part of the LAP program (Fig. 9e).
5. The tracks are then calculated and displayed as overlays using either the track index or other track properties (Fig. 9f). The merging or splitting of particles is calculated after the tracks have been assigned. Figure 9g and H compare the tracks in a trimmed and untrimmed sequence. The trimming was done to eliminate the several of the large ER bodies in the cytoplasm. In the trimmed sequence, the distance for connection between particles in subsequent frames was decreased from four times the particle diameter (0.5 μm) to three times the particle diameter. The track statistics are saved in data tables and can be accessed by spreadsheet programs such as Microsoft Excel. They can also be plotted by track length and time of entry into the field of view or by simply plotting things like track duration vs. track maximum speed, track median speed, or track standard deviation. Track speed standard deviation gives a measure of active flow because its value indicates the degree to which the velocity field varies—high values being more active than low values. By identifying the tracks with higher track speed standard deviation, the regions within the network that have more active flows can be determined.

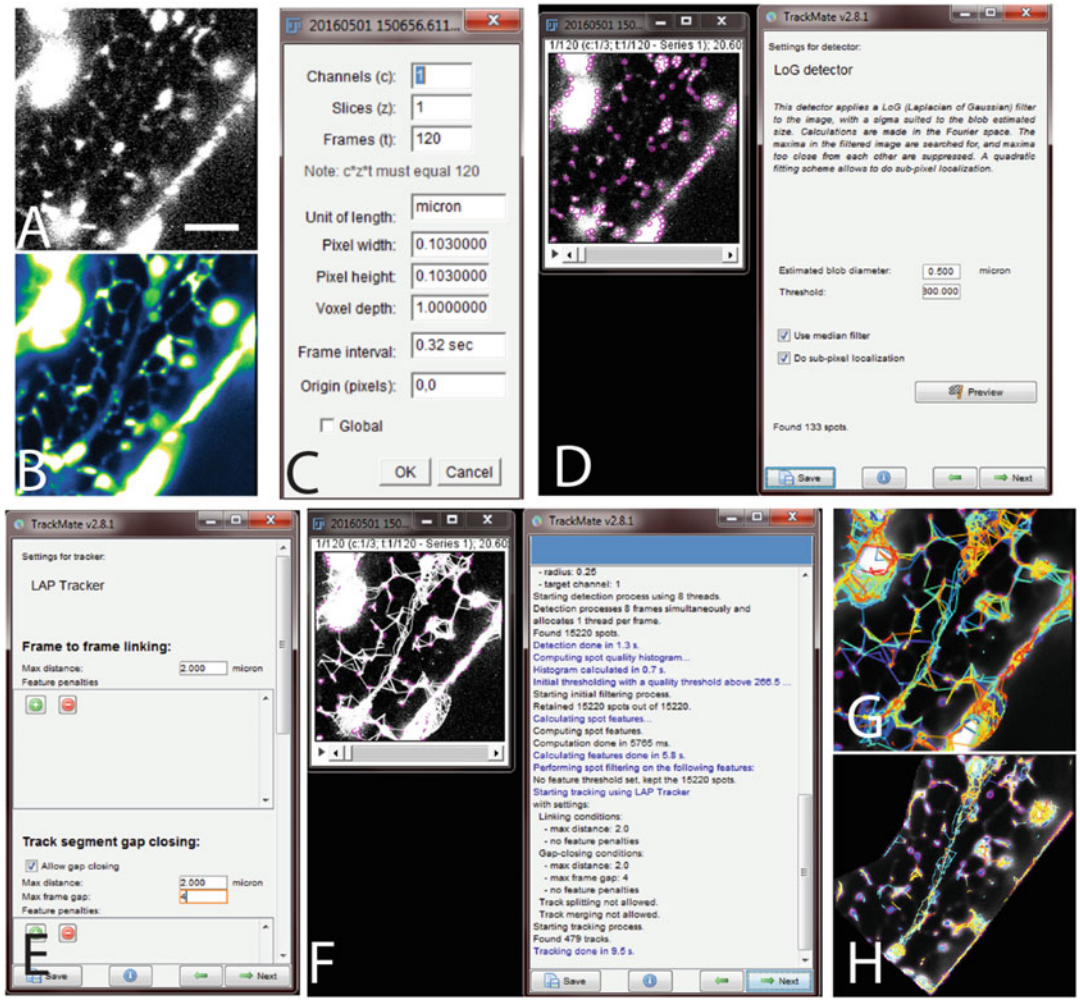

Fig. 9 Analysis of particle movement inside slightly stressed ER using TrackMate. (**a**) ER network as seen in a single frame of a time series in *ceh-1* mutant of arabidopsis which has a low level of constitutive ER stress. Scale bar = 5 μm. (**b**) Summed time sequence of ER dynamics of region in (**a**) showing that the tracks of the ER aggregates move along a typical ER tubule network (low intensity, *blue color*). (**c**) Dialog box from Image>Properties command in ImageJ showing that the sequence is a time interval (not a Z-stack), what the time interval is between stacks, and how big the pixels are. It is important to set this up correctly before running TrackMate. (**d**) Dialog box in TrackMate (Plugins>Tracking>TrackMate). Object identification dialog box (*right-hand side*) allowing particle size and minimum intensity to be selected. Identified objects are previewed as *small purple circles* (*right-hand image*). (**e**) Dialog box for user-entered calculation constraints for the Linear Assignment Problem (LAP) algorithm in TrackMate, showing frame-to-frame linking and gap closing variables in μm and frame to frame gap closing in time. (**f**) Output of track assignment showing calculations and calculation steps (*right-hand side*) and tracks (*left-hand side*). (**g**, **h**) Comparison of tracks using four frame, 3 μm particle gaps (**g**) and two frame, 2 μm particle gaps (**h**)

4 Notes

1. Fluorescent dyes are not recommended for examining ER dynamics in tobacco and arabidopsis.
2. The final preparation of the solvent should be equal to or less than a 1:1000 dilution, this is particularly true with DMSO which we do not recommend in arabidopsis.
3. There are Matlab (https://www.mathworks.com/products/matlab.html) and Python (https://www.python.org/downloads/) implementations of some of these algorithms, but Matlab is proprietary (Octave is the open source project, https://www.gnu.org/software/octave/) and many of the useful Python implementations use Python as an interpreted (non-compiled) wrapper for imaging libraries written in C++ (https://www.visualstudio.com/vs/cplusplus/), e.g., VTK and ITK (www.kitware.org). The great advantage of both the Python and Matlab implementations is that a specific image processing pipeline can be coded for larger data sets from sequential files in sequential directories, but the syntax and file management commands for these languages are beyond the scope of these methods. The additional plugins used are the Image Stabilizer plugin of Kang Li (http://www.cs.cmu.edu/~kangli/code/Image_Stabilizer.html), the Align_slices_in_stack plugin by Qingzong Tseng (https://sites.google.com/site/qingzongtseng/template-matching-ij-plugin), the FRAP plugin of Jeff Hardin (http://worms.zoology.wisc.edu/research/4d/4d.html#frap)—for ImageJ 1.45 s—and LPixel's LPX plugin package (https://lpixel.net/ijp/lpx_iij_plugins_s.jar).
4. Make sure to place the plant grown in 0.9% w/v washed agar in half-strength Murashige–Skoog medium on a slide that already has ~50 μl of buffer, 10 mM MES pH 5.8, on it so that it does not dry out.
5. For young seedlings of arabidopsis and other species, growth and streaming is inhibited by the pressure of the drying coverslip, so elevating the coverslip with two 2 mm × 10 mm single folded strips of Kim Wipe tissues or single strips of filter paper soaked in buffer (about 350 μm thick total) is recommended.
6. Recording Macros is a little tricky for the novice because every click on each window is recorded, but those records can be removed by editing the Macro file (Fig. 1) which appears as the Macro is being recorded in the Macro dialog box.
7. Drift can be avoided (but not always eliminated) by putting VALAP around the coverslip of the object being imaged, so that drying doesn't occur [22]. Drift can also be avoided with

the use a perfusion vessel (however, there may be movement during flow of the perfusion media). During osmotic shock, where the tissue visibly shrinks during analysis (even prior to plasmolysis) and image stabilization is therefore necessary.

8. This algorithm assumes that an image stack is a 3D stack of *z*-dimensional optical sections. In order to evaluate the whole stack, they can be simply made into a montage using the command, Image>Stacks>Make montage. However, this approach makes it difficult to get the information for each image in the stack independently.
9. This algorithm implements a different 3D thinning algorithm [38], written by Ignacio Arganda-Carreras, based on an implementation of the 3D thinning algorithm in ITK (Insight Registration and Segmentation Toolkit, http://itk.org).
10. Large moving cisternae may not be detected as moving within the interval because they are large, i.e., a large region that moves over another large region will be "subtracted out" and not revealed as moving. This is a form of the standard aperture problem, whereby some large object that takes up the region of interest may move, but since its moving edges are outside of the region of interest, the direction and magnitude of the movement cannot be determined.
11. FRAP'ing a region repeatedly can produce ER stress, and immediate ER stress is seen following photostimulation or photobleaching of the chloroplast-ER nexus with 405 nm laser [39]. Although photobleaching with laser lines at 456 and 488 nm does not induce a visible stress response, other work has shown that blue light lasers can cause reorientation of the cortical microtubules in hypocotyl cells [40].

References

1. Griffing LR (2015) Chapter 1: Plant and cell architecture. In: Taiz L, Zeiger E, Moeller I, Murphy A (eds) Plant physiology and development, 6th edn. Sinauer, Sunderland, MA
2. Griffing L (2010) Networking in the endoplasmic reticulum. Biochem Soc Trans 38L:747–753
3. Sparkes I, Runions J, Hawes C, Griffing L (2009) Movement and remodeling of the endoplasmic reticulum in nondividing cells of tobacco leaves. Plant Cell 21:3937–3949
4. Griffing L, Gao H, Sparkes I (2014) ER network dynamics are differentially controlled by myosins XI-K, XI-C, XI-E, XI-1, and XI-2. Front Plant Sci 5:218
5. Griffing LR, Lin C, Perico C, White RR, Sparkes I (2016) Plant ER geometry and dynamics: biophysical and cytoskeletal control during growth and biotic response. Protoplasma. doi:10.1007/s00709-016-0945-3
6. Madison S, Nebenfuehr A (2013) Understanding myosin functions in plants: are we there yet? Curr Opin Plant Biol 16:710–717
7. Muehlhausen S, Kollmar M (2013) Whole genome duplication events in plant evolution reconstructed and predicted using myosin motor proteins. BMC Evol Biol 13:202
8. Tamura K, Iwabuchi K, Fukao Y, Kondo M, Okamoto K, Ueda H, Nishimura M, Hara-Nishimura I (2013) Myosin XI-I links the nuclear membrane to the cytoskeleton to control nuclear movement and shape in Arabidopsis. Curr Biol 23:1776–1781

9. Ueda H, Yokota E, Kutsuna N, Shimada T, Tamura K, Shimmen T, Hasezawa S, Dolja VV, Hara-Nishimura I (2010) Myosin-dependent endoplasmic reticulum motility and F-actin organization in plant cells. Proc Natl Acad Sci U S A 107:6894–6899
10. Lackner LL, Ping H, Graef M, Murley A, Nunnari J (2013) Endoplasmic reticulum-associated mitochondria-cortex tether functions in the distribution and inheritance of mitochondria. Proc Natl Acad Sci U S A 110:458–467
11. Runions J, Brach T, Kuehner S, Hawes C (2006) Photoactivation of GFP reveals protein dynamics within the endoplasmic reticulum membrane. J Exp Bot 57:43–50
12. Koehler R, Schwille P, Webb W, Hanson M (2000) Active protein transport through plastid tubules: velocity quantified by fluorescence correlation spectroscopy. J Cell Sci 113:3921–3930
13. Dayel M, Hom E, Verkman A (1999) Diffusion of green fluorescent protein in the aqueous-phase lumen of endoplasmic reticulum. Biophys J 76:2843–2851
14. Nagaya H, Tamura T, Higa-Nishiyama A, Ohashi K, Takeuchi M, Hashimoto H, Hatsuzawa K, Kinjo M, Okada T, Wada I (2008) Regulated motion of glycoproteins revealed by direct visualization of a single cargo in the endoplasmic reticulum. J Cell Biol 180:129–143
15. Natesan S, Sullivan J, Gray J (2009) Myosin XI is required for actin-associated movement of plastid stromules. Mol Plant 2:1262–1272
16. Sbalzarini I, Mezzacasa A, Helenius A, Koumoutsakos P (2005) Effects of organelle shape on fluorescence recovery after photobleaching. Biophys J 89:1482–1492
17. Sbalzarini I, Hayer A, Helenius A, Koumoutsakos P (2006) Simulations of (an)isotropic diffusion on curved biological surfaces. Biophys J 90:878–885
18. Means S, Smith AJ, Shepherd J, Shadid J, Fowler J, Wojcikiewicz R, Mazel T, Smith G, Wilson B (2006) Reaction diffusion modeling of calcium dynamics with realistic ER geometry. Biophys J 91:537–557
19. Sbalzarini I (2013) Modeling and simulation of biological systems from image data. Bioessays 35:482–490
20. Ölveczky B, Verkman A (1998) Monte Carlo analysis of obstructed diffusion in three dimensions: application to molecular diffusion in organelles. Biophys J 74:2722–2730
21. Walley J, Xiao Y, Wang J-Z, Baidoo EE, Keasling JD, Shen Z, Briggs SP, Dehesh K (2015) Plastid-produced interoganellar stress signal MEcPP potentiates induction of the unfolded protein response in endoplasmic reticulum. Proc Natl Acad Sci U S A 112:6212–6217
22. Lutz DA, Inoué S (1986) Techniques for observing living gametes and embryos. Methods Cell Biol 27:89–110
23. Knebel W, Quader H, Schnepf E (1990) Mobile and immobile endoplasmic reticulum in onion bulb epidermis: short and long-term observations with a confocal laser scanning microscope. Eur J Cell Biol 52:238–340
24. Constantini L, Snapp E (2013) Probing endoplasmic reticulum dynamics using fluorescence imaging and photobleaching techniques. Curr Protoc Cell Biol 60:Unit 21.7
25. Leonhardt N, Marin E, Vavasseur A, Forestier C (1997) Evidence for the existence of a sulfonylurea-receptor-like protein in plants: modulation of stomatal movements and guard cell potassium channels by sulfonylureas and potassium channel openers. Proc Natl Acad Sci U S A 94:156–161
26. Jaquinod M, Villiers F, Kieffer-Jaquinod S, Hugouvieux V, Bruley C, Garin J, Bourquignon J (2007) A proteomics dissection of Arabidopsis thaliana vacuoles isolated from cell culture. Mol Cell Proteomics 6:394–412
27. Nelson BK, Cai X, Nebenführ A (2007) A multicolored set of in vivo organelle markers for co-localization studies in Arabidopsis and other plants. Plant J 51:1126–1136
28. Griffing L (2011) Laser stimulation of the chloroplast/endoplasmic reticulum nexus in tobacco transiently produces protein aggregates (boluses) within the endoplasmic reticulum and stimulates local ER remodeling. Mol Plant 4:886–895
29. Sparkes IA, Runions J, Kearns A, Hawes C (2006) Rapid, transient expression of fluorescent fusion proteins in plants and generation of stably transformed plants. Nat Protoc 1:2019–2025
30. Jain R, Joyce P, Molinete M, Halban P, Gorr S (2001) Oligomerization of green fluorescent protein in the secretory pathway of endocrine cells. Biochem J 360:645–649
31. Pedelacq J, Cabantous S, Tran T, Terwilliger T, Waldo G (2006) Engineering and characterization of a superfolder green fluorescent protein. Nat Biotechnol 24:79–88
32. Ueda H, Yokota E, Kuwata K, Kutsuna N, Mano S, Shimada T, Tamura K, Stefano G, Fukao Y, Brandizzi F, Shimmen T, Nishimura M, Hara-Nishimura I (2016) Phosphorylation of the C terminus of RHD3 has a critical role in

homotypic ER membrane fusion in Arabidopsis. Plant Physiol 170:867–880

33. Zhang TY, Suen C (1984) A fast parallel algorithm for thinning digital patterns. CACM 27:236–239
34. Zack GW, Rogers WE, Latt SA (1977) Automatic measurement of sister chromatid exchange frequency. J Histochem Cytochem 25:741–753
35. Hebert B, Costantino S, Wiseman PW (2005) Spatiotemporal image correlation spectroscopy (STICS) theory, verification, and application to protein velocity mapping in living CHO cells. Biophys J 88:3601–3614
36. Ji L, Danuser G (2005) Tracking quasi-stationary flow of weak fluorescent signals by adaptive multi-frame correlation. J Microsc 220:150–167
37. Jaqaman, K, Loerke, D, Mettlen, M, Kuwata, H, Grinsten, S, Schmid, SL, Danuser, G (2008) Robust single-particle tracking in live-cell time-lapse sequences. Nat. Methods 5:695–702
38. Arganda-Carreras I, Fernandez-Gonzalez R, Munoz-Barrutia A, Ortiz-De-Solorzano C (2010) 3D reconstruction of histological sections: application to mammary gland tissue. Microsc Res Tech 73:1019–1029
39. Griffing, L R (2011) Laser stimulation of the chloroplast/endoplasmic reticulum nexus produces aggregates (boluses) within the endoplasmic reticulum and stimulates local ER remodeling. Mol Plant 4:886–895
40. Lindeboom, J J, Nakamura, M, Hibbel, A, Shuyak, K, Guitierrez, R, Ketelaar, T, Emons, AM, Mulder, BM, Kirik, V, Ehrhardt, D W (2013) A mechanism for reorientation of cortical microtubule arrays driven by microtubule severing. Science 342:1245533

Chapter 8

Preparation of Highly Enriched ER Membranes Using Free-Flow Electrophoresis

Harriet T. Parsons

Abstract

Free-flow electrophoresis (FFE) is a technique for separation of proteins, peptides, organelles, and cells. With zone electrophoresis (ZE-FFE), organelles are separated according to surface charge. The ER is the only remaining major cellular compartment in Arabidopsis not to have been isolated using density centrifugation, immune-isolation, or any other method previously applied to purification of plant membranes. By using continuous-flow electrophoresis ER vesicles of similar surface charge, which may have been fragmented during cell lysis, can be focused. A large portion of these vesicles are of sufficiently different surface charge that separation from the majority of Golgi and other contaminants is possible. Here we adapt an earlier ZE-FFE Golgi isolation protocol for the isolation of highly pure ER vesicles and for tracking the migration of peripheral ER vesicles. Isolating ER vesicles of homogenous surface charge allows multi-'omic analyses to be performed on the ER. This facilitates investigations into structure–function relationships within the ER.

Key words Free-flow electrophoresis, Arabidopsis, Endoplasmic reticulum, Proteomics

1 Introduction

The endoplasmic reticulum (ER) is a dynamic, network-like, membranous organelle that extends throughout the cell via tubules connected by three-way junctions. It seemingly forms connections with most cellular compartments between where it surrounds the nucleus and extends out to tethering points at the plasma membrane (PM). Functionally, it is an important site of protein, lipid, and hormone synthesis, as well as protein quality control and modification, calcium storage and stress responses. Despite its essential biochemical roles, the ER remains one of the few locations within the plant cell which has not been isolated. Proteins have been localized to the arabidopsis ER by LOPIT [1] and fluorescent tagging, rather than the typical organelle-purification route by which most arabidopsis organelles proteomes have been obtained [2, 3]. The ER is the least structurally discrete of all cellular

Chris Hawes and Verena Kriechbaumer (eds.), *The Plant Endoplasmic Reticulum: Methods and Protocols*, Methods in Molecular Biology, vol. 1691, DOI 10.1007/978-1-4939-7389-7_8,

compartments, as shown by recent advances in imaging [4, 5], which no doubt contributes to the difficulty in capturing the ER within a single location on a density gradient. In an earlier "Methods in Molecular Biology" chapter, the isolation of high purity vesicles from the Golgi by free-flow electrophoresis was described [6]. Dynamic and varied structural features make both these organelles difficult to purify using density centrifugation but domains within each organelle that have uniform surface charge can be focused on an electrophoretic gradient, after an initial enrichment. This chapter builds on methods described previously for the Golgi [6] but with specific adaptations for the ER. Recognizing the increased diversity of tubular and cisternal structures within the ER, the initial enrichment gradient is simplified. Membrane washes are included before and after electrophoresis, as ribosomes and abundant ER-lumen proteins released from any ruptured vesicles may dominate proteomic analyses. The majority of ER proteins are focused within approximately ten fractions but, like the Golgi, the ER appears to show evidence of sub-domains with variable surface charge. This is not likely to arise from migration differences of rough vs. smooth ER, as ribosome migration resembles neither group. Additionally, a subgroup of ER proteins has been observed to co-migrate with the Golgi. Therefore particular emphasis is placed on suitable ER markers and tracking ER migration after electrophoretic separation and estimating purity. Instead of using western blotting to monitor marker proteins in FFE generated fractions, Selected Reaction Monitoring (SRM) offers an excellent way of rapidly monitoring membrane migration [7, 8], otherwise data-dependent acquisition and spectral counting can be used [9].

2 Materials

Prepare all solutions using ultrapure water and analytical grade reagents. Prepare all reagents at room temperature. Perform all centrifugation steps at 4 °C. Unless otherwise stated, prepare all buffers the day before and store at 4 °C.

2.1 Arabidopsis Protoplast Preparation

1. Arabidopsis cell suspension culture, temperature-controlled shaking incubator (22 °C, 120 rpm) with constant light (*see* **Note 1**).
2. Arabidopsis cell culture medium: 2% (w/v) glucose, α-naphthalenacetic acid (0.5 mg/L), kinetin (0.05 mg/L), 1× Murashige and Skoog basal salt mixture [10]. Prepare media and adjust to pH 5.7–5.8 with potassium hydroxide (KOH), autoclave for 20 min at 121 °C, and store at 4 °C.
3. Variable speed benchtop orbital shaker with wide orbital (*see* **Note 2**).

4. Protoplasting Buffer: 500 mM Sorbitol, 20 mM 2-(N-morpholino) ethanesulfonic acid (MES), adjust to pH 5.7–5.8 with KOH. Store at 4 °C. Just prior to use, add 1% (w/v) Cellulase "Onozuka" R-10 and 0.05% (w/v) pectolyase Y-23 (Duchefa Biochemie, Netherlands) by vortexing in 30 mL of Protoplasting Buffer.
5. Large capacity preparative centrifuge with 2 × 250 mL tube capacity, e.g., Sorvall SLA-1500.

2.2 Cell Rupture and Crude Membrane Enrichment

1. Homogenization Buffer: 1% (w/v) dextran (Mw 200,000), 0.4 M sucrose, 20 mM disodium hydrogen phosphate (Na_2HPO_4), 3 mM ethylenediaminetetraacetic acid (EDTA), 0.1% (w/v) bovine serum albumin (BSA), 5 mM dithiothreitol (DTT) and one cOmplete EDTA-free protease inhibitor tablet (Roche) (*see* **Note 3**), pH to 7.1 with sodium hydroxide (NaOH).
2. Glass-Teflon Dounce homogenizers (30–50 mL capacity), cooled on ice.
3. Preparative centrifuge with 4 × 50 mL tube capacity capable of 5000 × *g*, e.g., Sorvall SS-34.
4. Ultracentrifuge and swing-out rotor with 40 mL tube capacity capable of 100,000 × *g* for gradients, e.g., Beckman SW-32.
5. Gradient Buffer 1: 25% iodixanol, 20 mM Na_2HPO_4, 3 mM EDTA, pH 7.1 with NaOH (*see* **Note 4**).
6. Gradient Buffer 2: 1.0 M sucrose, 20 mM Na_2HPO_4, 3 mM EDTA, dextran Mw 200,000 (1% w/v), 5 mM DTT (*see* **Note 3**), pH 7.1 with NaOH, can store at −20 °C.
7. Gradient Buffer 3: 0.2 M sucrose, 20 mM Na_2HPO_4, 3 mM EDTA, dextran Mw 200,000 (1% w/v), 5 mM DTT (*see* **Note 3**), pH 7.1 with NaOH, can store at −20 °C.

2.3 Focusing of ER Membranes Using FFE

1. Free-Flow Electrophoresis System: BD™ FFE System (BD Diagnostics, NJ, USA for model years 2006–2010) or FFE System (FFE Service GmbH, Germany, http://www.ffeservice.com/ for model years 2011–present).
2. Spacers and filters for ZE-FFE including 0.5 mm spacer and 0.8 mm electrode filter papers for ZE-FFE (FFE Service GmbH, Germany).
3. 96-Well deep-well plates (2 mL).
4. UV-transparent 96-well plates, e.g., UV-Star (Greiner Bio One, NC, USA).
5. Microplate reader capable of reading absorbance at 280 nm, e.g., Single-Mode Microplate Readers (Molecular Devices, CA, USA).

6. FFE Buffer 1: 280 mM sucrose, 10 mM acetic acid, 10 mM triethanolamine, 1 mM EDTA, pH to 7.0 with NaOH (*see* **Note 5**).
7. FFE Buffer 2: 200 mM sucrose, 100 mM acetic acid, 100 mM triethanolamine, 10 mM EDTA, pH to 6.5 with NaOH (*see* **Note 5**).
8. FFE Buffer 3: 100 mM acetic acid, 100 mM triethanolamine, 10 mM EDTA, pH to 6.5 with NaOH (*see* **Note 5**).
9. Ultracentrifuge and fixed angle rotor with 10–15 mL tube capacity, capable of 100,000 × *g* for sample concentration.
10. 50 mM tris(hydroxymethyl)aminomethane (Tris–HCl), pH 8.0, stored at 4 °C.

2.4 Post-FFE Sample Analysis

1. High grade trypsin, e.g., Trypsin, from porcine pancreas (Sigma-Aldrich, MO, USA).
2. SpeedVac concentrator.
3. Ultra-micro Spin Columns with C_{18} (Harvard Apparatus, MA, USA).
4. ACN1 solution: 80% acetonitrile (v/v) with 0.1% trifluoroacetic acid (v/v).
5. ACN2 solution: 2% acetonitrile (v/v) with 0.1% trifluoroacetic acid (v/v).
6. LC-MS/MS Buffer A (98% water, 2% acetonitrile, 0.1% formic acid).
7. LC-MS/MS Buffer B (98% acetonitrile, 2% water, 0.1% formic acid).
8. Optional—Agilent Technologies (Santa Clara, CA) 6460QQQ mass spectrometer operating in SRM mode, with a Sigma (St. Louis, MO) Ascentis Peptide Express C-18 column (2.1 mm × 50 mm) or similar (*see* **Note 6**).
9. Tandem mass spectrometer (MS/MS) with online liquid chromatography (LC) capabilities (nanoflow or capillary flow rates) capable of data-dependent acquisition. Data in Fig. 1 was generated on a nano-ESI-Q-TOF (TripleTOF 5600 System, AB SCIEX) coupled to an Eksigent nano LC system (AB Sciex) and an Acclaim Pepmap100 C18 column (75 μm × 150 mm, Dionex-LC Packings) at 300 nL/min flow rate.
10. Search engine for analyzing mass spectrometry data to identify proteins, e.g., Mascot (Matrix Science, UK).
11. Optional—Targeted proteomics software, e.g., Skyline (freely available online at http://skyline.maccosslab.org) and Scaffold 4 (Proteome Software, OR, USA).

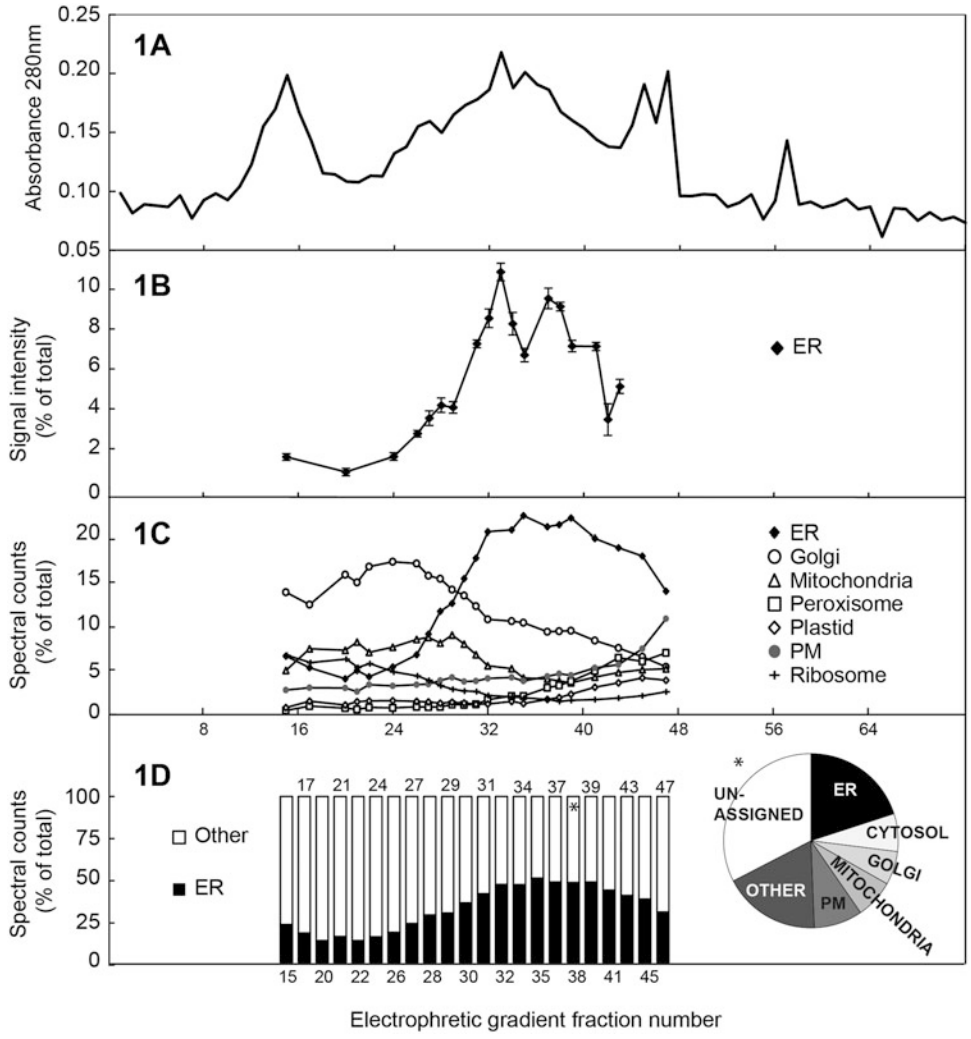

Fig. 1 Distribution of proteins along electrophoretic gradient, after ZE-FFE. (**a**) Total protein distribution was estimated by measuring the absorbance at 280 nm of 250 μL aliquots of fractions after electrophoresis. (**b**) Using the transitions and collision energies given in Table 1, the distribution of the ER was estimated using SRM measurements averaged from six proteins, each protein being averaged from two peptides. Peptide signal intensities were calculated by summing the two highest transition intensities, as described in [11]. (**c**) Spectra were summed for the proteins in each fraction that could be unambiguously assigned to subcellular compartments (based on experimental data housed at SUBA), and presented as a proportion of the total spectra for each fraction to give an estimation of ER migration relative to other organelles. (**d**) Spectral counts from all other organelles were summed and compared to summed spectral counts for ER-localized proteins, to give an estimate of the purity of the most ER-rich fractions. A pie chart gives an overview of protein numbers in ER-enriched fractions, showing that ER abundance is calculated from over 100 proteins in fraction 38*, from a total of 500 proteins with >5 spectra

3 Methods

3.1 Protoplast Preparation of Arabidopsis Cell Suspension Cultures

1. Maintain growing arabidopsis cells in 100 mL aliquots, subculture weekly at 1:10 ratio (*see* **Note 1**). Harvest cells from 4–6 flasks by centrifugation 800 × *g*, 20 °C for 5 min using a 250–500 mL capacity rotor and weigh pellet (*see* **Note 7**).
2. For up to 50 g cells (fresh weight), make 400 mL of Protoplasting Buffer. To 150 mL of Digestion Buffer add 1.0% (w/v) cellulase and 0.05% (w/v) pectolyase in a 4 L wide-bottomed, conical flask. Add cells, ensuring they are adequately suspended in the buffer. Place on an orbital shaker and rotate slowly in the dark for 2.5 h (*see* **Note 8**).
3. Protoplasts are harvested by centrifugation at 800 × *g* for 5 min, the supernatant discarded, and cells gently resuspended in the remaining 250 mL of Protoplasting Buffer without enzymes (*see* **Note 9**).
4. Centrifugation at 800 × *g* is repeated, the supernatant discarded, and cells resuspended in Homogenization Buffer using a ratio of 1:1 (w/v) using the original fresh weight of cells to buffer volume.

3.2 Homogenization of Protoplasts and pre-FFE Enrichment

1. Working at 4 °C, homogenize the protoplasts in Homogenization Buffer using 4–5 strokes at even pressure with a Dounce homogenizer (*see* **Note 10**).
2. Compare pre- and post-homogenized protoplasts under a light microscope to ensure adequate disruption (*see* **Note 10**).
3. Centrifuge homogenate at 5000 × *g* for 15 min (rotor with capacity for 50 mL samples, e.g., Sorvall SS-34).
4. Transfer the supernatant to thin-wall polypropylene tubes suitable for use in an SW-32 rotor, such that tubes are two-thirds full and underlay with 6 mL of Gradient Buffer 1 (*see* **Note 11**).
5. Ultracentrifuge at 100,000 × *g* for 1.5 h (*see* **Note 12**).
6. Remove the supernatant such that the cushion surface is disturbed as little as possible, then remove membranes from the cushion, gently mix in the same volume of homogenization buffer as previously, and repeat **steps 4** and **5** (*see* **Note 13**).
7. After removing the supernatant for a second time, gently layer 15–20 mL of Gradient Buffer 2 on to the membrane cushion, then 12–15 mL of Gradient Buffer 3, or until tubes are at least two-thirds full.
8. Ultracentrifuge samples at 100,000 × *g* for 1.5 h.
9. A single band should be present at the boundary between Gradient Buffer 2 and 3 (*see* **Note 14**).

10. Measure the protein concentration of the collected sample and dilute so the sucrose concentration is as close to FFE Buffer 1 as possible, although a total protein concentration less than 0.75 μg/μL is not recommended. Keep the desired band in a 15 mL tube on ice (*see* **Note 15**).

3.3 Separation of ER Membranes Using ZE-FFE

1. Ensure the FFE system is correctly set up for ZE-FFE, as detailed in Fig. 1 in [6], the temperature set to 8 °C, the media pump has been calibrated, and all necessary quality control tests have been undertaken (*see* **Note 16**).
2. Load *FFE Buffer 1* (inlet tubes 2–6), *FFE Buffer 2* (inlets 1 and 7), *FFE Buffer 3* (electrodes) and slowly fill chamber with buffers avoiding air bubbles. Set the media flow rate to 250 mL/h. Switch on electrode circuits, set the voltage, current, and power to 700 V, 150 mA, and 100 W, respectively, and switch on the voltage (*see* **Note 17**). Allow the system to equilibrate and stabilize for 20–30 min prior to use.
3. Load the sample at a flow rate of 2500–3000 μL/h. The sample should appear homogenous and be visible in the lower half of the separation chamber but is usually too dilute to be seen in the upper half (*see* **Note 18**).
4. After about 10 min, start collecting samples in the precooled 2 mL deep-well plates (*see* **Note 19**).
5. Throughout the ZE-FEE process, monitor protein distribution by removing 150–250 μL from plates and measuring at 280 nm using UV-transparent 96-well plates (Fig. 1a). Protein peak positions and profiles should remain constant throughout separation.
6. Assuming successful enrichment of membrane by density centrifugation, the main peak at 280 nm will constitute a mixture of cis-Golgi and ER membranes (Fig. 1c). The proportion of ER proteins will increase at the cathodic edge of this main peak, and the cis-Golgi to the anodic edge (Fig. 1b and c).
7. After electrophoretic separation, pool fractions from multiple plates and centrifuge at 100,000 × *g* for 60 min (*see* **Note 20**).
8. Remove the supernatant and rinse pellets gently in chilled water (*see* **Note 21**). Resuspend in 50 mM Tris–HCl (pH 8.0), then sonicate for 15 min at 30 s pulse intervals. Measure protein concentration using the Bradford's assay and store resuspended pellets at −80 °C.

3.4 Tryptic Digestion of Samples and Analysis by Mass Spectrometry

1. Reduce, alkylate, and digest at least 10 μg of protein overnight (37 °C) at a 1:40 trypsin:protein ratio in 50% (v/v) ACB.
2. Remove ACN in a SpeedVac concentrator, then resuspend in 50 μL ACN2.

3. Clean and concentrate samples in Ultra-micro SpinColumns (10–25 μL capacity), after washing columns once in ACN1 and priming twice in ACN2. Elute peptides in 50 μL ACN1.
4. Remove ACN in a SpeedVac concentrator, then resuspend in ACN2 to give a concentration of 1 μg/μL, assuming complete protein digestion.
5. Optional analysis using SRM: This method was developed using a 6460QQQ mass spectrometer operating in SRM mode (*see* Subheading 2.4, **item 8**), although other possibilities exist (*see* **Note 6**). Five micrograms of peptide were injected and separated at a flow rate of 400 μL/min over the following gradient: 95% Buffer, 5% Buffer B for 2 min, increased to 40% Buffer B over 15 min, rapidly increase to 90% B over 5 min, held at 90% B for 5 min, decreased rapidly to 5% B, and held for 2 min before the next run. Eluting peptides were ionized by using an Agilent Jet Stream source (sheath gas flow: 11 L/min, sheath gas temperature: 350 °C, nozzle voltage: 1000 V, nebulizing pressure: 30 psi, chamber voltage: 4500 V) operating in positive-ion mode. ER peptide transitions are given in Table 1. These parameters delivered the ER peptide-profiles shown in Fig. 1b.
6. If targeted proteomics analysis is not possible, then peptide samples can be analyzed by liquid chromatography tandem mass spectrometry (LC-MS/MS) using software such as Mascot (Matrix Science, UK). Organelle profiles in Fig. 1c and d were produced using instrumentation as detailed (*see* Subheading 2.4, **item 9**), with a gradient starting at 5% buffer B, increasing to 35% B over 60 min. Over 3 min Buffer B was increased to 90%, held for 15 min, then decreased to 5% Buffer B over 3 min and held for 15 min to re-equilibrate the column (*see* **Note 22**).
7. With sufficient protein of known localization to the ER and other cellular compartments, it is possible to monitor the migration of organelles (*see* **Note 23**). Information on all predicted and previous experimental localizations for proteins can be found at SUBA3 (suba3.plantenergy.uwa.edu.au). By assessing the proportion of proteins within a fraction that have a majority consensus to a given cellular location, the migration of the ER and other organelles can be mapped along the gradient, as in Fig. 1c and d. This proportion can be assessed by simply counting identifications, emPAI values, or the number of spectra associated with each protein [9] (*see* **Note 23**).

3.5 Summary and Future Uses of this Technique

In summary, this method describes how ER proteins can be enriched to approximately 50% of an endomembrane fraction. Some proteins identified in ER-rich fractions may have been substrates transiting the ER, so ER vesicles may comprise more than

Table 1
Transitions used for identification of ER-rich fractions using rapid gradient profiling by SRM

Protein identifier	Gene description	Peptide	Precursor *m/z*	Fragment *m/z*	Retention time (min)	Collision energy (eV)	Precursor ion charge	Fragment type	Fragment number	Fragment charge
AT5G61790.1	CNX	NSDYEGVWK	549.2	896.4	4.9	12.4	2.0	y	7	1
				781.4			2.0	y	6	1
AT5G61790.1	CNX	VVFDLLNK	474.3	848.5	11.0	8.6	2.0	y	7	1
				749.4			2.0	y	6	1
AT1G56340.1	CRT1	TLVFQFSVK	534.8	854.5	12.1	11.7	2.0	y	7	1
				755.4			2.0	y	6	1
AT1G56340.1	CRT1	YVGVELWQVK	534.8	755.4	11.6	15.6	2.0	y	7	1
				608.3			2.0	y	5	1
AT1G52260.1	PDIL1-5	FAEAATALK	461.3	703.4	4.4	8.0	2.0	y	7	1
				574.4			2.0	y	6	1
AT1G52260.1	PDIL1-5	YTVYDGSYK	548.3	732.3	2.5	12.4	2.0	y	6	1
				569.3			2.0	y	5	1
AT1G67490.1	GCS1	LPFTIDIPFISGIK	781.0	989.6	19.3	24.3	2.0	y	9	1
				761.5			2.0	y	7	1
AT1G67490.1	GCS1	TLSSGLDDYPR	612.3	1009.5	6.2	15.7	2.0	y	9	1
				835.4			2.0	y	8	1
AT5G13640.1	PDAT1	ITGPLPDPPGVK	595.8	709.4	8.7	14.8	2.0	y	7	1
				497.3			2.0	y	5	1
AT5G13640.1	PDAT1	LWGGTFGEVYK	628.8	1143.5	10.6	16.5	2.0	y	10	1
				957.5			2.0	y	9	1

Retention times and collisions energies refer to those used in this protocol using the Agilent 6460QQQ

50% of some fractions. Although this technique does not yield completely pure ER fractions, it is an appreciable increase on the purity achieved by density gradient centrifugation. As ER vesicles can be pelted from enriched fractions, this technique offers much interesting potential for lipidomic and metabolomic, as well as proteomic, investigation.

4 Notes

1. This protocol uses a *L. erecta* line similar to MMd2 cells [12] and tolerates a range of light levels. Whichever cell line is used, it is essential that it is a fine suspension culture which readily forms protoplasts.
2. A variable speed benchtop orbital shaker with a large orbital throw is optimal (at least 2 cm); this allows slow rotation while maintaining the cells in solution. This permits efficient enzymatic digestion of the cell wall.
3. DTT and protease inhibitors are added immediately prior to use and can be quickly solubilized by vortexing in 1.0 mL of buffer.
4. 25% iodixanol is prepared by diluting the stock solution twofold with 2× homogenization buffer (without BSA) to give a 30% solution, then diluting to 25% with homogenization buffer. This results in less osmolality extremes than the 1.6 M sucrose cushion used in previous protocols [6].
5. All FFE buffers must be used within 24 h and can be stored at 4 °C. Triethanolamine should be weighed. A generous volume of FFE Buffer 3, e.g., 800 mL for a 1–2 h run, is recommended so the electrode buffers are not exhausted. For FFE Buffer 1, about 1.5 L is required for a run using the conditions described.
6. Start with a minimum of 50 g fresh pellet weight. Before protoplasting, the cell pellet can be spooned out and weighed without damaging cells.
7. Rotate at the lowest possible speed at which cells remain in suspension. Enzymes should be added to the Protoplasting Buffer immediately before use. Enzymes are easily solubilized by vigorous shaking in a 30 mL aliquot of Protoplasting Buffer prior to their addition to the main solution.
8. The pellet/protoplasts are delicate; decant supernatent and resuspend gently to avoid breaking cells.
9. The idea is to rupture protoplasts while minimizing organelle rupture. This is dependent on the number of strokes, the force applied to each stroke, and the fit between the Teflon plunger and glass wall. It is recommended that this step be carefully

optimized, by examining the number of intact protoplasts under a light microscope and the efficiency with which chloroplasts can be pelleted at low speeds to leave a pale, beige but not green, supernatant.

10. Ideally, use around 15–20 g fresh weight starting material per gradient.
11. This step should result in a yellow-white colored band about 2 mm thick (assuming starting with 60 g fresh weight cells). Green coloration implies organelle rupture during protoplast homogenization. Elimination of green should be possible if starting from cell suspension culture but otherwise may not be possible if, e.g., liquid-grown plantlets are used as the starting material. Cytosolic contamination can be decreased by resuspending the band in homogenization buffer, then repeating this centrifugation step.
12. Complete removal of the supernatant is a compromise between quality of step gradient formation and disturbance of the cushion, with ensuing loss of yield.
13. A distinctly formed yellow-white band 1–3 mm thick at the 1.0 M/0.2 M interface will give optimize results obtained after FFE.
14. Ideally, **steps 1** and **2** (Subheading 3.2) should be completed as fast as practicably possible. Tubes containing Gradient Buffer 1 can be prepared in advance. Setup of the FFE and stabilization of the current should have been completed so as to coincide with **step 9**. The current normally takes not more than 20–30 min to stabilize. The conductivity may increase as the sample buffer enters the chamber. This can be rectified by lowering the voltage by, e.g., 20–30 V and waiting approximately 5 min before starting to collect samples.
15. This is a nontrivial task and some previous experience or instructions in the setup of the system for ZE-FFE has been assumed. Use of fresh filters, membranes, and electrode gaskets can improve separation performance considerably. Great care should be taken that the plastic spacer is exactly centered. Tubing sections under the peristaltic pumps should be checked thoroughly for hairline cracks prior to setup and changed if necessary. The sample inlet tubing should be exchanged if any kinks are present. Excessive indentation from the spacer or inlet tube on the lower, temperature cooled plate indicates a change of plastic cover sheeting is required for optimal separation. All FFE buffers should be made up precisely to the stated pH otherwise the conductivity will be too high and the current will not stabilize as desired. Much useful material, including references, is available at http://www.ffeservice.com.

16. Media flow rate and voltage are the two principal parameters that affect sample migration. For different types of sample preparation a ratio between the two should be optimized; however, below 200 MFR diffusion between streams of subcellular compartments may occur. The effect of changing parameters on protein distribution can be instantaneously verified by measuring protein content at 280 nm in UV-transparent 96-well plates.
17. If particulates are present in the sample, pass the sample once through a glass Pasteur pipette.
18. At a flow rate of 250 mL/h, plates will fill in approximately 17 min although shorter fill times will prevent sample warming if a plate cooling device is not available. Store plates at 4 °C and work at 4 °C for **steps 6** and 7 (Subheading 3.3).
19. Assuming eight plates at approximately 1.5 mL per well have been collected, pellets will be visible in all fractions above 0.15 A_{280} (measuring 250 μL at A_{280}), otherwise it may be necessary to pool fractions.
20. If only proteomic analysis of membrane proteins is required, pellets can be resuspended in 100 mM $NaCO_3$, shaken for 30 min at 4 °C and re-pelleted at 100,000 × *g* for 1 h. This will remove soluble proteins sticking to membranes but may result in vesicle rupture.
21. If analyzing ER membrane migration over many fractions, then analysis by a targeted proteomics technique such as SRM is recommended, using the transitions in Table 1. Using a QQQ mass spectrometer using microflow rates is ideal, as short gradients of 30 min or less can be used, dramatically reducing analysis time. Targeted analysis is also possible using a Triple-TOF running at microflow rates. Use of a Q-Exactive operating in PRM mode is also possible but as this must be conducted at nanoflow rates, there is little gain in analysis time.
22. When separating organelles by free-flow electrophoresis using the described methods, variations in instrument setup, buffer conductivity, and cell growth may combine to give a shift in absolute migration distances of about five fractions between experiments. This shift can be up to ten fractions when different instruments are used. However, the relative distribution of organelles should not change. It is therefore recommended that users carefully monitor organelle migration and relate to the total protein profile for several experiments, as in Fig. 1, until users are familiar with their experimental setup.
23. Software such as Scaffold 4.0 facilitates spectral counting but is not essential.

References

1. Dunkley TP et al (2006) Mapping the Arabidopsis organelle proteome. Proc Natl Acad Sci U S A 103:6518–6523
2. Agrawal GK et al (2011) Plant organelle proteomics: collaborating for optimal cell function. Mass Spectrom Rev 30:772–853
3. Drakakaki G et al (2012) Isolation and proteomic analysis of the SYP61 compartment reveal its role in exocytic trafficking in Arabidopsis. Cell Res 22:413–424
4. Kittelmann M, Hawes C, Hughes L (2016) Serial block face scanning electron microscopy and the reconstruction of plant cell membrane systems. J Microsc 263:200–211
5. Nixon-Abell J et al (2016) Increased spatiotemporal resolution reveals highly dynamic dense tubular matrices in the peripheral ER. Science 354(6311):aaf3928
6. Parsons HT, Fernández-Niño SM, Heazlewood JL (2014) Separation of the plant Golgi apparatus and endoplasmic reticulum by free-flow electrophoresis in plant proteomics. Methods Mol Biol 1072:527–539
7. Picotti P, Bodenmiller B, Aebersold R (2013) Proteomics meets the scientific method. Nat Methods 10:24–27
8. Aebersold R, Burlingame AL, Bradshaw RA (2013) Western blots versus selected reaction monitoring assays: time to turn the tables? Mol Cell Proteomics 12:2381–2382
9. Arike L, Peil L (2014) Spectral counting label-free proteomics. In: Martins-de-Souza D (ed) Shotgun proteomics: methods and protocols. Springer New York, New York, NY, pp 213–222
10. Murashige T, Skoog F (1962) A revised medium for rapid growth and bio assays with tobacco tissue cultures. Physiol Plant 15:473–497
11. Dahl RH et al (2013) Engineering dynamic pathway regulation using stress-response promoters. Nat Biotechnol 31:1039–1046
12. Menges M, Murray JA (2002) Synchronous Arabidopsis suspension cultures for analysis of cell-cycle gene activity. Plant J 30:203–212

Chapter 9

ER Microsome Preparation in *Arabidopsis thaliana*

Verena Kriechbaumer

Abstract

Microsomes are vesicles derived from the endoplasmic reticulum (ER) when cells are broken down in the lab. These microsomes are a valuable tool to study a variety of ER functions such as protein and lipid synthesis in vitro.

Here we describe a protocol to isolate ER-derived microsomes *Arabidopsis thaliana* seedlings and exemplify the use of these purified microsomes in enzyme assays with the auxin precursors tryptophan (Trp) or indole-3-pyruvic acid (IPyA) to quantify auxin synthetic capacity in microsomal and cytosolic fractions.

Key words Endoplasmic reticulum, Microsomal fraction, Enzyme assays, Arabidopsis

1 Introduction

Microsomes are generally described as vesicle-like structures with a diameter of 100–200 nm that are formed from pieces of the endoplasmic reticulum (ER) after eukaryotic cells are broken down experimentally (Fig. 1); hence microsomes are not found in healthy living cells. Microsomes are still capable of ER functions such as protein synthesis, protein glycosylation, Ca^{2+} uptake, and lipid synthesis and can be used to study all these functions in a test tube [1]. Therefore microsomes have found use in a plethora of experimental approaches and studies (Fig. 2).

Microsomes are purified from other cell compartments and membranes by differential centrifugation at 1,000,000 × *g*. Whole cells, nuclei, and mitochondria pellet at 10,000 × *g* [2] and chloroplasts already at 1000 × *g* [3, 4].

In his publication on the "constitution of protoplasm" Albert Claude named microsomes in 1943 [5] to distinguish these "small granules of undefined nature." He then used this fractionation technique to determine the localization of nucleic acid in leukemic cells [6]. Current applications and use of microsomes for research

Chris Hawes and Verena Kriechbaumer (eds.), *The Plant Endoplasmic Reticulum: Methods and Protocols*, Methods in Molecular Biology, vol. 1691, DOI 10.1007/978-1-4939-7389-7_9,

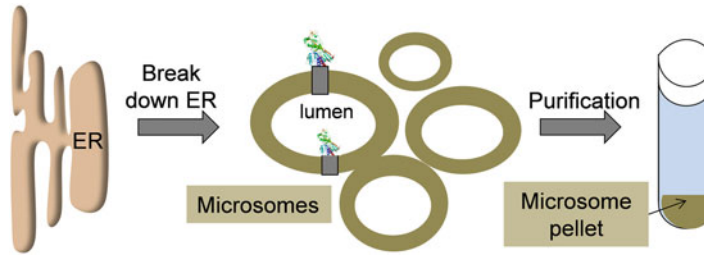

Fig. 1 Schematic representation of microsome purification

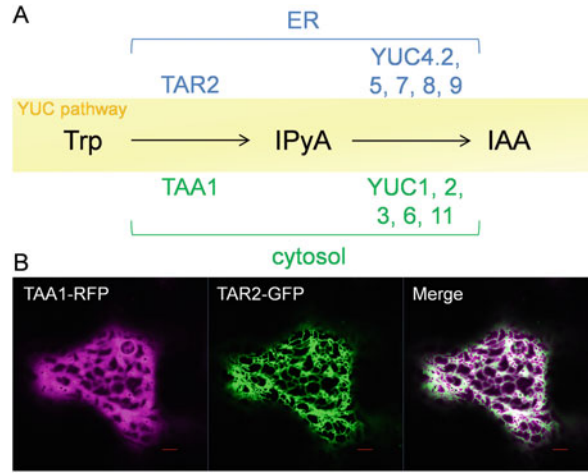

Fig. 2 Subcellular compartmentation of auxin biosynthesis in *Arabidopsis thaliana*. (**a**) YUC-route of auxin biosynthesis in arabidopsis. ER-located enzymes are labeled in *blue*, cytosolic enzymes in *green*. (**b**) Confocal localization for two enzymes in the first step of IAA biosynthesis. TAA1 is present in the cytosol, whereas TAR2 shows ER-location

are for example the areas of lipid secretion [7], P450 assays [8], or auxin biosynthesis [9–11].

A common source for microsomes are dog pancreas cells [12] or rabbit reticulocyte lysate [13]. For plant microsomes wheat germ is a good source [14] or they can be purified from soybeans [15].

Here I describe the isolation of microsomes from *Arabidopsis thaliana* seedlings (adapted from [9–11]).

2 Materials

2.1 Stock Solutions (See Note 1)

2.1.1 For Microsomal Preparation

1. M TEA-HOAc, pH 7.5.
2. 2 M KOAc, pH 7.5.
3. 0.1 M $Mg(OAc)_2$.
4. 1 M Sucrose.

5. 1 M DTT.
6. 0.5 M EDTA.

2.1.2 For IAA Quantification

1. 1 M Tris–HCl, pH 8.0.
2. 1 M Na_2CO_3.
3. 0.1 M NADPH.
4. 0.1 M FAD.
5. 0.1 M indole-3-pyruvic acid (IPyA).
6. 1 M Tryptophan (Trp).

2.2 Buffers

1. Buffer A: 25 mM TEA-HOAc (pH 7.5), 50 mM KOAc, (pH 7.5), 5 mM $Mg(OAc)_2$, 0.25 M Sucrose, 4 mM DTT.
2. Buffer B: 100 mM TEA-HOAc (pH 7.5), 20 mM EDTA.
3. Buffer C: 25 mM TEA-HOAc (pH 7.5), 25 mM KOAc (pH 7.5), 2 mM $Mg(OAc)_2$, 0.5 M Sucrose, 4 mM DTT.
4. Buffer D: 25 mM TEA-HOAc (pH 7.5), 0.25 M Sucrose, 1 mM DTT.

2.3 Equipment

1. Porcelain mortar and pestle.
2. Glass bottles for buffers.
3. Cheese cloth.
4. Refrigerated table centrifuge.
5. Ultracentrifuge with swing-out rotor (e.g., SW41, Beckman Coulter).
6. Ultracentrifuge corex tubes.
7. 2 ml Potter–Elvehjem homogenizer with glass rod.
8. Water bath (37 °C).
9. Speed-vac.
10. Nanodrop spectrophotometer, or equivalent, to determine protein concentration.

3 Methods

3.1 Endoplasmic Reticulum (ER) Microsome Preparation

(This part of the procedure will take between 3 and 4 h depending on sample size.)

1. All steps are carried out on ice or at 4 °C unless indicated otherwise.
2. All buffers, tubes, etc. used in the procedure should be pre-cooled (*see* **Note 2**).
3. 5 g of arabidopsis seedling tissue (7 days after germination, *see* **Notes 3–5**) are ground to fine powder in liquid nitrogen using a pre-cooled mortar and pestle.

4. The powder is then homogenized in 4 ml of ice-cold buffer A and transferred into a 50 ml falcon tube.
5. 4 ml of ice-cold buffer B are added to the tube and the suspension is incubated on ice for 10 min. Then the homogenate is centrifuged at 1000 × *g* for 10 min at 4 °C. The resulting supernatant is poured over four layers of cheese cloth into a fresh falcon tube. At this step, the resulting extract is considered total plant extract for later enzymatic assays. The extract is centrifuged again at 4500 × *g* for 25 min at 4 °C.
6. A 4 ml sucrose cushion (buffer C) is layered on the bottom of ultracentrifuge corex tubes.
7. The 8 ml of plant suspension is layered on top of this sucrose cushion by slightly angling the tube and carefully and slowly pipetting the suspension at the side of the tube. The tube is centrifuged for 90 min at 93,000 × *g* (ultracentrifuge with swing-out rotor, e.g., SW41).
8. The resulting pellet is removed from the ultracentrifuge tube if necessary with 20 μl of buffer D and transferred to a 2 ml Potter–Elvehjem homogenizer. The supernatant is kept and used as cytosolic extract in later IAA quantifications.
9. The final pellet was resuspended in 200 μl of buffer D using a glass rod and a 2 ml Potter–Elvehjem homogenizer. Protein content is measured using a Nanodrop spectrophotometer. Freshly prepared microsomes should be used for enzymatic assays straight away (*see* **Note 6**).

3.2 Purity of Microsomes

To check for the purity of the microsomal fraction both the microsomal and the cytosolic fraction can be probed with an anti-HSP70 antibody detecting cytosolic heat shock protein 70 (Fig. 3). The

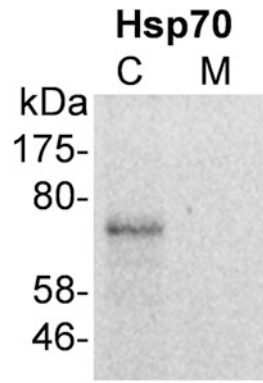

Fig. 3 Immunoblot analysis for purity of microsomal fractions. Microsomal (M) and cytosolic (C) fractions were tested for heat shock protein 70 (HSP70) using immunoblot analysis. 100 μg of protein from each fraction were probed with anti-HSP70 antibodies (1:1000) recognizing the cytosolic HSP70

HSP70 band is only detected in the cytosolic fraction indicating a rather pure microsomal fraction.

Further purity tests using immunoblot analysis could include testing for the presence of plasma membrane or mitochondrial proteins in the microsomal fraction.

3.3 Example for Microsomal Enzymatic Tests

The YUC-route of auxin biosynthesis is a two-step process (Fig. 2): In arabidopsis TAA-proteins (Tryptophan Aminotransferase of Arabidopsis), TAA1, TAR1, and TAR2 are converting tryptophan (Trp) to indole-3-pyruvic acid (IPyA) [16] which is then converted by YUC proteins to IAA (YUC1-11) [17]. It was shown that TAR2, YUC4.2, 5, 7, 8, and 9 are located on the ER, whereas TAA1 and YUC1, 2, 3, 6, and 11 are located in the cytosol [10].

Enzymatic activity tests (100 µl total volume) with microsomal and cytosolic fractions were carried out in the following manner:

1. In 2 ml Eppendorf tubes mix carefully: 20 µl of microsomal or cytosolic extract, 1 mM NADPH, 100 µM FAD, 100 µM IPyA or Trp (depending on experimental interest).
2. 100 mM Tris–HCl (pH 8.0) up to a total volume of 100 µl.
3. The assays are incubated for 1 h in a 37 °C water bath and snap-frozen in liquid nitrogen straight after the incubation time.
4. At this stage the assays can be stored at −20 °C before the IAA analysis is carried out.

3.4 Auxin Biosynthetic Capacity in Arabidopsis Microsomes

Representative data for the conversion of tryptophan and IPyA to IAA in arabidopsis seedlings is shown in Fig. 4 [10].

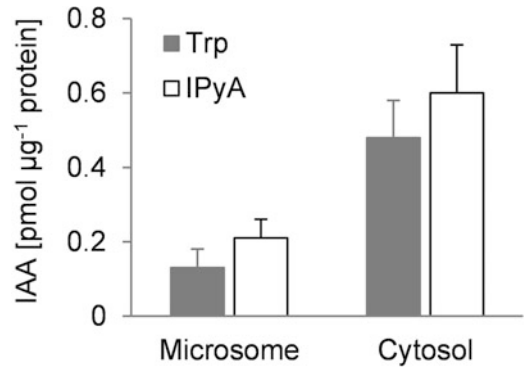

Fig. 4 Auxin biosynthetic capacity in arabidopsis seedlings. Enzymatic conversion of tryptophan to IAA by microsomal (Microsome) fractions or cytosolic (Cytosol) fractions from arabidopsis seedlings 7 days after germination. Standard errors are indicated. $n = 3$

4 Notes

1. Filter buffers 1–4 through 0.45 μm syringe filters. Add DTT from 1 M stock fresh prior to use.
2. Pre-chill tubes, glassware, buffers, centrifuges, etc. and keep your samples on ice as much as possible.
3. Tissue: depending on the biological question instead of using whole seedlings for the microsomal preparation it can, e.g., be distinguished between root and shoot or other ages and developmental stages can be used.
4. This preparation has also been successfully used for maize [9] and tobacco tissues (unpublished).
5. Collect plant material straight into a chilled falcon tube that is kept on ice and try to collect the material as quickly as possible.
6. Where possible timewise freshly prepared microsomes should be used for enzyme assays. Freezing in 20% glycerol for later assays is possible but not recommended.

Acknowledgements

This work was supported by a research scholarship from the Korean Federation of Science and Technology Societies (KOFST) awarded to Dr. Verena Kriechbaumer and the British Biotechnology and Biological Sciences Research Council (grant no. BB/J004987/1 research grant) awarded to Prof. Chris Hawes.

References

1. Alberts B, Johnson A, Lewis J, Morgan D, Raff M, Roberts K, Walter P (2014) Molecular biology of the cell, 6th edn. Science, Garland
2. Nagahashi J, Hiraike K (1982) Effects of centrifugal force and centrifugation time on the sedimentation of plant organelles. Plant Physiol 69:546–548
3. Tobin AK, Bowsher CG (2004) Subcellular fractionation of plant tissues: isolation of plastids and mitochondria. Methods Mol Biol 244:53–63
4. Kriechbaumer V, Shaw R, Mukherjee J, Bowsher CG, Harrison AM, Abell BM (2009) Subcellular distribution of tail-anchored proteins in Arabidopsis. Traffic 10:1753–1764
5. Claude A (1943) The constitution of protoplasm. Science 97:451–456
6. Claude A (1944) The constitution of mitochondria and microsomes, and the distribution of nucleic acid in the cytoplasm of a leukemic cell. J Exp Med 144(80):19–29
7. Yao Z, Zhou H, Figeys D, Wang Y, Sundaram M (2013) Microsome-associated lumenal lipid droplets in the regulation of lipoprotein secretion. Curr Opin Lipidol 24:160–170
8. Clausen M, Kannangara RM, Olsen CE, Blomstedt CK, Gleadow RM, Jørgensen K, Bak S, Motawie MS, Møller BL (2015) The bifurcation of the cyanogenic glucoside and glucosinolate biosynthetic pathways. Plant J 84:558–573
9. Kriechbaumer V, Seo H, Park WJ, Hawes C (2015) Endoplasmic reticulum localization and activity of maize auxin biosynthetic enzymes. J Exp Bot 66:6009–6020
10. Kriechbaumer V, Botchway SW, Hawes C (2016) Localization and interactions between Arabidopsis auxin biosynthetic enzymes in the

TAA/YUC-dependent pathway. J Exp Bot 67:4195–4207

11. Kriechbaumer V (2016) ER microsome preparation and subsequent IAA quantification in maize coleoptile and primary root tissue. Bio-protocol 6(9):e1805
12. .Walter P, Blobel G (1983) Preparation of microsomal membranes for cotranslational protein translocation. Methods Enzymol 96:84–89
13. Jackson R, Hunt T (1983) Preparation and use of nuclease-treated rabbit reticulocyte lysates for the translation of eukaryotic messenger RNA. Methods Enzymol 96:50–74
14. Erickson AH, Blobel G (1983) Cell-free translation of messenger RNA in a wheat germ system. Methods Enzymol 96:38–50
15. Abell BM, Holbrook LA, Abenes M, Murphy DJ, Hills MJ, Moloney MM (1997) Role of the proline knot motif in oleosin endoplasmic reticulum topology and oil body targeting. Plant Cell 9:1481–1493
16. Zhao Y, Christensen SK, Fankhauser C, Cashman JR, Cohen JD, Weigel D, Chory J (2001) A role for flavin monooxygenase-like enzymes in auxin biosynthesis. Science 291:306–309
17. Stepanova AN, Robertson-Hoyt J, Yun J, Benavente LM, Xie DY, Dolezal K, Schlereth A, Jürgens G, Alonso JM (2008) TAA1-mediated auxin biosynthesis is essential for hormone crosstalk and plant development. Cell 133:177–191

Chapter 10

ER Membrane Lipid Composition and Metabolism: Lipidomic Analysis

Laetitia Fouillen, Lilly Maneta-Peyret, and Patrick Moreau

Abstract

Plant ER membranes are the major site of biosynthesis of several lipid families (phospholipids, sphingolipids, neutral lipids such as sterols and triacylglycerols). The structural diversity of lipids presents considerable challenges to comprehensive lipid analysis. This chapter will briefly review the various biosynthetic pathways and will detail several aspects of the lipid analysis: lipid extraction, handling, separation, detection, identification, and data presentation. The different tools/approaches used for lipid analysis will also be discussed in relation to the studies to be carried out on lipid metabolism and function.

Key words Ceramides, GC-FID, GC-MS, Glucosylceramides, HPTLC, LC-MS, Long chain bases (LCB), Phospholipids, Phytosterols, Triacylglycerols

1 Introduction

ER membranes are known to be involved in many key cellular functions and understanding more precisely their role, being able to analyze their lipid composition and metabolism/homeostasis is as crucial as it is for ER proteins.

Of course to be able to perform such lipid analysis, we must handle highly purified ER membranes devoid of other membrane contaminants, something which is not so obvious as it will depend on the plant material considered. According to the starting material, different methodologies with various efficiencies in isolating highly purified ER membranes (differential ultracentrifugation, free-flow electrophoresis, two phase partition systems, affinity purification) alone or in combination have to be used ([1–3] and references therein).

Table 1 details the lipid composition of the ER membranes from different plant species and tissues, that have been combined from the literature to give a simplified view of the different lipid families/species and their relative abundance. The corresponding biosynthetic pathways of the different lipid classes of the ER

Chris Hawes and Verena Kriechbaumer (eds.), *The Plant Endoplasmic Reticulum: Methods and Protocols*, Methods in Molecular Biology, vol. 1691, DOI 10.1007/978-1-4939-7389-7_10,

Table 1
Lipid composition of plant ER membranes in mol%[a]

PA°	lPC	PC	PE	PG	PI	PS	GlcCer	Free sterols	Conjugated sterols
0.5–7	0.8–1.7	36–65	11–23	3.5–5	2.5–17.5	1–7	2–8	3–14	1–4

°Generally, PA is considered and found to be low/very low in the ER membranes and in most plant cell membranes because it is an intermediary metabolite and a signaling phospholipid. So most of the time, high amounts of PA are probably due to Phospholipase D activation during material handling and/or lipid extraction

[a]Data combined from several plant species and tissues ([12–14] and references therein, and unpublished results). *PA* Phosphatidic Acid, *lPC* lysoPhosphatidylCholine, *PC* PhosphatidylCholine, *PE* PhosphatidylEthanolamine, *PG* PhosphatidylGlycerol, *PI* PhosphatidylInositol, *PS* PhosphatidylSerine, *GlcCer* Glucosylceramides. Conjugated sterols: sum of sterol glycosides + steryl esters

membranes are presented in Fig. 1 for phospholipids, in Fig. 2 for glucosylceramides, and in Fig. 3 for sterols.

The pretty large variations in lipid amounts which can be observed (Table 1) can be due of course to the differences in the plant species/tissues but also to some extent to the purity of the ER membranes according to the isolation procedures used. Anyway, Table 1 indicates that the major lipid families/species are represented by the phospholipids, followed by the sterols (free and conjugated) and the glucosylceramides (GluCer). Other lipid species such as phosphoinositides (PIP, PIP2), acyl-CoAs, and ceramides (precursors of GluCer) are also present but in lower amounts. The levels of diacylglycerol in ER membranes (precursors of phospholipids and also of triacylglycerols for lipid bodies) are not mentioned because their levels can even be more variable.

The purpose of this chapter is not to give an extensive overview of the various lipid methodologies because this has already been done by well-recognized lipid experts in exhaustive set of publications such as in the AOCS Lipid Library (http://lipidlibrary.aocs.org) or in the arabidopsis book [4], but to select some lipid technologies that were, are and will be relevant for studying several aspects of plant ER membranes lipid metabolism.

2 Materials

2.1 Technologies/ Equipment

1. Lipid extraction-preparation/Bench centrifuge, 110 °C dry bath incubator, 110 °C resistant screwed glass tubes, bench vortex.
2. Densitometric analysis/TLC sampler Linomat 5 (Camag, Muttenz, Switzerland), TLC scanner 3 (CAMAG, Muttenz, Switzerland).
3. HPTLC (High Performance Thin Layer Chromatography)/ADC2 automatic developing chamber (Camag, Muttenz, Switzerland), HPTLC plates F254 (Merck, Darmstadt, Germany).

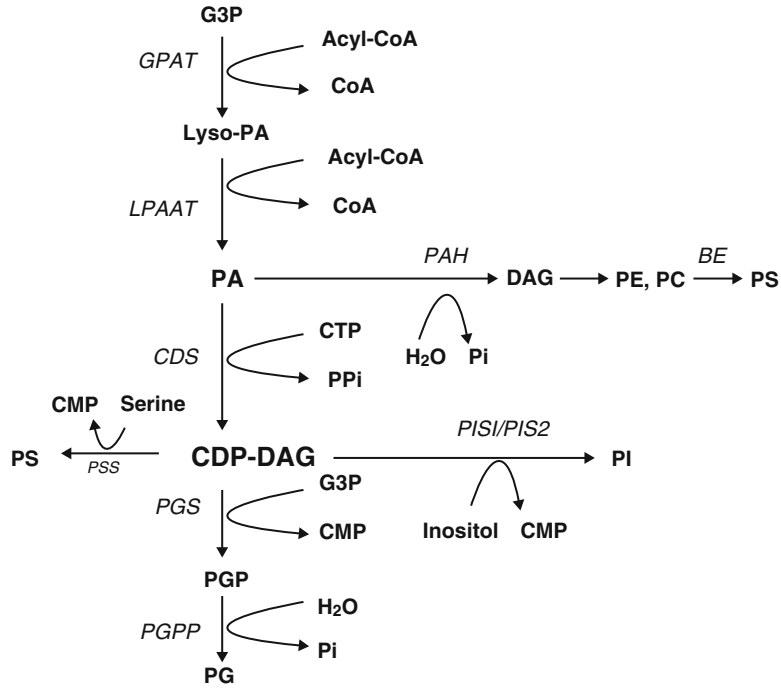

Fig. 1 Simplified phospholipid biosynthetic pathways in the ER. *CDP-DAG* cytidine diphosphate diacylglycerol, *CoA* coenzyme A, *CMP* cytidine monophosphate, *CTP* cytidine triphosphate, *DAG* diacylglycerol, *G3P* glycerol-3-phosphate, *Lyso-PA* lysophosphatidic acid, *PA* phosphatidic acid, *PC* phosphatidylcholine, *PE* phosphatidylethanolamine, *PG* phosphatidylglycerol, *PGP* phosphatidylglycerol phosphate, *PI* phosphatidylinositol, *PS* phosphatidylserine. *Enzymes*: *CDS* cytidine-diphosphate diacylglycerol synthase; *GPAT* glycerol-3-phosphate acyltransferase, *LPAAT* lysophosphatidic acid acyltransferase; *PAH* phosphatidic acid phosphohydrolase; *PGPP* phosphatidylglycerol phosphate phosphatase; *PGS* phosphatidylglycerol phosphate synthase; *PIS* phosphatidylinositol synthase; PSS phosphatidylserine synthase

4. GC-FID (Gas Chromatography-Flame Ionization Detector)/ Agilent 7890 gas chromatograph equipped with flame ionization detection (Santa Clara, CA, USA), Agilent GC Column DB-Wax 15 m × 0.53 mm × 1.0 μm.
5. GC-MS (Gas Chromatography-Mass Spectrometry)/Agilent 6850 gas chromatograph coupled with a MS detector MSD 5975-EI (Santa Clara, CA, USA), HP-5MS capillary column (5% phenyl-methyl-siloxane), 30-m, 250-mm, and 0.25-mm film thickness (Agilent, Santa Clara, CA, USA).
6. LC-MS (Liquid Chromatography-Mass Spectrometry)/QTRAP 5500 (ABSciex) mass spectrometer coupled to a liquid chromatography system (Ultimate 3000, Dionex). Luna C8 150 × 1 mm column with 100-Å pore size and 5-mm particles (Phenomenex).
7. Radiolabeling analysis/PhosphorImager (such as STORM or TYPHOON from GE Healthcare).

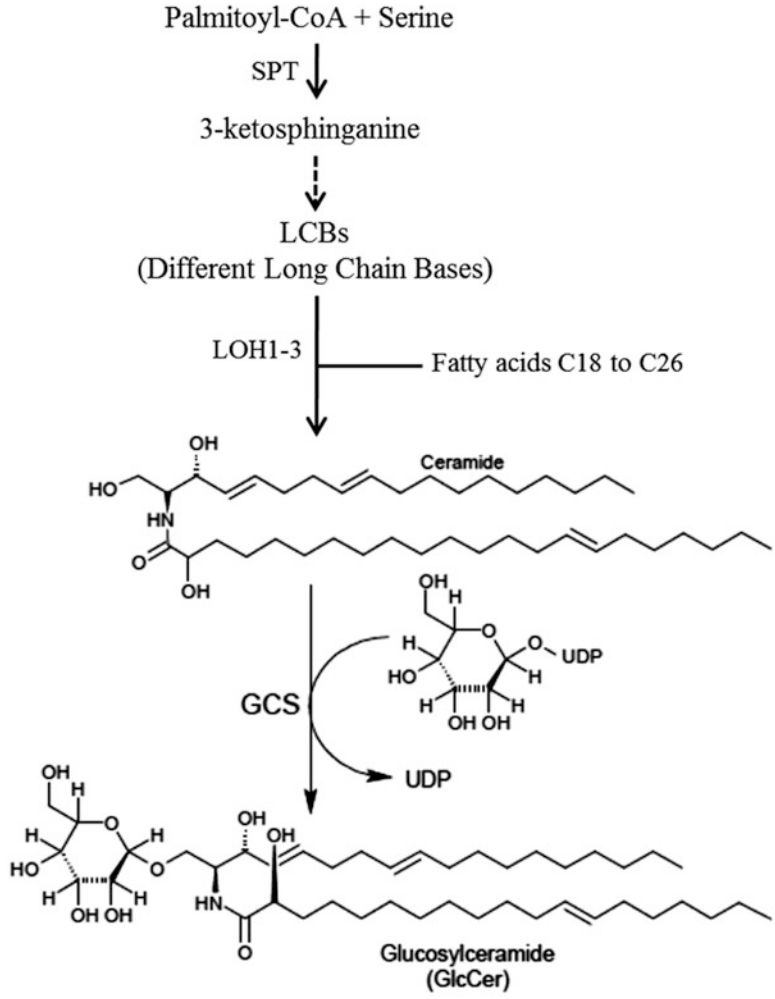

Fig. 2 Simplified GlcCer biosynthetic pathway in the ER. *GCS* glucosylceramide synthase, *LOH1–3* ceramide synthases 1, 2, and 3, *SPT* serine palmitoyl transferase. The *dotted arrow* indicates several enzymatic steps. All the enzymes involved in the biosynthesis of glucosylceramides and its precursors are located in the ER

2.2 Lipid Standards

1. Lipid standards are purchased from Avanti Polar Lipids (Alabaster, AL, USA), Nu-Chek-Prep (Elysian, MN, USA), Matreya, (State College, PA, USA), and/or Sigma (St. Louis, MO, USA). *See* **Note 1**.
2. For HPTLC analysis, all the phospholipid standards (PC, PE, PI, PG and PS) are from soybean extracts excepted PA which can be from any other source, DAG (for example di-18:1), TAG (for example tri-18:1), ceramides (bovine extract), glucosylceramides (soybean extract), sterol (plant extract). *See* also **Note 2**.

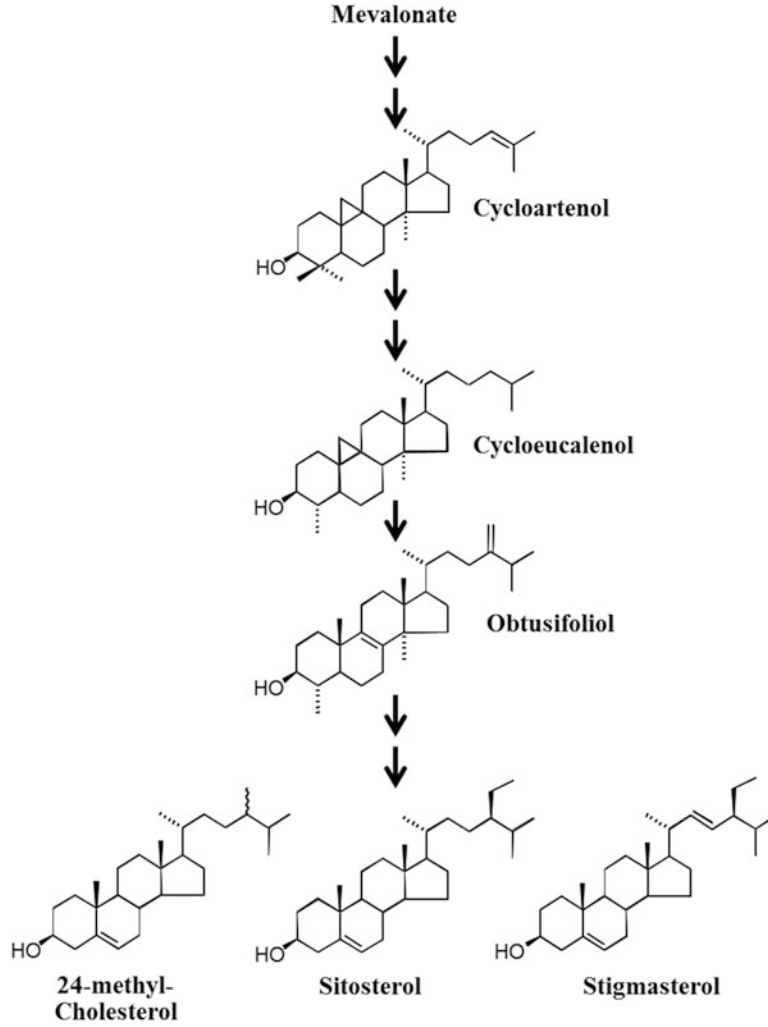

Fig. 3 Simplified sterol biosynthetic pathway in the ER. The *two successive arrows* indicate two or more enzymatic steps. The biosynthesis of the precursor mevalonate by the HMG-CoA reductase is the first step of the sterol biosynthetic pathway which is located in the ER

3. For GC-FID or GC-MS analysis, C17:0, h14:0, d20:0, t17:0, d14:1$^{4(E)}$, and cholestanol.
   For LC-MS analysis, PC, 17:0/17:0; PI, 17:0/14:1; PE, 17:0/17:0; PG, 17:0/17:0; PS, 17:0/17:0, TAG 17:0/17:0/17:0, DAG 17:0/17:0.

2.3 Solutions

1. Eluent A: isopropanol/methanol/H_2O 5/1/4, v/v containing 0.2% formic acid and 0.028% NH_3.
2. Eluent B: isopropanol containing 0.2% formic acid and 0.028% NH_3.

3. Eluent C: acetonitrile/methanol/H_2O (19/19/2, v/v) containing 0.2% formic acid and 0.028% NH_3.
4. Eluent D: isopropanol containing 0.2% formic acid and 0.028% NH_3.

3 Methods

3.1 Lipid Extraction

Whatever the isolation procedure of the purified ER membranes (differential ultracentrifugation, free-flow electrophoresis, two phase partition systems, affinity purification), the ER fraction will be generally obtained as a pellet after centrifugation in order to concentrate the membranes.

Analyzing lipids requires extraction using organic solvents. Extraction should be rapid in order to avoid lipid modifications during treatment. In the case of ER membranes, extraction should be carried out immediately after recovering the ER membranes; otherwise the membranes can be stored at −80 °C (but there is a risk of changes to the lipids).

1. The pellet should be suspended in a small volume (100–300 μl) of distilled H_2O (if protein activity is not necessary to be measured) or in buffer, by gentle grinding rather than vortexing, and transferred into glass tubes (with Teflon protected screw caps) for lipid extraction (plastic apparatus and containers (other than Teflon) should be avoided). One part (5%) of the aliquot should be conserved for protein measurement.
2. Then extract the lipids with chloroform/methanol 2/1, v/v [5] (*see* **Note 3** for acyl-CoAs), using a ratio of chloroform, methanol, and aqueous phase in the final mixture close to 8/4/3, v/v to be efficient.
3. The solution is vortexed or shaken for 5 min, at room temperature. Centrifuge the solution (10 min 3000 rpm) and discard the upper phase (as well as interphase).
4. This organic phase is washed with ¼ of volume of H_2O or 0.9% NaCl; after vortexing for 1 min, the solution is centrifuged (10 min, 3000 rpm (3000 × *g*)) and the lower phase recovered in a new glass tube.
5. The organic solvent is evaporated under air (or nitrogen if particular protection of unsaturated fatty acids is needed). Resuspended the lipids into appropriate solvents required for the subsequent analysis.

The principal methods for lipid class analysis are HPTLC and LC-MS/MS, and for their fatty acid content are GC-FID or GC-MS. Long chain bases of sphingolipids and sterols can be analyzed by GC-MS (a general scheme of lipid analysis is given in Fig. 4).

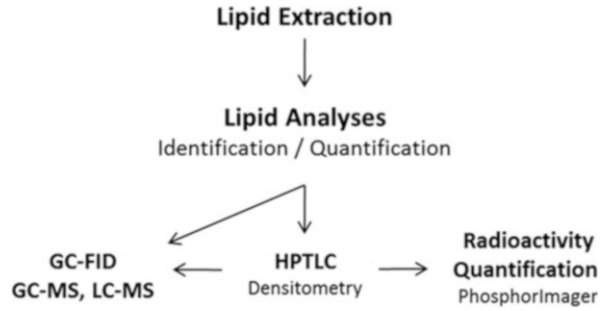

Fig. 4 Different steps of lipid analysis processes. The principal methods for lipid class analysis are HPTLC and LC-MS, and for their fatty acid content are GC-FID or GC-MS. Long chain bases of sphingolipids, and sterols, can be analyzed by GC-MS. *GC-FID* gas chromatography-flame ionization detector, *GC-MS* gas chromatography-mass spectrometry, *SPE* solid phase extraction, *HPTLC* high performance thin layer chromatography

3.2 HPTLC Analysis of Phospholipids and Acyl-CoAs

1. For analysis of phospholipids with HPTLC plates, the lipids should be resuspended into 50–200 μl of chloroform/methanol 2/1, v/v. Close the cap until use to prevent solvent loss and changes in lipid concentration.
2. Phospholipids may be analyzed by loading the extract, using a CAMAG Linomat IV, onto 10 × 10 or 10 × 20 cm HPTLC plates, which are developed in methyl acetate/n-propanol/chloroform/methanol/0.25% aqueous KCl (25/25/25/10/9, v/v) according to Heape et al. [6].
3. External phospholipid standards (10 μg per standard; *see* **Note 2**) are loaded on the same plates as the samples to be analyzed.
4. The migration may be carried out into a simple developing chamber (20 min saturation/45 min migration/45 min drying; developing solvent volume 20 ml) or into an ADC2 automatic developing chamber (developing solvent volume 10 ml; program: migration distance 85 mm; drying time 5 min; saturation time 0 min).
5. Lipids can be detected by dipping the plates into a 3% copper acetate (w/v) in 8% aqueous phosphoric acid solution [7, 8], followed by heating at 110 °C during 30 min.
6. Densitometric analysis of phospholipids must then be performed in the following hour (stability of coloration), using for example a TLC scanner 3 at 366 nm. Lipids are quantified (μg of lipids) by comparing lipids and standard lipids peak areas (*see* **Note 2**).
7. If analysis of the fatty acid content is needed, the lipids from the HPTLC plates are only labeled by iodine vapors. Place the chromatogram 5–15 min into a strong iodine atmosphere (into a covered beaker in which some iodine resublimed

crystals have been placed); double bonds containing lipids will be stained in yellow over a few minutes. The desired lipid bands are scraped off and transferred into glass tubes (with Teflon covered screw caps) for further analysis by GC-FID or GC-MS.

8. For HPTLC analysis of acyl-CoAs, the lipids should be resuspended into 50–200 μl of chloroform/methanol/H_2O, 3/3/1, v/v.

3.3 GC-FID Analysis of Fatty Acids from Phospholipids

1. Fatty acid methyl esters (FAMEs) are prepared by resuspending the scraped lipid bands in 1 ml of 2.5% H_2SO_4 (v/v) in methanol using heptadecanoic acid 2 μg/ml as internal standard.
2. Tubes are heated at 80 °C for 1 h and cooled to room temperature.
3. Then 400 μl hexane and 1.5 ml H_2O are added to extract fatty acid methyl esters.
4. The tubes are vortexed vigorously for at least 1 min and centrifuged 10 min at 2000 rpm (2000 × *g*) with a bench centrifuge and the organic (upper) phase is transferred (preferentially with a syringe) to injection GC vials.
5. GC-FID can be performed using an Agilent 7890 gas chromatograph equipped with an Agilent GC Column DB-Wax 15 m × 0.53 mm × 1.0 μm and flame ionization detection, with Helium as carrier gas at a flow rate of 3 ml/min (4 psi).
6. The temperature gradient conditions can be: 160 °C for 1 min, increase to 190 °C at 20 °C/min, increase to 210 °C at 5 °C/min and then remaining at 210 °C for 5 min.
7. FAMES are identified by comparing their retention times with commercial fatty acid standards and quantified using ChemStation to calculate the peak areas, and then comparing them with the response of an internal standard (C17:0).

3.4 Phospholipidomic Analysis by LC-MS

1. For the analysis of phospholipids by LC-MS, phospholipid extracts were dissolved in 100 μl eluent A.
2. Synthetic internal lipid standards (PE, 17:0/17:0; PS, 17:0/17:0; PC, 17:0/17:0; PI, 17:0/14:1; and PG, 17:0/17:0) were added at different amounts adapted for the detection.
3. LC-MS/MS (multiple reaction monitoring mode) analysis can be performed with a model QTRAP 5500 mass spectrometer coupled to a liquid chromatography system Ultimate 3000. Analysis was performed in the negative (PE, PS, PI, and PG) and positive (PC) modes with fast polarity switching (50 ms); nitrogen was used for the curtain gas (set to 15), gas 1 (set to 20), and gas 2 (set to 0). Needle voltage was at −4500 or +5500 V without needle heating; the collision gas was also nitrogen. The multiple reaction monitoring mode is based on

the loss of the fatty acid part for the negative analysis (PE, PS, PI, and PG), and on the loss of the polar head in positive mode for PC analysis. The declustering potential was adjusted at −160 V for PE, −130 V for PG, −90 V for PS, −85 V for PI, and +40 V for PC; collision energy is set to −48 eV for PE and PG, −60 eV for PS, −62 eV for PI, and +47 eV for PC. The dwell time was set up to 3 ms. Reverse-phase separations are performed at 50 °C on a Luna C8 150 × 1 mm column with 100-Å pore size and 5-mm particles. During the run, the proportions of eluent A and eluent B vary: 0 min, 30% B; 5 min, 50% B; 30 min, 80% B; 31–41 min, 95% B; 42–52 min, 30% B. The flow rate is set up at 40 µl/min, and 3 µl sample volumes are injected. The areas of LC peaks are determined using the MultiQuant software for phospholipid quantification.

3.5 Long Chain Bases (LCB) Analysis by GC-MS

The long chain bases (LCB) are extracted from sphingolipids by basic hydrolysis. The free LCB are chemically oxidized in their aldehyde form to be analyzed in GC-MS [9].

Add 1 ml of 10% (w/v) of barium hydroxide (dissolved in H_2O) to the ER membrane lipid extract. Be sure that the aqueous solution was well shaken before pipetting and place the samples in tubes of about 8 ml (*see* **Note 4**). Add 1 ml of dioxane with standards (d20:0, t17:0, and d14:$1^{4(E)}$, *see* **Note 5**). Incubate at 110 °C overnight, then, after cooling add 6 ml of distilled H_2O, and transfer the content in a new bigger tube (approximate volume of 12 ml). Add 4 ml of ether 100%. Shake vigorously and centrifuge at 700 × *g* for 5 min. Pick up the upper phase and place it in a new tube of about 8 ml. Add another 4 ml of ether 100% in the previous 12 ml tube, and shake vigorously and centrifuge at 700 × *g* for 5 min. Pick up the upper phase and place it in the previous 8 ml tube. Evaporate with N_2 gas flow. Do not warm in a H_2O bath, as LCBs are quite labile. After complete evaporation, add 1 ml of methanol. Add 100 µl of a 0.2 M metaperiodate ($NaIO_4$) solution in H_2O (*see* **Note 6**). Incubate at room temperature *in the dark* for 1 h sharp and shake slightly. Add 1 ml of hexane 99% and 1 ml of distilled H_2O and shake vigorously. Centrifuge at 700 × *g* for 5 min. Pick up the upper phase. Transfer to a new tube (8 ml) and evaporate with N_2 gas flow at room temperature (do not warm in a H_2O bath for evaporation as fatty aldehydes might be unstable in this condition). Suspend in 100 µl of hexane 99% and vortex. Transfer to GC vials and run GC-MS.

GC-MS can be performed using an Agilent 6850 gas chromatograph coupled to a MS detector MSD 5975-EI. An HP-5MS capillary column (5% phenyl-methyl-siloxane, 30-m, 250-mm, and 0.25-mm film thickness) can be used with Helium carrier gas at 2 ml/min; injection is done in splitless mode; injector and mass spectrometry detector temperatures are set to 250 °C; the

oven temperature is held at 50 °C for 1 min, then programmed with a 25 °C/min ramp to 150 °C (2-min hold) and a 10 °C/min ramp to 320 °C (6-min hold).

3.6 Ceramide and Glucosylceramide Analysis by HPTLC and GC-MS Analysis of Their Fatty Acids

Under the conditions of polar lipid (phospholipids) separation described above, glucosylceramides and sterylglucosides do not separate. These lipids are separated on HPTLC plates using the solvent system chloroform/methanol (85/15, v/v) [10]. In this elution system, ceramides can also be isolated on HPTLC plates. Quantification by densitometry using ceramide and glucosylceramide standards (10 μg per standard) can be performed as explained for phospholipids in 3.2.

For acyl-chain characterization of ceramides and glucosylceramides by GC-MS, scraped lipid bands (after iodine vapor revelation, *see* Subheading 3.2) are directly incubated with 1 ml of 5% sulfuric acid solution in methanol (implemented with standards: 5 μg/ml of C17:0 and 5 μg/ml of h14:0) for transesterification which is made overnight at 85 °C to produce FAMEs. Those are then washed by adding 1 ml of NaCl 2.5% and 1 ml of hexane 99%. After vigorous shaking and centrifugation at 700 × *g* for 5 min at room temperature, the higher phase is harvested, placed in a new tube and buffered with 1 ml of 100 mM Tris, 0.09% NaCl, pH 8 with HCl. After vigorous shaking and centrifugation at 700 × *g* for 5 min at room temperature, the higher phase is harvested, placed in a new tube and evaporated with needles evaporating pan. Then, 200 μl of N,OBis(trimethylsilyl)trifluoroacetamide + 1% trimethylsilyl (BSTFA + 1% TMCS) are added and incubated at 110 °C for 20 min. After evaporation, FAMEs are resuspended in 100 μl of 99% hexane and run on GC-MS with the same program described in Subheading 3.3.

3.7 Neutral Lipid Analysis by HPTLC and GC-FID

To isolate and quantify neutral lipids (including phytosterols, DAG, FFA, TAG, and steryl esters), the lipids, resuspended into 50–200 μl of chloroform/methanol 2/1, v/v, are loaded onto 10 × 10 or 10 × 20 cm HPTLC plates developed with hexane/ethylether/acetic acid (90/15/2, v/v) as described [8, 11]. External neutral lipid standards (10 μg per standard; *see* **Note 2**) are loaded on the same plates than the samples to be analyzed. The migration may be carried out into a simple developing chamber (10 min saturation/20 min migration/30 min drying; developing solvent volume 20 ml) or into an ADC2 automatic developing chamber (developing solvent volume 10 ml; program: migration distance 85 mm; drying time 5 min; saturation time 0 min). Quantification by densitometry can be performed as explained for phospholipids in Subheading 3.2.

For GC-FID analysis of fatty acids from fatty acid-containing neutral lipids, FAMEs are analyzed and quantified as described in Subheading 3.2.

3.8 Phytosterol Analysis by GC-MS

Phytosterols are prepared by resuspending the corresponding scraped lipid bands in 1 ml of ethanol containing the internal standard α-cholestanol (25 mg/ml) in screwed glass tubes. For saponification, add 100 µl of 11 N KOH (56.11 g/mol, 12.3 g/20 ml H_2O), close the tube(s) under nitrogen, incubate in a dry bath incubator at 80 °C for 1 h, add 1 ml of hexane, vortex for 15 s, add 2 ml of distilled H_2O, vortex for 15 s, centrifuge 5 min at 2000 rpm in a bench centrifuge, and recover the phytosterol-containing upper phase in a new screwed glass tube and evaporate the solvent under an N_2 gas stream. For silylation of phytosterols, add 200 µl of BSTFA/TMCS, incubate 15 min at 110 °C in a dry bath incubator, evaporate the solution to dryness under nitrogen.

GC-MS analysis: add 200 µl of hexane before injection on GC-MS and use the same program as described in Subheading 3.3.

3.9 LC-MS Analysis of DAG and TAG

For the analysis of DAG and TAG by LC-MS, phospholipid extracts were dissolved in 100 µl of eluent C; synthetic internal lipid standards (DAG 17:0/17:0; TAG, 17:0/17:0/17:0) were added at different amounts adapted for the detection.

LC-MS/MS (multiple reaction monitoring mode) analysis is performed with a model QTRAP 5500 mass spectrometer coupled to a liquid chromatography system Ultimate 3000. The multiple reaction monitoring mode is based on the loss of the fatty acid part during the fragmentation.

Analysis was achieved in positive mode and nitrogen was used as curtain gas (set to 30), gas1 (set to 25) and gas2 (set to 0). Needle voltage was at +5500 V without needle heating. The collision gas was also nitrogen. The multiple reaction monitoring mode is based on the loss of the fatty acid part of the TAG or DAG molecules. The declustering potential was set at +40 V for TAG and +86 V for DAG; collision energy was adjusted at +34 V for TAG and DAG. The dwell time was set to 3 ms. Reversed phase chromatography was carried out at 30 °C using a Luna 3u C8 150 × 1 mm column, with 100-Å pore size, 3-µm particles. Eluent C and eluent D were then used as follows. The gradient elution program was 0–5 min, 15% D; 5–35 min, 15–40% D; 35–50 min, 55% D; 51–58 min, 80% D; 59–70 min, 15% D. The flow rate was 40 µl/min and injection volume was 3 µl. The relative levels of DAG and TAG species were determined using MultiQuant and normalizing to the area of the DAG or TAG internal standards (Yuan et al., submitted).

3.10 Radiolabeling In Vivo

Radiolabeled lipid precursors can be used for incubation with plant cells/tissues to investigate ER membrane lipid metabolism in vivo. According to the starting material, ER membranes can be isolated through different methodologies (*see* Subheading 1). Subsequently, ER membrane lipids are then extracted and washed as detailed in Subheading 3.1. Polar and neutral lipids can then be separated onto HPTLC plates as described in the corresponding

paragraphs. Their radiolabeling can then be determined using a PhosphorImager equipment. HPTLC plates are generally exposed to the adapted screens for 24–48 h and then the screens are scanned with the PhosphorImager. The ImageQuant software translates the radioactivity on HPTLC plates into peaks and gives a surface area for each. Then, from a calibrating curve (made with any radioactive standard) defining the correspondence between peak surface area and labeling amount, we can calculate for each lipid the level of labeling, and from the specific radioactivity of the lipid precursor used, we can determine the amount of each lipid in moles.

3.11 Radiolabeling In Vitro

Radiolabeled lipid precursors can also be used for incubation with ER membranes to investigate in vitro the enzymatic activity of ER membrane enzymes involved in lipid metabolism. According to the starting material, ER membranes can be isolated through different methodologies (*see* Subheading 1). Subsequently, ER membrane lipids are then extracted and washed as detailed in Subheading 3.1. Polar and neutral lipids can then be separated onto HPTLC plates as described in Subheading 3.2. Their radiolabeling can then be determined using a PhosphorImager equipment. The procedure determining the formed products amounts in moles is described above.

4 Notes

1. All chemicals and solvents were either of analytical or mass spectrometric grades. Prepare all solutions using deionized H_2O (18.2 MΩ cm at 25 °C), for example produced using a Synergy UV Millipore System. Follow all disposal regulations when disposing waste material.
2. For HPTLC analysis, each of the lipid classes should be calibrated with appropriate standards, i.e., with a similar fatty acid degree of unsaturation to the samples because the revelation with both cupric acetate/phosphoric acid or iodine vapor solutions is sensitive to the degree of fatty acid unsaturation.
3. If acyl-CoAs are required, lipids should be extracted with six times the sample's volume of chloroform/methanol 1/1 in order to obtain a homogeneous phase permitting to conserve the more polar molecules such as the acyl-CoAs.
4. Be extremely careful that all tube caps contain a Teflon disk.
5. Standards (for example, d20:0, t17:0, and d14:$1^{4(E)}$) should be added in the dioxane. Each standard initial concentration (1 g/L in methanol) should be added at 5 μg/ml final, i.e., 10 μl in the 2 ml of barium hydroxide + dioxane.
6. The $NaIO_4$ stock concentration should be prepared only freshly.
   Equivalent instrumentation can be used.

Acknowledgments

Metabolome Facility-MetaboHUB (ANR-11-INBS-0010) of the Functional Genomic Center of Bordeaux.

References

1. Morré DJ, Panel C, Morré DM, Sandelius AS, Moreau P, Andersson B (1991) Cell-free transfer and sorting of membrane lipids in spinach. Donor and acceptor specificity. Protoplasma 160:49–64
2. Parsons HT, Drakakaki G, Heazlewood JL (2013) Proteomic dissection of the Arabidopsis Golgi and trans-Golgi network. Front Plant Sci 3:298
3. Parsons HT, Fernández-Niño SM, Heazlewood JL (2014) Separation of the plant Golgi apparatus and endoplasmic reticulum by free-flow electrophoresis. Methods Mol Biol 1072:527–539
4. Li-Beisson Y, Shorrosh B, Beisson F, Andersson MX, Arondel V, Bates PD, Baud S, Bird D, DeBono A, Durrett TP, Franke RB, Graham IA, Katayama K, Kelly AA, Larson T, Markham JE, Miquel M, Molina I, Nishida I, Rowland O, Samuels L, Schmid KM, Wada H, Welti R, Xu C, Zallot R, Ohlrogge J (2013) Acyl-lipid metabolism. Arabidopsis Book 11:e0161
5. Folch J, Lees M, Stanley GHS (1957) A simple method for the isolation and purification of total lipides from animal tissues. J Biol Chem 226:497–509
6. Heape AM, Juguelin H, Boiron F, Cassagne C (1985) Improved one dimensional thin layer chromatographic technique for polar lipids. J Chromatogr 332:391–395
7. Macala LJ, Yo RK, Ando S (1983) Analysis of brain lipids by high performance TLC and densitometry. J Lipid Res 24:1243–1250
8. Laloi M, Perret AM, Chatre L, Melser S, Cantrel C, Vaultier MN, Zachowski A, Bathany K, Schmitter JM, Vallet M, Lessire R, Hartmann MA, Moreau P (2007) Insights into the role of specific lipids in the formation and delivery of lipid microdomains to the plasma membrane of plant cells. Plant Physiol 143:461–472
9. Cacas JL, Melser S, Domergue F, Joubès J, Bourdenx B, Schmitter JM, Mongrand S (2012) Rapid nanoscale quantitative analysis of plant sphingolipid long-chain bases by GC-MS. Anal Bioanal Chem 403:2745–2755
10. Hillig I, Leipelt M, Ott C, Zahringer U, Warnecke D, Heinz E (2003) Formation of glucosylceramides and sterol glucoside by a UDP-glucose-dependent glucosylceramide synthase from cotton expressed in Pichia pastoris. FEBS Lett 553:365–369
11. Juguelin H, Heape MA, Boiron F, Cassagne C (1986) A quantitative developmental study of neutral lipids during myelinogenesis in the peripheral nervous system of normal and trembler mice. Brain Res 390:249–252
12. Brown DJ, Dupont FM (1989) Lipid composition of plasma membranes and endomembranes prepared from roots of barley *(Hordeum vulgare* L.): effects of salt. Plant Physiol 90:955–961
13. Grindstaff KK, Fielding LA, Brodl MR (1996) Effect of gibberellin and heat shock on the lipid composition of endoplasmic reticulum in barley aleurone layers. Plant Physiol 110:571–581
14. Moreau P, Bessoule JJ, Mongrand S, Testet E, Vincent P, Cassagne C (1998) Lipid trafficking in plant cells. Progr Lipid Res 37:371–391

Chapter 11

2in1 Vectors Improve In Planta BiFC and FRET Analyses

Dietmar G. Mehlhorn, Niklas Wallmeroth, Kenneth W. Berendzen, and Christopher Grefen

Abstract

Protein–protein interactions (PPIs) play vital roles in all subcellular processes and a number of tools have been developed for their detection and analysis. Each method has its unique set of benefits and drawbacks that need to be considered prior to their application. In fact, researchers are spoilt for choice when it comes to deciding which method to use for the initial detection of a PPI, and which to corroborate the findings. With constant improvements in microscope development, the possibilities of techniques to study PPIs in vivo, and in real time, are continuously enhanced, and expanded. Here, we describe three common approaches, their recent improvements incorporating a 2in1-cloning approach, and their application in plant cell biology: ratiometric Bimolecular Fluorescence Complementation (rBiFC), FRET Acceptor Photobleaching (FRET-AB), and Fluorescent Lifetime Imaging (FRET-FLIM), using *Nicotiana benthamiana* leaves and *Arabidopsis thaliana* cell culture protoplasts as transient expression systems.

Key words Protein–protein interaction, rBiFC, FRET, Acceptor photobleaching, FLIM, Gateway, SEC61, 2in1

1 Introduction

Core cellular processes such as signal perception and transduction, vesicle trafficking, transport activities, and metabolic pathways rely on formation of complex protein networks. Analysis of the biochemical mechanisms at the molecular level requires a fundamental understanding of the protein–protein interactions (PPIs) involved. Over the past decades, a number of techniques such as Co-immunoprecipitation (CoIP), the Yeast Two-Hybrid (Y2H), the Split Ubiquitin System (SUS), Förster Resonance Energy Transfer (FRET) and related methods, as well as Bimolecular Fluorescence Complementation (BiFC) have become routine laboratory techniques to dissect PPIs (reviewed in [1]). Technological advancements in microscope development have enhanced possibilities further by facilitating real/life-time imaging of PPIs. Even techniques that were thought to be predominantly in vitro techniques such as

Chris Hawes and Verena Kriechbaumer (eds.), *The Plant Endoplasmic Reticulum: Methods and Protocols*, Methods in Molecular Biology, vol. 1691, DOI 10.1007/978-1-4939-7389-7_11,

CoIP are now applicable for microscopy analysis at the single-molecule level [2].

Recently, our lab has introduced 2in1 cloning, a gateway-compatible approach to simultaneously clone two genes-of-interest into two independent expression cassettes on the same T-DNA/plasmid [3] (Fig. 1a). This cloning system is well suited for PPI techniques that rely on transient transfection systems, as a mixture of two (or more) independent *Agrobacteria* each carrying their own plasmid can lead to unequal gene dosage resulting in high variability of coexpression [4]. We have combined the 2in1-cloning system with Bimolecular Fluorescence Complementation [3] as well as with a range of suitable fluorophores for enhanced FRET/FLIM analysis [4].

This chapter describes the application of the optimized 2in1 vector sets that can be used for ratiometric Bimolecular Fluorescence Complementation (rBiFC), FRET-Acceptor Photobleaching (FRET-AB), and Fluorescent Lifetime Imaging (FRET-FLIM), using either *Nicotiana benthamiana* leaves or *Arabidopsis thaliana* cell culture protoplasts as expression system [3, 4].

1.1 Ratiometric Bimolecular Fluorescence Complementation (rBiFC)

Bimolecular Fluorescence Complementation (BiFC) is a protein fragment complementation analysis whose first application was in bacteria [5]. The principle of BiFC is straightforward: a previously split fluorescent protein (FP) reconstitutes due to an interaction of two proteins of interest that are fused to the complementary nonfluorescent fragments (Fig. 1b). One major advantage of BiFC is the applicability of the system to almost all types of proteins (cytosolic, nuclear, organellar, or membrane-bound), and the detection of interaction in an in vivo context. It also allows visualization of PPIs at their site of first interaction—which should not be confused with the subcellular position where these proteins normally reside or are trafficked to—a misconception that is often inferred. Nevertheless, the flaws of the technique almost match the advantages. Overexpression of fusion proteins as well as their FP fragment tag can lead to mis-localization and alter the likelihood of a positive readout. Reassembly of the FP is irreversible, promoting and stabilizing weak or transient interactions, but thereby also causing artifactual results even in the absence of a true interaction [1, 6]. However, the biggest disadvantage in conventional BiFC systems used in the plant field is the use of two individual plasmids and their co-infiltration in transient transformation. This leads to very high variability in gene dosage and only about 70–80% of coexpression ratios [4]. In other words, out of four or five cells analyzed, one does not contain both fusion proteins present making a meaningful interpretation of the results very hard. In addition, classical BiFC constructs do not contain concurrent reference markers making quantification against presumed negative controls (which could be non- or unequally transformed cells) a cherry-picking exercise (Fig. 2).

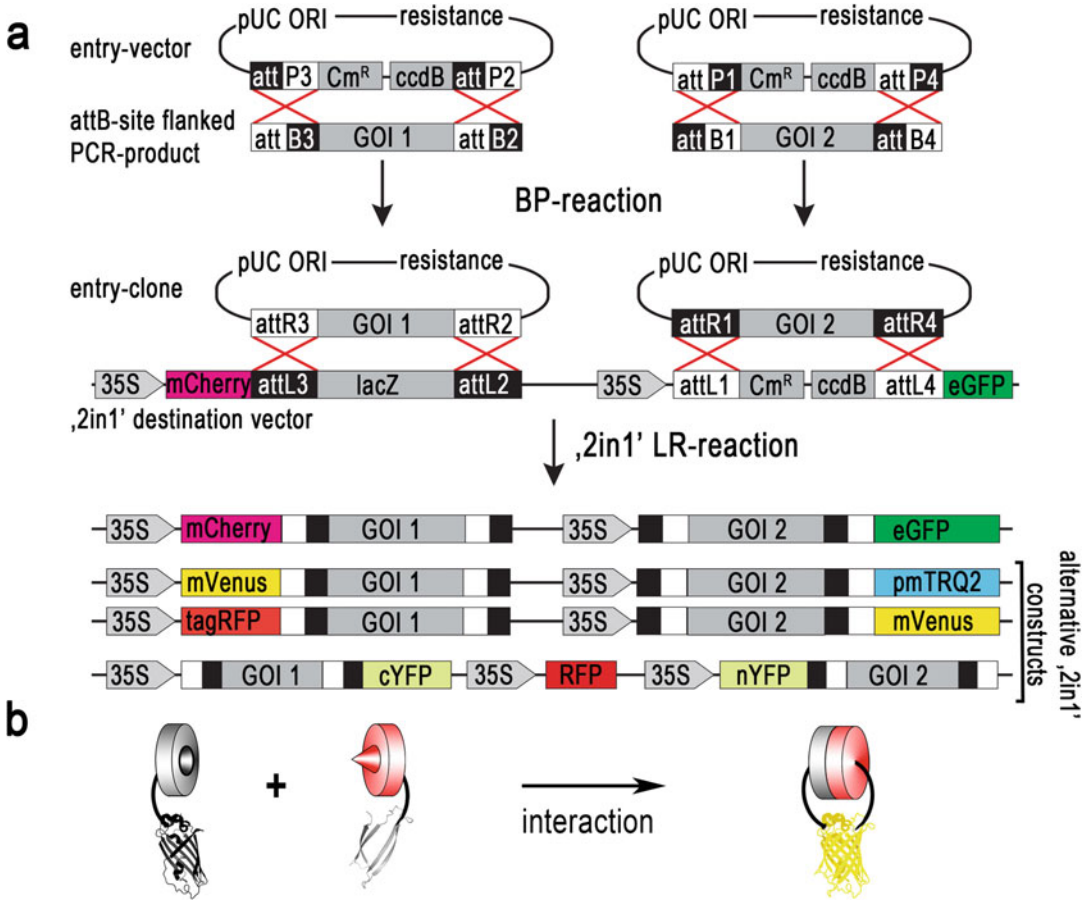

Fig. 1 Concepts of 2in1 cloning, Bimolecular Fluorescence Complementation and Förster Resonance Energy Transfer. (**a**) Site-specific BP recombination of PCR products and Entry vectors generates Entry clones. A subsequent one-step LR reaction recombines the two genes-of-interest (GOI) simultaneously in a 2in1 Destination vector. Depicted are the "2in1" vectors used in this chapter. *See* Table 1 for details. *35S* cauliflower mosaic virus 35S promoter and omega translational enhancer sequence, *pUC ORI* origin of replication, *Cm*^{R} chloramphenicol acetyltransferase resistance gene, *ccdB* gyrase inhibitor gene, *lacZ* lacZ expression cassette. (**b**) Cartoon depicting the concept of bimolecular fluorescence complementation (BiFC). Two proteins (*grey* and *red*) are tagged with nonfluorescent YFP fragments, nYFP and cYFP, respectively. Interaction of both proteins leads to reconstitution of fluorescent YFP. (**c**) Simplified Jablonski diagram depicting the excitation of an electron in a cyan-fluorescing protein (CFP). After internal conversion (*black wavy arrow*) to the S1 ground state (*cyan solid arrow*) a crossing of the energy barrier between S1 and S0 can cause the emission of a photon at a longer wavelength (red shifted, Stokes shift; i.e., fluorescence). If an acceptor molecule is in close enough proximity (here, YFP attached to a red-colored interacting protein), the energy can be transferred non-radiatively to the acceptor molecule. (**d**) Absorbance/fluorescence spectrum of mTurquoise2 and mVenus. The *dark grey surface* depicts the λ^4 weighted overlap integral. Acceptor and donor spectral bleed through are shown in *magenta* and *green*, respectively. (**e**) Example of a FRET acceptor photobleaching experiment. A nucleus expressing two interacting proteins attached to a donor and an acceptor fluorophore. After bleaching (right), the acceptor fluorescence is almost completely lost, but an increase in donor fluorescence can be detected. (**f**) Exemplary fluorescence lifetime decay curve of a putative donor molecule when FRET is occurring (*red solid curve*; *t*1) or in the absence of FRET (*cyan solid line*; *t*2). Fluorescence lifetime *t* is the average time that a fluorescent protein resides in the excited state and at which fluorescence intensity decreased to 1/*e* of its initial value. (**b**–**f**) modified from [1, 4]

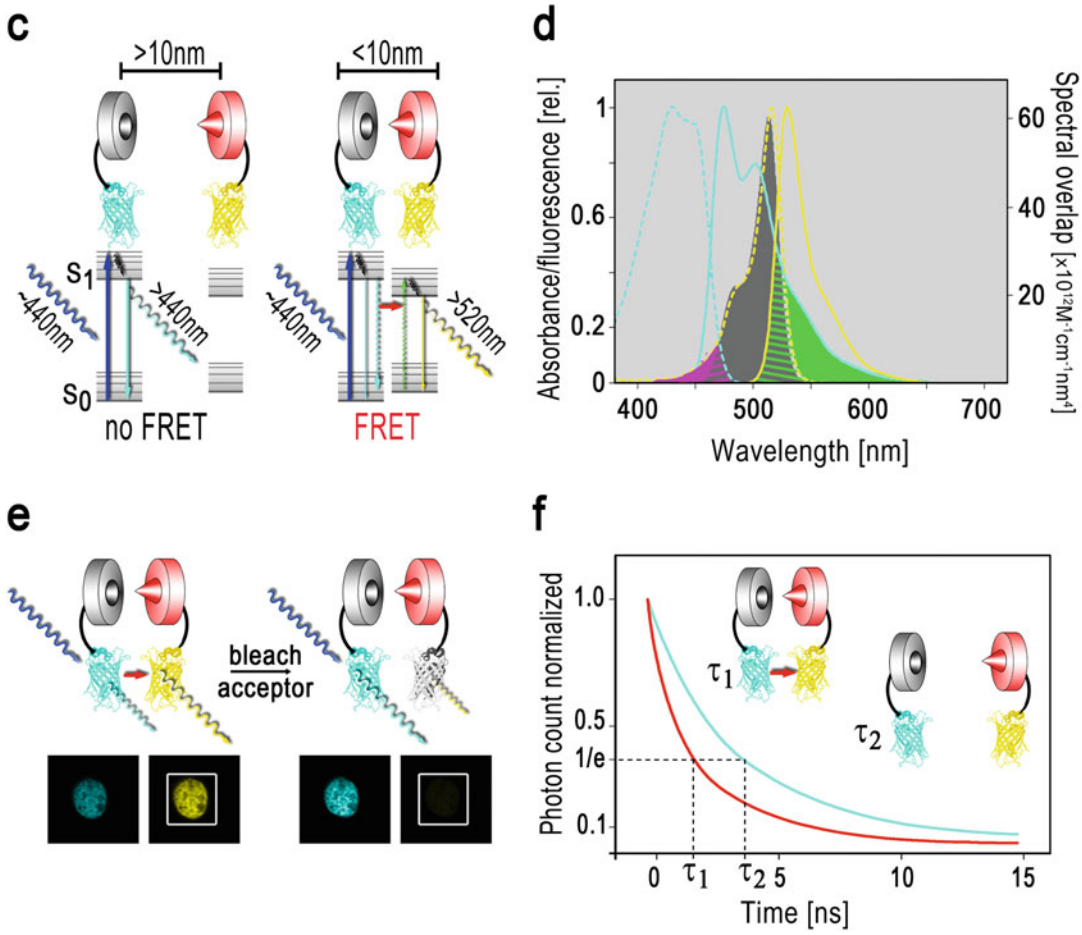

Fig. 1 (continued)

Contrary to classical BiFC, the ratiometric BiFC (rBiFC) approach addresses most of these issues and provides means for internal, ratiometric quantification of results [3]. Placing both FP fragments on the same T-DNA guarantees equal gene dosage of both nonfluorescent fusion proteins and the inclusion of a soluble RFP marker provides a readout for ratiometric analysis and transformation control of the cell under study [3] (Fig. 3). The technique has since been used in a number of studies for the detection of PPIs or their structure-function analysis [7–13, 24] (*see* **Note 1**).

1.2 Förster Resonance Energy Transfer-Acceptor Bleaching (FRET-AB)

An alternative, more reliable, yet sophisticated technique exploits the physical phenomenon of resonance energy transfer which was first postulated by Theodor Förster in 1946 and has been named after him as commemoration [14] (Fig. 1c–f). The principle of FRET is a non-radiative energy transfer from an excited donor fluorophore to an acceptor molecule—often, but not

Table 1
Available 2in1 expression vector sets for rBiFC and FRET experiments[a]

	Origin of replication		Resistance marker				
Name	***E. coli***	***A. tumefaciens***	**Bacteria**	**Plant**	**Promoter**	**FPs[a]**	**Reference**
pBiFC-2in1	ColE1	pVS1	Spectinomycin	None	CaMV35S	nYFP, cYFP, RFP[b]	[3]
pFRETcg-2in1	ColE1	pVS1	Spectinomycin	Basta	CaMV35S	mCherry, mEGFP	[4]
pFRETvt-2in1	ColE1	pVS1	Spectinomycin	Basta	CaMV35S	mVenus, mTRQ2	[4]

[a]Plasmids exist in all possible tag combinations of fluorescent proteins (FPs)
[b]RFP fluorescence serves as transformation control and ratiometric marker

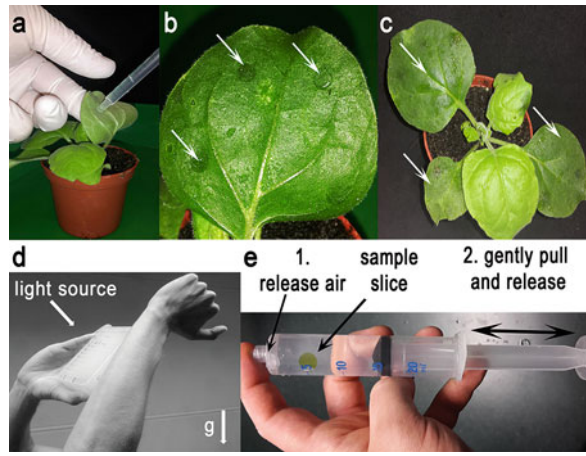

Fig. 2 Method handling. (**a**) Infiltration of 3–4-week-old *N. benthamiana* leaves using a syringe as described in Subheading 3.2. (**b**) *White arrows* point at areas of infiltration at the abaxial side of the leaves. (**c**) The first two youngest (*top*) leaves of a 4–6-week-old *N. benthamiana* plant should *not* be used for infiltration. Instead, slightly older leaves (*white arrows*) are ideal with respect to suitability for injection and transgene expression [23]. (**d**) "Tapping method" for gentle mixing of protoplasts with DNA. (**e**) Preparation of a *N. benthamiana* leaf disc for microscopic analysis. The syringe is filled with water, which – by application of a vacuum – replaces the air in the intercellular space of the leaf epidermis enhancing image quality

necessarily—fluorescent itself. Prerequisite is an overlap of the donor emission with the excitation spectrum of the acceptor. FRET only occurs if donor and acceptor are in close enough proximity of 10 nm or less [15, 16]. Such resolution of molecular distances is more than a magnitude lower than the diffraction limit of light microscopy at 200 nm, allowing distinction of protein co-localization from interaction.

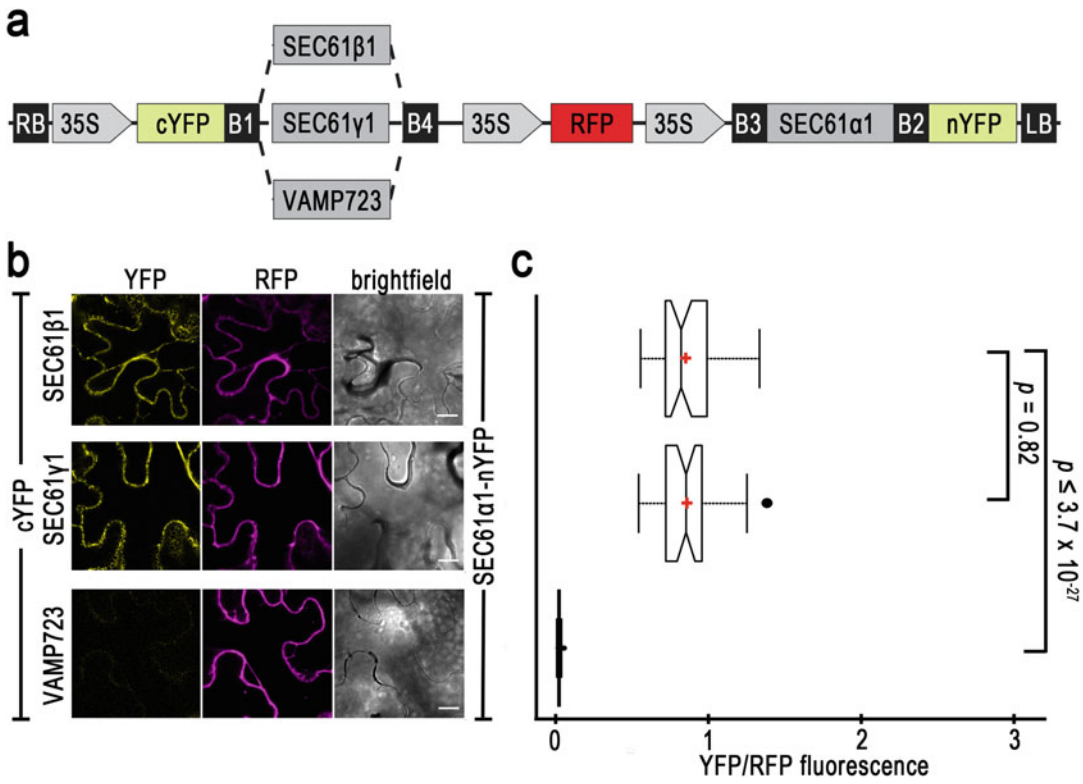

Fig. 3 rBiFC analysis of putative *Arabidopsis* SEC61 subunits in *N. benthamiana* leaves and *A. thaliana* protoplasts. (**a**) Cartoon of the "2in1" rBiFC destination constructs used in this experiment [3]. (**b**) Representative images of *N. benthamiana* leaves expressing SEC61α1-nYFP (At2g34250), RFP, and either cYFP-SEC61β1 (At2g45070), cYFP-SEC61γ (At5g50460), or, cYFP-VAMP723 (At2g33110), respectively. (**d**) At least 40 images were recorded per construct, and YFP/RFP mean fluorescence intensity calculated. *Box plot* depicts the median with outer limits at the 25th and 75th percentile, respectively. Notches indicate the 95% confidence intervals; Tukey whiskers extend to the 1.5× IQR and outliers are depicted as *black dots*. *Red crosses* mark sample means of each dataset. Exemplary *p*-values (*t*-test) are indicated in graph. (**d**) Representative images of *Arabidopsis* protoplasts expressing the same constructs. (**e**) At least ten protoplasts were recorded per construct, and YFP/RFP mean fluorescence intensity calculated. Boxplot as before. (**f**) Immunoblot analysis of HA-tagged SEC61α1, MYC-tagged proteins of interest and soluble RFP expressed in *Arabidopsis* protoplasts used for rBiFC analysis. *Asterisks* indicate expected protein size. Scale bar in (**b**, **d**) = 10 μm

In fluorescence microscopy, the FRET phenomenon can be detected using different approaches. Classical FRET approaches simply measure fluorescence of the acceptor when the donor is excited. However, this can lead to artifactual results due to spectral bleed through, a phenomenon deriving from an overlap of excitation spectrum of the donor with the emission spectrum of the acceptor, which—unfortunately—is a common property with most current FRET FP couples.

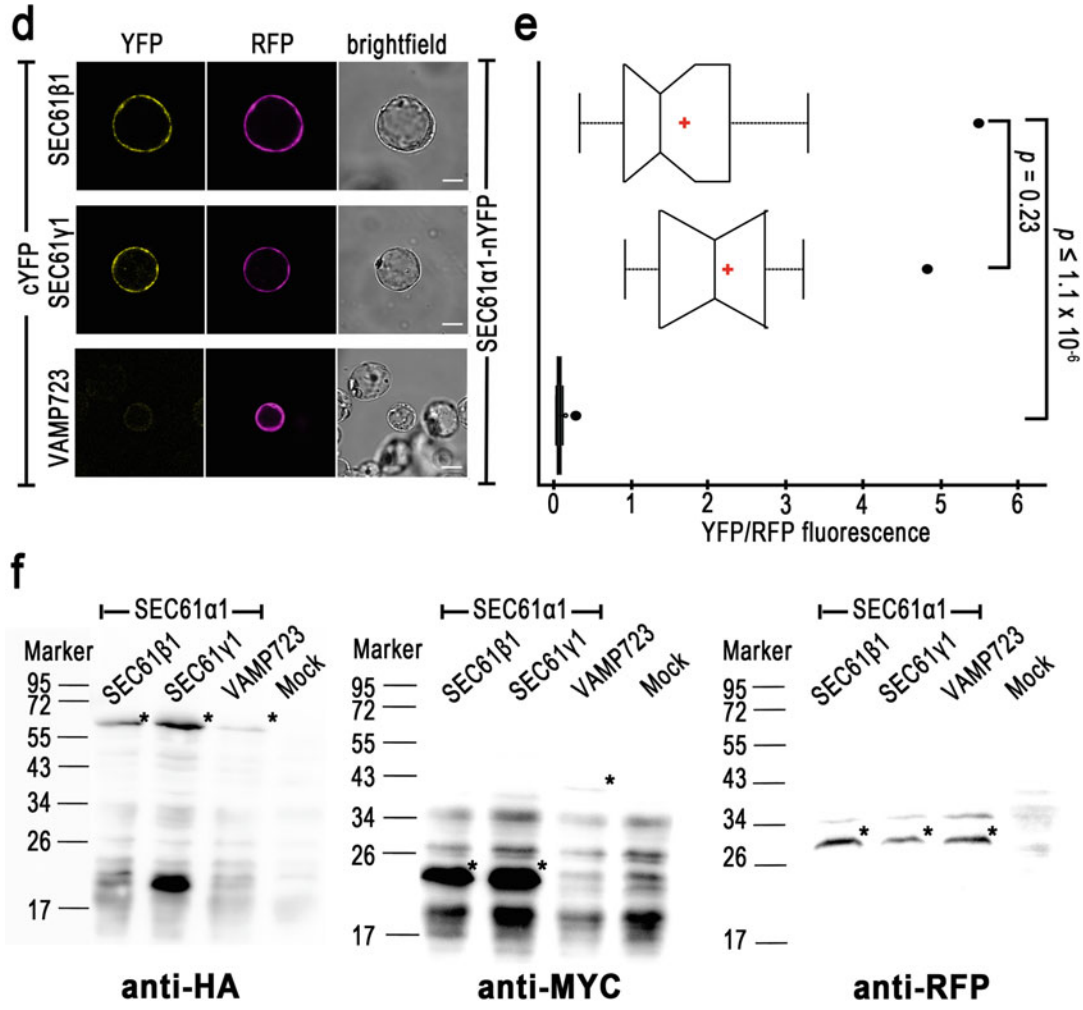

Fig. 3 (continued)

An alternative, more credible method based on FRET is "Acceptor Photobleaching" (FRET-AB). Here, the intensities of the donor fluorophore before and after photobleaching of the acceptor are measured in a specified region of interest (ROI). Bleaching of the acceptor leads to an increase in donor fluorescence in the ROI as the energy that would have been transferred to the acceptor remains within the donor, leading to increased fluorescence of the latter.

AB does not require high-end microscopes and can be carried out at any fluorescence microscope which is an advantage compared to Fluorescence Lifetime Imaging Microscopy (FLIM) measurements [15] (*see* below). However, photobleaching in AB can potentially photo-damage the samples and is therefore not suitable in prolonged time-lapse experiments. Other pitfalls are concomitant bleaching of acceptor and donor, as well as movement of the cytoplasm, both of which may lead to unfeasible results.

1.3 Fluorescence Lifetime Imaging Microscopy (FLIM)

Classical FRET and FRET-AB are both intensity-based methods and—as such—can be compromised by suboptimal fluorophore concentration ratios. Measurement of fluorescence lifetime, however, might overcome this issue [16, 17]. Briefly, irradiation leads to raising of the FP to an excited—S_1—state before relaxation to the ground—S_0—state. The average time the fluorophore resides in the excited state represents its fluorescence lifetime and is unique for each FP [18]. When an acceptor molecule is in close enough range (<10 nm), it can serve as energy sink, resulting in a lifetime "decay" of the donor molecule. Such reduction in lifetime can be compared to negative controls or "donor only" samples which inform on the original lifetime of an FP—the difference between the two informs on PPI (Fig. 4).

Still, while small imbalances in concentration of donor and acceptor do not affect FLIM measurements, the lifetime of fluorophores is affected by other factors such as for example changes in redox state, pH, or temperature. Yet, FRET-FLIM delivers more credible results as it is almost unaffected by concentration differences and spectral properties compared to FRET-AB; but it requires sophisticated and expensive equipment as well as considerable training and experience of the scientist who handles it.

2 Materials

2.1 Bacteria and Plants

For transient transformation of *Nicotiana benthamiana* leaves via infiltration, *Agrobacterium tumefaciens* strain GV3101 pMP90 carrying the selection markers for growth on rifampicin and gentamicin was chosen [19, 20].

2.2 Media and Reagents (Tobacco Leaf Infiltration)

1. Luria-Bertani (LB) medium: 1% tryptone, 0.5% yeast extract, 0.5% NaCl, pH 7.0–7.5 (for solid media add 2% agarose).
2. Antibiotics (1000× stock solution): gentamicin (20 mg/mL in distilled water), spectinomycin (100 mg/mL in distilled water), and rifampicin (50 mg/mL in DMSO).
3. AS medium: 10 mM $MgCl_2$, 10 mM MES-KOH, pH 5.6, 150 μM acetosyringone.
4. Sterile distilled water.

2.3 Media and Reagents (Protoplasts)

2.3.1 Sterile Filtration

The most economic sterile filtration method is to acquire a peristaltic pump and use membrane filters with a Swinnex Filter Holder (Millipore).

2.3.2 Sterile Erlenmeyer Flasks for Cell Culture

250 mL Erlenmeyer flasks are stoppered with Rotilabo®-culture plugs and covered well by aluminum foil. Sub-culturing is performed under highly sterile conditions and the flasks are flamed when opened to prevent contamination.

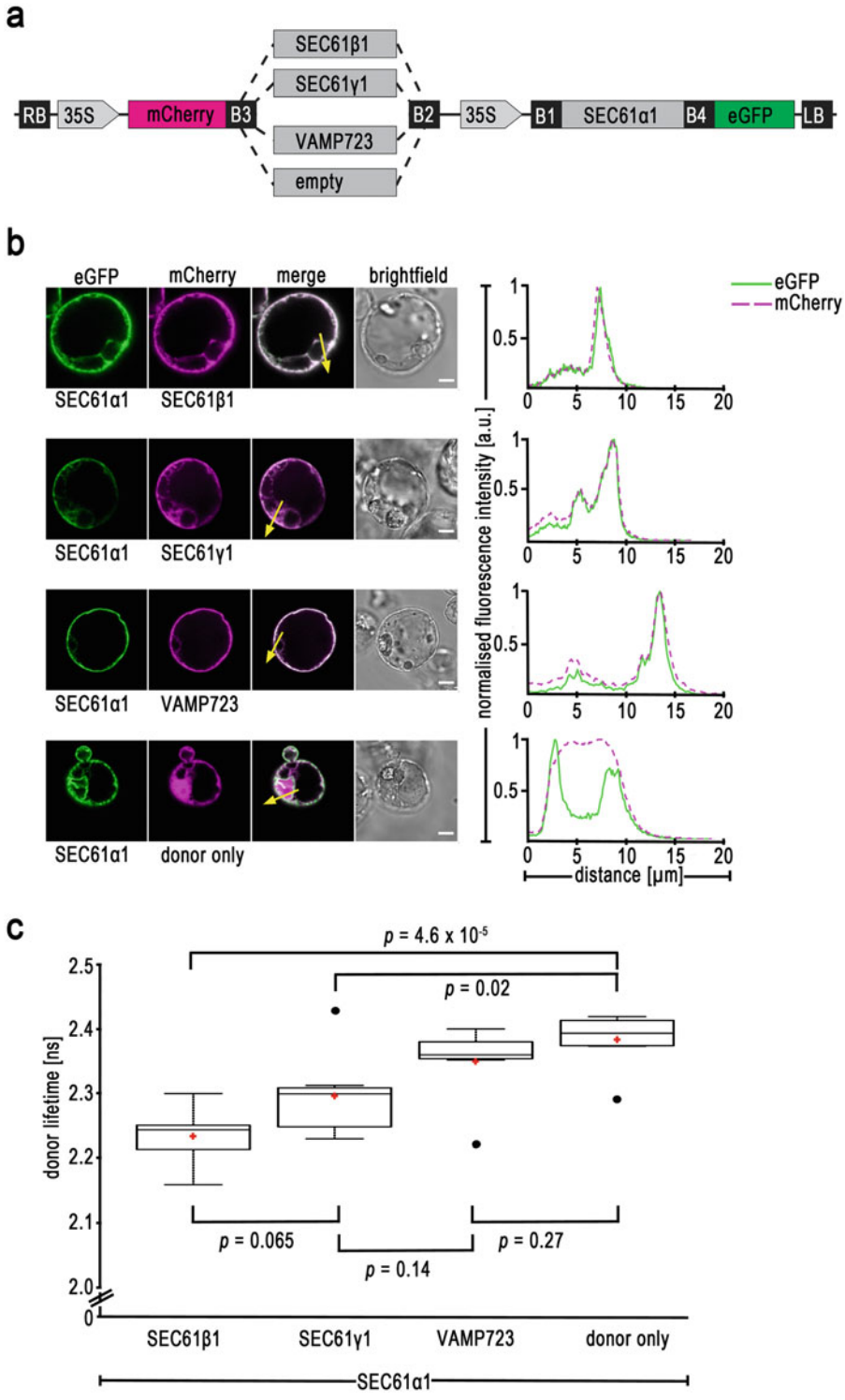

Fig. 4 FRET-FLIM analysis of putative *Arabidopsis* SEC61 subunits in *A. thaliana* protoplasts. (**a**) Cartoon of the "2in1" FRET destination constructs used in this experiment [4]. (**b**) Representative images of *A. thaliana*

2.3.3 Pipetting of Protoplasts

We use 200 μL, cut tips to handle protoplasts and try to aim for a diameter of 2–3 mm. Protoplasts are extremely sensitive to shearing stress and larger tip pore sizes circumvent this.

2.3.4 Cell Culture Maintenance Media

1. MS Col Medium (for 1 L): 4.3 g/L Murashige and Skoog Basal Salt Mixture (MS), 5 mL of NPT-Vitamin Stock, 100 mg/mL *myo*-Inositol, 30 g/L Sucrose, pH 5.8 with KOH. After autoclaving and before use, add 2,4-D to 1 mg/L. Store at 4 °C in the dark.
2. NPT-Vitamin Stock: 1 mg/mL Nicotinic acid, 1 mg/mL Pyridoxine-HCl, 10 mg/mL Thiamine-HCl in dH_2O. Sterilize by filtration (0.22 μm) and store at −20 °C.
3. 2,4-D Stock (for 100 mL): Dissolve 100 mg in 10 mL absolute ethanol and bring to 100 mL with dH_2O. Concentration is 1 mg/mL. Sterilize by filtration (0.22 μm) and store at −20 °C.

2.4 Media for Protoplast Generation

1. Wall digestion solution without enzymes: 8 mM $CaCl_2 \cdot 2H_2O$, 0.4 M Mannitol, pH 5.5 with KOH. Sterilize by filtration (0.22 μm).
2. Wall digestion solution: 1% Cellulase, 0.25% Macerozyme, 8 mM $CaCl_2 \cdot 2H_2O$, 0.4 M Mannitol, pH 5.5 with KOH. Sterilize by filtration (0.22 μm), use immediately or store at −20 °C.
3. W5: 154 mM NaCl, 125 mM $CaCl_2$, 5 mM KCl, 5 mM Glucose, pH 5.8–6.0 with KOH. Sterilize by filtration (0.22 μm) or autoclave.

2.5 Media for Protoplast Transfection

1. 40% PEG-1500: 10 g w/v PEG (1500), 1.275 g Mannitol, 0.413 g $Ca(NO_3)_2 \cdot 4H_2O$, 4 mM MES, pH 6 with KOH. Dissolve mannitol and calcium nitrate in 17.5 mL ddH_2O first and then add the PEG. Thereafter, adjust the pH with KOH. Sterilize by filtration (0.45 μm) and prepare aliquots and store at −20 °C. After defrosting make sure that all salts are

Fig. 4 (continued) protoplasts expressing SEC61α1-eGFP with either mCherry-SEC61β1, mCherry-SEC61γ, mCherry-VAMP723, or, mCherry, respectively. Line histograms to the right show normalized intensities of either eGFP or mCherry fluorescence along *yellow arrows* in merged images. *a.u.* arbitrary units. Scale bar = 10 μm. (**c**) Box plot of SEC61α1-eGFP donor lifetime in ns of at least seven independent measurements for each of the various acceptor samples. *Center lines* of *boxes* represent the median with outer limits at the 25th and 75th percentile, respectively. Notches indicate the 95% confidence intervals; Tukey whiskers extend to the 1.5× IQR and outliers are depicted as *black dots*. *Red crosses* mark sample means of each dataset. Exemplary *p*-values (*t*-test) are indicated in graph

dissolved, if not, shake vigorously until they are; slightly warming of the solution helps.

2. MM: 0.4 M Mannitol, 5 mM MES, pH 6.0 with KOH. Sterilize by filtration (0.22 μm) or autoclave.
3. K3 (for 100 mL)**:** 10 mL macro stock, 0.1 mL micro stock, 0.1 mL vitamin stock, 0.5 mL EDTA stock, 1 mL Ca-Phosphate stock, 10 mg *myo*-Inositol, 25 mg D(+)-Xylose, 13.7 g Sucrose, pH 5.6 with KOH. Sterilize by filtration (0.22 μm), prepare aliquots (15–40 mL) and store at −20 °C.
4. Macro stock (for 1 L): 1.5 g $NaH_2PO_4 \cdot H_2O$, 9 g $CaCl \cdot 2H_2O$, 25 g KNO_3, 2.5 g NH_4NO_3, 1.34 g $(NH_4)_2SO_4$, 2.5 g $MgSO_4 \cdot 7H_2O$, add H_2O up to 1 L and autoclave.
5. Micro stock (for 100 mL): 75 mg KI, 300 mg H_3BO_3, 1 g $MnSO_4 \cdot 7H_2O$ (or 0.6 g $MnSO_4 \cdot H_2O$), 200 mg $ZnSO_4 \cdot 7H_2O$, 25 mg $Na_2MoO_4 \cdot 2H_2O$, 2.5 mg $CuSO_4 \cdot 5H_2O$, 2.5 mg $CoCl_2 \cdot 6H_2O$, add H_2O up to 100 mL. Sterilize by filtration (0.22 μm) and store at −20 °C.
6. Vitamin stock (for 100 mL): 100 mg Nicotinic acid, 100 mg Pyridoxine-HCl, 1 g Thiamine-HCl, add H_2O up to 100 mL. Sterilize by filtration (0.22 μm) and store at −20 °C.
7. EDTA stock (for 1 L): dissolve 7.46 g EDTA in 300 mL pre-warmed H_2O (approx. 30 °C), separately, dissolve 5.56 g Fe (II)$SO_4 \cdot 7H_2O$ in 300 mL pre-warmed H_2O (approx. 30 °C). Combine and add H_2O up to 1 L. Autoclave, aliquot, and store in the dark at 4 °C. Protect from light.
8. Ca-Phosphate stock (for 200 mL): 1.26 g $CaHPO_4 \cdot 2H_2O$, add H_2O up to 200 mL, pH 3 with 25% HCl. Autoclave and keep in the dark at 4 °C. Protect from light.

3 Methods

3.1 Agrobacteria Preparation

1. Select a single colony of transformed *Agrobacteria* which contains the 2in1-vector plasmid or any other plasmid of choice.
2. Inoculate 5 mL LB medium containing the appropriate antibiotics (rifampicin 50 μg/mL, gentamicin 20 μg/mL, and the plasmid specific antibiotic) with the *Agrobacterium* colony and grow it overnight (28 °C, 200–230 rpm) (*see* **Note 2**).
3. Transfer 500 μL of the overnight culture into 4.5 mL of fresh LB medium supplied with rifampicin, gentamycin, and specific antibiotic and grow for another 3–4 h (28 °C, 200 rpm) to an OD_{595} of approximately 0.2–0.8.
4. Determine the OD_{595}.

5. Centrifuge at 4000 × *g* for 15 min at 4 °C and wash the pellet once or twice with 5 mL of 4 °C cold water.
6. Adjust to a final OD_{595} of 0.5 with 4 °C cold AS medium. (Calculation: $OD_{595}/0.5 \times 5$ mL = Volume (in mL) of AS medium needed.)
7. Before proceeding with transient transformation of *Nicotiana benthamiana* leaves, incubate samples at least 1 h on ice.

3.2 Transient Transformation of Nicotiana benthamiana Leaves

1. Water 3–4-week-old (8th–10th leaf stage) *Nicotiana benthamiana* plants 4–6 h prior to infiltration.
2. Start preparation of *Agrobacteria* as mentioned in Subheading 3.1.
3. Inject with a 1 mL syringe (without cannula) *Agrobacterium* suspension into the abaxial side of the third to fifth youngest leaves. For this purpose, position the syringe between leaf-veins and support injection by gentle counter pressure with a finger on the adaxial side (Fig. 2a–c).
4. After infiltration, cover and return plants to the growth chamber.
5. After approximately 36–72 h post-infiltration, proceed to Subheading 3.6.

3.3 Cell Culture Maintenance (Protoplasts)

The particular cell culture in this protocol (*Arabidopsis thaliana*, Col-0, root derived) was generated and donated by Mathur and Koncz [21].

1. Cell cultures are maintained in 250 mL Erlenmeyer flasks under constant shaking (120 rpm) in the dark at 23.5 °C ± 1 °C.
2. The cell culture is propagated by reinoculation every 7 days by transferring 10 mL of a one-week-old (7-day-old) culture to a fresh, sterile 250 mL Erlenmeyer flask with 50 mL MSCol medium. The final, total volume is 60 mL.

3.4 Generation of Protoplasts

1. Protoplasts should be generated from cells 3 days after subcultivation when they are in their peak growth phase (*see* **Note 3**).
2. Aliquot 10 mL of cells into 12 mL Poly-Propylene (PP) round-bottom tubes and collect them at 400 × *g* for 5 min (4–25 °C okay).
3. Wash cells by resuspension with 10 mL "wall digestion solution without enzymes" and spin down at 400 × *g* for 5 min (4–25 °C okay).
4. Re-suspend pellet in 7 mL "wall digestion solution" and dispense into a 90 mm diameter Petri dish.

5. Incubate by shaking at 50 rpm for 6 h at 23.5 °C ± 1 °C in the dark.
6. Collect protoplasts from one Petri dish in a 12 mL PP tube. Centrifuge at 100 × g for 5 min at 4 °C. Discard the supernatant.
7. Wash protoplasts by resuspension in up to 10 mL "wall digestion solution without enzymes" and spin down at 100 × *g* for 5 min at 4 °C. This is Wash #1.
8. Remove supernatant and dissolve pellet in remaining solution. Add up to 10 mL with W5 solution slowly and mix slowly. This is Wash #2. Spin down the cells at 100 × *g* for 5 min at 4 °C.
9. Re-suspend cells in 10 mL W5 solution as in **step 8**. This counts as Wash #3. Take 20 μL (use cut 200 μL tips to handle protoplasts) to determine cell concentration with a hemocytometer.
10. Adjust the cells to 1.5×10^6 cells/mL. Leave cells in the refrigerator (4 °C) for at least 20 min; overnight is also okay.
11. Determine the protoplast concentration you will use. Transfection will occur in ranges of 1.5×10^6 cells/mL up to 6.7×10^6 cells/mL. Our standard concentrations are 6.6×10^6 cells/mL and 3.5×10^6 cells/mL. Use higher cell concentrations when working with multiple plasmid species ($\geq$3) and the lower concentration for $\leq$2 plasmids. It is recommended that you test this for each experimental condition.
12. Collect the protoplasts under 50 × *g* at room temperature (RT).
13. Decant the supernatant (some W5 will remain, $\leq$500 μL) and adjust to the determined cell concentration with MM and incubate cells for 10–30 min (but not longer) at RT.
14. The cells are ready for transfection.

3.5 Protoplast Transfection

This protocol was designed to transfect protoplasts in 96-well plate format (2.2 mL, round-bottom, deep-well) using the "Liquidator™ 96 Manual Pipetting System" (Mettler-Toledo) but it can also be executed using 8- or 12-channel pipettes. It is recommended to mix after each row as soon as you add PEG. A small set of reactions can be performed in 2 mL round-bottom Eppendorfs; mix as soon as you add PEG.

1. Prepare up to 16 μg of high-quality DNA in 20 μL H_2O in each reaction-well.
2. Add 60 μL of cell suspension to the DNA and mix the plate from every side by tapping the plate against your forearm (Fig. 2d) until no cell clumps are visible. Make sure that the DNA is evenly mixed in the total volume.

3. Add 60 μL of PEG and start a timer to a 5 min countdown. Mix the plate from every side by tapping the plate against your forearm until the PEG is evenly dispensed. This will take approximately 1 min. You can see the solution mixing if you hold the plates or tubes against the lighting in your laboratory so that you see light diffraction through the liquid. After 3 min, mix again.
4. Add 60 μL of MM solution and mix as before.
5. Add 500–700 μL of K3 medium, mix gently, and cover the plate with a film that allows gas exchange (e.g., AeraSeal™ film, SIGMA) (*see* **Note 4**).
6. Incubate the cells in the dark at 25 °C from 3 to 24 h depending on your assay (*see* **Note 5**).

3.6 Mounting for Microscopy (Tobacco Leaf Infiltration)

1. Cut a leaf section of approximately 1 cm^2 and transfer it to a 20 mL syringe half filled with water. Use your finger to stop water loss at the syringe's exit, insert the plunger, and carefully remove the remaining air in the syringe (Fig. 2e).
2. Close the tip of the syringe again and pull the plunger back. This will produce a partial vacuum in the syringe.
3. Releasing the plunger gently will replace air space within the leaf slice with water.
4. Repeat **steps 3** and **4** several times until the tissue appears translucent.
5. Take out the slice and mount it upside down on a slide. Drop a bit of water on the slide and place a coverslip over the tissue.
6. Tap coverslips gently to remove air bubbles.

3.7 Mounting for Microscopy (Protoplasts)

Tightly wrap two stripes of tape around a microscope slide with a gap of around 5 mm between them. These will serve as spacers. Put approx. 50–100 μL of cell suspension between the stripes and place a coverslip on top (*see* **Note 6**).

3.8 Confocal Imaging

Our studies are done using the Leica TCS SP8 confocal microscope with laser lines diode 405, pulsed 440, pulsed 470, Argon 488, 496, 514, DPSS 561, HeNe 594, and HeNe 633, respectively. The microscope is equipped with a fast 8 kHz resonant scanner, HyD detectors, and FLIM unit (PicoQuant). Leica Application Suite (LAS) X software was used for image acquisition.

3.8.1 rBiFC

1. Set up the confocal microscope for YFP fluorescence with 514 nm excitation and 520–560 nm emission range and for RFP fluorescence with 561 nm excitation and 570–630 nm emission range. To avoid spectral overlap, sequential scanning should be applied. Include a bright field channel for guidance from transmission of either laser line.

2. Use a 40×/0.75 NA water-immersion objective to focus on epidermal cells. A zoom factor between 3 and 4 is recommended.
3. Start with a positive control and collect several images while adjusting gain and—if necessary—offset, for an optimal dynamic range. Settings should be adjusted to yield a mean fluorescence intensity ratio between YFP and RFP of one (*see* **Note 7**). Once the parameters are adjusted, select and save for quantification of 20–40 images of randomly selected areas (*see* **Note 8**).

3.8.2 Image Analysis

For image analysis, we use the ImageJ software (freely available at http://imagej.net/Downloads) with the Bio-Formats plugin which must be installed separately before using it for the first time.

1. Open the *.lif file with the ImageJ software. Using the Bio-Format tool the first time, choose "view stack with: Hyper-stack" and set a mark in the "split channels" box. Select all series.
2. Close brightfield images.
3. Select the first RFP image and press button M, or STRG-M (measure). A table with different values (Area, Mean, Min, Max) will appear.
4. Select the corresponding YFP image and measure again.
5. Proceed for all images as described in **steps 2–4**. Afterwards you can copy the data table into Microsoft Excel.
6. Calculate the ratio between the mean fluorescence intensity values of YFP and RFP for each image and use for graphical display after/including statistical analysis.

3.8.3 FRET-AB

1. Set up the confocal microscope for eGFP fluorescence with 488 nm excitation and 490–530 nm emission range, and for mCherry fluorescence with 561 nm excitation and 565–610 nm emission range. To avoid spectral overlap, sequential scanning should be applied. Include a bright field channel for guidance from transmission of either laser line.
2. Use a 40×/0.75 NA water-immersion objective.
3. Adjust gain and offset settings for your sample exploiting the full dynamic range.
4. Switch to the FRET-AB mode from the dropdown menu in the LAS X software and adjust donor and acceptor settings as before. Set acceptor-excitation-laser intensity in the "bleach" tab to 100% and frames between 300 and 500.
5. Search an area where both proteins of interest are sufficiently expressed, set up an ROI, and start the bleaching procedure.

LAS X software automatically captures images before and after bleaching and calculates the FRET efficiency (*see* **Note 9**) according to the following formula:

$$\mathrm{FRET}_{\mathrm{eff}} = \left(D_{\mathrm{post}} - D_{\mathrm{pre}}\right)/\left(D_{\mathrm{post}}\right)$$

with D_{pre} and D_{post} as mean fluorescence intensities prior and after bleach, respectively.

3.8.4 Image Analysis

Note the values provided by the LAS X software under the "Quantification" tab for further statistical evaluation and graphical display.

3.8.5 FLIM

For FLIM applications, LAS X software and SymPhoTime 64 (from PicoQuant) software are used.

1. Switch the microscope to FLIM-mode. Start SymPhoTime, and create a new workspace.
2. Start lasers, and set the laser combining unit to 0.
3. Click on the tab "Setup Imaging" in the Leica software, and choose your appropriate laser and detectors.
4. Go to the tab "Setup FLIM", and choose the detector that is connected to the time-correlated single photon counting (TCSPC) module. Choose the wavelength to excite the donor.
5. Under "Acquisition" set resolution to 256 × 256, and scanning speed to 20–50 MHz while adjusting pixel dwell time to approximately 20 μs.
6. Set up the pulsed laser.
7. Choose the number of photons per pixel that should be counted. We recommend 500–1000. Pick a region of interest (ROI), and run a FLIM test. The kilo counts/s should not exceed 10% of the excitation frequency (e.g., 2 kilo counts/s for 20 MHz). If necessary, close the shutter of the laser combining unit to get less counts/s.
8. Run FLIM measurements at 7–10 different positions/cells/protoplasts. Zoom in and define ROIs for measurement. We recommend performing at least three independent biological replicates for FLIM measurements.
9. Measure donor-only samples, as well as a meaningful noninteracting candidate as negative controls.

3.8.6 Measure Instrument Response Function (IRF)

Since the microscope, objective, coverslip, and the pulse type of the laser do have an influence on the detection, the IRF must be measured for later evaluation.

1. Put only a coverslip on the objective without sample.
2. Set the mode from *xyz* to *xzy*, the laser to 5%, and the required wavelength of the donor (e.g., for GFP: 488 nm). Choose one

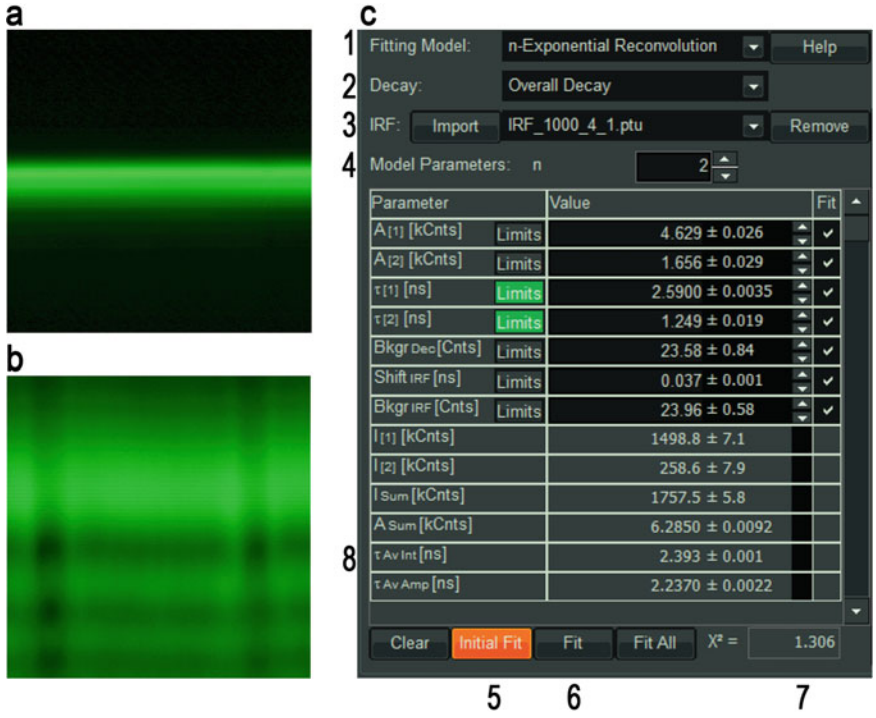

Fig. 5 Comparison between the edge of (**a**) the upper coverslip which is needed for measuring the IRF and (**b**) the edge of the microscope slide which should not be measured. (**c**) Section of SymPhoTime 64 software for evaluation of FRET-FLIM data. (*1*) The "Fitting Model" should be "n-Exponential Reconvolution" while the (*2*) "Decay" should be "Overall Decay." (*3*) The experimentally measured IRF (Subheading 3.8.6) has to be imported here (*4*). "Model Parameters – n" have to be set up according to the decay variant of the donor. Calculation is started with (*5*) "Initial Fit" and (*6*) Fit (*7*). If χ^2 is in the range of approximately 1–2, the fluorescence lifetime τ in [8] can be copied for further evaluation

PMT detector for emission at the same wavelength as the excitation (e.g., GFP: 488 nm).

3. Set the donor fluorescence to reflexion in the tab "AOBS."
4. Set up FLIM as before in Subheading 3.8.5 but use the PMT to detect exactly at the same wavelength as the pulsed laser.
5. Search the upper edge of the coverslip (Fig. 5a).
6. In the tab "fluorifier disc setting," deselect the autoselect and choose an empty position for the filters.
7. Close the laser combining unit.
8. Run a FLIM test with kilo counts per second at approximately 2000.
9. Measure IRF once and save it.

3.8.7 Evaluation

1. Open SymPhoTime and load your data. Choose one ".ptu" file, click Analysis → Imaging → FLIM → Start.

2. Set up "n-Exponential Reconvolution," overall decay and load your measured IRF sample in the designated tab. Choose the "Model Parameter – n" according to the decay variant of your donor fluorophore (e.g., mono- or bi-exponential decay) (Fig. 5).
3. We recommend decreasing the front border-width (e.g., 0.55 ns).
4. Press "Initial FIT" and afterwards "FIT." The χ^2 should be approximately between 1 and 2. Higher values indicate that the measured decay does not correlate to the calculated ideal decay (Fig. 5).
5. Lifetime values for further statistical evaluations are: "τ av. int (ns)" (Fig. 5).
6. Note these values in a .txt file or excel and use them for statistical evaluation and graphical display.

4 Notes

1. For structure-function analysis using alanine-scanning mutagenesis, we routinely design primers using our SDM-assist program that allows—in addition to the desired mutation—introduction of a silent restriction site to distinguish different point mutants via endonuclease digest [22].
2. We recommend construct verification of *Agrobacteria* clones used for transfection through plasmid rescued in *E. coli* followed by restriction analysis [20]. Even antibiotic resistant *Agrobacteria* colonies sometimes do not carry the recombinant plasmid, and we had cases, where plasmid restriction digests revealed significant alterations in plasmids. Verified *Agrobacteria* clones should be stored at −80 °C in 7% DMSO.
3. To gain more *Arabidopsis* protoplasts, it is possible to subculture 10 mL of a 3-day-old culture into 50 mL fresh MSCol medium. Cells for protoplast generation are taken 3 days after this second subculture. These cells are nicknamed "Turbo Cells" and produce finer and smaller protoplasts. You must not use these Turbo Cells for your main culture though, otherwise, the culture will outgrow itself too fast.
4. It is not necessary to wash out the PEG (1500) as its effective concentration is diluted in subsequent steps; alternatively, addition of a washing step with MM or W5 can be included.
5. Reporter assays benefit from shorter incubation times as they have better signal-to-noise ratios when applying treatments, whereas an overnight incubation is sufficient for localization or interaction assays.

6. Living cells will float on the top of the solution when they are in K3. Alternative incubation buffers found in the literature can also be used: for example, WI or TEX.
7. The ratio needs to be set up for a positive control and should be examined on several different epidermal cells. A ratio of 1 is preferred but not always feasible due to overall low expression. It is important that once the parameters are adjusted, there will be no change in settings over the complete set of samples to assure comparability.
8. Even though RFP acts as an expression and transformation/transfection control, verification of protein expression via immunoblot is recommended. The 2in1 plasmid used contains a 3xHA tag as well as a MYC tag fused to the proteins of interest for antibody detection (Fig. 3f).
9. Due to temporal delay in recording caused by the bleaching step, cellular movement leads to a shift of the region of interest out of the focal plane making measurements meaningless. To avoid this issue, we fixed samples in 4% (w/v) paraformaldehyde (PFA) in microtubule stabilization buffer (MTSB) (50 mM PIPES, 5 mM EGTA, 5 mM $MgSO_4 \cdot 7H_2O$, pH ~7 (KOH)).

Acknowledgements

We are grateful to Eva Schwörzer and Laure Grefen for excellent technical support. Work in our lab is supported through seed funding of the SFB1101 and an Emmy Noether fellowship of the German Research Foundation (DFG) to C.G. (GR 4251/1-1).

References

1. Xing S, Wallmeroth N, Berendzen KW, Grefen C (2016) Techniques for the analysis of protein-protein interactions in vivo. Plant Physiol 171:727–758
2. Husbands AY, Aggarwal V, Ha T, Timmermans MC (2016) In planta single-molecule pull-down reveals tetrameric stoichiometry of HD-ZIPIII:LITTLE ZIPPER complexes. Plant Cell 28:1783–1794
3. Grefen C, Blatt MR (2012) A 2in1 cloning system enables ratiometric bimolecular fluorescence complementation (rBiFC). Biotechniques 53:311–314
4. Hecker A, Wallmeroth N, Peter S, Blatt MR, Harter K, Grefen C (2015) Binary 2in1 vectors improve in planta (co-) localisation and dynamic protein interaction studies. Plant Physiol 168:776–787
5. Ghosh I, Hamilton AD, Regan L (2000) Antiparallel leucine zipper-directed protein reassembly: application to the green fluorescent protein. J Am Chem Soc 122:5658–5659
6. Horstman A, Tonaco IA, Boutilier K, Immink RG (2014) A cautionary note on the use of split-YFP/BiFC in plant protein-protein interaction studies. Int J Mol Sci 15:9628–9643
7. Grefen C, Karnik R, Larson E, Lefoulon C, Wang YZ, Waghmare S, Zhang B, Hills A, Blatt MR (2015) A vesicle-trafficking protein commandeers Kv channel voltage sensors for voltage-dependent secretion. Nat Plants 1:15108

8. Lipka E, Gadeyne A, Stockle D, Zimmermann S, De Jaeger G, Ehrhardt DW, Kirik V, Van Damme D, Muller S (2014) The phragmoplast-orienting kinesin-12 class proteins translate the positional information of the preprophase band to establish the cortical division zone in *Arabidopsis thaliana*. Plant Cell 26:2617–2632
9. Albert I, Bohm H, Albert M, Feiler CE, Imkampe J, Wallmeroth N, Brancato C, Raaymakers TM, Oome S, Zhang HQ, Krol E, Grefen C, Gust AA, Chai JJ, Hedrich R, Van den Ackerveken G, Nurnberger T (2015) An RLP23-SOBIR1-BAK1 complex mediates NLP-triggered immunity. Nat Plants 1:15140
10. Karnik R, Zhang B, Waghmare S, Aderhold C, Grefen C, Blatt MR (2015) Binding of SEC11 indicates its role in SNARE recycling after vesicle fusion and identifies two pathways for vesicular traffic to the plasma membrane. Plant Cell 27:675–694
11. Zhang B, Karnik R, Wang Y, Wallmeroth N, Blatt MR, Grefen C (2015) The arabidopsis R-SNARE VAMP721 interacts with KAT1 and KC1 K+ channels to moderate K+ current at the plasma membrane. Plant Cell 27:1697–1717
12. Kumar MN, Hsieh YF, Verslues PE (2015) At14a-Like1 participates in membrane-associated mechanisms promoting growth during drought in *Arabidopsis thaliana*. Proc Natl Acad Sci U S A 112:10545–10550
13. Le CT, Brumbarova T, Ivanov R, Stoof C, Weber E, Mohrbacher J, Fink-Straube C, Bauer P (2016) Zinc finger of Arabidopsis thaliana12 (ZAT12) interacts with FER-Like Iron Deficiency-Induced Transcription Factor (FIT) linking iron deficiency and oxidative stress responses. Plant Physiol 170:540–557
14. Forster T (1946) Energiewanderung und Fluoreszenz. Naturwissenschaften 33:166–175
15. Ishikawa-Ankerhold HC, Ankerhold R, Drummen GP (2012) Advanced fluorescence microscopy techniques—FRAP, FLIP, FLAP, FRET and FLIM. Molecules 17:4047–4132
16. Bucherl CA, Bader A, Westphal AH, Laptenok SP, Borst JW (2014) FRET-FLIM applications in plant systems. Protoplasma 251:383–394
17. Wallrabe H, Periasamy A (2005) Imaging protein molecules using FRET and FLIM microscopy. Curr Opin Biotechnol 16:19–27
18. De Los SC, Chang CW, Mycek MA, Cardullo RA (2015) FRAP, FLIM, and FRET: detection and analysis of cellular dynamics on a molecular scale using fluorescence microscopy. Mol Reprod Dev 82:587–604
19. Koncz C, Schell J (1986) The promoter of Tl-DNA Gene5 controls the tissue-specific expression of chimeric genes carried by a novel type of agrobacterium binary vector. Mol Gen Genet 204:383–396
20. Blatt MR, Grefen C (2014) Applications of fluorescent marker proteins in plant cell biology. Methods Mol Biol 1062:487–507
21. Mathur J, Koncz C (1997) Method for preparation of epidermal imprints using agarose. Biotechniques 22:280–282
22. Karnik A, Karnik R, Grefen C (2013) SDM-assist software to design site-directed mutagenesis primers introducing "silent" restriction sites. BMC Bioinformatics 14:105
23. Sparkes IA, Runions J, Kearns A, Hawes C (2006) Rapid, transient expression of fluorescent fusion proteins in tobacco plants and generation of stably transformed plants. Nat Protoc 1:2019–2025
24. Shuping Xing, Dietmar Gerald Mehlhorn, Niklas Wallmeroth, Lisa Yasmin Asseck, Ritwika Kar, Alessa Voss, Philipp Denninger, Vanessa Aphaia Fiona Schmidt, Markus Schwarzländer, York-Dieter Stierhof, Guido Grossmann, Christopher Grefen, (2017) Loss of GET pathway orthologs in causes root hair growth defects and affects SNARE abundance. Proceedings of the National Academy of Sciences 114(8):E1544–E1553

Chapter 12

Metabolons on the Plant ER

Verena Kriechbaumer and Stanley W. Botchway

Abstract

Metabolons are protein complexes that contain all the enzymes necessary for a metabolic pathway but also scaffolding proteins. Such a structure allows efficient channeling of intermediate metabolites from one active site to the next and is highly advantageous for labile or toxic intermediates. Here we describe two methods currently used to identify metabolons via protein–protein interaction methodology: immunoprecipitations using GFP-Trap®_A beads to find novel interaction partners and potential metabolon components and FRET-FLIM to test for and quantify protein–protein interactions in planta.

Key words Endoplasmic reticulum, Metabolon, Enzymes, Protein complex, Protein–protein interaction, Co-immunoprecipitation, GFP-trap, FRET-FLIM

1 Introduction

The plant ER has been shown to be dynamic and constantly remodeling [1]. Specific ER microdomains with unique lipid composition are suggested to direct proper anchoring of proteins and to facilitate and stabilize the subsequent assembly of components required to form a specific protein complex capable of carrying out a complete metabolic pathway [2]. These so-called metabolons enable metabolic processes to take place in the necessary highly coordinated and regulated processes in an efficient manner. Metabolons contain sequential enzymes plus scaffolding proteins allowing for efficient channeling of metabolic intermediates from one active site directly to the next [2]. The concept of these so-called metabolons was introduced in 1985 by Paul Srere in the context of glycolytic and Krebs cycle enzymes [3]. Sequential enzymes of a specialized biosynthetic pathway are transiently linked together by noncovalent binding typically stabilized by membrane or cytoskeletal anchoring [4]. Such a mechanism increases substrate concentration and turnover rates, prevents unwanted diffusion and metabolic interference, and is beneficial for containment of labile or toxic intermediates. Such complex organization has been shown

Chris Hawes and Verena Kriechbaumer (eds.), *The Plant Endoplasmic Reticulum: Methods and Protocols*, Methods in Molecular Biology, vol. 1691, DOI 10.1007/978-1-4939-7389-7_12,

for protein translocases in the endoplasmic reticulum, in chloroplasts and mitochondria [5–7] allowing coordinated and efficient transport potentially also preventing back-flux.

Metabolons will typically be comprised of sequential enzymes in the pathway together with scaffolding proteins allowing for efficient channeling of metabolic intermediates from one active site to the next [2]. Candidate proteins for such scaffolding are chaperones as well as membrane-anchored cytochrome P450 enzymes that can serve as nucleation points and platforms for metabolon formation [2]. In addition to this TA proteins were shown to have the potential to localize metabolons to specific organelle surfaces, for example in the TOM complex where the tail-anchors operate as assembly signal [8]. This can also stabilize proteins compared to their cytosolic versions as shown for tobacco expression of the HIV gene product Nef which has been researched in the context of HIV vaccination [9].

Also membrane-structural proteins have been suggested to play a role in metabolon formation, e.g., P450 enzymes involved in a lignin biosynthetic metabolon were co-purified with reticulon proteins (RTN) [10] which contribute to ER tubule shaping [11].

In plants, metabolons have been shown for several enzymatic pathways in secondary and primary metabolism [12]. Most metabolons involved in secondary metabolism involve less stable interactions than described for metabolons in primary metabolism demanding refined microscopy methods and computational analysis to prove their interactions [13].

Metabolons have been shown, e.g., for the production of flavonoids [14] and sporopollenin [15] in arabidopsis and the glucoside dhurrin [16] in sorghum. Recently a soybean isoflavonoid metabolon tethered to the ER has been reported [17]. An ER-localized metabolon for the biosynthesis of the auxin indole-3-acetic acid (IAA) has been suggested [18].

The metabolon complexes producing phenylpropanoids [19] and flavonoids [14, 20] seem to cater for specific metabolites made from shared intermediate products. The enzyme composition in the flavonoid pathway complex can change, resulting in varying end products [12, 14]. Membrane-anchored cytochrome P450 enzymes are reported to serve as nucleation points and platforms for the metabolon formation. Most P450 monooxygenases are membrane-bound to the ER via an N-terminal tether, enhancing metabolon formation on this membrane system [2, 21].

Metabolons for the glucoside dhurrin in sorghum are formed in specific ER domains [22] and metabolon formation between the three enzymes involved in dhurrin biosynthesis is suggested to be highly advantageous as the dhurrin precursor p-hydroxymandelonitrile is very unstable. Another ER-localized metabolon is the biosynthesis of sporopollenin in tapetal cells. Colocalization and protein–protein interaction of these enzymes

indicate the existence of a sporopollenin metabolon on the ER [15]. This benefits a coordinated and quick production of pollen cell wall components allowing for rapid pollen development.

Molecular distances (1–10 nm) can be measured using energy transfer processes. Förster or fluorescence resonance energy transfer (FRET), first described by Theodor Förster over 50 years ago [23], relies on the non-radiative energy transfer from an excited fluorescent donor molecule to a different non-excited fluorescent acceptor molecule in its vicinity. The very short distances required for this process to occur (<10 nm) means the two molecules, in this case two proteins, needs to be physically close to one another. For FRET to occur, the donor emission spectrum must overlap sufficiently with the acceptor absorption spectrum; the donor and acceptor dipoles display a mutual molecular orientation. The rate of the energy transfer k_T is described and calculated using Eq. 1:

$$k_T = \left(\frac{1}{\tau_D}\right)\left(\frac{R_0}{R}\right)^6 \quad (1)$$

where τ_D is the donor excited-state lifetime in the absence of the acceptor, R is the distance between D and A, and R_0 is the Förster radius. At the Förster radius, 50% of the donor molecules will emit fluorescence while the rest will undergo energy transfer. Since the energy transfer process is strongly distance dependent with $1/R^6$, FRET can be used to measure distance and examine molecular interactions on an nm spatial scale. During FRET, the rate of decay is reduced by a quenching process that depletes the excited state of the donor fluorophore, i.e., the donor fluorescence lifetime is shortened. By measuring changes in the excited-state lifetime of the donor at each pixel making up an image, steady-state FRET is enhanced. This is described as fluorescence lifetime imaging microscopy or FRET-FLIM. Generally the two proteins under investigation are tagged with GFP and its variants. We have used GFP and RFP as the donor and acceptor respectively in our work. We describe here two methods that have been used in metabolon work: Immunoprecipitations using GFP-Trap®_A beads to find novel interaction partners and potential metabolon components and FRET-FLIM to test for and quantify protein–protein interactions in planta.

2 Materials

2.1 Buffers and Media for Immunoprecipitations

1. Murashige and Skoog (MS) medium: 4.4 g/L Murashige and Skoog basal salts, pH 5.7, 10 g/L agar.
2. Lysis buffer: 10 mM Tris–HCl pH 7.5, 150 mM NaCl, 0.5 mM EDTA, 0.5% NP-40, 1 mM PMSF, protease inhibitor according to manufacturers' instructions.
3. Equilibration buffer: 10 mM Tris–HCl pH 7.5, 150 mM NaCl, 0.5 mM EDTA.

2.2 Buffers and Media for FRET-FLIM

For plant infiltration and expression in tobacco, *see* protocols in chapter "Labeling the ER for light and fluorescence microscopy."

2.3 Equipment for Immunoprecipitations

1. Petri dishes (large, with lid L × W × H: 245 mm × 245 mm × 25 mm).
2. 50-ml Falcon tubes.
3. Glass bottles for buffers.
4. Cheese cloth.
5. Refrigerated table centrifuge.

2.4 Equipment for FRET-FLIM

1. At least two-channel confocal and one-channel FLIM setup.
2. Becker and Hickl SPC 830 or SPC150 time-correlated single-photon counting card.
3. SPCImage analysis software version 5.1 (Becker and Hickl).

3 Methods

3.1 Immunoprecipitation Using GFP-Trap®_A Beads

(This part of the procedure will take between 4 and 5 h depending on sample size.) This protocol uses GFP-Trap®_A beads (Chromotek, Martinsried, Germany) and the procedure is carried according to the company's protocol with slight modifications (*see* **Note 1**):

Arabidopsis thaliana seedlings expressing the protein of interest fused to a fluorescent tag (*see* Protocol "Labeling the ER for light and fluorescence microscopy" for preparation of stable arabidopsis transformants) are grown for 2 weeks on MS plates (*see* **Note 2**).

1. Approximately 5 g of whole seedling plant material are ground first in liquid nitrogen to a fine powder and then in 5-ml lysis buffer until liquid. The extract is then distributed into three 2-ml Eppendorf tubes.
2. The extracts are incubated on ice for 30 min and then centrifuged at 10,000 × *g* for 10 min at 4°C.
3. The supernatant (about 4 ml) is poured into fresh 50-ml Falcon tubes via two layers of cheese cloth.
4. 100 μl of GFP-Trap®_A beads per sample are equilibrated in 500 μl equilibration buffer and centrifuged at 2500 × *g* for 2 min. The supernatant is being discarded and this wash is repeated twice.
5. 100 μl of the washed beads are added to the plant extract and the mixture is shaken on ice for 2 h with the tubes being placed horizontally in the ice.
6. After this, tubes are centrifuged at 2500 × *g* for 2 min at 4°C and the supernatant is being carefully discarded without disturbing the agarose pellet.

7. The resulting agarose pellet is then washed twice with dilution buffer.
8. This pellet can be used straight away for tryptic peptide digest and mass spectrometry analysis for containing proteins [24].

3.2 Real-Time Imaging of Metabolon Protein–Protein Interactions Using Two-Photon FRET-FLIM

Potential interaction candidates resulting from the immunoprecipitation are tested for interactions in planta with the bait protein. This procedure is done using agrobacterium-mediated transient expression in tobacco leaf epidermal cells (*see* Protocol "Labeling the ER for light and fluorescence microscopy" for transient expression in tobacco).

1. Epidermal samples of infiltrated tobacco leaves are excised, and both confocal and multiphoton FRET-FLIM data capture is performed by a two-photon microscope [25] (*see* **Note 3**).
2. The two-photon microscope built around a Nikon TE2000-U inverted microscope is used with a modified Nikon EC2 confocal scanning system to allow for near-infrared laser wavelength for FLIM [26].
3. Laser light at a wavelength of 920 nm is produced by a mode-locked titanium sapphire laser (Mira; Coherent Lasers), with 200-fs pulses at 76 MHz, pumped by a solid-state continuous wave 532-nm laser (Verdi V18; Coherent Laser).
4. The laser beam is focused to a diffraction limited spot using a water-immersion objective (Nikon VC; 360, numerical aperture of 1.2) to illuminate specimens on the microscope stage.
5. Fluorescence emission is collected without descanning (no pinhole), bypassing the scanning system, and passed through a BG39 (Comar) filter to block the near-infrared laser light. Line, frame, and pixel clock signals are generated and synchronized with an external detector in the form of a fast microchannel plate photomultiplier tube (Hamamatsu R3809U).
6. Linking these via a time-correlated single-photon counting PC module SPC830 (Becker and Hickl) generated the raw FLIM data. Prior to FLIM data collection, the GFP and mRFP expression levels in the plant samples within the region of interest are confirmed using a Nikon EC2 confocal microscope with excitation at 488 and 543 nm, respectively.
7. A 633-nm interference filter is used to significantly minimize the contaminating effect of chlorophyll autofluorescence emission that would otherwise obscure the mRFP as well as GFP emission.
8. Data are analyzed by obtaining excited-state lifetime values first on a pixel by pixel basis then of a region of interest on the nucleus, and calculations are made using SPCImage analysis software version 5.1.

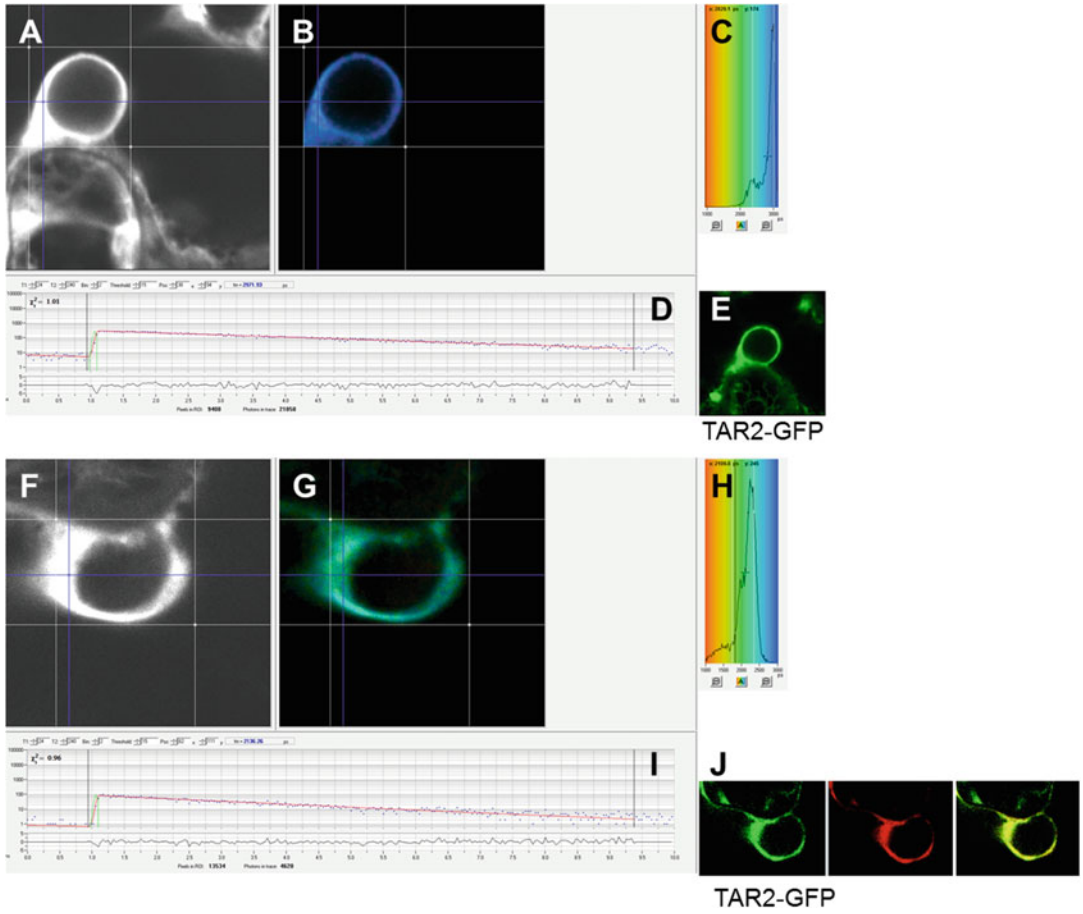

Fig. 1 FRET-FLIM analysis of TAR2 without an interaction partner (**a**–**e**) or with YUC8 (**f**–**j**). (**a**, **f**) Raw FRET-FLIM data; (**b**, **g**) pseudocolored lifetime maps showing the lifetime values for each point within the region of interest; (**c**, **h**) distribution of lifetimes across the image. *Blue shades* represent longer GFP fluorescence lifetimes than *green ones*. (**d**, **i**) Representative decay curves of a single point with an optimal single exponential fit, where $\chi 2$ values from 0.9 to 1.2 were considered an excellent fit to the data points (a binning factor of 2 was applied). The confocal images for the analysis in (**e**, **j**) show the GFP construct in green and the mCherry construct in red. This example of FRET-FLIM analysis shows TAR2-GFP alone as a negative control and YUC8 for protein–protein interaction. The fluorescence lifetime values for TAR2-GFP + YUC8-mCherry are 2.8 ± 0.02 ns and therefore statistically lower than the lifetime values for the TAR2-GFP fusion alone (3.04 ± 0.03 ns)

9. The distribution of lifetime values within the region of interest is generated and displayed as a curve. Only values with a χ^2 between 0.9 and 1.4 are taken.
10. The median lifetime, minimum and maximum values for one-quarter of the median lifetime values from the curve are taken to generate the range of lifetimes per sample.
11. The ER associated with at least three nuclei from a minimum of three independent biological samples per protein–protein combination are analyzed, and the average of the ranges is taken.

12. The degree or efficiency of energy transfer (E), from one protein to the other, may be determined using Eq. 2:

$$E\% = \left[1 - \left(\frac{\tau_{DA}}{\tau_D}\right)\right] \times 100 \quad (2)$$

where τ_D and τ_{DA} are the measured excited-state lifetime of the donor and acceptor, respectively.

Example data is shown in Fig. 1.

4 Notes

1. Gloves have to be worn for the whole procedure to reduce contamination.
2. This protocol can also be carried out with tobacco transiently expressing the protein of interest but will result in reduced yield of interacting proteins and will of course only show interactors in tobacco.
3. Best measurement results for the ER have been shown for the nuclear envelope and associated ER. Latrunculin B can be applied to the leaf disks to depolymerize the actin cytoskeleton and therefore inhibit any movement of the ER. This may not be necessary with high expression levels of the donor protein which result in shorter time for data capture and therefore movement is less critical.

Acknowledgements

This work was supported by the Science and Technology Facilities Council Program (grant no. 14230008) awarded to Prof. Chris Hawes.

References

1. Hawes C, Kiviniemi P, Kriechbaumer V (2015) The endoplasmic reticulum: a dynamic and well-connected organelle. J Integr Plant Biol 57:50–62
2. Jørgensen K, Rasmussen AV, Morant M, Nielsen AH, Bjarnholt N, Zagrobelny M, Bak S, Møller BL (2005) Metabolon formation and metabolic channelling in the biosynthesis of plant natural products. Curr Opin Plant Biol 8:280–291
3. Srere PA (1987) Complexes of sequential metabolic enzymes. Annu Rev Biochem 56:89–124
4. Hoppert M, Mayer F (1999) Principles of macromolecular organization and cell function in bacteria and archaea. Cell Biochem Biophys 31:247–284
5. Jarvis P, Chen LJ, Li H, Peto CA, Fankhauser C, Chory J (1998) An Arabidopsis mutant defective in the plastid general protein import apparatus. Science 28:100–103
6. Werhahn W, Niemeyer A, Jansch L, Kruft V, Schmitz UK, Braun H (2001) Purification and characterization of the preprotein translocase of the outer mitochondrial membrane from Arabidopsis. Identification of multiple forms of TOM20. Plant Physiol 125:943–954
7. Van den Berg B, Clemons WM, Collinson I, Modis Y, Hartmann E, Harrison SC, Rapoport

TA (2004) X-ray structure of a protein conducting channel. Nature 427:36–44

8. Horie C, Suzuki H, Sakaguchi M, Mihara K (2003) Targeting and assembly of mitochondrial tail-anchored protein Tom5 to the TOM complex depend on a signal distinct from that of tail-anchored proteins dispersed in the membrane. J Biol Chem 278:41462–41471
9. Marusic C, Nuttall J, Buriani G, Lico C, Lombardi R, Baschieri S, Benvenuto E, Frigerio L (2007) Expression, intracellular targeting and purification of HIV Nef variants in tobacco cells. BMC Biotechnol 7:12
10. Bassard JE, Richert L, Geerinck J, Renault H, Duval F, Ullmann P, Schmitt M, Meyer E, Mutterer J, Boerjan W, De Jaeger G, Mely Y, Goossens A, Werck-Reichhart D (2012b) Protein-protein and protein-membrane associations in the lignin pathway. Plant Cell 24:4465–4482
11. Sparkes I, Tolley N, Aller I, Svozil J, Osterrieder A, Botchway S, Mueller C, Frigerio L, Hawes C (2010) Five plant reticulon isoforms share ER localisation, topology, ER membrane shaping properties. Plant Cell 22:1333–1343
12. Winkel-Shirley B (2002) Evidence for enzyme complexes in the phenylpropanoid and flavonoid pathways. Plant Physiol 107:142–149
13. Bassard JE, Mutterer J, Duval F, Werck-Reichhart D (2012) A novel method for monitoring the localization of cytochromes P450 and other endoplasmic reticulum membrane associated proteins: a tool for investigating the formation of metabolons. FEBS J 279:1576–1583
14. Hrazdina G, Wagner GJ (1985) Metabolic pathways as enzyme complexes: evidence for the synthesis of phenylpropanoids and flavonoids on membrane associated enzyme complexes. Arch Biochem Biophys 237:88–100
15. Lallemand B, Erhardt M, Heitz T, Legrand M (2013) Sporopollenin biosynthetic enzymes interact and constitute a metabolon localized to the endoplasmic reticulum at tapetum cells. Plant Physiol 162:616–625
16. Nielsen KA, Tattersall DB, Jones PR, Møller BL (2008) Metabolon formation in dhurrin biosynthesis. Phytochemistry 69:88–98
17. Dastmalchi M, Bernards MA, Dhaubhadel S (2016) Twin anchors of the soybean isoflavonoid metabolon: evidence for tethering of the complex to the endoplasmic reticulum by IFS and C4H. Plant J 85:689–706
18. Kriechbaumer V, Botchway SW, Hawes C (2016) Localization and interactions between Arabidopsis auxin biosynthetic enzymes in the TAA/YUC-dependent pathway. J Exp Bot 67:4195–4207
19. Stafford HA (1974) Possible multienzyme complexes regulating the formation of C6-C3 phenolic compounds and lignins in higher plants. Recent Adv Phytochem 8:53–79
20. Winkel-Shirley B (2001) Flavonoid biosynthesis: a colorful model for genetics, biochemistry, cell biology and biotechnology. Plant Physiol 126:485–493
21. Ralston L, Yu O (2006) Metabolons involving plant cytochrome P450. Phytochem Rev 5:459–472
22. Winkel BS (2004) Metabolic channelling in plants. Annu Rev Plant Biol 55:85–107
23. Förster T (1948) Zwischenmolekulare Energiewanderung und Fluoreszenz. Ann Phys 437:55–75
24. Kriechbaumer V, Botchway SW, Slade SE, Knox K, Frigerio L, Oparka K, Hawes C (2015) Reticulomics: protein-protein interaction studies with two plasmodesmata-localized reticulon family proteins identify binding partners enriched at plasmodesmata, endoplasmic reticulum, and the plasma membrane. Plant Physiol 169:1933–1945
25. Schoberer J, Botchway SW (2014) Investigating protein-protein interactions in the plant endomembrane system using multiphoton-induced FRET-FLIM. Methods Mol Biol 1209:81–95
26. Botchway SW, Scherer KM, Hook S, Stubbs CD, Weston E, Bisby RH, Parker AW (2015) A series of flexible design adaptations to the Nikon E-C1 and E-C2 confocal microscope systems for UV, multiphoton and FLIM imaging. J Microsc 258:68–78

Chapter 13

Using Optical Tweezers Combined with Total Internal Reflection Microscopy to Study Interactions Between the ER and Golgi in Plant Cells

Imogen Sparkes, Rhiannon R. White, Benjamin Coles, Stanley W. Botchway, and Andy Ward

Abstract

Optical tweezers have been used to trap and micromanipulate several biological specimens ranging from DNA, macromolecules, organelles to single celled organisms. Using a combination of the refraction and scattering of laser light from a focused laser beam, refractile objects are physically captured and can be moved within the surrounding media. The technique is routinely used to determine biophysical properties such as the forces exerted by motor proteins. Here, we describe how optical tweezers combined with total internal reflection fluorescence (TIRF) microscopy can be used to assess physical interactions between organelles, more specifically the ER and Golgi bodies in plant cells.

Key words Optical trap, ER, Golgi, Tweezers, GFP

1 Introduction

Trapping and micromanipulation for biological samples using optical tweezers has a wide range of applications from DNA, macromolecules, organelles to single celled organisms (reviewed in [1]). The basic premise of optical traps is that only microscopic particles that display a significantly different refractive index to the surrounding medium will be trapped in the focused infrared laser beam (Fig. 1). Infrared laser beams are routinely used as they generally result in the lowest sample absorbance and therefore cause the least photon damage. Optical traps can either be fixed in position, and therefore require lateral stage movement to move the sample relative to the trapped object, or the system can use mirrors, acousto-optic deflectors, or spatial light modulation to move the position of the trap and therefore the object [2]. Here, we present our system which utilizes a single beam gradient trap that is fixed in position combined with TIRF microscopy. Readers

Chris Hawes and Verena Kriechbaumer (eds.), *The Plant Endoplasmic Reticulum: Methods and Protocols*, Methods in Molecular Biology, vol. 1691, DOI 10.1007/978-1-4939-7389-7_13,

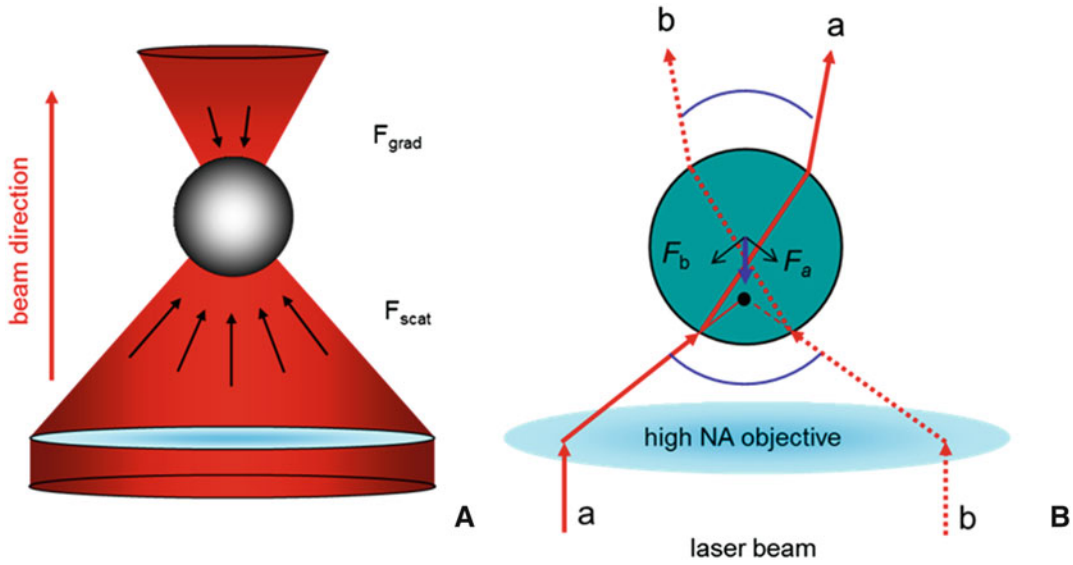

Fig. 1 Mechanism of action of a gradient optical trap. (**A**) Scattering and gradient forces are balanced in a tightly focused laser beam using a high numerical aperture objective lens to form a stable three-dimensional trap. (**B**) Gradient restoring forces (F_a, F_b) result from the refraction of the laser beam as it passes through the trapped object, with rays of light (*a* and *b*) depicting the paths taken by the edges of the beam

are directed to Ketelaar et al. [3] for discussion of integrating optical traps with confocal microscope systems.

Optical trapping has been used to probe several aspects of subcellular architecture in plant cells (reviewed in [3]). For example, the effects of nuclear positioning on root hair growth [4], interactions between several organelle pairings including peroxisome-chloroplasts [5], ER-Golgi [6] and ER-chloroplasts [7], and cytoskeletal organization [8]. We have used optical tweezers to characterize interactions between several organelles in plants (ER-Golgi and peroxisome-chloroplast), where the measurement of such interactions is only possible if one of the organelles is preferentially trapped. The efficiency with which organelles are trapped is related to a number of factors including refractive index, size, shape, and laser wavelength. For example, unlike the endoplasmic reticulum (ER), Golgi bodies in leaf epidermal cells are amenable to being trapped and moved within the confines of the cell. Since the ER and Golgi are functionally linked through the secretory pathway, this raised the question as to whether they were also physically linked. Using optical tweezers, we were able to show that lateral movement of trapped Golgi bodies resulted in the remodeling of the ER indicative of a physical association between the two organelles [6]. These studies provided a qualitative analysis of the interaction between the two structures. Here, we provide an overview of our current optical trapping platform which enables the user to quantify interactions between organelles. We have used this

system successfully to characterize the physical interaction between peroxisomes and chloroplasts, which are functionally linked through the photorespiratory pathway [5]. We will discuss important considerations relating to system calibration, sample generation, developing a quantifiable platform for measuring interactions and post-acquisition analysis. We also include caveats to force measurement calculations in plant cells. Of course, variations will apply subject to the optical trap system available to the user, but the general premise and pitfalls herein are universal.

2 Materials

2.1 System Setup and LabVIEW Interface

An optical trap with a two-channel TIRF microscope (TIRF-M) was constructed around a Nikon Ti-U inverted microscope. The near infrared (NIR) trapping laser at 1090 nm was delivered to the trapping objective (100×, oil immersion, NA 1.49 with both temperature and cover glass correction ring) using a commercial Elliot Scientific optical trapping platform. Fluorescence excitation for the TIRF-M imaging was obtained from an Omicron laser hub fiber coupled to a manual Nikon TIRF-M unit. For GFP and RFP chromophores fused to the proteins of interest, 488 and 561 nm were used, respectively. Fluorescence emissions were detected using two electron multiplying charge-coupled device (EMCCD, iXon, Andor) cameras. These are connected via a twin-cam (Cairn) unit (Fig. 2). This allowed the flexibility of full field of view per imaging channel as well as the ability to further magnify the image without restricting the observation area. A single camera may be used for a dual channel imaging (requiring technologies such as the Cairn OptoSplit II). This leads to restricted field of view but has the advantage of reduced cost and no need for synchronization of two separate cameras.

2.2 Microscopy Consumables

1. Standard glass slides (76 mm × 26 mm, 1 mm thick) to fit the stage.
2. Borosilicate No. 1 coverslips (*see* **Note 1**).
3. Electrical tape.
4. Polystyrene beads (1 μm diameter) are commercially available.

3 Methods

Carry out all procedures at room temperature unless otherwise stated.

3.1 Calibrating the Optical Trap Against Known Standards

The trap position, optical trapping force, and laser power transmission at the microscope objective are measured daily and compared for consistency to ensure the laser trapping setup is performing to

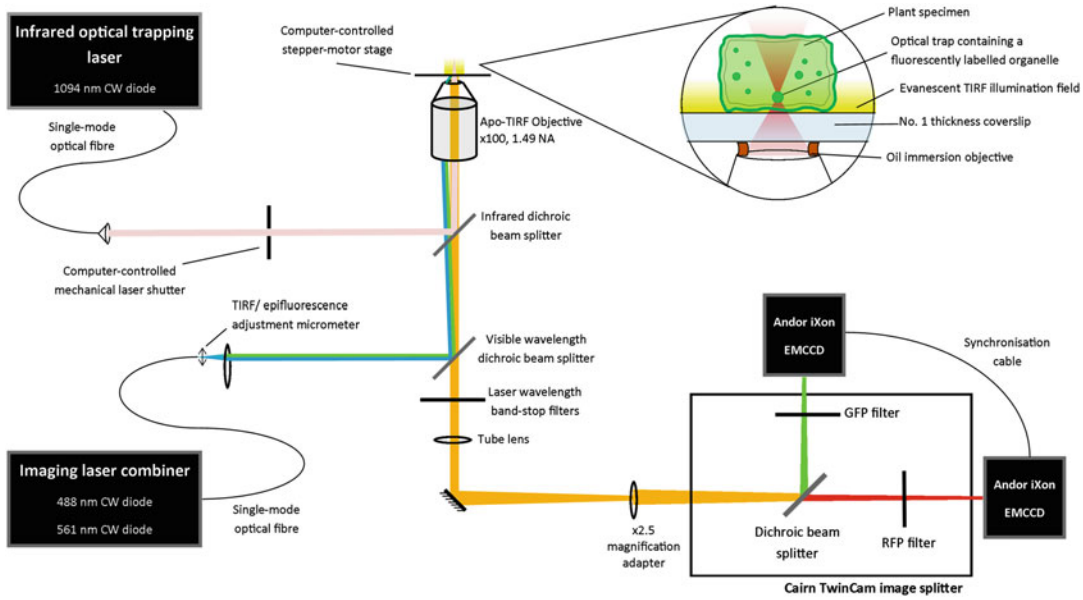

Fig. 2 Schematic of the microscope and optical trap system setup. The infrared trapping laser and visible-wavelength imaging lasers are fiber-coupled to independent microscope ports. The TIRF angle is tuned by adjusting the position of the fiber aperture in relation to the collimating lens using a micrometer. A computer-controlled mechanical shutter is placed in the trapping laser beam path which provides fast shuttering of the optical trap. The sample is mounted on a computer-controlled variable speed (Märzhäuser) stepper motor stage. The fluorescence is imaged through a (Nikon) ×100 1.49 NA objective and ×2.5 magnification adapter on two (Andor) EMCCD cameras, filtered for GFP and RFP fluorescent dyes, respectively. The associated computer-controlled hardware is interfaced using National Instruments LabVIEW which provides full automation for each trapping routine

specification. You are referred to **Note 2** for a critical evaluation of objective lenses for tweezers and TIRF microscopy.

3.2 Nominal Laser Power Transmission at the Sample

Using a power meter set to the wavelength of the trapping laser (1090 nm), a range of power readings of the optical trap laser transmission (0–130 mW) at the objective are measured on a daily basis. Large fluctuations of these readings (i.e., >5% change) between daily experimental runs could be indicative of changes in laser performance and stability or changes in laser alignment affecting the percentage transmission at the objective.

3.3 Trap Position and Force

Trap position is determined by trapping a 1 μm diameter polystyrene bead dispersed in water and imaging the position under bright field illumination or directly observing a significantly attenuated laser using the EMCCDs with the infrared filter removed.

To assess the trap strength, the escape force of spherical polystyrene beads is calculated. This is a relationship between the power of the optical trap that is required to maintain beads in the trap at a given stage speed, and is carried out as follows:

1. Place a drop of polystyrene beads on a coverslip and leave to settle for ~30 min.
2. Trap a polystyrene bead at the upper end of the optical trap power spectrum (*see* **Note 3**).
3. Move the stage back and forth with a preset velocity of 100 μm/s.
4. Repeat **step 3** after decreasing the power incrementally.
5. Note down the trap laser power at which the bead escapes the trap at 100 μm/s stage oscillation.
6. Repeat **steps 2–5** using 200, 300, 400, and 500 μm/s stage speeds.
7. Using the equation for Stokes viscous drag, calculate the escape force at which the bead escapes the trap (i.e., is no longer trapped) for each of the five different stage speeds.

$$F_{\text{drag}} = 6\pi\mu r v$$

where F_{drag} is the viscous drag force acting on the bead, μ is the fluid viscosity (water, 0.00089 Pa s), r is the object radius (bead), and v is the velocity measured.

8. Plot laser power against escape force for each stage speed (i.e., calculate the F_{drag} for the given velocity at which the bead escapes the trap). For beads, the relationship is linear as there are no constraints on moving the bead other than viscosity (Fig. 3).

Comparison between escape force profiles between different experimental runs enables the user to determine whether the trap "strength" has altered, i.e., is it "easier" or "harder" to maintain beads in the trap at a given stage speed. Similar bead trapping

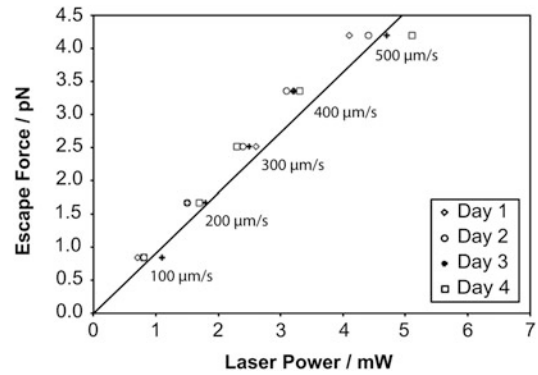

Fig. 3 Calculation of the optical trap escape force of a 1 μm polystyrene bead. Example plot of laser power (mW) against bead escape force (pN) for a range of indicated stage speeds (100–500 μm/s). Data displayed was collected on 4 consecutive days

profiles ensures that the system is behaving in a consistent manner and therefore allows results from biological samples to be directly compared.

3.4 Sample Preparation

To be able to specifically trap Golgi bodies, fluorophores need to be introduced which are specifically targeted to, and highlight the Golgi. Similarly, fluorophores for ER, or other organelles are required if monitoring the effects of interaction between two organelles. Genetically encoded fusions to targeting sequences, or functional proteins can be introduced into the plant material through agrobacterium-mediated transformation. Integration and expression can either be stable or transient. Readers are referred to standard protocols for these transformation procedures [9, 10]. Note, a bank of fluorescent organelle markers generated by the Nebenführ lab [11] are available either as plasmids or stable transgenic Arabidopsis lines through public repositories (ABRC or NASC).

Plant leaf material expressing the relevant fluorescent markers to be subjected to optical trapping is prepared in the following manner:

1. Pieces of tissue (~5 mm^2) are cut from the plant leaves and immersed in latrunculin b (25 μM for 1 h) to depolymerize actin and prevent organelle movement (*see* below).
2. The leaf samples are carefully mounted on the microscope slide and a No. 1 coverslip secured over the top using thin strips of electrical tape at either end of the slide.
3. Slides are mounted coverslip down onto the microscope stage and secured with spring clips. We are aiming to minimize the working distance between the coverslip and leaf to enable efficient trapping and uniform TIRF illumination. If the samples are incorrectly mounted, then trapping efficiency and imaging can be compromised.
4. To this end, a metal plate with a hole to allow imaging of the sample is placed under the slide and the spring clips of the slide holder placed over the top. The metal plate allows equal pressure to be applied evenly over the slide to help minimize the distance between sample and coverslip (i.e., plane of optimal trap force). Note, the level of pressure does not affect cell viability as evidenced through cytoplasmic streaming in samples which have not been treated with latrunculin b.
5. Regions of the sample are imaged ensuring the level of excitation lasers for the fluorophores is minimal so as to reduce any effects from fluorophore bleaching.

We have been able to trap Golgi bodies in both *Arabidopsis thaliana* [6] and *Nicotiana tabacum* leaf epidermal cells (Figs. 4 and 5). Both ER and Golgi are highly motile and so to be able to

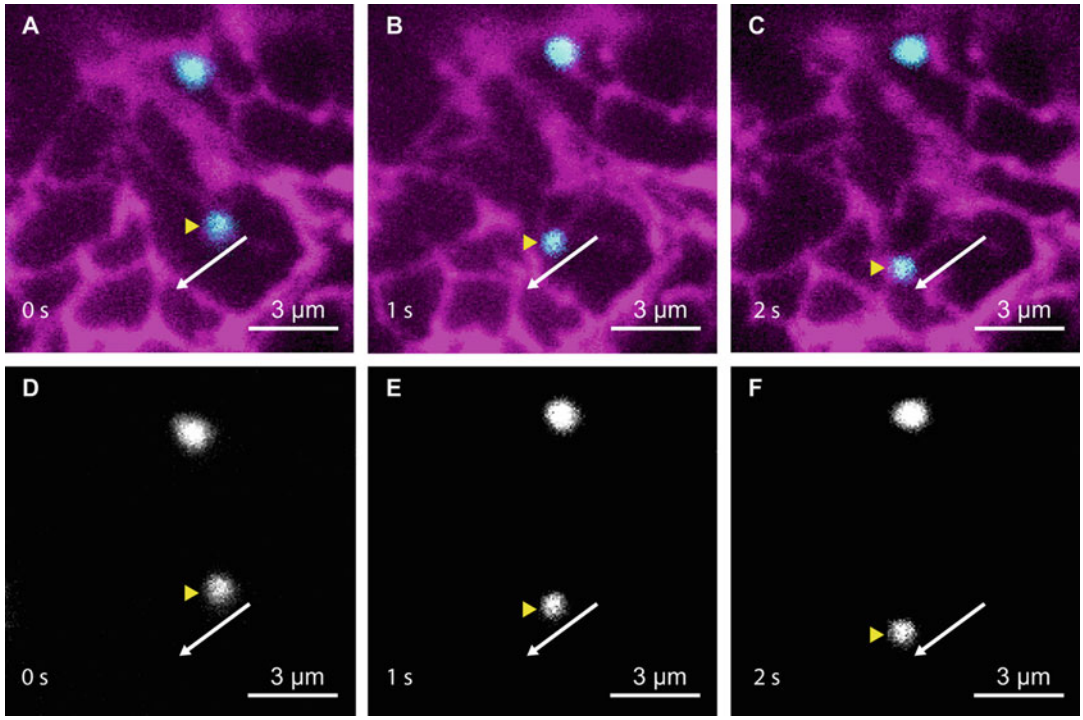

Fig. 4 Optical trapping and movement of an ER-associated Golgi body in tobacco leaf epidermal cells. Micrographs showing sequential frames of a movie of a Golgi (**d**–**f**) that is trapped under the force of the optical trap as the microscope stage is moved a distance of 6 μm at 6 μm/s. This movement is referred to as the stage translation. Panels (**a**)–(**c**) show the same frames of the trapped Golgi (*cyan*) in relation to the position of the surrounding ER (*magenta*). The ER is observed to be attached to and to move with (behind) the trapped Golgi. The *yellow* arrow indicates the position of the trapped Golgi and the *white arrow* indicates the direction of movement of the ER behind the trapped Golgi body. Scale bar, 3 μm

carefully dissect interaction the movement of both organelles needs to be inhibited [6]. Any subsequent motion is therefore due to the trapping and micromanipulation of the trapped object. Figure 4 highlights trapping of Golgi in a motile system. Comparisons between image frames highlight dynamic rearrangement of the ER making it difficult to observe the resulting changes in the ER as a result of trapping and moving a Golgi body which is physically associated with the ER. Figure 5 clearly shows trapping and movement of Golgi which are not attached to the ER.

3.5 Developing an Automated Trapping Routine

Qualitative analysis of interaction between ER and Golgi can be carried out by trapping and manually moving the Golgi and observing the effects on the ER [6]. To quantify interactions, the relationship between trap strength and organelle trapping efficiency and behavior is required (*see* **Note 3**).

1. Prior to data acquisition, a live image is displayed on the computer monitor and a potential organelle of interest is

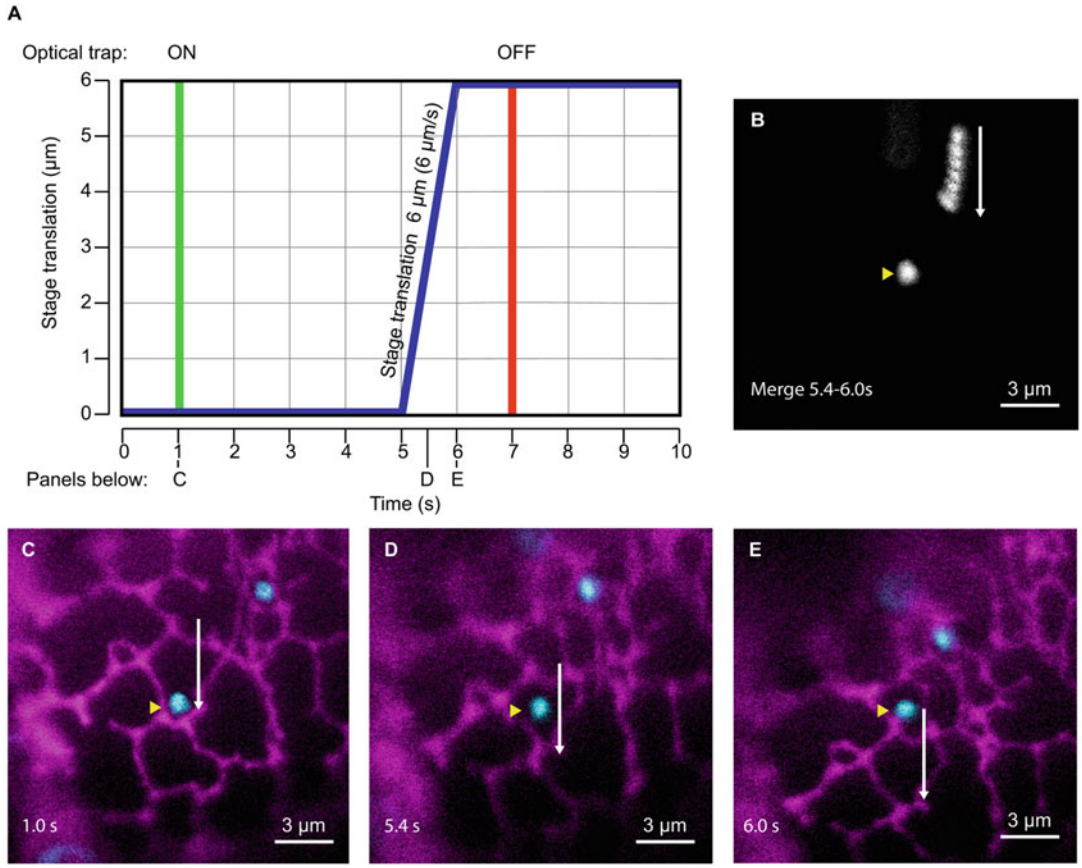

Fig. 5 Automated trapping routine applied to a Golgi body in tobacco leaf epidermal cells. Schematic representation of the position of the optical trap as considered radially from the starting point of the trapping routine (**a**). The TIRF image is recorded from 0 s, the trap is turned on after 1 s, the stage movement (translation) of 6 μm at 6 μm/s begins at 5 s and ends at 6 s, the trap is turned off after 7 s, and the image recording ends at 10 s. Images taken from a representative movie where the trapping routine (**a**) was used to trap a Golgi (*cyan*) and record the event in relation to the surrounding ER (*magenta*) are depicted; the moment the trap is turned on (**c**), the midpoint of the translation (**d**), and the end of the translation before the trap is turned off (**e**). The *yellow arrow* indicates the position of the trapped Golgi and the *white arrow* indicates the direction of movement of the stage. In this case, the Golgi is not attached to the ER and as it is moved the ER does not follow (**d**). Merged frames of the Golgi signal that correspond to 5.4–6.0 s of the routine are provided (**b**). The trapped Golgi (*yellow arrow*) does not change position relative to the field of view as the stage moves relative to the trapped object. Merged image therefore shows the trapped organelle as a single point (*yellow arrow*), whereas an organelle which was not trapped appears to be moving in the merged composite (*white arrow*) as its position changes relative to the field of view as the stage moves. Scale bar, 3 μm

located manually using a joystick and aligned with the optical trapping position.

2. The organelle then undergoes a recorded trapping routine such as that highlighted in Fig. 5. Here, the trap is turned on, stage moved laterally at a fixed speed over a fixed distance (referred to as stage translation), trap turned off, and the movement of the organelle post trapping monitored.

3. Organelles are scored as either being stably trapped (i.e., remaining in the trap during stage translation), or escaping the trap during the stage translation, or are not trapped during the procedure.
4. Distribution of trapping outcomes among these three categories can serve to determine the relative differences in trapping efficiency between different conditions, and can be compared when optical trapping power is changed [5]; tethered organelles will tend to require greater force to trap and move them a fixed distance than organelles which are not tethered. This procedure was followed for characterizing interactions between peroxisomes and chloroplasts [5].
5. The major considerations are the laser power used to trap the organelle, and the distance and speed at which to move the surrounding environment relative to the trapped organelle. If the trapping force is too strong, it will simultaneously trap several refractile objects, and if it is too weak, then the object will not be trapped. Similarly, if the object is moved too quickly, or too far (i.e., beyond the cell boundary), it will escape the trap.

Through development of the experiment we have built a custom system to allow the interface between imaging and optical trapping to be integrated. The major benefit of an integrated system is that customized scripts can be written in LabVIEW® to control the stage lateral motion (i.e., speed and distances traversed), the timing of trap activation, and the subsequent data capture [5]. The essential components are therefore:

1. An optical trap.
2. A means of turning the trap on and off (we use a shutter that can be automated).
3. A microscope stage that can be moved at the sub-micron resolution scale at controlled velocity.
4. A means of imaging the organelles of interest in a real-time (TIRF).

3.6 Setting the Optical Trap Laser Power

If the optical trap is too strong, it will likely trap the majority of organelles it is centered over (which includes organelles which do not contain fluorophores). If the goal is to determine whether trapping efficiency is affected by molecular perturbation, then it is important that not all organelles can be trapped under control conditions. Therefore, trapping 20 organelles and assessment of whether they remain in the trap during the micromanipulation procedure (*see* above) is deemed necessary. In practice, we classify organelles that have undergone the trapping routine into three categories: stably trapped (i.e., stay in the trap over the entire

movement), escape the trap (i.e., "fall out" of the trap during the stage movement), or are not trapped at all. Once this distribution has been ascertained, a full characterization can be carried out with at least five samples from each condition where at least ten organelles are trapped per sample.

3.7 Optimizing Distance and Speed at Which to Move the Trapped Organelle

Determining the distance to move the trapped organelle is an important consideration, too far and organelles may escape the trap due to opposing force components encountered (e.g., moving it into cytoplasmic streams if working in a motile system or encountering other subcellular structures), too short and it will be difficult to assess whether the trapped organelle is still attached to the ER.

3.8 Post-Acquisition Data Analysis

Analysis of data generated from the integrated TIRF-M optical tweezer setup requires certain META data to be assigned to each data set. The META data enables the user to determine the coordinates of the optical trap, to overlay trails of trapping events for ease of initial analysis and indicates the crucial time points during the trapping routine (e.g., trap on/off).

3.9 META Data Output for Post-Acquisition Analysis

For each recorded trapping event, five data files are generated based on post-acquisition analysis requirements:

1. and 2. Raw images acquired from the synchronized EMCCDs as 16-bit TIFF stacks, one for each fluorescent channel.
3. An 8-bit false-color (RGB) TIFF stack containing overlaid channels for quick reference.
4. A txt file containing the lateral (x/y) trap (shutter) position at the start of the routine and any additional META data (e.g., optional notes).
5. A csv file containing lateral (x/y) positions as measured in μm relative to the top-left stage limit. These positions are measured at the end of each frame but could be measured more often if required.

3.10 Data Analysis

Data can be analyzed based on the distribution of organelles into the three categories (stable, escaped, not trapped classification), and how this changes with optical trap power or under molecular perturbation. In addition, the distance and rate at which stably trapped organelles move back towards their original pre-trap position after the trap has been turned off can be measured. These measurements enable the user to understand the nature of physical interaction or the surrounding environment of the organelle. Assuming constant viscosity, differences in recoil rate can be used to model the physical tethering process [5]. Statistical analysis undertaken is dependent on the hypothesis under test and the nature of the material. Keeping sample sizes constant over experimental runs allows for less complicated downstream statistical analysis. Commercial or free software such as ImageJ can be used to

analyze the TIFF stacks post acquisition, and using python or similar programming language the lateral stage positions can be used to map and subtract the movement of the stage for automatic/batch analysis of the relative movement (e.g., speed, distance, recoil) of the trapped organelle. Determination of precise force components in vivo is difficult owing to variability in the biological specimen; slight variations in organelle size and morphology, changes in microenvironments within the cell such as viscosity, cytoplasmic streaming events and potential shear forces from boundary layers generated in the constrained cytoplasmic environment. Due to these inherent complications generating variation of trapping efficiencies across the cell environment, a large number of interaction events need to be probed to obtain statistically significant data; we routinely trap at least 50 organelles in total taken from several samples from at least three independent plants from independent transformations.

4 Notes

1. Some batches or individual coverslips can have aberrations in the glass making trapping difficult. A manifestation of these issues is a significant change in Z focus upon trapping. If this occurs, move to another area on the slide or make a fresh sample.
2. Using a high numerical aperture TIRF objective lens to create a single beam gradient trap (laser tweezers) requires some care. The TIRF objectives with oil immersion have aberration when used in aqueous environments such as plant cells which reduces the effective numerical aperture for trapping from 1.49 to a value between 1.0 and 1.1. This both reduces the efficiency of trapping from a focusing perspective but also means that not all the laser power entering the objective is used for trapping. While we have used the TIRF objective in a conventional manner by slightly overfilling the input pupil, other researchers have found more efficient trapping by underfilling the objective. The transmission of laser light at 1090 nm of our TIRF objective was determined to be 70% using the double objective method suggested by Mahamdeh et al. [12].
3. Beads which have settled and adhered to the coverslip cannot be trapped and moved laterally. Beads which are “free floating” can undergo the trapping routine.

Acknowledgements

This work is supported by The Leverhulme Trust (RPG-2015-106) and STFC (PM-1216).

References

1. Hawes C, Osterrieder A, Sparkes IA, Ketelaar T (2010) Optical tweezers for the micromanipulation of plant cytoplasm and organelles. Curr Opin Plant Biol 13:731–735
2. Osterrieder A, Sparkes IA, Botchway SW, Ward A, Ketelaar T, de Ruijter N, Hawes C (2017) Stacks off tracks: a role for the golgin AtCasp in plant endoplasmic reticulum – Golgi tethering. J Exp Bot [Epub ahead of print]
3. Ketelaar T, de Ruijter N, Niehren S (2014) Optical trapping in plant cells. Methods Mol Biol 1080:259–265
4. Ketelaar T, Faivre-Moskalenko C, Esseling JJ, de Ruijter NCA, Grierson CS, Dogterom M, Emons AMC (2002) Positioning of nuclei in Arabidopsis root hairs: an actin-regulated process of tip growth. Plant Cell 14:2941–2955
5. Gao H, Metz J, Teanby NA, Ward AD, Botchway SW, Coles B et al (2016) In vivo quantification of peroxisome tethering to chloroplasts in tobacco epidermal cells using optical tweezers. Plant Physiol 170:263–272
6. Sparkes IA, Ketelaar T, de Ruitjer NCA, Hawes C (2009) Grab a Golgi: laser trapping of Golgi bodies reveals in vivo interactions with the endoplasmic reticulum. Traffic 10:567–571
7. Andersson M, Goksor M, Sandelius AS (2007) Optical manipulation reveals strong attracting forces at membrane contact sites between endoplasmic reticulum and chloroplasts. J Biol Chem 282:1170–1174
8. Van der Honing HS, de Ruijter NCA, Emons AMC, Ketelaar T (2009) Actin and myosin regulate stiffness in plant cells: a study using optical tweezers. New Phytol 185:90–102
9. Clough SJ, Bent AF (1998) Floral dip: a simplified method for Agrobacterium-mediated transformation of Arabidopsis thaliana. Plant J 16:735–743
10. Sparkes IA, Runions J, Kearns A, Hawes C (2006) Rapid, transient expression of fluorescent fusion proteins in tobacco plants and generation of stably transformed plants. Nat Protoc 1:2019–2025
11. Nelson BK, Cai X, Nebenführ A (2007) A multicolored set of in vivo organelle markers for co-localization studies in Arabidopsis and other plants. Plant J 51:1126–1136
12. Mahamdeh M, Campos CP, Schäffer E (2011) Under-filling trapping objectives optimizes the use of the available laser power in optical tweezers. Opt Express 19:11759–11768

Chapter 14

Protein Biosynthesis and Maturation in the ER

Emanuela Pedrazzini and Alessandro Vitale

Abstract

The endoplasmic reticulum takes care of the folding, assembly, and quality control of thousands of proteins destined to the different compartments of the endomembrane system, or to be secreted in the apoplast. Here we describe how these early events in the life of all these proteins can be followed biochemically by using velocity or isopycnic ultracentrifugation, metabolic labeling with radioactive amino acids, and immunoprecipitation in various conditions.

Key words Protein synthesis, Endoplasmic reticulum, Chaperones, Protein folding, Protein oligomerization, Protein–protein interactions, Pulse-chase, Immunoprecipitation, Ultracentrifugation

1 Introduction

In a given plant cell, thousands of different polypeptides are synthesized by ribosomes bound to the endoplasmic reticulum (ER) membrane, to be introduced into the ER lumen or integrated in its limiting membrane. Most of these proteins will then proceed along the secretory pathway, to reach the correct destination within the endomembrane system or to be secreted. Before starting their journey, all these polypeptides undergo folding and in many cases assembly into oligomers, with the assistance of ER resident folding helpers and, if these events fail, the same helping machinery directs the defective polypeptides to degradation [1–3]. The extent of interactions with the folding machinery is often predictive of whether folding defects can explain observed effects in activity, intracellular sorting, or turnover, resulting from natural mutations or protein engineering [4–8].

Here we describe biochemical techniques to determine protein localization and structural maturation in the ER, and interactions with the Binding Protein (BiP), the ER member of the heat shock protein 70 family and the most promiscuous chaperone of the ER [2]. These techniques can be used to define the steady-state situation or, when coupled with pulse-chase radioactive labeling, to

Chris Hawes and Verena Kriechbaumer (eds.), *The Plant Endoplasmic Reticulum: Methods and Protocols*, Methods in Molecular Biology, vol. 1691, DOI 10.1007/978-1-4939-7389-7_14,

analyze the time-course dynamics of events. Protein radioactive pulse-chase was developed several decades ago and has been used in plant biology since the end of 1950s [9], but it still remains the major approach of choice for subsequent fine biochemical analysis of a given protein regarding its in vivo time-course of assembly, interactions with folding helpers, and traffic.

2 Materials

2.1 Protein Extraction from Leaves or Protoplasts (See Note 1)

2.1.1 Leaf Homogenization

1. Leaf Homogenization Buffer (HB): 200 mM NaCl, 1 mM EDTA, 50 mM Tris–Cl, 0.2% Triton X-100, pH 7.8. Store at −20 °C in small aliquots and supplement with protease inhibitors cocktail immediately before use.
2. Reducing HB: same as HB, but supplemented with 4% (v/v) 2-mercaptoethanol (*see* **Note 2**).
3. Ice-cold mortar.

2.1.2 Protoplast Homogenization

1. 15 or 1.5 mL polypropylene tubes.
2. Protoplast Homogenization Buffer (ptsHB): 150 mM NaCl, 1.5 mM EDTA, 1.5% Triton X-100, 150 mM Tris–Cl pH 7.5. This is a 1.5× stock. Store at −20 °C in small aliquots and supplement with protease inhibitors cocktail immediately before use.
3. Reducing protoplast homogenization buffer: same as ptsHB but supplemented with 4% (v/v) 2-mercaptoethanol (*see* **Note 2**).

2.2 Subcellular Fractionation on Isopycnic Sucrose Gradients

1. Buffer A: 10 mM KCl containing either 2 mM $MgCl_2$ or 1 mM EDTA (*see* **Note 3**), 100 mM Tris–Cl, pH 7.8. Store at −20 °C if not autoclaved.
2. 12%, 16%, 55%, 65% (w/w) sucrose buffer: dissolve sucrose in buffer A (with 2 mM $MgCl_2$ or 1 mM EDTA) to 12%, 16%, 55%, 65% (w/w). To dissolve 55% or 65% sucrose heat the solution to 40–50 °C, because sucrose is at the limit of solubility. Once dissolved, it will not precipitate even upon freezing. Do not autoclave (the solution will turn yellowish-brown, indicating sucrose alterations). Store at −20 °C, otherwise it gets easily contaminated: sucrose is very good for bacterial and fungal contamination.
3. 13 mL polypropylene ultracentrifuge tubes.

2.3 Velocity Sucrose Gradient Centrifugation

1. Sucrose gradient buffers: 5% sucrose (w/v) in 150 mM NaCl, 0.1% Triton X-100, 25 mM Tris–Cl, pH 7.5; 25% sucrose (w/v) in 150 mM NaCl, 0.1% Triton X-100, 50 mM Tris–Cl, pH 7.5. Store at −20 °C.
2. Molecular mass markers: prepare a mixture with 0.33 μg/μL each of cytochrome *c* (12.4 kDa), ovalbumin (43 kDa), bovine

serum albumin (67 kDa), aldolase (161 kDa), and catalase (232 kDa) in HB.

3. 13 mL polypropylene ultracentrifuge tubes.

2.4 Metabolic Labeling with Radioactive Amino Acids

1. K3 medium: 3.78 g/L Gamborg's B5 basal medium with minimal organics, 750 mg/L $CaCl_2$ $2H_2O$, 250 mg/L NH_4NO3, 136.2 g/L sucrose, 250 mg/L xylose, 1 mg/L 6-benzylaminopurine (from a 5 mg/mL stock in 1 N NaOH), 1 mg/L 1-naphtalenacetic acid. Bring to pH 5.5 with a few drops of 1 M KOH, filter sterilize and store at −20 °C.
2. W5 medium: 9 g/L NaCl, 0.37 g/L KCl, 18.37 g/L $CaCl_2$ $2H_2O$, 0.9 g/L glucose. Filter sterilize, aliquot, and store at −20 °C.
3. ^{35}S Met/Cys mix.
4. Unlabeled Met/Cys (10× stock): 15 mg/mL Met, 6.05 mg/mL Cys in K3. Store at −20 °C (*see* **Note 4**).
5. Bovine serum albumin, 4 mg/mL stock in K3. Store at −20 °C in aliquots.
6. 1/2MS10 medium: half the normal concentration of Murashige and Skoog medium, 10% sucrose. Bring to pH 5.6 with KOH.

2.5 Protein Immunoselection

1. Gelatin stock: 2% gelatin from porcine skin in distilled water. Autoclave and, when at around 30–40 °C but before it starts forming the gel, add NaN_3 to 0.02% to avoid microorganism growth and store at 4 °C. Melt in microwave oven before use. It can undergo many melting cycles without deteriorating.
2. Immunoselection gelatin buffer (Nonidet-EDTA-Tris-gel buffer, NET-gel): 50 mM Tris–HCl, pH 7.5, 150 mM NaCl, 1 mM EDTA, 0.1% octylphenoxy poly(ethyleneoxy)ethanol, branched (Nonidet P-40 or IGEPAL® CA-630), 0.25% gelatin, 0.02% sodium azide.
3. Washing buffer (NET buffer): same as NET-gel buffer, but without gelatin.
4. Protein A-Sepharose 10% suspension: work at room temperature. Swell Protein A-Sepharose in NET buffer for at least 3 h with occasional agitation, in a graduated 50 or 15 mL polypropylene tube, and wait until it sediments. Discard the supernatant using a pasteur pipette connected to a water pump. Add 1 M Tris–HCl pH 7.5. Allow to stand for 1 h with occasional agitation. Spin down the bead at 5000 × *g*, 5 min at room temperature, and discard supernatant. Wash the bead 1× with NET buffer. Spin down and note volume occupied by the bead (1 g of dry powder should give about 3.5 mL of bead). Discard supernatant and add 9 bead volumes of NET buffer. Store at 4 °C for up to several months.

3 Methods

3.1 Total Protein Extraction from Leaves or Protoplasts (See Note 5)

3.1.1 Leaf Homogenization

1. Collect arabidopsis rosette leaves or small (4–7-cm long) leaves from tobacco grown in axenic conditions or in soil, weight them, and transfer them (*see* **Note 6**) to an ice-cold mortar kept on ice and containing 5–7 v/w of ice-cold HB supplemented, immediately before use, with protease inhibitor cocktail. Rapidly homogenize the leaves keeping the mortar on ice. Alternatively, use reducing HB and follow the same procedure (*see* **Note 7**).
2. Transfer the homogenate to an appropriate tube (depending on the volume) and clarify the homogenate by centrifugation at 1500 × *g*, 10 min at 4 °C. Collect the supernatant and discard the pellet (*see* **Note 8**). The clarified homogenate can be stored frozen at −20 °C for several months.

3.1.2 Protoplast Homogenization

1. Add to protoplasts two volumes of ice-cold ptsHB, by pipetting 4–5 times through a 200 µL tip and freeze-thawing the suspension in liquid nitrogen. Alternatively, use reducing ptsHB and follow the same procedure (*see* **Note 7**).
2. Clarify the homogenate by centrifugation at 1500 × *g*, 10 min at 4 °C (*see* **Note 9**). Protoplast homogenate can be stored at −20 °C for several months.

3.2 Subcellular Fractionation to Determine Protein Localization

3.2.1 Subcellular Fractionation on Isopycnic Sucrose Gradients

1. To prepare linear 16–55% or 16–65% (w/w) (*see* **Note 10**) sucrose gradients, gently stratify with a micropipette 6 mL of 16% sucrose buffer (with magnesium or EDTA) onto 6 mL of 55% (or 65%) sucrose buffer (with magnesium or EDTA) in a 13 mL ultracentrifuge tube. Seal the tube with Parafilm™ and gently turn it to a perfectly horizontal position. Keep it in this position for 4 h at room temperature, then gently turn it back to a vertical position and store for at least 10 h at 4 °C before using it.
2. For leaves: homogenize small leaves (3–8-cm long) in an ice-cold mortar with ice-cold 12% (w/w) sucrose buffer (with magnesium or EDTA) supplemented with protease inhibitor cocktail, using 4–7 mL of buffer per gram of fresh leaf tissue.
3. For protoplasts: homogenize pelleted protoplasts in ice with ice-cold 12% sucrose buffer supplemented with protease inhibitor cocktail, using the same buffer/protoplast pellet ratio as above. With a 200 µL micropipette tip, pipette the suspension up and down about 20 times, to break protoplasts. Do not let the material warm up.

4. With a micropipette, load the homogenate (up to 600 μL) on top of the gradient. Keep everything in ice (*see* **Note 11**).
5. Ultracentrifuge at 150,000 × *g* (r_{av}), in a swinging rotor at 4 °C for 2 h.
6. Collect fractions (usually of about 500–600 μL each) (*see* **Note 12**). A pellet will be visible at the bottom of the tube: do not discard it. Fractions and the tube with its pellet can be stored at −20 °C.
7. Take an equal aliquot of each fraction and add 0.5 volumes of 3× SDS-PAGE denaturation buffer. Solubilize the pellet at the bottom of the centrifuge tube with a volume of 1× SDS-PAGE corresponding to the same volume of each original fraction.
8. Denature the aliquots from the gradient and the solubilized pellet at 90 °C, 5 min. Analyze by SDS-PAGE and protein blot or fluorography each fraction and an equal aliquot of the solubilized pellet. Remember to load an aliquot of denatured total 12% sucrose homogenate, as a control (*see* **Note 13**).

3.2.2 Rapid Isolation of Microsomes

1. Homogenize leaves or protoplast in 12% sucrose buffer and clarify as described above.
2. Load the clarified homogenate on a cushion made of 17% (w/w) sucrose buffer. Ultracentrifuge in a swinging rotor 90 min at 100,000 × *g* (r_{av}), 4 °C (*see* **Note 14**).
3. Collect the supernatant, resuspend the pellet, and analyze both fractions by SDS-PAGE and protein blot (or fluorography).

3.3 Determination of the Assembly Grade of Proteins

3.3.1 Velocity Centrifugation on Sucrose Gradient

1. Prepare linear 5–25% (w/v) sucrose gradients following the procedure described in Subheading 3.2.1, **step 1**, but using the buffers for velocity sucrose gradient centrifugation.
2. Homogenize leaves or protoplast as described in Subheading 3.1.1 or 3.1.2.
3. Load the clarified lysate on the top of the 12 mL linear 5–25% (w/v) sucrose gradient.
4. In parallel, load an additional gradient with 600 μL of the molecular mass marker mixture.
5. Centrifuge at 200,000 × *g* (r_{av}) for 25 h at 4 °C in an ultracentrifuge swinging rotor.
6. Fractionate the gradients from the top into 18–22 fractions of about 500–600 μL each (*see* **Note 12**).
7. Solubilize equal volumes of each fraction with 0.5 volumes of 3× SDS-PAGE loading buffer. The pellet at the bottom of the centrifuge tube is solubilized with 500–600 μL of 1× SDS-PAGE loading buffer.

Take equal aliquots of fractions and pellet, denature at 90 °C, 5 min and analyze by SDS-PAGE and protein blot (or fluorography). Remember to load an aliquot of denatured total homogenate, as a control. Similarly denature 40 μL of each fraction from the molecular mass marker gradient, analyze by SDS-PAGE and stain the gel with Coomassie Blue. The easily detected bands will serve as size markers along the gradients.

3.4 Protein Metabolic Labeling with Radioactive Amino Acids

3.4.1 Pulse-Chase Labeling of Protoplasts

1. Pulse: Label protoplasts in K3 medium using 100 μCi/mL of ^{35}S-label Met/Cys mixture. Incubate for 1 h at 25 °C (tobacco) or 20 °C (arabidopsis) in the dark. A workable concentration of protoplasts for the subsequent steps is 1–2 millions/mL.
2. Stop pulse labeling by diluting protoplasts with four volumes of ice-cold W5 solution; centrifuge at 100 × *g* for 5 min at 4 °C.
3. Chase: Resuspend the pelleted protoplasts in K3 medium supplemented with unlabeled Met/Cys to a final concentration of 10 and 5 mM, respectively, using the Met/Cys 10× stock (*see* **Note 15**). Incubate at 25 °C (tobacco) or 20 °C (arabidopsis) in the dark for the desired chase time points.
4. Collect an aliquot of protoplasts (usually 100–250 μL) at each chase time point, add three volumes of ice-cold W5, and centrifuge 10 min at 60 × *g*. Remove the supernatant (and save it if secretion needs to be studied), leaving about 50 μL covering the protoplast pellet.
5. Quickly freeze in liquid nitrogen and store at −80 °C until homogenization. Alternatively, homogenize immediately using the buffer required according to subsequent analysis that will be performed.

3.4.2 Pulse-Chase Labeling of Intact Leaves

1. Pulse: Put 150 μL of 1/2MS10 medium supplemented with 150 μCi/mL ^{35}S-label Met/Cys mixture in a conical 10 or 15 mL plastic tube.
2. Cut one leaf (not longer than 5 cm) from axenic plant and insert it into the tube, so that the petiole touches the bottom of the tube.
3. Incubate under vacuum for 1 min, to favor entrance of the labeling medium into the vascular system.
4. Incubate for 1–3 h or longer at 25 °C (tobacco) or 20 °C (arabidopsis) in the dark, covering the tube with its unscrewed cap.
5. Carefully remove the incubation medium with a micropipette and replace it with 150 μL 1/2 MS10. Incubate 1 h as above, to favor as much as possible incorporation of the radioactive

amino acids before starting the chase. You can homogenize leaves now (as described above) or continue with the chase.

6. Chase: Remove the medium and replace it with 1/2 MS10 supplemented with unlabeled Met/Cys to 10 and 5 mM, respectively, using the Met/Cys 10× stock (*see* **Note 16**).
7. At the desired time points, homogenize leaves as described above.

3.5 Immunoselection

1. Add NET-gel buffer to protoplast or leaf homogenates prepared as in Subheadings 3.1.1 and 3.1.2, or to aliquots from isopycnic or velocity gradient fractions (no more than 400 μL of sample), up to a final volume of 1 mL. Mix well by vortexing. Use 1.5 mL polypropylene tubes.
2. Spin twice (4 min at 4 °C at maximum speed in minifuge) to pellet any insoluble material. Transfer supernatant to a new tube each time.
3. Add the appropriate antibody or antiserum. The final concentration of immunoglobulins depends on the affinity of each antibody/antiserum and must be previously determined, but the volume should be limited to a few microliters. Incubate 2 h on ice (*see* **Note 17**).
4. Add 100–150 μL of a 10% suspension of Protein A-Sepharose. Incubate for 1 h at 4 °C under gentle agitation (the resin must be in continuous movement).
5. Pellet the resin (30 s to 2 min at maximum speed in minifuge), and discard supernatant.
6. Wash the resin three times with 1 mL of NET-gel buffer. Spin as above and discard supernatant after each wash. Leaving each time about 1 mm of buffer over the resin.
7. Add to the bead equal volume of 2× SDS-PAGE buffer (bead is usually 30–40 μL).
8. Mix well, denature 5 min at 90 °C, spin and load the solution on SDS-PAGE. If you use a Hamilton syringe, this is easy because the bead will not enter the needle.
9. Radioactive polypeptides can be revealed by fluorography or autoradiography of the dried gel.

3.6 Analysis of Protein Interaction with BiP

1. Protoplast or leaf homogenate is immunoselected as describe above with anti-BiP antiserum (commercially available or prepared in the investigator's laboratory).
2. After washing three times with NET-gel buffer, split the beads into three aliquots: one aliquot is washed again twice for 30 min with 500 μL of NET-gel buffer only, one with NET-gel buffer containing 6 mM $MgCI_2$ and one with NET-gel

buffer containing 6 mM $MgCI_2$ and 3 mM ATP (*see* **Note 18**). Treatments are performed on ice.

3. The material still bound to the beads after these treatments is directly analyzed by SDS-PAGE.
4. The ATP-released material is re-immunoselected using antiserum or antibody against the protein of interest, following the procedure described above, **steps 3–9** of Subheading 3.5.
5. As a further control, repeat the entire procedure from **step 1** in reverse order, that is using first the antiserum or antibody against the protein of interest and then selecting the ATP-released material with anti-BiP antiserum.

4 Notes

1. The described methods can be used to analyze samples both from *Nicotiana tobacum* and from *Arabidopsis thaliana* [5, 8, 10].
2. 2-Mercaptoethanol is volatile and highly toxic. Avoid breathing vapors or skin contact. Always work under a ventilated hood when working with the stock chemical or any solution containing it. Discard solutions, tubes and pipet tips in appropriate containers, separated from other disposed material.
3. Magnesium will preserve ribosomes, and therefore the ones attached to the ER will remain there. EDTA dissociates the ribosome subunits and releases them from the ER membrane. As a result, the density of the ER is higher in the presence of magnesium (because the ratio protein/lipid is higher) [6, 10, 11].
4. When melting the unlabeled aminoacid mix, check it for precipitates: after several freezing and melting, the solution may become cloudy. If this occurs, discard and prepare a new stock.
5. The methods in this section are used to prepare proteins for all subsequent analysis described in this chapter, with the exception of the analysis of protein subcellular localization: nonionic detergents dissolve membranes and therefore destroy the integrity of subcellular compartments. As described in Subheading 2.2, the homogenization buffers to analyze subcellular localization therefore do not contain ionic detergents.
6. If you start from frozen leaves, work fast and do not allow them to warm up before homogenization, because freezing breaks membranes and thus vacuolar proteases will have access to all proteins as the tissue is defrosted.
7. HB contains salts and ionic detergent sufficient to bring into solution the vast majority of soluble and integral membrane

proteins. However, certain proteins are not solubilized unless their disulfide bonds are reduced. The most striking examples are constituted by many prolamins of cereal seeds [12]. Therefore, if their recombinant forms are expressed in leaves of transgenic plants or transiently in protoplasts, the use of reducing HB or reducing ptsHB is mandatory for their solubilization [13, 14]. Other proteins that fold in the ER oxidizing environment may also require reducing conditions to be solubilized. When working on a new protein introduced in the secretory pathway, it is thus recommended to first compare its solubility in reducing and nonreducing homogenization buffers.

8. The pellet mainly contains cell wall polysaccharides and starch from plastids. Unbroken cells may also be present, as well as insoluble proteins that may require reducing conditions to enter into solution (*see* **Note 7**), or even strong denaturing agents such as SDS or urea. However, the use of strong denaturants will preclude further analysis of assembly or interactions with chaperones.
9. The pellet of protoplast homogenates may be not easy to see, especially if you are homogenizing less than 30,000 protoplasts. Proceed anyway to collect the supernatant, taking care of avoiding touching the bottom of the tube.
10. 16–65% sucrose is recommended to fractionate highly dense organelles, such as ER protein bodies [10].
11. Remember to load each gradient with homogenate made in the *SAME* buffer (magnesium or EDTA)!
12. Use a 1 mL micropipette. Slowly and carefully collect each fraction by remaining as close as possible to the top of the gradient. Unavoidably, a very low amount of the top of the gradient will remain in the tube as you remove the different fractions. Due to the increasing difference in density, this will not contaminate the other fractions, until it will remain at the bottom of the tube where it will slightly contaminate the last fraction.
13. In the presence of $MgCl_2$, the plant ER has a density corresponding to 1.17–1.18 g/mL sucrose. When Mg^{2+} is chelated by EDTA, ribosomes are detached from the ER membrane, which thus becomes less dense, with a consequent shift in migration along the gradient [6, 10, 11].
14. Microsomes derived from Golgi and ER, tonoplast and plasma membrane fragments, vesicles, mitochondria, and chloroplasts will precipitate at the bottom of the tube. Cytosolic proteins as well as soluble proteins of vacuoles (vacuoles break during homogenization) will remain in the 12% supernatant [6].

15. If proteins secreted by protoplasts into the incubation medium are the object of study, 150 μg/mL of bovine serum albumin (from the 4 mg/mL stock) should be added to the K3 medium. This will constitute a very abundant substrate for secreted proteases, thus strongly lowering the probability of degradation of the newly secreted polypeptides.
16. Upon the addition of nonradioactive amino acids to protoplast samples, the incorporation of radioactive ones into protein rapidly drops to almost undetectable levels. This occurs within a few minutes from the starting of chase. Do not expect the same to occur when leaves are labeled, because of the much slower incorporation in intact tissue and the variability between different leaves. This makes very difficult to analyze the time course of events occurring within relatively short times (1–2 h) when leaves are labeled. Keep this in mind when you interpret your results.
17. Immunoprecipitation works also if homogenization is performed in reducing conditions, such as in the presence of 4% 2-mercaptoethanol [14, 15]. The immunoglobulin tetramer contains interchain disulfide bonds, but its assembly depends mainly on other types of interactions and therefore it is not disrupted by 2-mercaptoethanol in the absence of strong denaturants such as SDS.
18. Like the other members of the heat shock 70 protein family, BiP is an ATPase and releases its bound ligands upon ATP hydrolysis. Because ATPase activity requires magnesium, the presence of EDTA during homogenization and immunoselection ensures that ligands are not released from the chaperone. Subsequent treatment with buffer supplemented with ATP and magnesium, but not with magnesium alone, promotes the release of polypeptides that have been immunoselected because BiP is acting on them as a molecular chaperone, rather than because of unspecific interactions [5, 6, 14, 16].

Acknowledgements

We thank the present and past members of our laboratories for their fundamental contributions in developing and continuously improving the methods described here.

References

1. Vitale A, Ceriotti A, Denecke J (1993) The role of the endoplasmic reticulum in protein synthesis modification and intracellular transport. J Exp Bot 44:1417–1444
2. Vitale A, Boston R (2008) Endoplasmic reticulum quality control and the unfolded protein response: insights from plants. Traffic 9:1581–1588

3. Liu XJ, Howell SH (2016) Managing the protein folding demands in the endoplasmic reticulum of plants. New Phytol 211:418–428
4. Zhang F, Boston RS (1992) Increases in binding protein (BiP) accompany changes in protein body morphology in three high lysine mutants of maize. Protoplasma 171:142–152
5. Pedrazzini E, Giovinazzo G, Bollini R, Ceriotti A, Vitale A (1994) Binding of BiP to an assembly-defective protein in plant cells. Plant J 5:103–110
6. Pedrazzini E, Giovinazzo G, Bielli A, de Virgilio M, Frigerio L, Pesca M, Faoro F, Bollini R, Ceriotti A, Vitale A (1997) Protein quality control along the route to the plant vacuole. Plant Cell 9:1869–1880
7. Hong Z, Jin H, Tzfira T, Li J (2008) Multiple mechanism-mediated retention of a defective brassinosteroid receptor in the endoplasmic reticulum of Arabidopsis. Plant Cell 20:3418–3429
8. Maîtrejean M, Wudick MM, Voelker C, Prinsi B, Mueller-Roeber B, Czempinski K, Pedrazzini E, Vitale A (2011) Assembly and sorting of the tonoplast potassium channel AtTPK1 and its turnover by internalization into the vacuole. Plant Physiol 156:1783–1796
9. Pollard JK, Steward FC (1959) The use of proline-C14 by growing cells: its conversion to protein and hydroxyproline. J Exp Bot 10:17–32
10. Ceresoli V, Mainieri D, Del Fabbro M, Weinstein R, Pedrazzini E (2016) A fusion between domains of the human bone morphogenetic protein-2 and maize 27 kD γZein accumulates to high levels in the endoplasmic reticulum without forming protein bodies in transgenic tobacco. Front Plant Sci 7:358
11. Barbante A, Irons S, Hawes C, Frigerio L, Vitale A, Pedrazzini E (2008) Anchorage to the cytosolic face of the endoplasmic reticulum membrane: a new strategy to stabilize a cytosolic recombinant antigen in plants. Plant Biotechnol J 6:560–575
12. Pedrazzini E, Mainieri D, Marrano CA, Vitale A (2016) Where do protein bodies of cereal seeds come from? Front Plant Sci 7:1139
13. Shani N, Rosenberg N, Kasarda DD, Galili G (1994) Mechanisms of assembly of wheat high molecular weight glutenins inferred from expression of wild-type and mutant subunits in transgenic tobacco. J Biol Chem 269:8924–8930
14. Mainieri D, Rossi M, Archinti M, Bellucci M, De Marchis F, Vavassori S, Pompa A, Arcioni S, Vitale A (2004) Zeolin, a new recombinant storage protein constructed using maize gamma-zein and bean phaseolin. Plant Physiol 136:3447–3456
15. Pompa A, Vitale A (2006) Retention of a bean phaseolin/maize γ-zein fusion in the endoplasmic reticulum depends on disulfide bond formation. Plant Cell 18:2608–2621
16. Foresti O, Frigerio L, Holkeri H, de Virgilio M, Vavassori S, Vitale A (2003) A phaseolin domain directly involved in trimer assembly is a BiP binding determinant. Plant Cell 15:2464–2475

Chapter 15

ER Membrane Protein Interactions Using the Split-Ubiquitin System (SUS)

Lisa Yasmin Asseck, Niklas Wallmeroth, and Christopher Grefen

Abstract

Protein–protein interactions (PPIs) play fundamental roles in all cellular processes. Especially membrane proteins facilitate a range of important biological functions in stimuli perception, signaling, and transport. Here we describe a detailed protocol for the yeast mating-based Split-Ubiquitin System (mbSUS) to study PPIs of ER membrane proteins in vivo. In contrast to the prominent Yeast Two-Hybrid, mbSUS enables analysis of full-length membrane proteins in their native cellular context. The system is based on the ubiquitin proteasome pathway leading to the release of an artificial transcription factor followed by activation of reporter genes to visualize PPIs. The mating-based approach is suitable for both small- and large-scale interaction studies. Additionally, we describe protocols to apply the recently established SUS Bridge assay (SUB) which is optimized for the detection of ternary protein interactions.

Key words Protein–protein interaction, Ternary interaction, Yeast, Split Ubiquitin, mbSUS, SUB, Membrane proteins, Gateway

1 Introduction

Protein–protein interactions (PPIs) are prerequisite for a wide range of cellular functions. A large number of biophysical and biochemical techniques have been developed to unravel PPI networks for a better understanding of cellular complexities (for review, *see* [1]). For example, a technique such as the yeast two hybrid is often applied for their ease of use and applicability to large-scale approaches. One downside of this particular technique, however, is the obligatory nuclear localization of the interaction partners which imposes truncation of membrane or large proteins to facilitate their nuclear (mis-)localization. Truncation and artificial nuclear localization in turn might cause artifacts and misinform on interactions among—for example—membrane proteins. Yet, many key processes in cell signaling and vesicle trafficking are mainly coordinated by interactions between or with membrane

Chris Hawes and Verena Kriechbaumer (eds.), *The Plant Endoplasmic Reticulum: Methods and Protocols*, Methods in Molecular Biology, vol. 1691, DOI 10.1007/978-1-4939-7389-7_15,

proteins, which due to their natural environment and hydrophobic composition has remained experimentally difficult.

The mating-based Split-Ubiquitin System (mbSUS, [2]) described in this chapter is an approach well-suited to elucidate full-length membrane protein interactions in vivo. The system relies on reassembly of the N- (Nub) and C-terminal (Cub) ubiquitin moieties that reconstitute a functional molecule when brought into close proximity by interacting proteins fused to these fragments [3]. To prevent spontaneous reassembly, Nub is mutated at residue Ile13 to either glycine or alanine that reduces its affinity for Cub [4] (*see* **Note 1**). Upon reconstitution, ubiquitin is recognized by cytosolic ubiquitin-specific proteases (USPs), which cleave off the artificial transcription factor PLV (ProteinA-LexA-VP16) fused to the C-terminus of Cub [5]. The released transcription factor then translocates into the nucleus to mediate activation of reporter genes allowing auxotrophy selection (*ADE2*, *HIS3*) and quantification of the relative interaction strength (*lacZ*). Thus, split ubiquitin as interaction sensor circumvents the use of mis-localized or truncated versions of fusion proteins significantly reducing artifacts associated with such protein modifications.

The mating-based strategy can be used not only to assay the interaction between two known proteins but is particularly adapted for large-scale interaction tests to screen a multitude of potential binding partners (*see* **Note 2**). In such screens, the mating approach simplifies and accelerates the experimental procedure compared to sequential transformations or co-transformations. Experimentally verified, binary interactions represent an idealized condition of the real-world biological complexity of multi-protein complexes. However, only a few methods have thus far been established to study multimeric interactions, an increasingly important task for our understanding of the cellular interactome. The SUS Bridge assay (SUB) is adapted from the classical Split-Ubiquitin System with the addition of a third (tagged or untagged) protein being expressed that can either facilitate, enhance, or inhibit a nonexistent, weak, or previous interaction between bait and prey, respectively [6, 7].

In this book chapter, we detail the application of both the mbSUS and SUB technique, respectively, to detect interactions between membrane proteins. As textbook example of an ER-membrane complex we choose the subunits of the heterotrimeric SEC61 translocon complex of *Arabidopsis*. Via Blastp analysis we identified the *Arabidopsis* orthologues of the mammalian SEC61 translocon subunits. Assembly of the three α, β, and γ SEC61 subunits yields the ER-membrane localized channel, which mediates translocation of secretory proteins across and integration of membrane proteins into the lipid bilayer [8]. Here we show that the Sec61 subunit isoform α1 of *Arabidopsis thaliana* (At2g34250) directly interacts with Sec61β1 (At2g45070) and γ1 (At5g50460), respectively (Fig. 1).

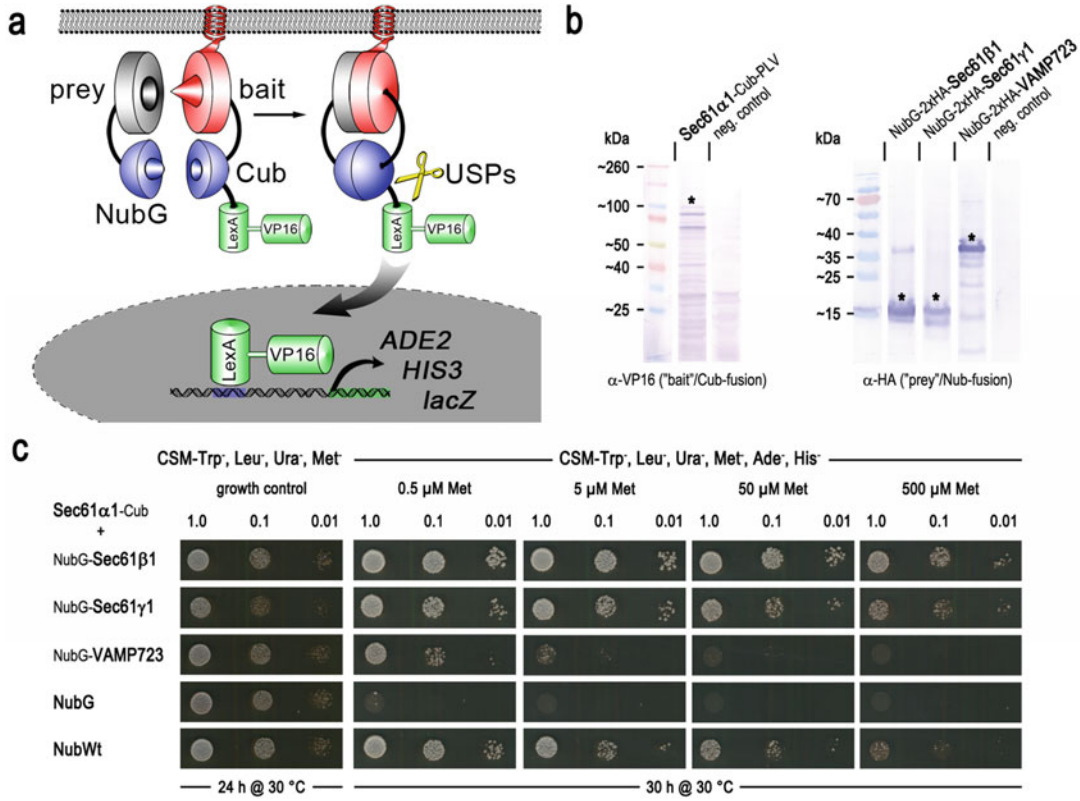

Fig. 1 mbSUS analysis of the *Arabidopsis* Sec61 subunit α1 with Sec61β1 and Sec61γ1. (**a**) Schematic depiction of the SUS principle. Upon interaction of bait (*red*) and prey (*grey*) NubG and Cub reassemble to ubiquitin which is recognized by ubiquitin-specific proteases (USPs) that cleave off the LexA-VP16 transcript activator. Diffusion of this construct into the nucleus activates reporter genes *ADE2*, *HIS3*, and *lacZ* which can be monitored by growth or colorimetric assays. (**b**) Western blot analysis of haploid yeast prior mating and used in (**c**) with antibodies detecting the VP16 domain of the chimeric PLV and the HA-tag fused between NubG and GOI, respectively. (**c**) Growth assay of diploid yeast expressing the indicated fusion proteins. Yeast was dropped in serial dilutions (of OD_{600} from 1.0 to 0.01) on vector-selective (CSM-Leu$^-$, Trp$^-$, Ura$^-$) and interaction-selective (CSM-Leu$^-$, Trp$^-$, Ura$^-$, Ade$^-$, His$^-$) media with increasing methionine concentrations. NubWt was used as positive control, and NubG as well as VAMP723 as negative controls (*see* **Note 3**). Sec61α1-Cub-PLV (~106 kDa), NubG-2xHA-Sec61β1 (~16 kDa), NubG-2xHA-Sec61β1 (~15 kDa), NubG-2xHA-VAMP723 (~32 kDa)

2 Materials

2.1 Vectors and Strains

The Gateway-compatible (exception: pNubWt-Xgate) mbSUS and SUB vectors which are necessary for interaction analysis are listed in Table 1. Maps and sequences of the vectors can be downloaded from http://www.zmbp.uni-tuebingen.de/dev-genetics/grefen/resources/yeast-vectors.html. The yeast strains that are used in this book chapter are listed in Table 2.

Table 1
Destination vectors for mbSUS and SUB analysis

		Origin		Selection			
Plasmid name	**Promoter**	***E. coli***	**Yeast**	***E. coli***	**Yeast**	**Function**	**Reference**
pMetYC- Dest	Met25	pUC	ARS/CEN	Amp, Cm	LEU2	Met-repressible fusion protein with C-terminal Cub-PLV	[9]
pNX35-Dest	ADH1	pUC	2μ	Amp, Cm	TRP1	Constitutive expression with N-terminal NubG-2xHA	[7]
pXNubA22-Dest	ADH1	pUC	2μ	Amp, Cm	TRP1	Constitutive expression with C-terminal NubA-3xHA	[10]
pNubWt-Xgate	ADH1	pUC	2μ	Amp, Cm	TRP1	Positive control vector, NubWt peptide; not a Gateway vector	[2]
pMZU-Dest	ADH1	pUC	2μ	Spec, Cm	URA3	Constitutive expression with N-terminal myc	[7]
pZMU-Dest	ADH1	pUC	2μ	Spec, Cm	URA3	Constitutive expression with C-terminal myc	[6]

Table 2
Yeast strain genotypes

Name	**Organism**	**Genotype**	**Function**	**Reference**
THY.AP4	*S. cerevisiae*	MATa; *ade2*$^-$, *his3*$^-$, *leu2*$^-$, *trp1*$^-$, *ura3*$^-$; lexA::ADE2, lexA::HIS3, lexA::lacZ	Reporter strain, used for transformation of Cub-clones, used for SUB assay	[2]
THY.AP5	*S. cerevisiae*	MATα; *ade2*$^-$, *his3*$^-$, *leu2*$^-$, *trp1*$^-$	Used for transformation of Nub-clones; mate with THY.AP4 for binary interactions	[2]

2.2 Media and Solutions for Growth and Transformation of Yeast

1. YPD media: 2% peptone, 2% glucose, 1% yeast extract; adjust pH to 6–6.3 with KOH before adding 2% oxoid agar.
2. Sterile deionized water (ddH_2O).
3. 1 M lithium acetate (LiAc): dissolve LiAc in ddH_2O. Adjust pH to 7.5 with acetic acid, sterilize by filtration.
4. 50% polyethylene-glycol 3350 (PEG 3350): dissolve PEG 3350 in deionized water to a final concentration of 50% (w/v), sterilize by filtration. Avoid water loss through autoclaving or during storage as this significantly decreases the transformation efficiency.
5. Single-stranded carrier DNA (ssDNA): dissolve 10 mg/ml ssDNA in deionized water, sonicate, and/or boil for 10 min following cooling on ice before use.

6. CSM-Ade$^-$, His$^-$, Leu$^-$, Met$^-$, Trp$^-$, Ura$^-$ as dropout.
7. Chemicals for auxotrophy selection, each dissolved in 100 ml water and sterilized by filtration; store in darkness at 4 °C:

   ADE: 0.4 g of adenine sulfate (add 5 ml per liter media).

   HIS: 0.4 g of L-histidine HCl (add 5 ml per liter media).

   LEU: 2.0 g of L-leucine (add 5 ml per liter media).

   TRP: 1.0 g of L-tryptophane (add 5 ml per liter media).

   URA: 0.4 g of uracil (add 5 ml per liter media).

   MET: 1.5 g of methionine (equals a 100 mM stock; add appropriate amount to obtain 0.5, 5, 50, and 500 μM final concentrations).
8. Selection media: 0.17% YNB (without amino acids), 0.5% ammonium sulfate, 2% glucose, 0.056% CSM-dropout mix; adjust pH to 6–6.3 with KOH before adding 2% oxoid agar; add appropriate auxotrophy selection chemicals before or after autoclaving, e.g., ADE, HIS, TRP, and URA for transformation of THY.AP4 in the mbSUS assay (*see* **Note 4**).

2.3 Solutions for Western Blot Analysis

1. Lyse and load (LL-) buffer: 50 mM Tris (pH 6.8), 4% SDS, 4 M urea, 30% glycerol, 0.1 M DTT, 0.005% bromophenol blue; store at −20 °C.
2. Acid-washed glass beads (0.25–0.5 mm).
3. 20 ml SDS-PAGE resolving gel (12.5%): 6.2 ml H_2O, 8.4 ml acrylamide mix (30%), 5.0 ml 1.5 M Tris (pH 8.8), 0.2 ml SDS (10%), 0.2 ml $(NH_4)_2S_2O_8$ (10%), 0.008 ml TEMED.
4. 5 ml SDS-PAGE stacking gel (5%): 3.4 ml H_2O, 0.83 ml acrylamide mix (30%), 0.63 ml 1 M Tris (pH 8.8), 0.05 ml SDS (10%), 0.05 ml $(NH_4)_2S_2O_8$ (10%), 0.005 ml TEMED.
5. 10× SDS running buffer: 250 mM Tris, 1.9 M glycine, 0.15% SDS.
6. 100% methanol.
7. PVDF membrane.
8. 10× TBS: 250 mM Tris, 1.5 M NaCl, 20 mM KCl; adjust pH 7.4 (HCl).
9. Washing buffer, 1× TBS-Tween: 100 ml 10× TBS, 900 ml H_2O, 0.1% Tween20.
10. Blocking buffer: 1× TBS-Tween, 5% milk powder.
11. Antibodies (dilute 1:1000 in 1× TBS-Tween, add 0.1% NaN_3).
    (a) Primaries: α-VP16, α-HA, α-myc.
    (b) Secondaries: anti-rabbit IgG alkaline phosphatase, anti-mouse IgG alkaline phosphatase.

12. Staining buffer: 100 mM Tris (pH 9.5), 100 mM NaCl, 5 mM $MgCl_2$.
13. NBT-solution: 50 mg/ml Nitro blue tetrazolium chloride in 70% DMF; aliquot and store at −20 °C.
14. BCIP solution: 50 mg/ml 5-Bromo-4-chloro-3-indolylphosphate-p-Toluidin in 100% DMF; aliquot and store at −20 °C.
15. Staining solution: 66 µl NBT-solution, 33 µl BCIP solution in 10 ml staining buffer; always prepare freshly.

3 Methods

The mbSUS technique allows fast screening of PPIs in vivo. The flowchart in Fig. 2 should provide a detailed overview of the steps necessary for execution of the methods and includes their approximate duration to aid in planning of the experiment.

3.1 Yeast Transformation

3.1.1 mbSUS Transformation

1. Streak THY.AP4 and THY.AP5 yeast strains out on YPD plates and incubate for 2 days at 30 °C.
2. Pick one colony and inoculate into 5 ml YPD liquid media each. Grow overnight at 30 °C while shaking (200 rpm).

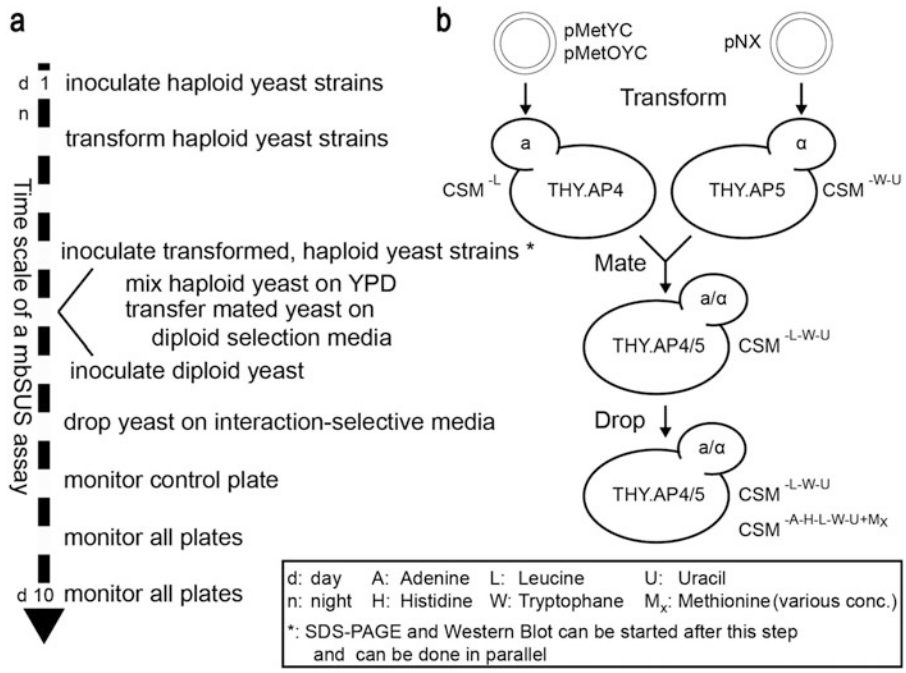

Fig. 2 Flowchart of mbSUS analysis. (**a**) Timeline listing the necessary steps of an mbSUS analysis in consecutive order. (**b**) Cartoon depicting the different ploidy states of the yeast at the different stages of an mbSUS protocol

3. Add 2 ml of the overnight culture to 100 ml of fresh YPD and incubate for 3–5 h at 30 °C while shaking (200 rpm) until the OD_{600} reaches 0.5–0.8.
4. Harvest cells by centrifugation (5 min at 2000 × *g*) in sterile 50 ml tubes. Discard the supernatant.
5. Wash with 20 ml of sterile ddH_2O and centrifuge again (5 min at 2000 × *g*). Discard the supernatant.
6. Resuspend the pellet in 1 ml of 0.1 M LiAc and transfer to a 2 ml tube. Spin down (2 min at 1000 × *g*) and discard the supernatant.
7. Resuspend the cells in an appropriate amount of 0.1 M LiAc (20 µl per transformation) and incubate at room temperature for 30 min.
8. Meanwhile prepare sterile PCR stripes with 10 µl ssDNA and 5 µl of plasmid DNA for each transformation (*see* **Note 5**).
9. Prepare a master mix by mixing 70 µl of 50% PEG, 10 µl 1 M LiAc, and 20 µl of competent yeast (**step 7**) for each transformation.
10. Distribute 100 µl of the master mix into each PCR tube and mix carefully with the prepared DNA-mixture.
11. Incubate for 20 min at 30 °C using a PCR cycler. Mix the reactions by gently pipetting up and down several times with a multichannel pipette.
12. Incubate an additional 10 min at 30 °C.
13. Heat shock at 43 °C for 15 min.
14. Spin down briefly. Carefully remove the supernatant using a pipette.
15. *Optional:* Wash the pellet with 100 µl of sterile ddH_2O.
16. Resuspend the cells in 100 µl of sterile ddH_2O.
17. Plate the entire volume on appropriate selective minimal media (THY.AP4: CSM-Leu^-, THY.AP5: CSM-Trp^-, Ura^-).
18. Seal the plates and incubate for 3 days at 30 °C.

3.1.2 Bridge Assay Transformation

The transformation protocol is the same as that in Subheading 3.1.1 with the following exceptions:

1. Use haploid THY.AP4 cells exclusively.
2. Prepare DNA-mix with only 9 µl ssDNA and 2 µl each of the three different plasmid DNAs. For efficient transformation use more highly concentrated plasmid DNA (*see* **Note 5**).
3. Plate on CSM-Leu^-, Trp^-, Ura^- media. Incubate for 3 days at 30 °C.

3.2 Mating

1. Pool several colonies per transformation and grow shaking overnight in 5 ml of appropriate selective media at 30 °C.
2. Harvest 2 ml each for western blot analysis. Store the pellet at −20 °C.
3. Harvest 2 ml each by centrifugation (5 min at 1000 × *g*) and resuspend the pellet in 200 µl YPD. Scale up the volume for a higher number of crossings (20 µl per mating).
4. Mix 20 µl each, bait (THY.AP4) and prey (THY.AP5) of any desired combination in sterile PCR stripes.
5. Drop 5 µl of each mating onto a YPD plate.
6. Incubate (right side up) for 6–8 h at 30 °C.
7. Transfer mated yeast on CSM-Leu$^-$, Trp$^-$, Ura$^-$ plates using sterile pipette tips or a replicator stamp. Be careful NOT to transfer YPD medium with the cells.
8. Incubate overnight at 30 °C (*see* **Note 6**).

3.3 Screening Approach

1. Transform bait construct in THY.AP4 as described in Subheading 3.1.1 (*see* **Notes 7** and **8**).
2. Inoculate 5–10 colonies in 50 ml selective media (CSM-Leu$^-$) and incubate shaking overnight at 30 °C until an OD_{600} of ~10^8 is reached. Determine the total number of cells using a Neubauer Chamber.
3. Harvest cells by centrifugation (5 min at 1000 × *g*). Discard the supernatant.
4. Resuspend the cells in 1 ml of YPD (pH 4.5).
5. Simultaneously, transform prey library in THY.AP5 in ten small-scale approaches.
6. Collect cells from the plates with selective media (CSM-Trp$^-$, Ura$^-$).
7. Harvest cells by centrifugation (5 min at 1000 × *g*). Discard the supernatant.
8. Resuspend the pellet in 10 ml of CSM-Trp$^-$, Ura$^-$. Determine the total cell number.
9. Mix both transformations 1:1. Fill up to 2 ml with YPD (pH 4.5).
10. Incubate 2 h at 30 °C, shaking at 35 rpm.
11. Plate in 300 µl aliquots on complete medium (YPD pH 4.5) on square plates (12 × 12 cm).
12. Incubate 5 h at 30 °C.
13. Wash cells with 15 ml ddH_2O.
14. Harvest cells by centrifugation (10 min at 1000 × *g*). Discard the supernatant.

15. Resuspend the cells in 5 ml ddH_2O.
16. Plate in 100 µl aliquots on CSM including 500 µM methionine and incubate for 3 days at 30 °C.
17. A total of ~10^6 colonies should be obtained.
18. Transfer colonies using sterile pipette tips on fresh CSM including 500 µM methionine and incubate for 3 days at 30 °C. Be careful NOT to transfer too much yeast material to avoid growth of false-positives.
19. Analyze by colony PCR (Subheading 3.6) and sequencing.

3.4 Detection Assay

1. Inoculate in 2 ml selective media (CSM-Leu^-, Trp^-, Ura^-) and grow shaking overnight at 30 °C.
2. Pipette 100 µl in a 1.5 ml tube and 100 µl into a cuvette containing 900 µl H_2O.
3. Determine 1:10 diluted OD_{600}. Note the values.
4. Harvest cells in the tubes by centrifugation (2 min at 2000 × *g*). Carefully remove the supernatant by pipetting.
5. Add appropriate volume of sterile ddH_2O to reach a final OD_{600} of 1.0 (e.g., 1:10 dilution has an OD_{600} value of 0.450; resuspend yeast pellet in 450 µl sterile H_2O).
6. Make tenfold serial dilutions (1:10, 1:100): Prepare tubes with 900 µl of sterile ddH_2O. Add 100 µl of the appropriate yeast ($OD_{600} = 1.0$) and mix well by shaking by hand. For the 1:100 dilution, transfer 100 µl of the 1:10 dilution into another tube containing 900 µl ddH_2O.
7. Drop 7 µl yeast of each dilution on selective plates containing increasing methionine concentrations as well as on vector-selective media (CSM-Leu^-, Trp^-, Ura^-) as growth control. Allow the drops to dry (*see* **Notes 9** and **10**).
8. Seal the plates and incubate for 1–3 days at 30 °C. Remove the vector-selective growth control after 24 h of incubation to see the gradient of the yeast ODs.
9. Document results by scanning or photography using a black background.

3.5 Western Blot

1. Harvest 2 ml of overnight yeast culture or use deep-frozen aliquots.
2. Add ~50 µl glass beads.
3. Resuspend cells in 200 µl LL-buffer by vortexing for approx. 2 min.
4. Incubate shaking for 10 min at 65 °C.
5. Centrifuge at 16,500 × *g* for 10 min.
6. Transfer the supernatant to a fresh tube.

7. Load 10–20 µl on a SDS-PAGE gel. *Optional:* Store at −80 °C.
8. Run gel with appropriate conditions.
9. Run western blot (e.g., semidry transfer on PVDF membrane).
10. Block membrane in blocking buffer on a shaker for 1 h at room temperature. *Optional:* overnight at 4 °C.
11. Wash three times, 10 min each with 1× TBST.
12. Transfer membrane into primary antibody solution. Incubate at least 1 h at room temperature. *Optional:* overnight at 4 °C.
13. Wash three times, 10 min each with 1× TBST.
14. Transfer membrane into secondary antibody solution. Incubate at least 1 h at room temperature. *Optional:* overnight at 4 °C.
15. Wash three times, 10 min each with 1× TBST.
16. Equilibrate membrane in staining buffer for 1 min.
17. Transfer membrane into staining solution. Incubate until clear signals can be monitored. Stop substrate reaction by washing with H_2O.

3.6 Yeast Colony PCR and Sequencing

1. Prepare sterile PCR tubes, strips, or plates with 50 µl ddH_2O (*see* **Note 11**).
2. Add small amount of yeast material using a sterile pipette tip.
3. Boil the samples at 100 °C for 10 min using a PCR cycler.
4. Cool and spin down briefly to avoid cross-contaminations when opening.
5. Prepare fresh tubes with 20 µl PCR master mix.
6. Use 10 µl of supernatant as sample and add into each well.
7. Run the following PCR program:
   (a) 95 °C—2.00 min
   (b) 95 °C—0.30 min
   (c) 58 °C—0.30 min
   (d) 72 °C—1.30 min
   (e) 72 °C—3.00 min
   (f) Repeat **steps (b)–(d)** 37 times.
8. Run 5 µl on a 1.5% agarose/TAE gel to determine successful amplification and insert size. Use the remainder for sequencing.

4 Notes

1. Depending on the presence of signal peptides or transmembrane domains, prey proteins can be tagged with either N-terminal NubG or C-terminal NubA. As mentioned in the

introduction, mutating the isoleucine at position 13 prevents spontaneous reassembly with Cub. Replacement by alanine shows a slightly increased affinity towards Cub [4] and can hence be used in the C-terminal Nub vectors that usually perform weaker compared with the N-terminal Nubs [1, 10].

2. The mbSUS is ideally suited for structure function analysis of proteins [12, 13] since the mating-based approach allows biased screening of many different mutants against the same interaction partner. Generation of mutants can best be done by including a point mutation together with a silent mutation that introduces a restriction site as identifier for each mutation [14].
3. In order to correctly interpret your data, it is crucial to always include the whole set of controls, comprising both NubWt as positive control and "empty" vectors as negative controls. Moreover, biological negative controls might provide additional evidence for the specificity of an interaction.
4. For solid media, add a magnetic stir bar before autoclaving. To give uniform growth conditions, measure 80 ml medium per square plate (12 × 12 cm) or 30 ml into round plates (diam. 9 cm), respectively. Try to avoid air bubbles.
5. Efficient (co-)transformation of yeast depends on the cell concentration as well as on the amount of carrier and plasmid DNA. Therefore we recommend to use at least 1 μg of plasmid DNA. However, it is important to note that transforming three plasmids at once results generally in lower transformation efficiency which can be counterbalanced through upscaling of the transformation mixture.
6. Red/white selection of diploid yeasts can be used as a preliminary tool to estimate positive/negative interactions. The effect is based on the *ADE2* reporter gene, which encodes an enzyme involved in the de novo synthesis of adenine. If *ADE2* is not activated due to the lack of interaction between bait and prey peptides, cells accumulate a red colored intermediate, whereas cells expressing interacting proteins become white.
7. The native structure and topology of an integral membrane protein are important parameters that have to be considered to determine tag orientation of bait proteins. It should always be taken into account that the Cub-PLV tag has to reside in the cytosol (not in the lumen of the ER or other compartments), as the USPs are cytosolic enzymes and the cleaved PLV needs to be able to diffuse into the nucleus. Also, the bait protein should be large, and attached or integrated into a membrane to prevent leakage of the fusion protein into the nucleus. Tools for the prediction of membrane protein topology and signal peptides such as "TMHMM" (http://www.cbs.dtu.dk/services/TMHMM/) and "SignalP" (http://www.cbs.dtu.dk/

services/ SignalP/) might be helpful to decide which bait should be used.

To determine the interaction with soluble baits, we recommend "cytoSUS" using a vector with an N-terminal OST4 transmembrane domain to artificially anchor the protein to the ER membrane [11, 15]. Otherwise the construct itself might diffuse into the nucleus and activate reporter genes due to its PLV fusion, leading to false-positive results.

8. Before starting an experiment, yeast expressing the bait/Cub-fusion proteins should be mated with soluble NubG and NubWt peptides, respectively, to verify functionality/stability and excluding self-activation (*see* **Note 12**). This includes growth assays as well as immunoblots of the bait proteins (Subheadings 3.4 and 3.5).
9. Increased assay stringency is achieved by expressing bait fusions in low-copy ARS/CEN vectors under the control of the methionine-repressible Met25 promoter. To identify both strong and weak interactions, we usually apply methionine concentrations of 0.5 μM–500 μM. However, methionine above 500 μM should be avoided as yeast growth becomes negatively affected by such concentrations.
10. It is helpful to print a dropping scheme and stick it under the media plates to guide pipetting. To avoid satellite colonies, the yeast drops should be placed carefully, and under no circumstances should the second pressure point of the pipette be used. The surface of the media should be relatively dry to prevent dispersion of the spots. Also, high (500 μM) levels of methionine seem to break the surface tension of the solid media causing carefully placed yeast drops to disperse on the surface. For this reason, we recommend not to place more than eight by eight yeast drops on a 12 cm square plate.
11. Contrary to our previous protocol [6], we repeatedly found in the evaluation of colony PCR results since that DMSO seems to inhibit the PCR reaction and should hence be omitted from the PCR mix. Also, addition of 0.2 M NaOH which should aid in lysis of yeast cells seems to negatively affect PCR fidelity. Instead, boiling the yeast colonies in water should suffice to extract an appropriate amount of template DNA for subsequent PCR amplification.
12. If one of your fusion proteins is not expressing well, it might be related to protein instability due to the tagging and thereby masking of signal peptides or other recognition/processing sites, especially in the N-terminal region. Also codon bias has a crucial role in heterologous gene expression and nonoptimal codon usage can limit the expression. Prior to codon optimization, we recommend to verify single colonies by western blot (Subheading 3.5).

Acknowledgements

We are grateful to Eva Schwörzer and Laure Grefen for excellent technical support. Work in our lab is supported through seed funding of the SFB1101 and an Emmy Noether fellowship of the German Research Foundation (DFG) to C.G. (GR 4251/1-1).

References

1. Xing S, Wallmeroth N, Berendzen KW, Grefen C (2016) Techniques for the analysis of protein-protein interactions in vivo. Plant Physiol 171:727–758
2. Obrdlik P et al (2004) K+ channel interactions detected by a genetic system optimized for systematic studies of membrane protein interactions. Proc Natl Acad Sci U S A 101:12242–12247
3. Johnsson N, Varshavsky A (1994) Split ubiquitin as a sensor of protein interactions in vivo. Proc Natl Acad Sci U S A 91:10340–10344
4. Raquet X, Eckert JH, Muller S, Johnsson N (2001) Detection of altered protein conformations in living cells. J Mol Biol 305:927–938
5. Stagljar I, Korostensky C, Johnsson N, Heesen S (1998) A genetic system based on split-ubiquitin for the analysis of interactions between membrane proteins in vivo. Proc Natl Acad Sci U S A 95:5187–5192
6. Grefen C (2014) The split-ubiquitin system for the analysis of three-component interactions. Methods Mol Biol 1062:659–678
7. Grefen C, Blatt MR (2012) Do calcineurin B-like proteins interact independently of the serine threonine kinase CIPK23 with the K+ channel AKT1? Lessons learned from a menage a trois. Plant Physiol 159:915–919
8. Park E, Rapoport TA (2012) Mechanisms of Sec61/SecY-mediated protein translocation across membranes. Annu Rev Biophys 41:21–40
9. Grefen C, Lalonde S, Obrdlik P (2007) Split-ubiquitin system for identifying protein-protein interactions in membrane and full-length proteins. Curr Protoc Neurosci. Chapter 5:Unit 5.27
10. Grefen C, Obrdlik P, Harter K (2009) The determination of protein-protein interactions by the mating-based split-ubiquitin system (mbSUS). Methods Mol Biol 479:217–233
11. Karnik R et al (2015) Binding of SEC11 indicates r role in SNARE recycling after vesicle fusion and identifies two pathways for vesicular traffic to the plasma membrane. Plant Cell 27:675–694
12. Zhang B et al (2015) The Arabidopsis R-SNARE VAMP721 interacts with KAT1 and KC1 K^+ channels to moderate K^+ current at the plasma membrane. Plant Cell 27:1697–1717
13. Grefen C et al (2015) A vesicle-trafficking protein commandeers Kv channel voltage sensors for voltage-dependent secretion. Nat Plants 3:15108
14. Karnik A, Karnik R, Grefen C (2013) SDM-assist software to design site-directed mutagenesis primers introducing "silent" restriction sites. BMC Bioinformatics 14:105
15. Xing S, Mehlhorn DG, Wallmeroth N, Asseck LY, Kar R, Voss A, Denninger P, Schmidt VAF, Schwarzländer M, Stierhof Y-D, Grossmann G, Grefen C (2017) Loss of GET pathway orthologs in causes root hair growth defects and affects SNARE abundance. Proc Natl Acad Sci 114(8):E1544–E1553

Chapter 16

Analysis of Protein Glycosylation in the ER

Jennifer Schoberer, Yun-Ji Shin, Ulrike Vavra, Christiane Veit, and Richard Strasser

Abstract

Protein N-glycosylation is an essential posttranslational modification which is initiated in the endoplasmic reticulum. In plants, the N-glycans play a pivotal role for protein folding and quality control. Through the interaction of glycan processing and binding reactions mediated by ER-resident glycosidases and specific carbohydrate binding proteins, the N-glycans contribute to the adoption of a native protein conformation. Properly folded glycoproteins are released from these processes and allowed to continue their transit to the Golgi where further processing and maturation of N-glycans leads to the formation of more complex structures with different functions. Incompletely folded glycoproteins are removed from the ER by a highly conserved degradation process to prevent the accumulation or secretion of misfolded proteins and maintain ER homeostasis. Here, we describe methods to analyze the N-glycosylation status and the glycan-dependent ER-associated degradation process in plants.

Key words N-glycosylation, Glycoprotein, Oligosaccharyltransferase, Quality control, ERAD

1 Introduction

Glycosylation is a ubiquitous modification of newly synthesized proteins in the endoplasmic reticulum (ER). Dependent on the linkage of the oligosaccharide to the amino acid side chain of the protein, there are two major types of glycosylation: N- and O-glycosylation. O-glycosylation is quite diverse and various types of O-glycans have been described for secretory proteins in eukaryotes including mucin-type O-linked N-acetylgalactosamine (GalNAc) or O-mannosylation [1, 2]. These O-glycosylation reactions are initiated by the transfer of a single monosaccharide to serine or threonine residues of proteins. While the O-glycan biosynthesis can already be initiated in the ER, the majority of the O-glycan modifications take place in the Golgi. In plants, it has been proposed that the plant-specific serine O-galactosylation of extensins or arabinogalactan proteins is initiated in the ER while further maturation of glycans takes place in the Golgi [3].

Chris Hawes and Verena Kriechbaumer (eds.), *The Plant Endoplasmic Reticulum: Methods and Protocols*, Methods in Molecular Biology, vol. 1691, DOI 10.1007/978-1-4939-7389-7_16,

In contrast to O-glycosylation, N-glycosylation and early N-glycan processing steps are highly conserved in all eukaryotes [4]. A hallmark of N-glycosylation is the en bloc transfer of a common preassembled oligosaccharide ($Glc_3Man_9GlcNAc_2$) from the lipid carrier dolichol pyrophosphate to selected asparagine residues in the sequence Asn-X-Ser/Thr (X ≠ P) within nascent polypeptides [5] (*see* **Note 1**). The transfer of the oligosaccharide takes place at the luminal side of the ER and is catalyzed by the oligosaccharyltransferase (OST) complex. In the ER, the attached N-glycans are crucial for protein folding and for quality control processes. Notably, by exposing defined motifs the N-glycans orchestrate the fate of glycoproteins in the ER [6]. In contrast to the conserved role of ER-type oligomannosidic structures, complex N-glycans are generated in the Golgi and serve different protein-specific roles that are not well understood in plants (Fig. 1a) [7–9].

1.1 N-Glycosylation

The biosynthesis of the lipid-linked oligosaccharide starts on the cytosolic side of the ER membrane by a number of different glycosyltransferases that have been initially characterized in yeast (asparagine-linked glycosylation proteins—ALGs) [10]. The synthesized $Man_5GlcNAc_2$-PP-Dol is flipped through the ER membrane (Fig. 1b) and further elongated in the lumen of the ER by three α-mannosyltransferases (ALG3, ALG9, and ALG12) and three α-glucosyltransferases (ALG6, ALG8, and ALG10) (Fig. 1b). Putative orthologs of these enzymes are present in the plant genome and mutants with defects in the assembly of the oligosaccharide precursor have been described [4]. For example, knockout of the *Arabidopsis thaliana* ALG10 gene results in an incomplete synthesis of the oligosaccharide precursor leading to reduced glycosylation efficiency of proteins [11]. The observed underglycosylation defect affects different glycoproteins and results in a leaf growth phenotype.

The fully assembled oligosaccharide precursor is transferred by OST to asparagine resides within the consensus sequence. In yeast, OST is a heteromeric membrane-bound protein complex [12] consisting of one catalytically active subunit (STT3) and several different non-catalytic subunits that contribute to N-glycosylation by regulation of the substrate specificity, stability, or assembly of the complex [12]. Mammals harbor two different catalytic isoforms (STT3A and STT3B) that are present in distinct OST complexes and differ in their catalytic activity and acceptor substrate selectivity [13]. While STT3A is predominately involved in co-translational glycosylation, STT3B displays a preference for posttranslational glycosylation [14]. The transfer of the preassembled oligosaccharide in plants involves a similar OST multi-subunit complex, which is still poorly characterized. In *A. thaliana*, two proteins (STT3A and STT3B) with homology to yeast and mammalian catalytic subunits have been identified [15]. STT3A-deficient plants are

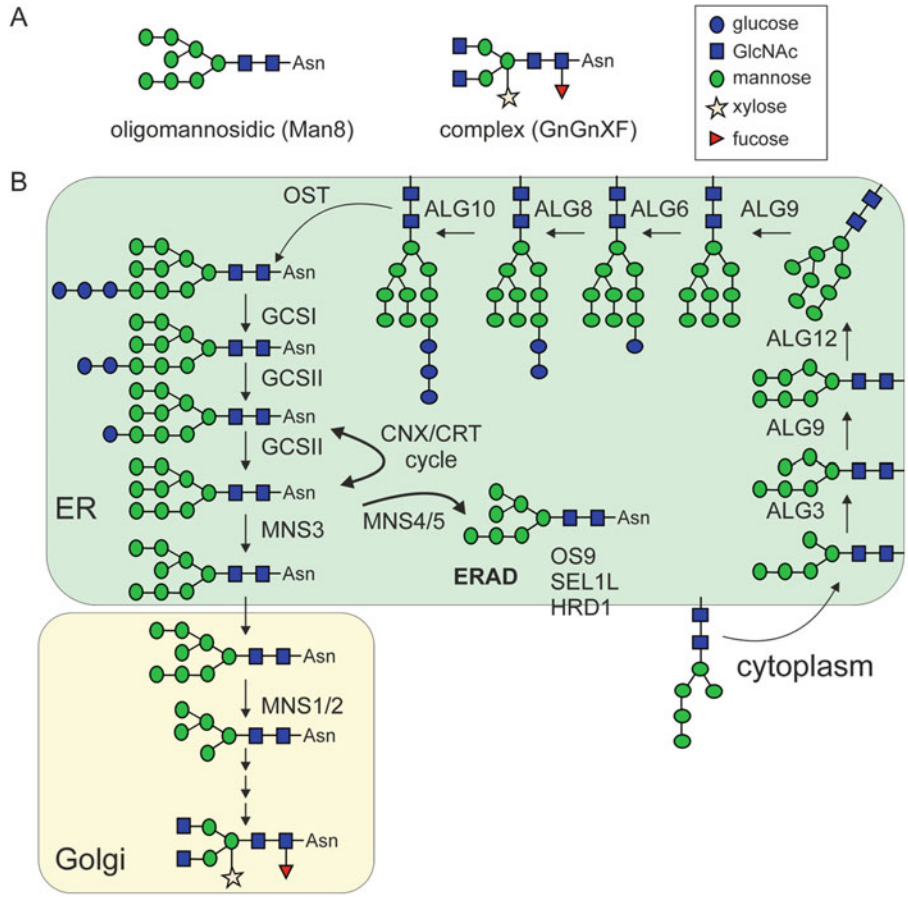

Fig. 1 (**a**) Schematic representation of two major N-glycan structures in plants: ER-type oligomannosidic and Golgi-processed complex N-glycans. (**b**) N-glycosylation and N-glycan processing in the ER of plants. The dolichol-linked $Man_5GlcNAc_2$ intermediate is translocated from the cytosol into the lumen of the ER (the preceding cytosolic biosynthesis steps are not shown). In the lumen of the ER, mannose residues are sequentially added by the α-mannosyltransferases ALG3, ALG9, and ALG12. Further elongation of the oligosaccharide is carried out by the α-glucosyltransferases ALG6, ALG8, and ALG10. The fully assembled $Glc_3Man_9GlcNAc_2$ oligosaccharide is transferred to selected asparagine residues by the oligosaccharyltransferase (OST) complex. Upon transfer, terminal glucose residues are trimmed by α-glucosidase I (GCSI) and II (GCSII). A terminal glucose residue is required for the interaction with calnexin (CNX) and calreticulin (CRT) that support folding of the glycoproteins. Properly folded proteins may be further processed in the ER by the α-mannosidase MNS3 [22] and are allowed to exit to the Golgi which is the site for complex N-glycan formation. In the ER, terminally misfolded proteins are subjected to processing by the α-mannosidases MNS4 and MNS5 which results in the degradation by the OS9-SEL1L-HRD1 complex [24]. The symbols for representation of the glycan structures follow the style of the Consortium for Functional Glycomics (www.functionalglycomics.org)

viable, but display a protein underglycosylation defect that impairs the biogenesis of different heavily glycosylated proteins, such as the pattern recognition receptor EF-TU RECEPTOR (EFR) or the endo-β1,4-glucanase KORRIGAN1 [7, 16, 17]. By contrast, much less is known about STT3B function and its substrates. Notably,

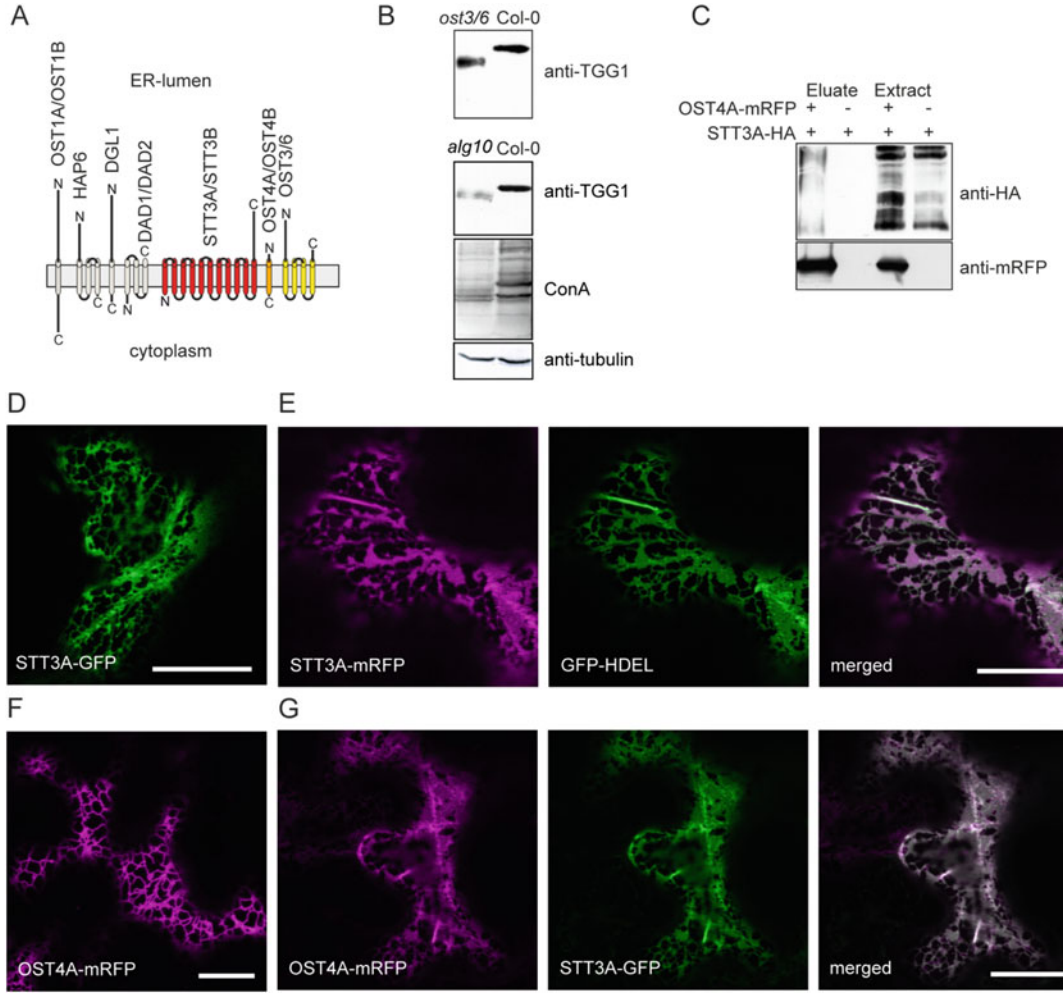

Fig. 2 (**a**) Schematic representation of the OST subunits and their predicted topology [4]. Subunits which likely interact (based on co-IP experiments) [19] are depicted in *red*, *orange*, and *yellow*. Other subunits are shown in grey. (**b**) Protein extracts from *A. thaliana* leaves were analyzed by immunoblotting with anti-TGG1 or anti-tubulin (non-glycosylated control) antibody. The shift in mobility indicates underglycosylation of TGG1 in the *ost3/6* and *alg10* mutants. The ConA lectin blot shows an overall weaker signal in the *alg10* mutant and some bands display an altered migration which is consistent with the underglycosylation defect. (**c**) OST4A-mRFP interacts with STT3A-HA. Proteins were transiently co-expressed in *N. benthamiana* leaves and extracts were analyzed 2 dpi. OST4A-mRFP was purified by RFP-Trap®_A beads and co-isolated STT3A-HA was monitored by immunoblotting with anti-HA antibodies. *Note*: due to the presence of numerous transmembrane helices STT3A-HA displays anomalous gel mobility. (**d**–**g**) Analysis of fluorescent proteins was done by confocal microscopy. Bars = 20 μm. The indicated constructs were transiently expressed in *N. benthamiana* leaves and analyzed 2 dpi

A. thaliana stt3a stt3b double knockouts are gametophytic lethal [15] highlighting the importance of the catalytic OST subunit for protein N-glycosylation in plants. Other subunits that have been characterized include DGL1 and OST3/6 [18, 19] (Fig. 2a). While

DGL1 appears essential for plants, OST3/6-deficient plants do not display any growth phenotype but are compromised in their immunity. In addition, it has recently been shown that OST3/6 is required for the interspecific gametophyte recognition in *A. thaliana* [20].

1.2 N-Glycan Processing in the ER

Specific processing of N-glycans in the ER generates distinct oligosaccharide structures that expose signals for quality control processes or degradation. Upon transfer of the preassembled oligosaccharide to the polypeptide chain, glucosidase I (GCSI) and II (GCSII) remove the two outermost glucose residues. The resulting monoglucosylated N-glycan can interact with the lectins calnexin (CNX) and calreticulin (CRT) to promote folding. In the current models, release from the CNX/CRT interaction requires the trimming of the remaining glucose by GCSII. Re-addition of the single glucose by the folding sensor UDP-glucose:glycoprotein glucosyltransferase (UGGT) facilitates prolonged interaction with CNX/CRT [21]. Several rounds of glucose trimming, re-glucosylation, and interaction with CNX/CRT are possible until proteins attain their final conformation and are released from this glycan-dependent quality control process.

The N-glycans from properly folded proteins or from folding intermediates may be subjected to further processing in the ER which is catalyzed by the α-mannosidase MNS3. Analysis of the substrate specificity revealed that MNS3 displays the typical ER-α-mannosidase I activity that has been described in mammals and yeast [22]. In contrast to yeast, however, MNS3 is mainly located in small punctate structures resembling Golgi bodies. Whether this characteristic subcellular localization of MNS3 is linked to its function in N-glycan processing is currently unclear. The processed glycoproteins typically carry the oligomannosidic N-glycans $Man_7GlcNAc_2$, $Man_8GlcNAc_2$, or $Man_9GlcNAc_2$. Further processing takes place in the Golgi and is initiated by Golgi α-mannosidase I (MNS1/MNS2)-mediated trimming of mannose residues resulting in the formation of $Man_5GlcNAc_2$.

1.3 N-Glycan-Dependent Quality Control and ER-Associated Degradation

To maintain protein homeostasis in the ER, all eukaryotic cells have a conserved machinery that selects aberrant or incompletely assembled proteins for degradation. In mammals and yeast, this ER-associated degradation (ERAD) pathway involves recognition of the misfolded protein, retro-translocation from the ER to the cytoplasm, ubiquitination of the protein and its subsequent disposal by the 26S proteasome [23]. While the latter steps have not been characterized in detail in plants, the selection and delivery reactions that take place in the lumen of the ER appear highly conserved. If folding attempts are unsuccessful, the α-mannosidases MNS4 and MNS5 cleave a terminal mannose residue from the C-branch of the oligomannosidic N-glycan [24]. The exposed

α1,6-linked mannose residue is recognized by the lectin-like protein OS9 and delivered to the SEL1L-HRD1 ERAD complex resulting in the degradation of the aberrant glycoprotein [25] (Fig. 1b).

Here, we provide protocols to address different aspects of protein N-glycosylation, N-glycan processing, and glycan-dependent ERAD that take place in the lumen of the ER.

2 Materials

1. *A. thaliana* seeds with characterized underglycosylation defects can be purchased from the European Arabidopsis Stock Center (*alg10-1*: NASC ID: N874475) [11, 15]. Seeds with defects in glycan-dependent ERAD are available from NASC (*os9-1*: N529413; *mns4 mns5*: double mutant can be obtained by crossing of N656907 and N162962) [24, 26]. The *bri1-9* seeds were kindly provided by Frans E. Tax. The *ost3/6-1* seeds can be requested from the Strasser group [19].
2. Mixer mill with steel beads.
3. Container with liquid nitrogen.
4. Refrigerated benchtop centrifuge with a relative centrifugal force of 9400 × *g* or higher and a rotor for 1.5/2 mL microcentrifuge tubes.
5. Thermo block.
6. Orbital shaker.
7. Vertical electrophoresis system.
8. Tank transfer system.
9. Power supply with at least 100 V and 400 mA.
10. SDS-PAGE (10–12%) gels.
11. Tris/glycine/SDS-PAGE running buffer: (25 mM Tris, 192 mM glycine, 0.1% (w/v) SDS.
12. 3× Laemmli sample buffer: 187.5 mM Tris pH 6.8, 30% (w/v) glycerol, 6% (w/v) SDS, 15% (v/v) β-mercaptoethanol, 0.15% (w/v) bromophenol blue.
13. Prestained protein standard.
14. Tris/glycine/methanol transfer buffer: 25 mM Tris, 192 mM glycine, 20% (v/v) methanol.
15. Blotting paper.
16. Nitrocellulose blotting membrane.
17. 1× PBS: phosphate buffered saline: 137 mM NaCl, 2.7 mM KCl, 10 mM Na_2HPO_4, 2 mM KH_2PO_4, pH 7.4.
18. PBST: 1× PBS + 0.1% (v/v) Tween 20.

19. 1× TBS: Tris buffered saline (25 mM Tris, pH 7.5, 150 mM NaCl, 2 mM KCl).
20. TBST: 1× TBS + 0.1% (v/v) Tween 20.
21. Blocking solution for immunoblots: TBST + 5% (w/v) skimmed milk powder or PBST + 3% (w/v) BSA.
22. Western blotting detection reagent: as an example, we use SuperSignal West PICO Chemiluminescent Substrate or ECL Prime Western Blotting Detection Reagent.
23. Sensitive films for detection: for example, we use Amersham Hyperfilm ECL (GE Healthcare).
24. Film developer and fixer solutions.
25. Rat monoclonal HA antibody (Roche 11867423001): 1:2000 diluted in TBST + 1% (w/v) BSA.
26. Polyclonal TGG1 antibody: custom-made antibody against the TGG1 peptide (AQNNQTIVPSDVHT): 1:10,000 diluted in PBST + 3% (w/v) BSA.
27. Polyclonal BRI1 antibody (Agrisera: AS12 1859): 1:5000 diluted in TBST + 5% (w/v) skimmed milk powder.
28. Rat monoclonal RFP antibody (ChromoTek: 5F8): 1:1000 diluted in PBST + 1% (w/v) BSA.
29. Mouse monoclonal GFP antibody (Roche: 11814460001): 1:2000 diluted in PBST + 3% (w/v) BSA.
30. Mouse monoclonal α-tubulin antibody (Sigma-Aldrich: T6074): 1:5000 diluted in PBST + 1% (w/v) BSA.
31. Concanavalin A-peroxidase (ConA-HRP, Sigma-Aldrich: L6397): ConA solution: 0.5 μg/mL Con A-HRP in PBST containing 1 mM $MnCl_2$, 1 mM $CaCl_2$, 1 mM $MgCl_2$.
32. Anti-rabbit IgG-peroxidase (such as Sigma A0545): 1:5000 diluted in TBST + 5% (w/v) skimmed milk powder for BRI1 detection and 1:50,000 diluted in TBST for TGG1 detection.
33. Anti-mouse IgG-peroxidase (such as Sigma A9044): 1:10,000 diluted in TBST for detection of GFP and α-tubulin.
34. Anti-rat IgG-peroxidase (Jackson): 1:10,000 diluted in PBST + 0.5% (w/v) BSA for detection of RFP and HA-tagged proteins.
35. Endoglycosidase H (Endo H, we use 500,000 units/mL, New England Biolabs) + GlycoBuffer 3 (New England Biolabs) + 10× Glycoprotein Denaturing Buffer (New England Biolabs).
36. Empty micro spin chromatography columns.
37. Nonidet P-40 (10% solution).
38. Kifunensine (Santa Cruz Biotechnology): class I α-mannosidase inhibitor, dissolved in ultrapure water.

39. RIPA buffer: 150 mM NaCl, 1.0% (v/v) Nonidet P-40, 0.5% (v/v) sodium deoxycholate, 0.1% (w/v) SDS, 50 mM Tris, pH 8.0.
40. RFP-Trap®_A beads (ChromoTek) for purification of RFP-tagged proteins.
41. Protein A Sepharose (such as rProtein A Sepharose Fast Flow from GE Healthcare).
42. Coomassie Brilliant Blue staining solution: 0.25% (w/v) Coomassie Brilliant Blue R-250, 10% (v/v) acetic acid, 50% (v/v) methanol.
43. Infiltration buffer: 0.5% (w/v) D-glucose, 50 mM 2-(N-morpholino)ethanesulfonic acid (MES), 2 mM Na_3PO_4, 0.1 mM acetosyringone.
44. *Agrobacterium tumefaciens* strain UIA143 pMP90 [27].
45. LB Broth (Lennox): 10 g/L tryptone, 5 g/L NaCl, 5 g/L yeast extract. Sterilize by autoclaving, supplement with 50 mg/L kanamycin 25 mg/L gentamicin.
46. MS medium: 0.5× Murashige and Skoog (MS) medium including MES buffer supplemented with 0.8% (w/v) agar and 1% (w/v) sucrose.

3 Methods

3.1 Monitoring of Protein Underglycosylation

N-glycosylation efficiency can be monitored by comparison of differences in mobility upon SDS-PAGE and immunoblotting of glycoproteins (*see* **Note 2**). Reduced N-glycosylation efficiency causes underglycosylation of glycoproteins which typically results in a faster migrating protein due to the reduced molecular weight (*see* **Note 3**). As a result, a single faster migrating band representing a partially or non-glycosylated variant can be detectable (Fig. 2b) or several bands might appear representing a mixture of differentially glycosylated proteins (fully glycosylated, partially glycosylated, and unglycosylated variants) (*see* **Note 4**). Protein underglycosylation has been described in several *A. thaliana* mutants which can be used as controls (e.g., mutants with defects in one of the OST subunits such as *stt3a-2* (15) or *ost3/6-1* [19] or mutants with defects in the assembly of the oligosaccharide precursor like *alg10* [11] (*see* **Note 5**). *A. thaliana* beta-thioglucoside glucohydrolase 1 (TGG1) is a heavily glycosylated protein that is expressed in high amounts in leaves [28] and has been used in several studies to show a reduction in protein glycosylation efficiency [11, 15]. In addition, protein underglycosylation can also be detected by an overall reduced signal with the lectin ConA that recognizes terminal α-linked mannose residues from oligomannosidic N-glycans (*see* **Notes 6** and **7**).

1. Harvest 10–100 mg of plant material (e.g., rosette leaves) from mutants and Columbia (Col-0) wild-type and transfer to 2 mL Eppendorf Safe-lock microcentrifuge tubes containing two steel beads (5 mm diameter) per tube.
2. Submerge 2 mL tubes with plant material in container with liquid nitrogen.
3. Mount 2 mL tubes in mixer mill and run mixing for 2 min at 50–60 amplitude.
4. Add 4 μL extraction buffer such as PBST per mg of plant material, vortex shortly, transfer mixture into a 1.5 mL tube.
5. Incubate on ice for 15 min, invert tube every 3 min.
6. Centrifuge two times 15 min, 9600 × *g* at 4 °C, transfer supernatant each time to a new tube.
7. Mix samples with 3× Laemmli sample buffer and heat to 95 °C for 5 min.
8. Load SDS-PAGE gel with 20 μL and run protein separation for 1.5 h at 100 V.
9. Soak nitrocellulose membrane, sponges, and blotting paper in transfer buffer.
10. Perform the gel-membrane assembly according to the user manual.
11. Blot for 1 h at 100 V, disassemble gel-membrane sandwich, and carefully rinse the membrane with ultrapure water.
12. Incubate in blocking solution for 1 h at room temperature.
13. Rinse briefly with PBST and incubate membrane on a shaker for 1.5 h at room temperature in the antibody solution (in our example, use a TGG1 antibody to detect changes in N-glycosylation and an antibody against a non-glycosylated protein like α-tubulin as a control).
14. After incubation, wash four times 5 min with TBST and add secondary antibody solution to the membrane, incubate 1.5 h at room temperature on a shaker. Omit this step for ConA detection, because the used ConA protein is covalently linked to horseradish peroxidase.
15. Wash four times 5 min in TBST, perform detection using the chemiluminescent substrate, and develop the film.

3.2 Co-IP and Subcellular Localization of OST Subunits

Agroinfiltration of *Nicotiana benthamiana* leaves is a fast procedure for protein expression and subsequent co-localization studies by confocal laser scanning microscopy or for monitoring of complex formation by co-immunoprecipitation (co-IP). These protocols have, for example, been used to characterize unknown subunits of the *A. thaliana* OST complex [19] (Fig. 2a and c).

1. Grow *A. tumefaciens* in LB liquid culture supplemented with the appropriate antibiotics for 16 h at 29 °C.
2. Spin down 500 μL of the overnight culture containing the construct for expression of the glycan-modifying enzyme and wash pellet twice with infiltration buffer. Dilute the agrobacteria suspension with infiltration buffer to an OD600 (optical density at 600 nm) of 0.1.
3. For co-localization of GFP and mRFP fusion proteins, mix two or more agrobacteria suspensions and co-infiltrate the whole mixture into fully expanded leaves of 5–6-week-old *N. benthamiana* plants using a 1 mL syringe without a needle. The analysis of subcellular localization by confocal microscopy has been described in detail previously [29].
4. Briefly, sections of infiltrated leaves are analyzed 1–3 days post-infiltration (dpi) on a Leica TCS SP5 confocal microscope equipped with ×63 and ×100 oil immersion objectives using appropriate spectral selections. Post-acquisition image processing is performed in IMAGEJ and ADOBE PHOTOSHOP CS (Fig. 2d–g).
5. For co-IP, harvest 500 mg of leaves and extract the proteins with RIPA buffer following the grinding steps as described in Subheading 3.1.
6. Per sample equilibrate 50 μL RFP-Trap®_A bead slurry in 500 μL of dilution buffer (RIPA buffer without detergents).
7. Centrifuge at 2500 × *g* for 2 min, discard the supernatant and repeat wash twice.
8. Add 2 mL of the clear protein extract to equilibrated RFP-Trap®_A beads and incubate for 1 h at 4 °C using an orbital shaker.
9. The RFP-Trap®_A beads with the bound proteins are washed four times with dilution buffer and proteins are eluted by incubation at 95 °C for 10 min in 50 μL 1× Laemmli buffer.
10. To collect the bound proteins, perform centrifugation at 2500 × *g* for 2 min using micro spin columns.
11. The protein extracts and the eluate are subjected to SDS-PAGE and immunoblotting with anti-HA and anti-mRFP antibodies as described above for monitoring of protein underglycosylation (*see* **Note 8**) (Fig. 2c).

3.3 Characterization of ER-Type Oligomannosidic N-Glycans

ER-resident proteins typically carry oligomannosidic N-glycans because these proteins are not in contact with the Golgi-located machinery for complex N-glycan processing (Fig. 1b). Such oligomannosidic N-glycans are sensitive to digestion by endoglycosidase H (Endo H) which cleaves between the chitobiose core to release the majority of the oligosaccharide (Fig. 3a). As a consequence,

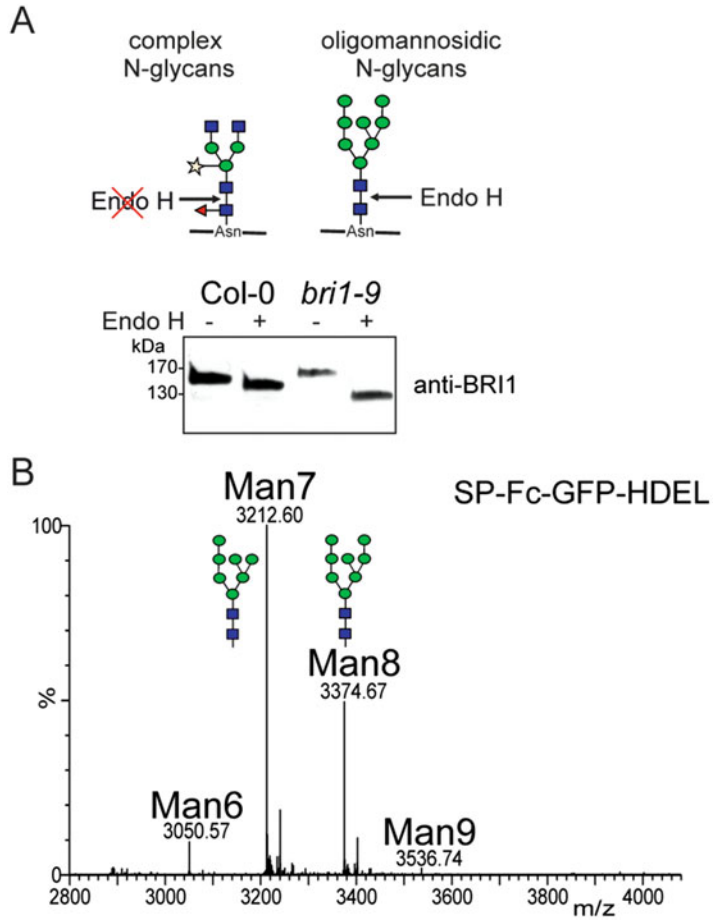

Fig. 3 (**a**) Endo H digestion and detection of BRI1 glycosylation in protein extracts from Col-0 wild-type and the *bri1-9* mutant. BRI1 in Col-0 is only partially deglycosylated (few oligomannosidic N-glycans are present) as visible by the minor shift in mobility (band >130 kDa). Endo H treatment of BRI1 in the mutant results in complete deglycosylation (band <130 kDa). The cartoon illustrates the cleavage specificity of Endo H. For description of sugar symbols, *see* Fig. 1. (**b**) Transiently expressed SP-Fc-GFP-HDEL was purified and the glycopeptide (peptide sequence: TKPREEQYNSTYR—N-glycosylation site is underlined) from the Fc domain was subjected to LC-ESI-MS analysis. Peak labels were made according to the ProGlycAn system (www.proglycan.com)

Endo H digestion of oligomannosidic N-glycans will result in a reduced molecular weight that can be monitored by SDS-PAGE and immunoblotting. Proteins with complex N-glycans are resistant to Endo H digestion and do not cause a similar change in the molecular weight (Fig. 3a). Endo H treatment has been used to show that a misfolded variant of the brassinosteroid receptor BRI1 accumulates in the ER in the *bri1-9* mutant [30]. By contrast, correctly folded BRI1 is secreted and carries primarily Golgi-processed complex N-glycans (*see* **Note 9**).

1. Incubate 22.5 μL protein extract with 2.5 μL 10× Glycoprotein Denaturing Buffer for 10 min at 50 °C, transfer to ice and cool for 5 min.
2. Mix 22.5 μL of the denatured glycoproteins with 3 μL 10× GlycoBuffer 3, 3 μL ultrapure water, and 1.5 μL Endo H.
3. For the control reaction, replace the 1.5 μL Endo H with ultrapure water.
4. Incubate for 90 min at 37 °C and stop the reaction by heating to 50 °C for 5 min.
5. Subject samples to SDS-PAGE and perform immunoblotting, for example with anti-BRI1 antibody (Fig. 3a) to distinguish between ER-retained and secreted BRI1 variants.
6. To confirm the presence of oligomannosidic N-glycans, glycoproteins can be purified and subjected to mass spectrometry.

   The attachment of the HDEL or KDEL ER-retrieval peptide sequence to the C-terminal end leads to the steady-state accumulation of proteins in the ER. An example for such a protein is a chimeric protein consisting of an N-terminal signal peptide, the Fc domain region from human IgG, GFP and the HDEL peptide (SP-Fc-GFP-HDEL). This protein can be expressed transiently in *N. benthamiana* leaves as described in Subheading 3.2 and ER accumulation can be monitored by confocal microscopy. Efficient one-step purification of this protein is achieved by affinity chromatography using binding of the Fc domain region to bacterial Protein A (*see* **Note 10**).
7. Harvest 1 g of leaves 2 dpi and extract proteins in RIPA buffer as described in Subheading 3.2.
8. Add 50 μL protein A sepharose that has been washed several times with 1× PBS.
9. Incubate for 1.5 h at 4 °C using an orbital shaker, spin down briefly, and discard the supernatant.
10. Wash the sepharose three times with 250 μL 1× PBS using micro spin columns.
11. Elute the Fc domain-containing protein from the column by adding 50 μL 1× Laemmli buffer.
12. Elute as described for the RFP-Trap®_A purification and separate by SDS-PAGE.
13. Stain the gel with Coomassie Brilliant Blue and excise the glycoprotein band from the gel. Perform S-alkylation, digestion with trypsin (*see* **Note 11**) and analyze the resulting glycopeptides by liquid chromatography-electrospray

ionization-mass spectrometry (LC-ESI-MS) (Fig. 3b). The detailed procedure for this MS-based glycopeptide analysis has been described recently [31].

3.4 Monitoring of Glycan-Dependent ERAD

Glycan-dependent ERAD is a major pathway for disposal of misfolded glycoproteins from the ER. To monitor whether a protein is subjected to glycan-dependent ERAD the class I α-mannosidase inhibitor kifunensine can be used. Kifunensine blocks the trimming of terminal α-linked mannose residues which is mediated by class I α-mannosidases [32]. The exposure of an α1,6-linked mannose residue (Fig. 1b) to the ERAD machinery (including proteins like OS9, SEL1L, and HRD1) is a highly conserved hallmark of glycan-dependent ERAD in different species [24, 33–35]. Kifunensine blocks the formation of the exposed α1,6-linked mannose residue and thus blocks the degradation of ERAD substrates (Fig. 4a) (*see* **Note 12**).

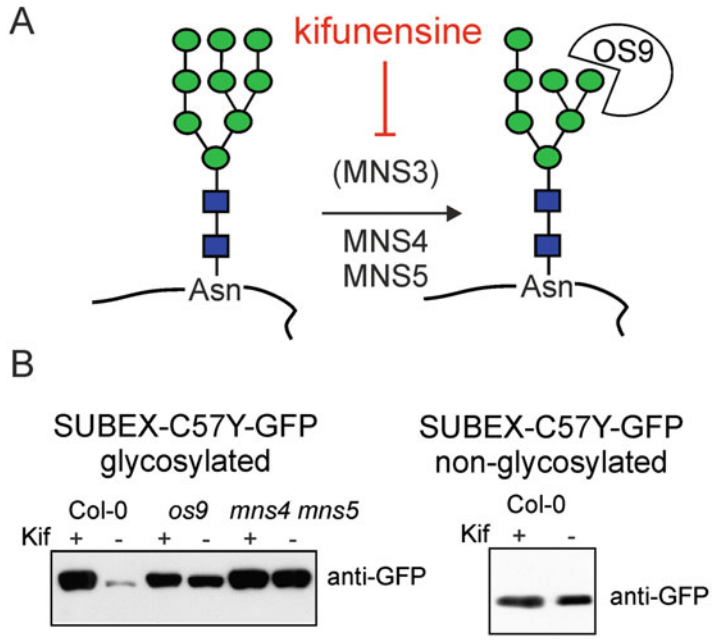

Fig. 4 (**a**) Illustration of the processing by MNS4/MNS5 which generates the N-glycan that serves as degradation signal for misfolded glycoproteins. The class I α-mannosidase inhibitor kifunensine (Kif) blocks the mannose trimming and leads to accumulation of misfolded glycoproteins (ERAD substrates) in the ER. Likewise, OS9 or MNS4/MNS5 deficiency blocks the degradation. MNS3 may act on the $Man_9GlcNAc_2$ N-glycan but is not necessary for glycan-mediated ERAD [24]. (**b**) The ERAD substrate SUBEX-C57Y-GFP consisting of a misfolded variant of the glycosylated extracellular domain from STRUBBELIG fused to GFP is degraded in Col-0 wild-type and accumulates in the *os9* or *mns4 mns5* mutants as well as in the presence of Kif [42]. A non-glycosylated variant of the misfolded protein is not degraded by the same pathway highlighting the glycan dependency of the protein disposal pathway

1. Detach leaves from 4-week-old *A. thaliana* plants, cut them into small pieces (alternatively whole seedlings can be used in the same way), and submerge in 0.5× MS medium supplemented with 20 μM kifunensine.
2. Incubate at 22 °C with gentle shaking under long day conditions (16 h light/8 h dark) for 24 h.
3. Harvest seedlings, remove excess liquid and extract protein as described under Subheading 3.1. To monitor the accumulation of the ERAD substrate, perform immunoblotting with appropriate antibodies (Fig. 4b).
4. An increased signal in the presence of the inhibitor indicates the involvement of a glycan-dependent degradation pathway.
5. To substantiate the finding, the fate of the misfolded glycoprotein can be analyzed in different mutants with distinct defects in glycan-dependent ERAD [24, 26].

4 Notes

1. Apart from Asn-X-Ser/Thr, there is the rare possibility for the use of noncanonical glycosylation sites like Asn-X-Cys [36, 37]. The sequon is necessary but not sufficient for N-glycosylation. N-glycosylation efficiency is dependent on many factors involving the amino acid sequence close to the N-glycosylation site, the secondary structure, the positioning of the site within the protein [13], and organism-specific difference in the composition and function of the OST subunits [12].
2. A shift in mobility can also be caused by other posttranslational modifications including proteolytic processing. Digestion of protein extracts with endoglycosidases that remove oligomannosidic or complex N-glycans is a way to support the observation of underglycosylation. However, complex N-glycans carrying core α1,3-fucose cannot be efficiently removed from whole proteins using endoglycosidases which can complicate the interpretation of the results. Additional blots with antibodies against complex/paucimannosidic N-glycans and lectins that bind to mannose residues can be used to further support a protein underglycosylation defect (*see* also the procedure for detection of glycoproteins that are recognized by ConA). Apart from the described immunoblot-based protocols, purification of the protein with subsequent mass spectrometric (MS) analysis and quantification of glycosylated versus non-glycosylated peptide should be used to confirm the underglycosylation defect [31].
3. In some cases, a clear protein band cannot be detected anymore in a protein underglycosylation mutant (e.g., KORRIGAN1 in

stt3a-2) [7]. Most likely, the absence of distinct N-glycans interferes with proper folding leading to degradation or aggregation (exposure of hydrophobic sequence stretches that are otherwise shielded by N-glycans) of these proteins.

4. These differences depend on the number of N-glycans and other protein intrinsic features that are involved in N-glycosylation. For example, some of the noncatalytic OST subunits have accessory function and can slow down protein folding to keep the polypeptide in a glycosylation-competent state [13].
5. Additional approaches can be used that suggest a possible reduction in glycosylation efficiency. These approaches involve treatment of seedlings with tunicamycin. Tunicamycin is an inhibitor that blocks N-glycosylation by interfering with one of the early steps of the lipid-linked oligosaccharide biosynthesis pathway. Plants with defects in N-glycosylation are typically more sensitive to tunicamycin [38].
6. An altered signal with ConA could also result from changes in complex N-glycan formation (e.g., increased signal in the *cgl1* mutant that lacks complex N-glycans). It is therefore recommended to combine the ConA lectin blot with immunoblots using antibodies against complex N-glycans [39].
7. In an alternative approach, protein underglycosylation can be detected in *A. thaliana* by restoration of complex N-glycan formation in the *cgl1* mutant. This approach has been described in detail recently [39].
8. While co-IP can be helpful to identify the components of a protein complex, it does not provide spatiotemporal information on direct interactions of the investigated proteins. Therefore, alternative approaches like FRET-FLIM should be applied for monitoring of real-time protein–protein interactions in cells [40].
9. Oligomannosidic N-glycans can also be found on secreted proteins that are not trafficking through the Golgi (e.g., due to direct ER-to-vacuole protein trafficking). In addition, some N-glycans are not accessible for Golgi-mediated N-glycan processing (e.g., steric hindrance of N-glycan processing) resulting in the presence of oligomannosidic N-glycans on some secreted or plasma-membrane anchored proteins (*see* also Endo H digestion of BRI1 in Col-0 in Fig. 3a). It is therefore necessary to perform additional experiments (e.g., confocal microscopy of fluorescent fusion proteins) to confirm ER localization.
10. Purification with an immobilized antibody against GFP could also be used instead of binding to Protein A. While such protocols work equally well with our fusion proteins, there are more suppliers for Protein A-related reagents than for reagents

that can be used for purification of GFP-tagged proteins. Consequently, Protein A-based purification is typically less expensive than purifications based on GFP-binding proteins. Alternatively, an antibody specific for an (ER-resident) glycoprotein can be used for purification and subsequent N-glycan analysis. Due to the low expression levels, such protocols typically require extensive optimization.

11. The choice of the protease is dependent on the amino acid sequence. Separate or sequential digestion with alternative enzymes, such as Glu-C, Asp-N, or chymotrypsin, is sometimes necessary to improve the detection of glycopeptides [31].
12. Although the components of the glycan-dependent ERAD pathway are already well known, the steps that lead to the recognition of aberrant glycoproteins as well as the downstream steps that lead to their disposal are currently unclear. In mammals and yeast, the ERAD degradation pathway involves translocation into the cytoplasm, ubiquitination, and proteasomal degradation. In plants, the involvement and role of the proteasome in degradation of glycoprotein ERAD substrates is unclear [41, 42].

Acknowledgements

We would like to thank Friedrich Altmann and Daniel Maresch (both Department of Chemistry) for LC-ESI-MS-analysis. This work was supported by grants from the Austrian Science Fund (FWF): P28218 and T655-B20.

References

1. Xu C, Ng DT (2015) O-mannosylation: the other glycan player of ER quality control. Semin Cell Dev Biol 41:129–134
2. Gill DJ, Clausen H, Bard F (2011) Location, location, location: new insights into O-GalNAc protein glycosylation. Trends Cell Biol 21 (3):149–158
3. Saito F, Suyama A, Oka T, Yoko-O T, Matsuoka K, Jigami Y, Shimma YI (2014) Identification of novel peptidyl serine α-galactosyltransferase gene family in plants. J Biol Chem 289:20405–20420
4. Strasser R (2016) Plant protein glycosylation. Glycobiology 26:926–939
5. Aebi M (2013) N-linked protein glycosylation in the ER. Biochim Biophys Acta 1833:2430–2437
6. Aebi M, Bernasconi R, Clerc S, Molinari M (2010) N-glycan structures: recognition and processing in the ER. Trends Biochem Sci 35:74–82
7. Kang J, Frank J, Kang C, Kajiura H, Vikram M, Ueda A, Kim S, Bahk J, Triplett B, Fujiyama K, Lee S, von Schaewen A, Koiwa H (2008) Salt tolerance of *Arabidopsis thaliana* requires maturation of N-glycosylated proteins in the Golgi apparatus. Proc Natl Acad Sci U S A 105:5933–5938
8. Fanata WI, Lee KH, Son BH, Yoo JY, Harmoko R, Ko KS, Ramasamy NK, Kim KH, Oh DB, Jung HS, Kim JY, Lee SY, Lee KO (2013) N-glycan maturation is crucial for cytokinin-mediated development and cellulose synthesis in *Oryza sativa*. Plant J 73:966–979
9. Harmoko R, Yoo JY, Ko KS, Ramasamy NK, Hwang BY, Lee EJ, Kim HS, Lee KJ, Oh DB, Kim DY, Lee S, Li Y, Lee SY, Lee KO (2016) N-glycan containing a core α1,3-fucose residue

is required for basipetal auxin transport and gravitropic response in rice (*Oryza sativa*). New Phytol 212:108–122

10. Lehle L, Strahl S, Tanner W (2006) Protein glycosylation, conserved from yeast to man: a model organism helps elucidate congenital human diseases. Angew Chem Int Ed Engl 45:6802–6818
11. Farid A, Pabst M, Schoberer J, Altmann F, Glössl J, Strasser R (2011) *Arabidopsis thaliana* alpha1,2-glucosyltransferase (ALG10) is required for efficient N-glycosylation and leaf growth. Plant J 68:314–325
12. Kelleher D, Gilmore R (2006) An evolving view of the eukaryotic oligosaccharyltransferase. Glycobiology 16:47R–62R
13. Cherepanova N, Shrimal S, Gilmore R (2016) N-linked glycosylation and homeostasis of the endoplasmic reticulum. Curr Opin Cell Biol 41:57–65
14. Ruiz-Canada C, Kelleher DJ, Gilmore R (2009) Cotranslational and posttranslational N-glycosylation of polypeptides by distinct mammalian OST isoforms. Cell 136:272–283
15. Koiwa H, Li F, McCully M, Mendoza I, Koizumi N, Manabe Y, Nakagawa Y, Zhu J, Rus A, Pardo J, Bressan R, Hasegawa P (2003) The STT3a subunit isoform of the Arabidopsis oligosaccharyltransferase controls adaptive responses to salt/osmotic stress. Plant Cell 15:2273–2284
16. Nekrasov V, Li J, Batoux M, Roux M, Chu Z, Lacombe S, Rougon A, Bittel P, Kiss-Papp M, Chinchilla D, van Esse H, Jorda L, Schwessinger B, Nicaise V, Thomma B, Molina A, Jones J, Zipfel C (2009) Control of the pattern-recognition receptor EFR by an ER protein complex in plant immunity. EMBO J 28:3428–3438
17. Saijo Y, Tintor N, Lu X, Rauf P, Pajerowska-Mukhtar K, Häweker H, Dong X, Robatzek S, Schulze-Lefert P (2009) Receptor quality control in the endoplasmic reticulum for plant innate immunity. EMBO J 28:3439–3449
18. Lerouxel O, Mouille G, Andème-Onzighi C, Bruyant M, Séveno M, Loutelier-Bourhis C, Driouich A, Höfte H, Lerouge P (2005) Mutants in DEFECTIVE GLYCOSYLATION, an Arabidopsis homolog of an oligosaccharyltransferase complex subunit, show protein underglycosylation and defects in cell differentiation and growth. Plant J 42:455–468
19. Farid A, Malinovsky FG, Veit C, Schoberer J, Zipfel C, Strasser R (2013) Specialized roles of the conserved subunit OST3/6 of the oligosaccharyltransferase complex in innate immunity and tolerance to abiotic stresses. Plant Physiol 162:24–38
20. Müller LM, Lindner H, Pires ND, Gagliardini V, Grossniklaus U (2016) A subunit of the oligosaccharyltransferase complex is required for interspecific gametophyte recognition in Arabidopsis. Nat Commun 7:10826
21. Caramelo JJ, Parodi AJ (2015) A sweet code for glycoprotein folding. FEBS Lett 589:3379–3387
22. Liebminger E, Hüttner S, Vavra U, Fischl R, Schoberer J, Grass J, Blaukopf C, Seifert G, Altmann F, Mach L, Strasser R (2009) Class I alpha-mannosidases are required for N-glycan processing and root development in Arabidopsis thaliana. Plant Cell 21:3850–3867
23. Vembar S, Brodsky J (2008) One step at a time: endoplasmic reticulum-associated degradation. Nat Rev Mol Cell Biol 9:944–957
24. Hüttner S, Veit C, Vavra U, Schoberer J, Liebminger E, Maresch D, Grass J, Altmann F, Mach L, Strasser R (2014) Arabidopsis class I α-mannosidases MNS4 and MNS5 are involved in endoplasmic reticulum-associated degradation of misfolded glycoproteins. Plant Cell 26:1712–1728
25. Liu Y, Li J (2014) Endoplasmic reticulum-mediated protein quality control in Arabidopsis. Front Plant Sci 5:162
26. Hüttner S, Veit C, Schoberer J, Grass J, Strasser R (2012) Unraveling the function of *Arabidopsis thaliana* OS9 in the endoplasmic reticulum-associated degradation of glycoproteins. Plant Mol Biol 79:21–33
27. Hamilton CM (1997) A binary-BAC system for plant transformation with high-molecular-weight DNA. Gene 200:107–116
28. Liebminger E, Grass J, Jez J, Neumann L, Altmann F, Strasser R (2012) Myrosinases TGG1 and TGG2 from Arabidopsis thaliana contain exclusively oligomannosidic N-glycans. Phytochemistry 84:24–30
29. Schoberer J, Runions J, Steinkellner H, Strasser R, Hawes C, Osterrieder A (2010) Sequential depletion and acquisition of proteins during Golgi stack disassembly and reformation. Traffic 11:1429–1444
30. Jin H, Yan Z, Nam K, Li J (2007) Allele-specific suppression of a defective brassinosteroid receptor reveals a physiological role of UGGT in ER quality control. Mol Cell 26:821–830
31. Gruber C, Altmann F (2015) Site-specific glycosylation profiling using liquid chromatography-tandem mass spectrometry (LC-MS). Methods Mol Biol 1321:407–415

32. Elbein AD, Tropea JE, Mitchell M, Kaushal GP (1990) Kifunensine, a potent inhibitor of the glycoprotein processing mannosidase I. J Biol Chem 265:15599–15605
33. Clerc S, Hirsch C, Oggier D, Deprez P, Jakob C, Sommer T, Aebi M (2009) Htm1 protein generates the N-glycan signal for glycoprotein degradation in the endoplasmic reticulum. J Cell Biol 184:159–172
34. Ninagawa S, Okada T, Sumitomo Y, Kamiya Y, Kato K, Horimoto S, Ishikawa T, Takeda S, Sakuma T, Yamamoto T, Mori K (2014) EDEM2 initiates mammalian glycoprotein ERAD by catalyzing the first mannose trimming step. J Cell Biol 206:347–356
35. Su W, Liu Y, Xia Y, Hong Z, Li J (2012) The Arabidopsis homolog of the mammalian OS-9 protein plays a key role in the endoplasmic reticulum-associated degradation of misfolded receptor-like kinases. Mol Plant 5:929–940
36. Zielinska DF, Gnad F, Schropp K, Wiśniewski JR, Mann M (2012) Mapping N-glycosylation sites across seven evolutionarily distant species reveals a divergent substrate proteome despite a common core machinery. Mol Cell 46:542–548
37. de Oliveira MVV, Xu G, Li B, de Souza Vespoli L, Meng X, Chen X, Yu X, de Souza SA, Intorne AC, de A. Manhães AME, Musinsky AL, Koiwa H, de Souza Filho GA, Shan L, He P (2016) Specific control of Arabidopsis BAK1/SERK4-regulated cell death by protein glycosylation. Nat Plants 2:15218
38. Hori H, Elbein AD (1981) Tunicamycin inhibits protein glycosylation in suspension cultured soybean cells. Plant Physiol 67:882–886
39. Veit C, Vavra U, Strasser R (2015) N-glycosylation and plant cell growth. Methods Mol Biol 1242:183–194
40. Schoberer J, Liebminger E, Vavra U, Veit C, Castilho A, Dicker M, Maresch D, Altmann F, Hawes C, Botchway SW, Strasser R (2014) The transmembrane domain of N-acetylglucosaminyltransferase I is the key determinant for its Golgi subcompartmentation. Plant J 80:809–822
41. Hong Z, Jin H, Tzfira T, Li J (2008) Multiple mechanism-mediated retention of a defective brassinosteroid receptor in the endoplasmic reticulum of Arabidopsis. Plant Cell 20:3418–3429
42. Hüttner S, Veit C, Vavra U, Schoberer J, Dicker M, Maresch D, Altmann F, Strasser R (2014) A context-independent N-glycan signal targets the misfolded extracellular domain of Arabidopsis STRUBBELIG to endoplasmic-reticulum-associated degradation. Biochem J 464:401–411

Chapter 17

The Unfolded Protein Response

Kazuki Tabara, Yuji Iwata, and Nozomu Koizumi

Abstract

Under the unfolded protein response (UPR), transcripts encoding the endoplasmic reticulum (ER) chaperones are increased and those encoding proteins synthesized in the ER are decreased. To reproducibly detect such changes of an expression profile, homogeneous growth of plants is desired. In addition, uniform treatment with drugs inducing the UPR is also necessary. Here we describe our methods of plant culture and drug treatment, and procedure to detect gene expression by quantitative RT-PCR.

Key words Quantitative RT-PCR, Tunicamycin, Dithiothreitol, L-Azetidine-2-carboxylic acid, Arabidopsis

1 Introduction

The unfolded protein response (UPR) or the endoplasmic reticulum (ER) stress response is a cellular response highly conserved among eukaryotes [1, 2]. In general, accumulation of misfolded or unfolded proteins induces transcription of genes encoding the ER chaperones during the UPR. Even though several environmental stresses may cause the UPR, effects of any of those stresses are not obvious especially in plants. Then, drugs that disturb folding of proteins are often used to induce the UPR not only in plant cells but also in other organisms such as yeast and animals. In addition to induction of genes encoding the ER chaperones and folding enzymes, degradation of mRNA encoding a wide range of proteins translated in the ribosomes attached to the ER membrane is observed during the UPR in plants as well as in other organisms with some exception [3–5]. This phenomenon has been known as regulated IRE1-dependent decay of mRNA (RIDD). Drugs are also used to observe RIDD. Popular drugs inducing the UPR are tunicamycin, a potent inhibitor of asparagine-linked glycosylation [6], dithiothreitol (DTT), a reducing agent disturbing disulfide bond formation [7], and L-azetidine-2-carboxylic acid (AZC), a proline analog that is incorporated to polypeptides and disturbs

Chris Hawes and Verena Kriechbaumer (eds.), *The Plant Endoplasmic Reticulum: Methods and Protocols*, Methods in Molecular Biology, vol. 1691, DOI 10.1007/978-1-4939-7389-7_17,

protein folding [8]. Treatment of yeast cells or cultured animal cells is considered to be easier than plant cells since they are mostly uniform cells. If cultured plant cells are available, it would be also useful. However, inducing cultured cells from plants such as arabidopsis is somewhat laborious and limits the use of a number of mutants to be tested. Then, a culture method of more or less homogeneous arabidopsis plantlets suitable for drug treatments is desired.

Here we describe our routine protocol of cultivation and drug treatment of arabidopsis plantlets [9–12]. Detection of induction of representative chaperone genes and degradation of RIDD target by quantitative RT-PCR (qRT-PCR) are also described [13].

2 Materials

Analytical grade reagents and pure water are used for preparation of medium and solution unless indicated otherwise. Medium and solution can be stored at room temperature also unless indicated.

2.1 Sterilized Plantlets

1. 70% ethanol: Dilute 99.5% EtOH with water.
2. 1% Hypochlorous acid (NaClO) solution: Dilute 5% NaClO with water.
3. 0.1% agar: Dissolve 0.1 g of agar in 100 mL of water and autoclave.
4. 1/2 MS medium with 1% sucrose: Dissolve premixed MS (Murashige and Skoog) salt (for 1 L) in 100 mL of water (this is 20× MS stock). Take necessary amount for the experiment, fill up with water, and add sucrose at a final concentration of 1% (*see* **Note 1**). Adjust pH to 5.6 with KOH and autoclave.
5. Sterilized 12- or 24-well titer plates.

2.2 Drugs Inducing the UPR

1. Tunicamycin stock solution (5 mg/mL): Dissolve 10 mg of tunicamycin in 2 mL of dimethyl sulfoxide (DMSO). Store at −20 °C (*see* **Note 2**).
2. DTT stock solution (1 M): Dissolve 154 mg of DTT in 1 mL of sterilized ultrapure water. Store at −20 °C.
3. AZC stock solution (2 M): Dissolve 101 mg of AZC in water. Store at −20 °C.

2.3 Extraction of RNA

1. 1.5 and 2 mL microtubes.
2. Aluminum oxide beads (Φ4 mm) (Nikkato Ltd.) (*see* **Note 3**).
3. Bead mill: TissueLyser II System (QIAGEN) (*see* **Note 4**).
4. RNA extraction buffer: 38% (V/V) of buffer saturated phenol, 0.8 M of guanidine thiocyanate, 0.4 M ammonium

thiocyanate, 0.1 M sodium acetate, and 5% glycerol (V/V). Ultrapure water is used for preparation of solution.

5. High salt buffer: 0.8 M sodium citrate and 1.2 M sodium chloride. Ultrapure water is used for preparation of solution.
6. 3 M sodium acetate.
7. Chloroform.
8. Isopropanol.

2.4 qRT-PCR

1. DNase (*see* **Note 5**).
2. Applied Biosystems™ High Capacity cDNA Reverse Transcription Kit.
3. THUNDERBIRD® SYBR qPCR Mix (TOYOBO LIFE SCIENCE).
4. 7300 Real Time PCR System, Applied Biosystems™ (*see* **Note 6**).
5. qRT-PCR primers: (*see* **Note 7**).

Housekeeping gene (internal standard):

Act8-F	TCAGCACTTTCCAGCAGATG
Act8-R	ATGCCTGGACCTGCTTCAT

UPR genes:

BiP1-F	TCAGTCCTGAGGAGATTAGTGCT
BiP1-R	TGCCTTTGAGCATCATTGAA
BiP3-F	CGAAACGTCTGATTGGAAGAA
BiP3-R	GGCTTCCCATCTTTGTTCAC

RIDD target genes:

MBL1-F	CTTTGATTCTCCCACCGACA
MBL1-R	CTTGGCTTCCATCACGAGAC
PR-4-F	GTGGGATGCTGATAAGCCGTA
PR-4-R	TGCAGCATTTGTTCTTGTGTTCT

3 Methods

3.1 Cultivation of Arabidopsis Plantlets in Sterilized Condition

1. Take arabidopsis seeds in a 1.5 mL microtube (*see* **Note 8**).
2. Add 1 mL of 70% EtOH and mix by vortex for 1 min (*see* **Note 9**).
3. Centrifuge briefly and discard 70% EtOH.
4. Add 1 mL of 1% hypochlorous acid (NaClO) solution.
5. Vortex for 5 min.
6. Centrifuge briefly and discard NaClO solution as much as possible.

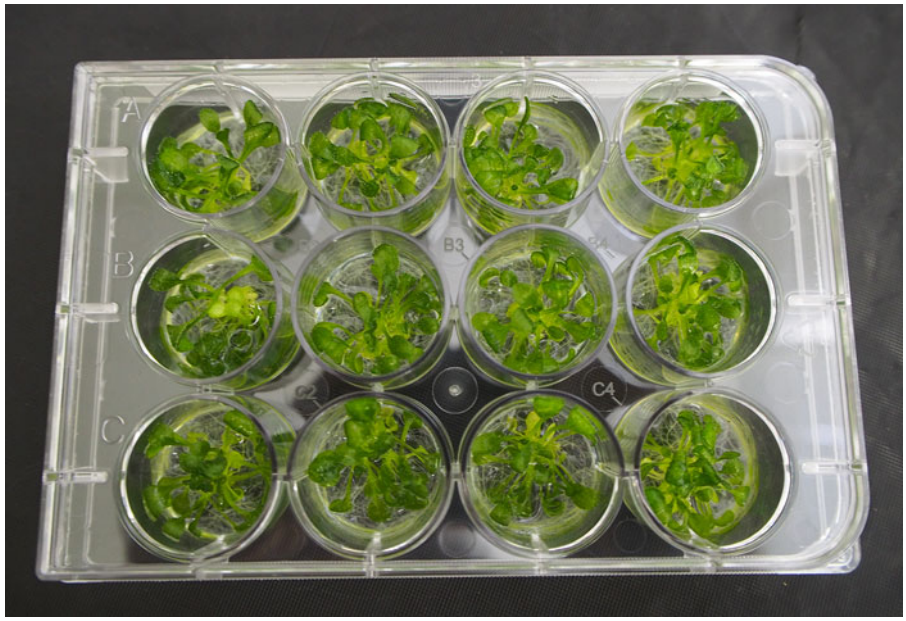

Fig. 1 Arabidopsis plantlets grown in a 24-well titer plate for 10 days under the condition described in Subheading 3.1

7. Add 1 mL sterilized water in a laminar flow hood and mix with vortex.
8. Centrifuge briefly and remove sterilized water in a laminar flow hood.
9. Repeat washing step by sterilized water four more times (*see* **Note 10**).
10. Discard sterilized water; add 1 mL of 0.1% sterilized agar and mix gently to disperse seeds.
11. Keep seeds in 0.1% agar at 4 °C for 2 days (*see* **Note 11**).
12. Prepare sterilized 24-well plates and add 1 mL of 1/2 MS medium with 1% sucrose (*see* **Note 12**).
13. Sow three to five seeds into each well using the micropipette (*see* **Notes 13** and **14**).
14. Incubate at 22 °C under 16-h light and 8-h dark condition with gentle shaking (90–100 rpm) until drug treatment and harvest (Fig. 1) (*see* **Note 15**).

3.2 Drug Treatment

1. Add stock solution of Tm, DTT, or AZC into culture medium directly. As mock treatment, add the same volume of the solvent (*see* **Note 16**).
2. Continue incubation for appropriate period (*see* **Note 17**).
3. Harvest plantlets into 2 mL microtube containing a bead and immediately freeze with liquid nitrogen.

3.3 RNA Extraction and DNase Treatment

1. Disrupt the plantlets with a bead mill (*see* **Note 18**).
2. Add 1 mL of RNA extraction buffer and vortex.
3. Leave at room temperature for 5 min.
4. Centrifuge at 20,000 × *g* for 10 min at 4 °C.
5. Transfer supernatant to a new tube, and add 200 μL of chloroform and vortex.
6. Leave at room temperature for 10 min.
7. Centrifuge at 20,000 × *g* for 10 min at 4 °C.
8. Transfer supernatant to a new tube, and add 250 μL of isopropanol and 250 μL of high salt solution.
9. Vortex and leave at room temperature for 10 min.
10. Centrifuge at 15,000 rpm for 15 min at 4 °C.
11. Discard supernatant and add 1 mL of 70% EtOH.
12. Vortex and centrifuge at 15,000 rpm for 5 min at 4 °C.
13. Discard 70% EtOH and dry up (*see* **Note 19**).
14. Dissolve RNA in 89 μL of ultrapure water.
15. Add 10 μL of 10× DNase buffer II (*see* **Note 20**).
16. Vortex and add 1 μL of DNase.
17. Incubate for 15 min at 37 °C.
18. Add 10 μL of Stop solution and incubate for10 min at 70 °C (*see* **Note 20**).
19. Add 11 μL of 3 M Na acetate and mix.
20. Add 300 μL of 99.5% EtOH and mix.
21. Centrifuge at 20,000 × *g* for 10 min at 4 °C.
22. Discard supernatant and add 1 mL of 70% EtOH.
23. Centrifuge at 15,000 rpm for 5 min at 4 °C.
24. Discard supernatant, air-dry EtOH, and dissolve in 50 μL ultrapure water.

3.4 cDNA Synthesis

1. Measure RNA concentration by an UV spectrophotometer.
2. Prepare 5 μL of RNA solution at a concentration of 20 ng/μL in PCR tubes.
3. Incubate for 5 min at 65 °C.
4. Using RNA solution, prepare reaction solution for reverse transcription according to the manufacturer's protocol of Applied Biosystems™ High Capacity cDNA Reverse Transcription Kit (*see* **Note 21**).
5. Perform reverse transcribe reaction as follows. Incubate for 10 min at 25 °C, 120 min at 37 °C, and 5 min at 85 °C.
6. Dilute cDNA solution with 20 μL of ultrapure water.

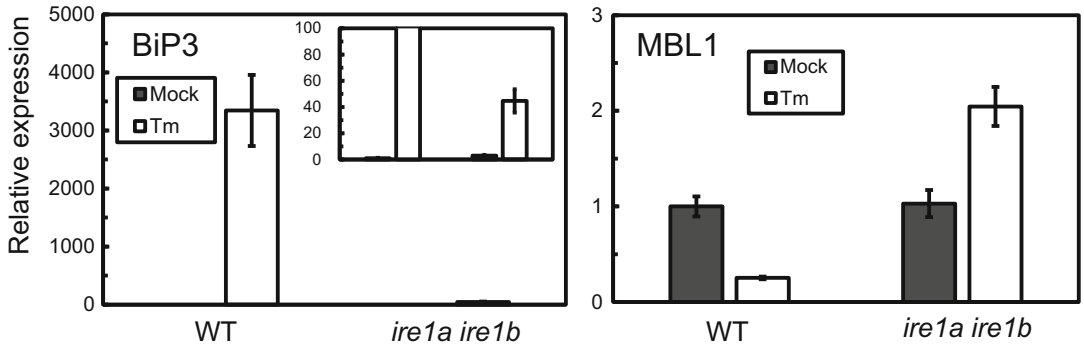

Fig. 2 Quantification of transcripts by qPCR after mock or Tm treatment. RNA was extracted from 10-day-old plantlets of wildtype (WT) and *ire1a ire1b* mutant treated with mock (0.1% DMSO) or 5 μg/mL Tm for 5 h. Quantitative RT-PCR for BiP3 and MBL1 was performed as described in Subheading 3 (reproduced from Ref. 13 with permission of Bioscience Biotechnology and Biochemistry)

3.5 Quantitative PCR

1. Prepare 20 μL of reaction solution as follows (*see* **Note 22**).

THUNDERBIRD® SYBR qPCR Mix	10.4 μL
PrimerA (20 μM)	0.3 μL (0.3 μM)
PrimerB (20 μM)	0.3 μL (0.3 μM)
cDNA	2–4 μL
Ultrapure water	7–5 μL
Total	20.0 μL

2. Conduct real-time PCR as follows. 95 °C for 2 min and (95 °C 15 s, 60 °C 50 s) × 40 cycle. Dissociation stage (95 °C 15 s, 60 °C 30 s, 95 °C 15 s) (*see* **Note 23**).
3. Examples of qRT-PCR to detect *BiP3* mRNA, which is increased by Tm treatment, and *MBL1* mRNA, which is decreased by Tm treatment, were shown in Fig. 2. Reproduced from [13] with permission from *Bioscience Biotechnology and Biochemistry*. In this case, RNA was prepared from cultured cells.

4 Notes

1. In most cases, medium up to 100 mL is more than enough. Then, we keep medium as 20× solution at −20 °C.
2. If tunicamycin was purchased as 10 mg of vial, DMSO can be directly added to the vial. It is recommended to store the stock solution as aliquots in the −20 °C freezer to avoid repeated freezing and thawing. This is also applicable to storage of DTT and AZC stock solutions.
3. Aluminum oxide beads can be substituted to zirconia or other equivalent beads.

4. The bead mill (QIAGEN) consists of a mixer and two tube holders. 24 of 2 mL microtubes can be set in each holder. Similar equipment can be substituted with the bead mill and in this case, follow manufacture's manual.
5. Although we purchase DNase from NIPPON GENE, any RNase-free DNase can be used instead.
6. Any other real-time PCR machine can be applicable.
7. PCR primers are dissolved in sterilized ultrapure water.
8. We do not recommend too much seeds in the tube from two reasons. First, too much seeds in a tube would result in inefficient sterilization. Second, as mentioned below, only 3–5 seeds are sown in each well and then small amount is sufficient for gene expression analysis.
9. Tapping the tube can be substituted for vortex.
10. It is important to remove NaClO thoroughly, otherwise seeds will not germinate.
11. This step serves as vernalization treatment to uniform germination.
12. 12-well plates are often used as well as 24-well plates. In this case, 2 mL of medium is added in each well.
13. Head of tips of micropipette are cut with sterilized razor blade or scissors to make seeds enter to the tips.
14. For qRT-PCR, we conduct at least three biological repeats. Since plantlets in each well do not necessarily grow equally, we usually prepare six wells for one treatment.
15. Usually we grow plantlets for 10 days after sowing. At this stage, the growth almost saturates as shown in Fig. 1.
16. Since plantlets absorb some of culture medium during cultivation, it is difficult to estimate the exact volume of the medium. On the assumption that the same amount of culture medium is present in each well, we add the same volume of drugs. Alternatively, culture medium can be discarded and 1/2 MS medium with 1% sucrose containing each drug can be added. Although we use different concentrations of drugs depending on experiments, we often use 5 μg/mL of tunicamycin, 2 mM of DTT, and 5 mM of AZC.
17. Treatment period also depends on experiments. We expose plantlets to drugs for 1–5 h to detect gene expression. In general, longer treatment is necessary when changes at protein level need to be observed. Treatment for long time such as more than 2 days is supposed to be meaningless since cell death started after 12 h when plantlets treated with 5 μg/mL of tunicamycin.
18. Tube holders of the bead mill are precooled in −80 °C freezer to prevent thawing the sample. Attach tubes in the holder and

begin shaking immediately at 30 times/s for 1 min. Subsequently, tubes are cooled by liquid nitrogen to avoid thawing and shake again for 1 min. A compatible bead mill can be used according to manufacturer's protocol.

19. Alternatively EtOH residue can be dried up by DNA110 SpeedVac Concentrator (Savant) or equivalent equipment.
20. 10× DNase buffer II and Stop solution are accompanied with DNase (NIPPON GENE).
21. If other kit was used, follow the manufacturer's protocol.
22. When other kits are used, follow the recommended protocol by the kit's manufacturer.
23. Calculation depends on real-time PCR equipment and reaction reagent. We performed at least three biological replicates to obtain results.

Acknowledgements

This work was supported by the Japan Society for the Promotion of Science (JSPS) [KAKENHI No. 22020031] to N.K.

References

1. Walter P, Ron D (2012) The unfolded protein response. Science 334:1081–1086
2. Iwata Y, Koizumi N (2012) Plant transducers of the endoplasmic reticulum unfolded protein response. Trends Plant Sci 17:720–727
3. Mishiba K, Nagashima Y, Suzuki E, Hayashi N, Ogata Y, Shimada Y, Koizumi N (2013) Defects in IRE1 enhance cell death and fail to degrade mRNAs encoding secretory pathway proteins in the Arabidopsis unfolded protein response. Proc Natl Acad Sci U S A 110:5713–5718
4. Hollien J, Lin JH, Li H, Stevens N, Walter P, Weissman JS (2009) Regulated Ire1-dependent decay of messenger RNAs in mammalian cells. J Cell Biol 186:323–331
5. Maurel M, Chevet E, Tavernier J, Gerlo S (2014) Getting RIDD of RNA: IRE1 in cell fate regulation. Trends Biochem Sci 39:245–254
6. Kuo S-C, Lampen JO (1974) Tunicamycin – an inhibitor of yeast glycoprotein synthesis. Biochem Biophys Res Commun 58:287–295
7. Braakman I, Helenius J (1992) Manipulating disulfide bond formation and protein folding in the endoplasmic reticulum. EMBO J 11:1717–1722
8. Beckmann RP, Mizzen LEEA, Welch WJ (1990) Interaction of Hsp 70 with newly synthesized proteins: implications for protein folding and assembly. Science 248:850–854
9. Koizumi N, Martinez IM, Kimata Y, Kohno K, Sano H, Chrispeel MJ (2001) Molecular characterization of two Arabidopsis Ire1 transmembrane protein kinases 1. Plant Physiol 127:949–962
10. Iwata Y, Koizumi N (2005) An Arabidopsis transcription factor, AtbZIP60, regulates the endoplasmic reticulum stress response in a manner unique to plants. Proc Natl Acad Sci U S A 102:5280–5285
11. Iwata Y, Fedoroff NV, Koizumi N (2008) Arabidopsis bZIP60 is a proteolysis-activated transcription factor involved in the endoplasmic reticulum stress response. Plant Cell 20:3107–3121
12. Iwata Y, Sakiyama M, Lee M-H, Koizumi N (2010) Transcriptomic response of Arabidopsis thaliana to tunicamycin-induced endoplasmic reticulum stress. Plant Biotechnol 27:161–171
13. Iwata Y, Hahashi N, Tabara K, Mishiba K, Koizumi N (2016) Tunicamycin-induced inhibition of protein secretion into culture medium of Arabidopsis T87 suspension cells through mRNA degradation on the endoplasmic reticulum. Biosci Biotechnol Biochem 76:1168–1171

Chapter 18

Unfolded Protein Response in Arabidopsis

Cristina Ruberti and Federica Brandizzi

Abstract

The unfolded protein response (UPR) is a highly regulated signaling pathway that is largely conserved across eukaryotes. It is essential for cell homeostasis under environmental and physiological conditions that perturb the protein folding in the endoplasmic reticulum (ER). Arabidopsis is one of the outstanding multicellular model systems in which to investigate the UPR. Here, we described a protocol to induce the UPR in plants, specifically arabidopsis, and to estimate their ability to cope with ER stress through the quantification of physiological parameters.

Key words Unfolded protein response, Endoplasmic reticulum stress, Temporary ER stress, Prolonged ER stress, Tunicamycin, Arabidopsis

1 Introduction

Adverse environmental changes and physiological conditions of growth can interfere with crucial biosynthetic processes and disturb proper protein folding in the endoplasmic reticulum (ER), leading to a potentially lethal condition generally termed "ER stress" [1, 2]. To overcome ER stress, the unfolded protein response (UPR), a highly regulated signaling pathway largely conserved across eukaryotes, is actuated [3]. The UPR activates a network of pathways, which generally promote cell adaptation and restore ER homeostasis; however, under unmitigated stress conditions they also can ignite programmed cell death (PCD) both in animals [1, 4] and plants [5, 6]. Despite the relevance of the UPR in cell growth and stress adaptation and the abundant information on the function of the canonical stress sensors and transducers in the UPR [5, 7, 8], we lack a complete understanding of the molecular players involved in the temporally distinct UPR-related events (i.e., UPR initiation, recovery from temporary ER stress, survival from mild and prolonged ER stress, and ignition of PCD under unmitigated ER stress), especially in plants [9].

Chris Hawes and Verena Kriechbaumer (eds.), *The Plant Endoplasmic Reticulum: Methods and Protocols*,
Methods in Molecular Biology, vol. 1691, DOI 10.1007/978-1-4939-7389-7_18,

Depending on the duration of ER stress, three main experimental approaches have been implemented to investigate the contribution of the UPR players in ER stress resolution. The downstream transcriptional initiation of the adaptive UPR signaling response can be monitored at a molecular level by assaying the expression levels of the UPR marker genes in time-course treatment with ER stress-inducing agents (for detailed methods, *see* [3, 10]). The plant ability to recover after temporary ER stress or to cope with prolonged and mild ER stress is evaluated at phenotypic level on seedlings transferred or germinated and grown on ER stress inducer-containing media [5, 6]. Finally, ER stress-induced cell death can be evoked by growing seedlings under prolonged and severe ER stress conditions and quantified by standard methods to test for PCD (e.g., ion leakage and TUNEL staining) [6, 11].

Common chemical agents used to experimentally induce ER stress and activate the UPR in plants are tunicamycin (Tm) or dithiothreitol (DTT) [5, 12, 13]. Tm inhibits the N-acetylglucosamine phosphotransferases; this prevents N-linked glycosylation of nascent polypeptides in the ER lumen. DTT is a potent reducing agent that prevents disulfide bond formation during folding of polypeptides in the ER (*see* **Note 1**). Here, we describe phenotypic analyses most commonly adopted to evaluate ER stress sensitivity of arabidopsis seedlings after a short ER stress-inducing treatment or during prolonged ER stress.

2 Materials

1. Basic equipment for plant sterile tissue culture.
2. Plant growth chamber conditions: continuous white light at 21 °C, 100 μEinstein/m^2 s, 65% humidity.
3. Plant growth medium: half-strength (1/2) Linsmaier and Skoog (LS) medium, 1% sucrose, pH 5.7.
4. Tunicamycin (Tm) from *Streptomyces* sp. (*see* **Note 2**): prepare 10 mg/mL of Tm stock solution by dissolving 0.005 g Tm in 0.5 mL of DMSO yielding a clear solution (*see* **Notes 3** and **4**).
5. Dimethyl sulfoxide (DMSO).
6. 70% ethanol.
7. 5% commercial bleach freshly prepared.
8. Acetone: 80% solution in water.
9. Petri dishes, square with grids, 100 mm × 100 mm, sterile, polystyrene.
10. Micropore gas-permeable surgical tape.
11. Sterilized toothpicks.
12. Razor blades.

13. Analytical balance.
14. Microplate, 96 well, flat bottom, clear.
15. Microplate reader equipped with 663 and 645 nm wavelengths.

3 Methods

3.1 Recovery After Temporary ER Stress Treatment

Carry out all procedures at room temperature and if aseptic conditions are required, work in a laminar flow hood.

1. Surface-sterilize the arabidopsis seeds (*see* **Note 5**): in a microcentrifuge tube, soak the seeds in 1 mL 70% ethanol for 1 min, suspend them by turning the tube or vortex, pour out the liquid, rinse two times in distilled sterile water, suspend the seeds in 1 mL 5% commercial bleach for 1 min, then rinse three times in sterile distilled water (*see* **Note 6**). Store the seeds at 4 °C for 2 days to synchronize them.
2. Autoclave for 25 min the plant growth medium with 12 g/L agar (*see* **Note 7**) and pour 40 mL into each square Petri dish.
3. Use a sterile toothpick to sow the arabidopsis seeds on the solid plant growth medium placing each seed at an equally spaced distance (Fig. 1a).

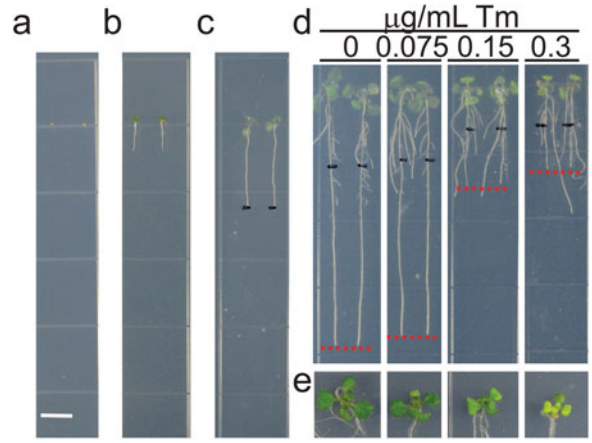

Fig. 1 Arabidopsis Col-0 growth phenotype after recovery from short-term Tm treatment. (**a**) Arabidopsis seeds sown at an equally spaced distance on ½ LS solid medium for vertical growth. Scale bar: 0.65 mm. (**b**) 5-day-old seedlings were transferred to ½ LS solid medium plates containing Tm or DMSO for short-term ER stress treatment. (**c**) 8-day-old seedlings were transferred from Tm-plates to ½ LS solid plates and the root tips were marked on the back of the plate using a black extra-fine point marker. (**d**) Root growth inhibition of Tm-treated seedlings compared to untreated seedlings after 3 days of recovery from short-term Tm treatment. *Red lines* show the primary root tip. (**e**) Close-up view of the shoot of seedlings shown in (**d**)

4. Seal the plates with one layer of micropore gas-permeable surgical tape to allow gaseous exchange.
5. Germinate and grow the seeds in vertical position in a plant growth chamber for 5 days.
6. Autoclave for 25 min the plant growth medium and store it at room temperature.
7. Prepare Tm stock solution (*see* **Notes 3** and **4**).
8. Freshly prepare 0.075, 0.15, and 0.30 mg/mL Tm stock solutions by 133, 66, and 33× dilution, respectively, of the 10 mg/mL Tm stock solution using 1/2 LS liquid medium.
9. Autoclave for 25 min the plant growth medium with 12 g/L agar (*see* **Note 5**). Cool down the medium until 50 °C (*see* **Note 8**) and keep it homogeneously mixed with a magnetic stir bar.
10. Add 0.075, 0.15, and 0.30 mg/mL Tm stock solutions, respectively, to the cooled down ½ LS medium by 1000 dilution to make plant growth medium containing 0.075, 0.15, and 0.30 μg/mL Tm (*see* **Notes 9** and **10**).
11. As mock control, the same preparation procedure is carried out replacing the Tm in the ½ LS medium with 0.0005% DMSO.
12. Transfer the 5-day-old seedlings using a sterile toothpick to plant growth medium plates containing DMSO, 0.075, 0.15, or 0.30 μg/mL Tm (Fig. 1b). Seal the plates with one layer of micropore gas-permeable surgical tapes to permit gaseous exchange and place them on vertical position into the plant growth chamber.
13. After 3 days, use a sterile toothpick to transfer the seedlings to plant growth medium plates without Tm (or DMSO). Mark the root tip on the back of the plate using an extra-fine point permanent marker and place the plates on vertical position into the plant growth chamber (Fig. 1c).
14. After 3 days, observe the growth phenotype (Fig. 1d and e) and quantify the plant growth parameters as described below.
15. If using Col-0 ecotype wild-type arabidopsis, the plants show growth defects already at 0.15 μg/mL Tm (Fig. 1d and e).

3.2 Prolonged ER Stress Treatment

Carry out all procedures at room temperature and if aseptic conditions are required, work in a laminar flow hood.

1. Autoclave for 25 min the plant growth medium and store it at room temperature.
2. Autoclave for 25 min the plant growth medium with 12 g/L agar (*see* **Note 5**).
3. Freshly prepare 0.04, 0.06, and 0.08 mg/mL Tm stock solutions by 250, 166, and 125× dilution of 10 mg/mL Tm stock solution, respectively, using 1/2 LS liquid medium.

4. Add 0.04, 0.06, and 0.08 mg/mL Tm stock solutions, respectively, to the cooled down ½ LS medium by 1000 dilution to make plant growth medium containing 40, 60, and 80 ng/mL Tm (*see* **Notes 9** and **11**). As mock control, the same preparation procedure is carried out replacing the Tm in the ½ LS medium with 0.0005% DMSO.
5. Surface-sterilize the arabidopsis seeds (*see* **Note 3**) and store them at 4 °C for 2 days.
6. Use a sterile toothpick to sow the surface-sterilized seeds on the ½ LS medium containing DMSO, 40, 60, and 80 ng/mL Tm. Place each seed at an equally spaced distance (Fig. 1a)
7. Seal the plates with one layer of micropore gas-permeable surgical tape to allow gaseous exchange.
8. Germinate and grow the seeds in vertical position in a plant growth chamber.
9. After 5 days, mark the root tip on the back of the plate using an extra-fine point marker (Fig. 2a) and place the plates back on vertical position into the plant growth chamber.
10. Observe the growth phenotype 7–14 days after germination (Fig. 2b and c), but check the plant growth each day during the assay to precisely monitor the ER stress sensitivity of the

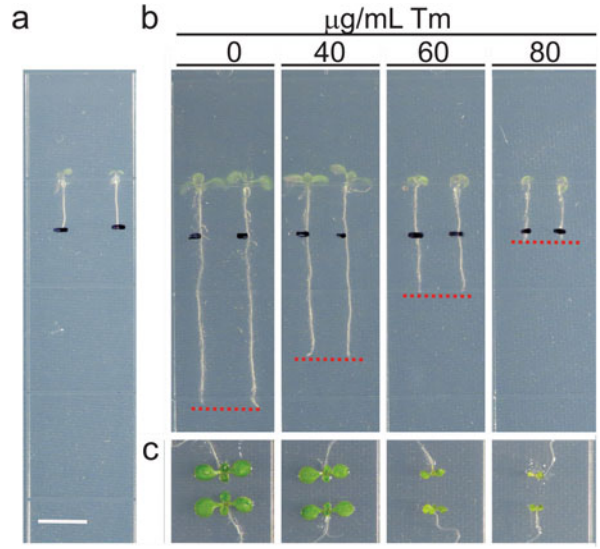

Fig. 2 Arabidopsis Col-0 growth phenotype after prolonged Tm treatment. (**a**) Root tips of 5-day-old seedlings were marked on the back of the plate using a black extra-fine point marker. Scale bar: 0.65 mm. (**b**) Root growth inhibition of Tm-treated seedlings compared to untreated seedlings grown for 10 days vertically. *Red lines* show the primary root tip. (**c**) Close-up view of the shoot of seedlings shown in (**b**)

seedlings. Quantify the plant growth parameters as described below.

11. If using Col-0 ecotype wild-type arabidopsis, the plants show growth defects starting from 40 ng/mL Tm (Fig. 2b and c).

3.3 Plant Growth Parameters

1. The effect of the prolonged ER stress on arabidopsis seeds can be quantified through the quantification of emergence of the true leaves (Fig. 2c). Count the number of seedlings having true leaves on Tm-containing plates and normalize this value with respect to the total number of all sown seeds. Similarly, count the number of seedlings having true leaves on DMSO-containing plates and normalize this value on the total number of all sown seeds [12].
2. Fresh shoot weight is an easy readout of plant sensitivity of both short-term ER stress and prolonged ER stress. Using a razor blade, cut the plant shoots at a consistent cut-position on the hypocotyl. Gently dry the shoots on a paper towel and measure the weight with an analytical balance. To quantify the relative growth values, the shoot weight of the seedlings grown on Tm is divided by the shoot weight of the seedlings grown on DMSO-plates. For each measurement, use a pool of 6–10 shoots for each of the at least six technical replicates for each of the three biological replicates.
3. Chlorophyll (Chl) content of the leaves can be used as an indicator of overall plant health after short-term or prolonged Tm treatment. After measuring fresh shoot weight, place the pool of leaves into a microcentrifuge tube and extract chlorophyll using 1 mL cold 80% acetone at 4 °C for 24 h (*see* **Note 12**) in the dark (*see* **Note 13**). Quickly transfer 0.3 mL of the supernatant to a flat-bottom 96-well microplate and use 0.3 mL 80% acetone blank as reference. Measure the absorbance (A) of the chlorophyll content using a microplate reader at 663 and 645 nm wavelengths. The chlorophyll concentration is calculated as follows: Chl (mg/g) = $[8.02 \times A_{663} + 20.20 \times A_{645}] \times \underline{V}/1000 \times W$, where V = volume of the extract (mL) and W = weight of fresh leaves (g) [13, 14].
4. The primary root elongation declines as the concentration of the ER stress inducer increases into the growth media in a dose-dependent manner (Figs. 1d and 2b) [15]. For this reason, ER stress sensitivity can be quantified measuring the primary root length of seedlings grown on Tm-plates. Take pictures of the plants treated as described in Subheading 3.1, **steps 1–14** or 3.2, **steps 1–10** (*see* **Note 14**). Measure the root length from the root tip to the mark made in the Subheading 3.1, **step 13** or 3.2, **step 9**. To quantify the relative root elongation value, the root length of the seedlings grown on Tm is divided by the root length of the seedlings grown on DMSO-plates.

4 Notes

1. Even if DDT is commonly used to cause protein misfolding in the ER, it is not a specific ER stress inducer, since it blocks disulfide bond formation both in the ER and in the cytosol, and causes oxidative stress and the expression of defense genes [12, 15].
2. The hazard category for Tm is acute toxicity, oral (category 2) H300 (fatal if swallowed). Tm is light sensitive.
3. To avoid formation of aerosols, directly inject the DMSO solvent using a 1-mL syringe with a needle through the lid of the tube containing the solution and mix.
4. To avoid freezing and thawing, aliquot the 10 mg/mL stock solution into relatively small amounts (0.01 mL aliquots) and store them at −20 °C freezer in the dark.
5. ER stress sensitivity is highly affected by the seeds quality. Use seeds with high germination quality and freshly collected from healthy plants.
6. Do not leave seeds in ethanol or bleach for too long because the treatment may be toxic to the seeds.
7. Mix homogeneously the solution with a magnetic stir bar before and after to autoclave, to avoid settling of unmelted agar at the bottom of the bottle.
8. Tm is sensitive to high temperature.
9. Prepare the Tm-containing medium plates right before using them.
10. The optimal range of concentration of Tm has to be experimentally determined. As initial screen, use 0.075 and 0.15 μg/mL Tm and then decrease or increase the Tm concentration depending on the degree of Tm sensitivity of the analyzed arabidopsis ecotype.
11. The optimal range of concentration of Tm has to be experimentally determined. As initial screen, use 20 and 40 ng/mL Tm and then decrease or increase the Tm concentration depending on the degree of Tm sensitivity of the analyzed arabidopsis ecotype and on the purpose of your assay. To evaluate Tm sensitivity under mild ER stress conditions, use low Tm concentration that can be increased to get unmitigated ER stress conditions and consequent cell death.
12. Complete chlorophyll extraction is fulfilled when the shoots are completely white. If the leaves are still partially green, keep the tissues at 4 °C in the darkness for longer time.

13. During chlorophyll extraction and analyses, keep the samples in the dark, because chlorophylls are light-sensitive pigments.
14. To better distinguish the roots, take pictures of the back of the plates.

Acknowledgements

This study was primarily supported by National Institutes of Health (GM101038) with contributing support from the Chemical Sciences, Geosciences and Biosciences Division, Office of Basic Energy Sciences, Office of Science, U.S. Department of Energy (award number DE-FG02-91ER20021), and AgBioResearch.

References

1. Chen Y, Brandizzi F (2013) IRE1: ER stress sensor and cell fate executor. Trends Cell Biol 23:547–555
2. Liu J-X, Howell SH (2016) Managing the protein folding demands in the endoplasmic reticulum of plants. New Phytol. doi:10.1111/nph.13915
3. Ruberti C, Brandizzi F (2014) Conserved and plant-unique strategies for overcoming endoplasmic reticulum stress. Front Plant Sci 5:69
4. Hetz C (2012) The unfolded protein response: controlling cell fate decisions under ER stress and beyond. Nat Rev Mol Cell Biol 13:89–102
5. Chen Y, Brandizzi F (2012) AtIRE1A/AtIRE1B and AGB1 independently control two essential unfolded protein response pathways in Arabidopsis. Plant J Cell Mol Biol 69:266–277
6. Mishiba K et al (2013) Defects in IRE1 enhance cell death and fail to degrade mRNAs encoding secretory pathway proteins in the Arabidopsis unfolded protein response. Proc Natl Acad Sci U S A 110:5713–5718
7. Liu J-X, Srivastava R, Che P, Howell SH (2007) An endoplasmic reticulum stress response in Arabidopsis is mediated by proteolytic processing and nuclear relocation of a membrane-associated transcription factor, bZIP28. Plant Cell 19:4111–4119
8. Iwata Y, Fedoroff NV, Koizumi N (2008) Arabidopsis bZIP60 is a proteolysis-activated transcription factor involved in the endoplasmic reticulum stress response. Plant Cell 20:3107–3121
9. Ruberti C, Kim S-J, Stefano G, Brandizzi F (2015) Unfolded protein response in plants: one master, many questions. Curr Opin Plant Biol 27:59–66
10. Chen Y, Brandizzi F (2013) Analysis of unfolded protein response in Arabidopsis. Methods Mol Biol 1043:73–80
11. Yang Z-T et al (2014) The membrane-associated transcription factor NAC089 controls ER-stress-induced programmed cell death in plants. PLoS Genet 10(3):e1004243
12. Sun L et al (2013) The lumen-facing domain is important for the biological function and organelle-to-organelle movement of bZIP28 during ER stress in Arabidopsis. Mol Plant 6:1605–1615
13. Ritchie RJ (2006) Consistent sets of spectrophotometric chlorophyll equations for acetone, methanol and ethanol solvents. Photosynth Res 89:27–41
14. Ni Z, Kim E-D, Chen ZJ (2009) Chlorophyll and starch assays. Available at: http://dx.doi.org/10.1038/nprot.2009.12
15. Deng Y, Srivastava R, Howell SH (2013) Protein kinase and ribonuclease domains of IRE1 confer stress tolerance, vegetative growth, and reproductive development in Arabidopsis. Proc Natl Acad Sci U S A 110:19633–19638

Chapter 19

Fluorescence Imaging of Autophagy-Mediated ER-to-Vacuole Trafficking in Plants

Hadas Peled-Zehavi and Gad Galili

Abstract

Macroautophagy (hereafter referred to as autophagy) is a conserved mechanism in eukaryotic cells that delivers unneeded cellular components for degradation in the lytic organelle. In plants, as in other eukaryotes, autophagy begins in the formation of cup-shaped double membranes that engulf cytosolic material. The double membrane closes to form autophagosomes that are then transported to the vacuole for degradation. Autophagy can function as a bulk nonselective process or as a selective process targeting specific proteins, protein aggregates, organelles, or other cellular components for degradation. The endoplasmic reticulum (ER) is linked to autophagy-related processes in multiple ways. The ER was suggested as a possible site for the nucleation of autophagosomes, and as a source for autophagosomal membranes. Furthermore, autophagy has an important role in ER homeostasis, and the ER is a target for a selective type of autophagy, ER-phagy, in response to ER stress. However, the detailed molecular mechanisms, especially in plants, are only now starting to be revealed.

In this chapter, we describe the use of confocal imaging to follow the delivery of fluorescently tagged ER-associated proteins to the vacuole. We also describe the utilization of fluorescent protein fusions to look at the co-localization of a protein of interest with the autophagosome marker protein ATG8, a core autophagy machinery protein that is essential for selective autophagy processes.

Key words Autophagy, ATG8, Concanamycin A, Confocal microscopy, Endoplasmic reticulum, Fluorescence, Vacuole

1 Introduction

Autophagy is a conserved eukaryotic endomembrane trafficking process that is essential for development, cellular homeostasis, and stress tolerance [1–3]. Autophagy involves the sequestration of cargo in double-membrane bounded autophagosomes that are further transported to the lytic organelle (the vacuole in plants) for degradation. Upon arrival of the autophagosomes to the vacuoles, their outer membranes fuse with the tonoplast, creating single-membrane vesicles inside the vacuole, termed autophagic bodies. The autophagic bodies and their contents are then degraded, providing recycled materials to build new

Chris Hawes and Verena Kriechbaumer (eds.), *The Plant Endoplasmic Reticulum: Methods and Protocols*, Methods in Molecular Biology, vol. 1691, DOI 10.1007/978-1-4939-7389-7_19,

macromolecules [1, 2, 4]. In plants, autophagy is one of the central cellular machineries required to survive biotic and abiotic stresses such as limiting light levels, nutrient deficiency, drought, and pathogen attack [2, 5, 6]. Autophagy was classically defined as a bulk nonselective process. However, in recent years it became evident that autophagy-related routes are more varied and also involve the selective transport of specific proteins, protein aggregates, organelles, or organelles components to the vacuole, thus regulating the steady-state levels of these specific components in response to specific cues [4, 6].

The core mechanism of autophagy is mediated by AuTophaGy-related or ATG

Genes [1, 2, 4, 7]. Though these genes were originally discovered in yeast, many of them are conserved in evolution, and homologs have later been found in many organisms including mammals and plants [8, 9]. A central protein of both bulk and selective autophagy is ATG8, which in plants exists as a gene family. ATG8 is synthesized as a proprotein and goes through several processing events that result in its covalent attachment to phosphatidylethanolamine (PE) at the autophagosomal membrane [10–13]. ATG8-PE located on the outer membrane of the autophagosome is cleaved off during autophagosome deposition by ATG4. ATG8-PE located on the inner membrane of the autophagosome enters the vacuole with the autophagic body [14, 15]. As ATG8 is found on the autophagosome from its formation to its lytic destruction in the vacuole, a green fluorescent protein (GFP) fusion of ATG8 is the most commonly used marker for autophagosomes [1, 2]. ATG8 is involved in autophagosome formation and membrane extension and is also essential for selective autophagy. It has been shown to mediate target recognition by specific binding to protein targets or adaptor proteins [1, 3, 4, 6]. Therefore, the demonstration of a specific interaction between ATG8 and a protein of interest strongly supports the involvement of this protein in selective autophagy processes.

The involvement of the ER in autophagic processes is multifaceted. The ER was suggested as a possible site for the nucleation of the cup-shaped phagophores that elongate and fuse to form autophagosomes, and as a source for autophagosomal membranes [7, 16–18]. The ER is also the target of a selective type of autophagy, termed reticulophagy or ER-phagy. ER-phagy was shown to be involved in ER degradation in response to induced ER stress in animals and yeast [19–22]. Similarly, treating *Arabidopsis thaliana* plants with ER stress agents was shown to trigger autophagy and to result in the appearance of autophagic bodies containing ribosome-decorated ER membranes within the vacuole lumen [23]. Interestingly, selective autophagy was also reported to act as a biogenesis-mediating process in special trafficking routes delivering vacuolar resident proteins to function in this organelle. The best known

example being the cytosol to vacuole targeting (Cvt) pathway of yeast [24]. Recently, it was suggested that analogous types of autophagy-dependent trafficking routes may exist also in plants in the form of a direct ER-to-vacuole, Golgi-independent, trafficking route [25].

The use of fluorescently tagged proteins and fluorescence microscopy to study the involvement of specific proteins in selective autophagy processes has proven to be a powerful research tool in the autophagy field [26]. In this chapter, we describe procedures utilizing confocal imaging to look at the in vivo co-localization of stably expressed fluorescently tagged ER-associated proteins with the autophagosome marker ATG8, and to follow their delivery to the vacuole. These procedures are combined with the use of Concanamycin A (conA). ConA inhibits the vacuolar H^+-ATPase, resulting in an increase in vacuolar pH and inhibition of vacuolar enzymes activity [1]. Under these conditions, autophagic bodies accumulate in the vacuole and there is an increase in the amount of autophagosomes in the cytoplasm [27], facilitating the visualization of autophagy processes.

2 Materials

2.1 Plant Growth Materials

1. Half-strength Murashige and Skoog (MS) medium: dissolve 2.15 g of MS basal salt mixture in 0.8 L of distilled water. Check and adjust pH to 5.6–5.8 using 1 M KOH and add distilled water to a final volume of 1 L. Add 8 g plant agar. Autoclave for 20 min at 121 °C and cool down to 45–50 °C before pouring into petri dishes under sterile conditions (laminar flow hood).
2. *Arabidopsis thaliana* seed surface sterilization solutions: 75% (v/v) ethanol, 3% sodium hypochlorite (v/v), sterile deionized or reverse osmosis purified water.
3. Sterile petri dishes.

2.2 Seedlings Treatment

1. Concanamycin A 100x: 100 μM conA (Santa Cruz) in DMSO. Aliquot and store at −20 °C protected from light.
2. Liquid half-strength MS medium: prepare as in Subheading 2.1, **item 1**, but do not add the plant agar.
3. Aluminum foil.

2.3 Confocal Imaging and Analysis

1. Glass microscope coverslips. We use 0.13–0.17 mm thick 24 × 60 mm and 18 mm coverslips.
2. Confocal laser scanning microscope. The images presented here were acquired using an inverted Nikon A1 microscope and the NIS-Elements AR imaging software.

3. Software: Imaris image processing and analysis software (Bitplane inc.) or ImageJ freeware with the coloc_2 plug-in (imagej.net/imagej), MS Excel.

3 Methods

3.1 General Considerations

Several vector systems for the generation of fluorescent protein fusion constructs in plant binary plasmids exist, utilizing both restriction enzyme based and recombination based cloning techniques. Examples of vectors available through the Arabidopsis Biological Resource Center (ABRC) include the pSAT/pZP and pMDC vector systems [28, 29]. In choosing the appropriate system, it is important to take into consideration the appropriate fusion orientation (*see* **Note 1**), the promoter that will be used to drive the expression (*see* **Note 2**) and the desirable fluorescent protein used for the fusion (*see* **Note 3**). Following *Arabidopsis thaliana* transformation with *Agrobacterium*, several lines with differing levels of fluorescence expression should be propagated for further characterization (*see* **Note 4**).

3.2 Plant Material and Growth Conditions

1. Sterilize arabidopsis seeds by washing them twice with 75% ethanol solution, followed by soaking for 5 min in 3% bleach solution. Wash 3–4 times in sterile water.
2. Plate the sterilized seeds on solid half-strength MS medium. Seal with micropore paper tape or parafilm and place the plates at 4 °C for 2 days for stratification.
3. Grow under long day conditions (16 h light) at 22 °C.

3.3 Treating Plants with conA

1. Transfer 6-day-old seedlings of each of the examined genotypes (5–10 seedlings will suffice) to a 24-well plate with 0.5 mL liquid half-strength MS medium complemented with 1 μM conA (*see* **Note 5**). For control treatment, transfer seedlings into liquid medium with the same volume of DMSO (used to dissolve the conA). The seedlings should be removed from the growing plate carefully using tweezers to prevent tearing the roots (*see* **Note 6**).
2. Seal the plates with parafilm and cover in double layered aluminum foil. Incubate with gentle shaking (80 rpm) for 20 h before imaging (*see* **Note 7**).

3.4 Co-Localization with Fluorescently Labeled ATG8 Marker

To look at co-localization with autophagosomes, *Agrobacterium tumefaciens* mediated transformation or crossing is used to generate transgenic lines co-expressing fluorescently tagged ATG8 and protein of interest (*see* **Note 8**).

3.5 Confocal Microscopy Imaging

1. Place 1–3 seedlings on a microscope glass coverslip, add a drop of distilled water, and cover with a second coverslip (we routinely use 0.13–0.17 mm thick 24 × 60 mm rectangular coverslip with a round 18 mm coverslip on top). Place on the stage of the confocal microscope for imaging.
2. Select the 20× objective, adjust the focus, and find the hypocotyl under bright field illumination (*see* **Note 9**).
3. Choose a suitable excitation laser and emission filter for image acquisition. For GFP or YFP fluorescence, use 488-nm laser excitation and a 525-nm emission filter. For mRFP or mCherry fluorescence, use 561-nm laser excitation and a 595-nm emission filter. For chlorophyll autofluorescence, use a 640-nm laser and a 700-nm emission filter (*see* **Note 10**).
4. Image the sample. Focus on different layers of the tissue to get an estimation of the fluorescence signal and a general view of the level of autophagy (*see* **Note 11**).
5. Switch the objective lens to 60×/1.2NA water immersion lens (or similar). Water immersion lens is preferable to oil immersion lens since the refractive index of water most closely matches that of live cells. Determine image acquisition parameters such as laser intensities, gain, and scan speed, and keep them constant for all images taken (*see* **Note 12**). Save the image in a file format that preserves the maximal amount of image data.
6. To look at transport of the protein of interest to the vacuole following conA treatment, capture Z-stacks of the sample and look for a focal plane through the vacuole. A focal plane through the vacuole will show a central space—the vacuole—surrounded by chloroplasts (as evident from the chlorophyll fluorescence). This is demonstrated in Fig. 1 using a GFP-labeled ATG8-interacting protein 1 (ATI1). ATI1 was characterized as an ATG8 binding protein in *Arabidopsis thaliana* that is partially associated with the ER under normal growth conditions. Following carbon starvation, ATI1 is localized on ER-associated bodies and on bodies associated with chloroplasts (ATI-bodies). These bodies are delivered to the vacuole in a process that requires active autophagy [30, 31]. As demonstrated in Fig. 1, untreated ATI1-GFP expressing plants show no or very few fluorescent puncta in the vacuole (Fig. 1a). However, in conA-treated plants, multiple fluorescent puncta are clearly visible in the vacuole (Fig. 1b) as a result of inhibited vacuolar degradation. A view through the cytoplasmic focal plane shows ATI1 fluorescence associated with a typical ER network-like structure (Fig. 1c).
7. Autophagic bodies in the vacuole typically move in a rapid and random manner [32]. To capture this typical movement, use

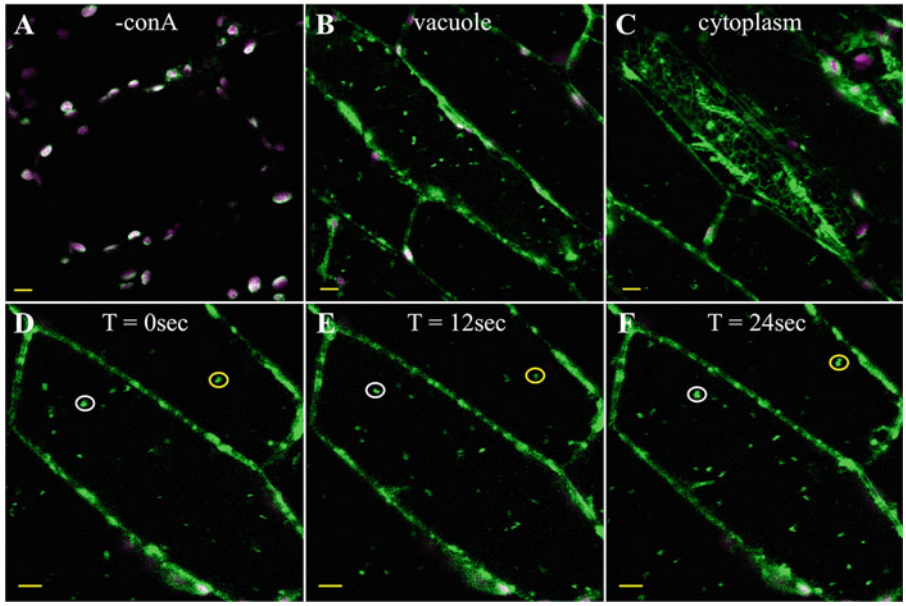

Fig. 1 Imaging of conA-treated *Arabidopsis thaliana* seedlings. Arabidopsis seedlings stably expressing ATI1-GFP driven by its endogenous promoter were exposed to 1 day of carbon starvation. ATI1-GFP fluorescence is shown in *green* and chlorophyll autofluorescence is shown in *magenta*. When viewed through the vacuolar plane of the cell, DMSO-treated control hypocotyl cells show no fluorescent puncta (**a**), while conA-treated hypocotyl cells accumulate multiple ATI1-GFP labeled bodies in the vacuole (**b**). A view through the cytoplasmic plane of conA-treated cells shows ATI1-GFP labeling typical ER structures (**c**). Time-lapse images, taken every 12 s, illustrate the random movement of ATI1-GFP labeled bodies in the vacuole (**d**)–(**f**) as illustrated by the GFP-labeled bodies highlighted by *white* and *yellow circles*. Scale bars = 5 μM

time-lapse imaging (for an example, *see* Fig. 1d and e). The confocal microscope requires relatively long acquisition time. Therefore, to capture the dynamic movement of autophagic bodies with minimal blurring, it might be necessary to increase the scan speed and eliminate frame averaging.

8. To look at the co-localization of the protein of interest with ATG8, sequential scanning (multitracking) should be used to avoid as much as possible bleed-through artifacts and to more accurately separate emission spectra. Depending on the protein of interest, different autophagy-inducing stress treatments can be used to enhance the co-localization. An example is shown in Fig. 2 using mRFP-ATG8f and ATI1-GFP. Following 24 h carbon starvation, ATI1 is partially localized to spherical bodies (green and yellow arrows). ATG8f is found on autophagosomes (red and yellow arrows), but also shows diffuse cytoplasmic distribution. ATG8f and ATI1 are co-localized on autophagosomes (yellow arrows), but there are some autophagosomes that do not carry ATI1 (red arrows). On the other hand, some spherical bodies are labeled by ATI, but not by ATG8f (green arrows).

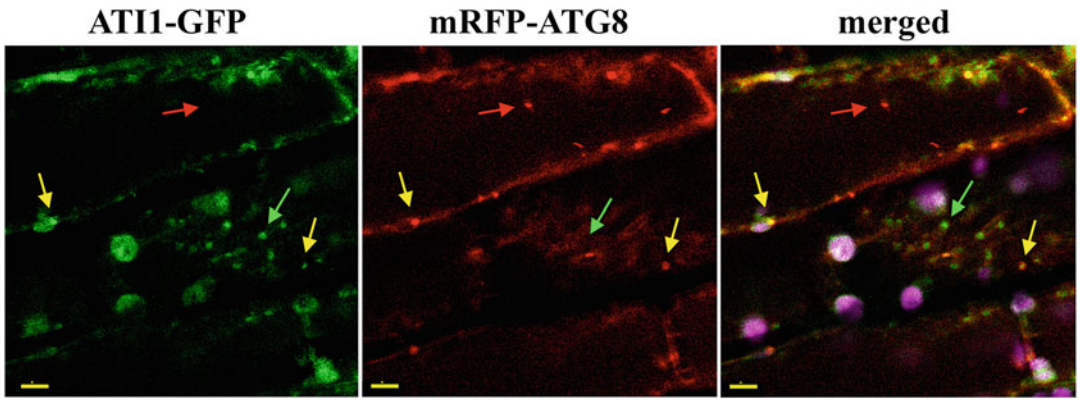

Fig. 2 Co-localization of ATI1 and ATG8f. Confocal images of hypocotyl cells of *Arabidopsis thaliana* seedlings stably co-expressing GFP-fused ATI1 (ATI1-GFP, *left panel*) and mRFP-fused ATG8f (mRFP-ATG8f, *middle panel*) were imaged following 24 h carbon starvation. Images of ATI1-GFP and mRFP-ATG8f fluorescence were combined (merged, *right panel*) to illustrate the relative localization of ATI1 and ATG8f. Chloroplasts autofluorescence is shown in magenta. ATI1 is partially co-localized with ATG8 on vesicles (*yellow arrows*). Vesicles containing ATI1 alone (*green arrows*) or ATG8f alone (*red arrows*) are also evident. Scale bars = 5 μM

9. ConA treatment can be combined with ATG8 co-localization studies to verify the identification of the protein of interest labeled puncta in the vacuole as autophagic bodies.

3.6 Quantification and Analysis

1. As the variability between imaged cells is considerable, reliable quantitative analysis requires sufficient sample size. It is advisable to quantitate about 50 images taken from several seedlings for each genotype/treatment.
2. The Pearson's correlation coefficient is widely used as a measure for the co-localization of two fluorescently tagged proteins and can be calculated using commercial software such as the Imaris image analysis software or co-localization plug-ins of the open source java application ImageJ/Fiji such as Coloc_2. However, when co-localization between an ER-associated protein and ATG8 is examined, calculating the Pearson's coefficient over the whole image can be misleading. If the protein of interest is associated with autophagy processes, it is expected to be co-localized with ATG8 on autophagosomes, but some of it will likely be localized to the ER. Similarly, ATG8 often shows a diffused cytoplasmic pattern besides its autophagosomal localization (*see* example in Fig. 2). Therefore, when quantitatively analyzing co-localization, there may be a significant difference between overall co-localization and co-localization on autophagosomes. To quantitatively analyze co-localization on autophagosomes, the spot detection and co-localization module of the Imaris image analysis software is very useful. Alternatively, it is possible to use ImageJ co-localization plug-ins and define the puncta visible in the images as regions of interest (ROI) (*see* **Note 13**).

3. Quantitative analysis of conA-treated samples is quite straightforward, as most of the fluorescence will be associated with autophagic bodies in the vacuolar plane (Fig. 1b). The number of autophagosome/autophagic bodies in each frame can be counted manually or using the spot detection module of the Imaris software. Proper statistical tools, such as standard deviation calculation, student's *t*-test, or one-way ANOVA, should be employed to compare different stress treatments or genetic backgrounds.

4 Notes

1. GFP (or other fluorescent proteins) can be fused at either the N-terminus or the C-terminus of the target protein. To determine the best fusion orientation, it is crucial to take into account possible targeting signals or known processing sites in the protein sequence. As N-terminal fusions can disrupt targeting to the ER, prediction software and literature search should be used to help determine the best fusion orientation. If possible, it is advisable to try both fusion orientations and validate expression and correct localization of the construct using transient transformation to *Nicotiana benthamiana*.
2. Using the Cauliflower mosaic virus 35S promoter to drive the expression of the fusion proteins is common and effective. However, excess protein can saturate the target compartment and cause mislocalization. Furthermore, overexpression of a protein might by itself cause cellular stress and the recruitment of the autophagic machinery. Therefore, where feasible, i.e., when the endogenous level of expression allows detection, it is prudent to verify the results using the target protein native promoter (*see* **Note 4**).
3. The GFP signal is sensitive to the acidic and/or proteolytic conditions of the vacuolar lumen, whereas mRFP or mCherry is more stable. Hence, mRFP or mCherry fusions might allow easier visualization of the target protein in the vacuole. For co-localization experiments with an ATG8 marker, fluorescent proteins that can be distinguished from one another should be chosen, for example GFP and mRFP or mCherry (*see* **Note 8**).
4. It is advisable to avoid using plant lines with very high expression levels, especially when using the strong 35S promoter, as these are more prone to silencing in later generations (*see* **Note 2**).
5. Use gloves when handling conA or conA-containing samples, as it is a carcinogen.
6. The same treatment can also be applied to detached mature rosette leaves.

7. Sealing the plates with parafilm prevents evaporation of the liquid during the incubation. As carbon starvation induces autophagy, we use liquid medium without sucrose and incubate the plates in the dark. This is also useful as conA is light sensitive. The gentle shaking of the plates allows mixing without damaging the seedlings.
8. *Arabidopsis thaliana* has nine ATG8 isoforms, all of which are thought to associate with the autophagosome membrane and can potentially be used as markers. GFP (or any other fluorescent protein) has to be fused to the N-terminus of the ATG8 protein, as ATG8 lipidation occurs at the C-terminus during autophagosome formation [10–13]. Different GFP-ATG8 transgenic seeds are currently available from the ABRC. These include two kinds of GFP-ATG8a transgenes that have different promoters. One transgene is under the control of the stronger Cauliflower mosaic virus 35S promoter (stock # CS39996) [12] while the other uses a promoter of the arabidopsis ubiquitin10 gene (stock # CS68819) [33]. Also available are 35S promoter driven GFP-ATG8e transgenic plants and constructs (stock # CS66943) [34]. Our lab has constructs of GFP- as well as mRFP-ATG8f under the control of the 35S promoter as well as transgenic lines expressing them [30].
9. We routinely image the hypocotyl as it is easy to detect the vacuole and autophagosomes in the elongated hypocotyl cells. It is of course possible to image other tissues as needed.
10. To prevent photodamage to the tissue, the laser intensity used for excitation should be kept low. If necessary, the pinhole can be opened to increase signal at the expense of *Z*-axis resolution. Alternatively, the detector gain can be increased and frame averaging can be used, at the cost of temporal resolution in time-lapse studies.
11. Plants contain a variety of autofluorescent compounds. While the most commonly encountered is the chlorophyll fluorescence from the chloroplast, we experience a lot of wide spectrum autofluorescence in stressed and damaged plant cells. This autofluorescence is typically present in multiple channels, and might be mistaken for co-localization of ATG8 and the protein of interest. Therefore, it is very important to image non-expressing and single expressing control plants that grew under the same conditions and went through the same treatments, to avoid artifacts.
12. To assure meaningful quantitative analysis of the images, it is imperative to adjust acquisition parameters such as laser intensities, gain, and exposure times, so that the fluorescence signal will be collected in the linear range of the detector system without saturating the signal.

13. Be careful not to change the original image while utilizing image analysis software. The image analysis should be performed on a copy of the original image.

Acknowledgments

We thank Dr. Tamar Avin-Wittenberg and Dr. Simon Michaeli for their critical comments on the manuscript. The work on ATI1-related autophagy pathways in the Galili lab is supported by a grant from the Israel Science Foundation (612/16). G.G. is the incumbent of the Bronfman Chair of Plant Sciences at The Weizmann Institute of Science.

References

1. Li F, Vierstra RD (2012) Autophagy: a multifaceted intracellular system for bulk and selective recycling. Trends Plant Sci 17:526–537
2. Liu Y, Bassham DC (2012) Autophagy: pathways for self-eating in plant cells. Annu Rev Plant Biol 63:215–237
3. Michaeli S, Galili G, Genschik P, Fernie AR, Avin-Wittenberg T (2016) Autophagy in plants—what's new on the menu? Trends Plant Sci 21:134–144
4. Reggiori F, Klionsky DJ (2013) Autophagic processes in yeast: mechanism, machinery and regulation. Genetics 194:341–361
5. Avin-Wittenberg T, Bajdzienko K, Wittenberg G, Alseekh S, Tohge T, Bock R, Giavalisco P, Fernie AR (2015) Global analysis of the role of autophagy in cellular metabolism and energy homeostasis in arabidopsis seedlings under carbon starvation. Plant Cell 27:306–322
6. Floyd BE, Morriss SC, Macintosh GC, Bassham DC (2012) What to eat: evidence for selective autophagy in plants. J Integr Plant Biol 54:907–920
7. Mizushima N, Yoshimori T, Ohsumi Y (2011) The role of Atg proteins in autophagosome formation. Annu Rev Cell Dev Biol 27:107–132
8. Avin-Wittenberg T, Honig A, Galili G (2012) Variations on a theme: plant autophagy in comparison to yeast and mammals. Protoplasma 249:285–299
9. Thompson AR, Vierstra RD (2005) Autophagic recycling: lessons from yeast help define the process in plants. Curr Opin Plant Biol 8:165–173
10. Fujioka Y, Noda NN, Fujii K, Yoshimoto K, Ohsumi Y, Inagaki F (2008) In vitro reconstitution of plant Atg8 and Atg12 conjugation systems essential for autophagy. J Biol Chem 283:1921–1928
11. Phillips AR, Suttangkakul A, Vierstra RD (2008) The ATG12-conjugating enzyme ATG10 is essential for autophagic vesicle formation in Arabidopsis thaliana. Genetics 178:1339–1353
12. Thompson AR, Doelling JH, Suttangkakul A, Vierstra RD (2005) Autophagic nutrient recycling in Arabidopsis directed by the ATG8 and ATG12 conjugation pathways. Plant Physiol 138:2097–2110
13. Yoshimoto K, Hanaoka H, Sato S, Kato T, Tabata S, Noda T, Ohsumi Y (2004) Processing of ATG8s, ubiquitin-like proteins, and their deconjugation by ATG4s are essential for plant autophagy. Plant Cell 16:2967–2983
14. Chung T, Phillips AR, Vierstra RD (2010) ATG8 lipidation and ATG8-mediated autophagy in Arabidopsis require ATG12 expressed from the differentially controlled ATG12A AND ATG12B loci. Plant J 62:483–493
15. Nair U, Yen WL, Mari M, Cao Y, Xie Z, Baba M, Reggiori F, Klionsky DJ (2012) A role for Atg8-PE deconjugation in autophagosome biogenesis. Autophagy 8:780–793
16. Le Bars R, Marion J, Le Borgne R, Satiat-Jeunemaitre B, Bianchi MW (2014) ATG5 defines a phagophore domain connected to the endoplasmic reticulum during autophagosome formation in plants. Nat Commun 5:4121
17. Zhuang X, Chung KP, Jiang L (2016) Origin of the autophagosomal membrane in plants. Front Plant Sci 7:1655
18. Zhuang X, Wang H, Lam SK, Gao C, Wang X, Cai Y, Jiang L (2013) A BAR-domain protein

SH3P2, which binds to phosphatidylinositol 3-phosphate and ATG8, regulates autophagosome formation in Arabidopsis. Plant Cell 25:4596–4615

19. Cebollero E, Reggiori F, Kraft C (2012) Reticulophagy and ribophagy: regulated degradation of protein production factories. Int J Cell Biol 2012:182834
20. Khaminets A, Heinrich T, Mari M, Grumati P, Huebner AK, Akutsu M, Liebmann L, Stolz A, Nietzsche S, Koch N et al (2015) Regulation of endoplasmic reticulum turnover by selective autophagy. Nature 522:354–358
21. Mochida K, Oikawa Y, Kimura Y, Kirisako H, Hirano H, Ohsumi Y, Nakatogawa H (2015) Receptor-mediated selective autophagy degrades the endoplasmic reticulum and the nucleus. Nature 522:359–362
22. Rashid HO, Yadav RK, Kim HR, Chae HJ (2015) ER stress: autophagy induction, inhibition and selection. Autophagy 11:1956–1977
23. Liu Y, Burgos JS, Deng Y, Srivastava R, Howell SH, Bassham DC (2012) Degradation of the endoplasmic reticulum by autophagy during endoplasmic reticulum stress in Arabidopsis. Plant Cell 24:4635–4651
24. Lynch-Day MA, Klionsky DJ (2010) The Cvt pathway as a model for selective autophagy. FEBS Lett 584:1359–1366
25. Michaeli S, Avin-Wittenberg T, Galili G (2014) Involvement of autophagy in the direct ER to vacuole protein trafficking route in plants. Front Plant Sci 5:134
26. Klionsky DJ, Abdelmohsen K, Abe A, Abedin MJ, Abeliovich H, Acevedo Arozena A, Adachi H, Adams CM, Adams PD, Adeli K et al (2016) Guidelines for the use and interpretation of assays for monitoring autophagy (3rd edition). Autophagy 12:1–222
27. Minina EA, Filonova LH, Fukada K, Savenkov EI, Gogvadze V, Clapham D, Sanchez-Vera V, Suarez MF, Zhivotovsky B, Daniel G, Smertenko A, Bozhkov PV (2013) Autophagy and metacaspase determine the mode of cell death in plants. J Cell Biol 203:917–927
28. Curtis MD, Grossniklaus U (2003) A gateway cloning vector set for high-throughput functional analysis of genes in planta. Plant Physiol 133:462–469
29. Tzfira T, Tian GW, Lacroix B, Vyas S, Li J, Leitner-Dagan Y, Krichevsky A, Taylor T, Vainstein A, Citovsky V (2005) pSAT vectors: a modular series of plasmids for autofluorescent protein tagging and expression of multiple genes in plants. Plant Mol Biol 57:503–516
30. Honig A, Avin-Wittenberg T, Ufaz S, Galili G (2012) A new type of compartment, defined by plant-specific Atg8-interacting proteins, is induced upon exposure of Arabidopsis plants to carbon starvation. Plant Cell 24:288–303
31. Michaeli S, Honig A, Levanony H, Peled-Zehavi H, Galili G (2014) Arabidopsis ATG8-INTERACTING PROTEIN1 is involved in autophagy-dependent vesicular trafficking of plastid proteins to the vacuole. Plant Cell 26:4084–4101
32. Takeshige K, Baba M, Tsuboi S, Noda T, Ohsumi Y (1992) Autophagy in yeast demonstrated with proteinase-deficient mutants and conditions for its induction. J Cell Biol 119:301–311
33. Shin KD, Lee HN, Chung T (2014) A revised assay for monitoring autophagic flux in Arabidopsis thaliana reveals involvement of AUTOPHAGY-RELATED9 in autophagy. Mol Cells 37:399–405
34. Contento AL, Xiong Y, Bassham DC (2005) Visualization of autophagy in Arabidopsis using the fluorescent dye monodansylcadaverine and a GFP-AtATG8e fusion protein. Plant J 42:598–608

Chapter 20

Imaging the ER and Endomembrane System in Cereal Endosperm

Verena Ibl, Jenny Peters, Eva Stöger, and Elsa Arcalís

Abstract

The cereal endosperm is a complex structure comprising distinct cell types, characterized by specialized organelles for the accumulation of storage proteins. Protein trafficking in these cells is complicated by the presence of several different storage organelles including protein bodies (PBs) derived from the endoplasmic reticulum (ER) and dynamic protein storage vacuoles (PSVs). In addition, trafficking may follow a number of different routes depending on developmental stage, showing that the endomembrane system is capable of massive reorganization. Thus, developmental sequences involve progressive changes of the endomembrane system of endosperm tissue and are characterized by a high structural plasticity and endosomal activity.

Given the technical dexterity required to access endosperm tissue and study subcellular structures and (seed storage protein) SSP trafficking in cereal seeds, static images are the state of the art providing a bulk of information concerning the cellular composition of seed tissue. In view of the highly dynamic endomembrane system in cereal endosperm cells, it is reasonable to expect that live cell imaging will help to characterize the spatial and temporal changes of the system. The high resolution achieved with electron microscopy perfectly complements the live cell imaging.

We therefore established an imaging platform for TEM as well as for live cell imaging. Here, we describe the preparation of different cereal seed tissues for live cell imaging concomitant with immunolocalization studies and ultrastructure.

Key words Cereal endosperm, Endomembrane system, Electron microscopy, Live cell imaging, Fluorescent organelle markers

1 Introduction

The endosperm of cereal seeds is a highly differentiated tissue containing specialized cells that are responsible for the synthesis and storage of proteins. The high specialization of the tissue is reflected in the endomembrane system. Storage protein synthesis requires a well-developed endoplasmic reticulum (ER) and involves different storage organelles that will form de novo during seed development [1, 2]. ER-derived protein bodies contain prolamin aggregates while the protein storage vacuole, far from being a plain

Chris Hawes and Verena Kriechbaumer (eds.), *The Plant Endoplasmic Reticulum: Methods and Protocols*, Methods in Molecular Biology, vol. 1691, DOI 10.1007/978-1-4939-7389-7_20,

post-Golgi compartment, accumulates different storage protein classes and often incorporates the content of ER-derived storage bodies in an autophagy-like process [3–6]. At the peak of storage protein production (as soon as 16 days after pollination [dap] in maize seeds), endosperm cells undergo programmed cell death (PCD) and generate a starchy endosperm core [7]. This sequence of intracellular changes in developing seeds challenges the endomembrane system that is a plastic and dynamic system capable of rapid morphological and functional adaptation (Fig. 1a). The massive reorganization of the endomembrane system during seed development involves significant morphological changes to the storage organelles and also affects the trafficking and distribution of storage proteins [5, 8–12].

The study of such a dynamic system can be approached by different, complementary imaging methods. Live cell imaging combined with fluorescent membrane markers can be used to follow the morphological changes in situ. This was reported in the context of barley endosperm development, comparing PSVs in the aleurone, subaleurone, and central starchy endosperm layers [10]. The use of TIP3-GFP marker lines, together with the use of fluorescent organelle dyes such as ER Tracker®, allowed the visualization of morphological changes in the PSVs along development and a spatiotemporal pattern could be established [10]. ER Tracker® and neutral red, as well as other organelle dyes such as FM4-64 and BCECF, are very convenient tools to identify and track organelles in cereal endosperm. It should be noted, however, that the staining patterns may be unexpected, due to the specialization of the endomembrane system and results should be interpreted with some caution and considering appropriate controls (Fig. 1e–m).

Protein trafficking and organelle reshaping can also be investigated by looking at the behavior of recombinant proteins, including storage proteins fused to fluorescent tags [5, 13–15]. Endogenous glycoproteins are rarely found in the endosperm [16] and are difficult to follow due to the lack of appropriate detection antibodies, so recombinant glycoproteins produced in the context of molecular farming are particularly useful because they can be traced by immunolocalization and by characterizing their glycan modifications. Accordingly, a significant reduction in the number of PSVs was observed during maize seed development and the fate of the recombinant glycoprotein phytase and the endogenous vacuolar maize proteins corn legumin-1 and α-globulin were found to change during endosperm development. All three proteins were found to locate to the PSVs in early development while closer to maturity they were found at the periphery of the ER-derived protein bodies [17]. This example reflects the flexibility and dynamics of a system, where interactions between organelles and changes in protein trafficking fulfill distinct developmental functions [18].

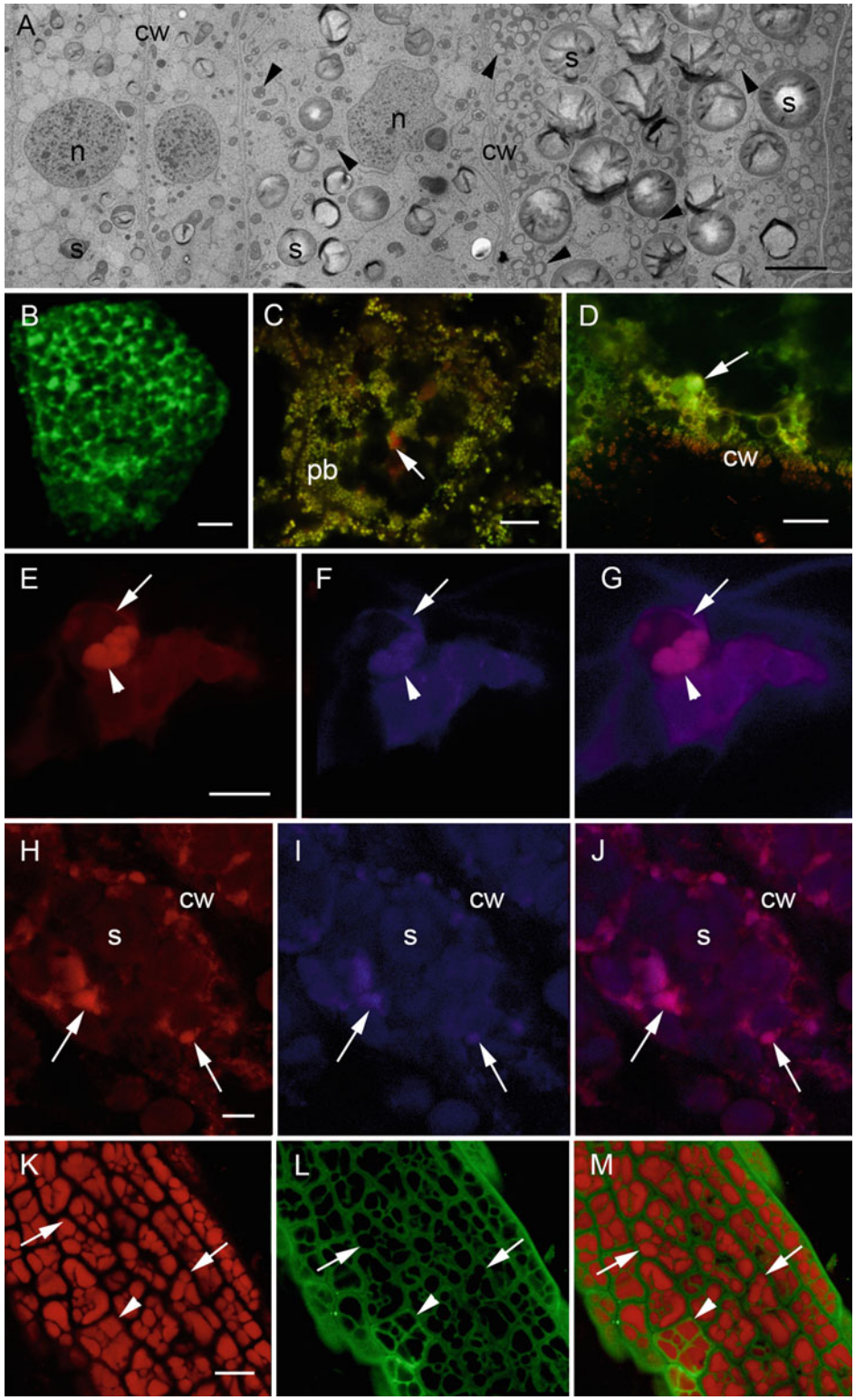

Fig. 1 Imaging the endomembrane system of the cereal endosperm. (**a**) Electron microscopy. Outer layers of maize endosperm (mid-developmental stage). *See* the changes in the ultrastructure of maize endosperm,

Cereal endosperm can be accessed by various imaging techniques, which differ from each other and offer specific advantages and disadvantages. With live cell imaging for example it has become possible to monitor dynamic endomembrane processes in real time, however at limited resolution. Electron microscopy on the other hand provides high resolution, but requires sample fixation and the information must be derived from static images. A combination of approaches, as here described, is therefore the best choice for obtaining maximum information.

2 Material

2.1 Plant Material

Maize plants (*Zea mays* L.), cv. Hi II (A188XB73) are grown in a climate-controlled growth chamber at 28 °C/24 °C day/night temperature with a 14 h photoperiod. Barley (*Hordeum vulgare* L., cv. Golden Promise) is grown at 16 °C and 70% relative humidity under a 16 h photoperiod. After tillering, cultivation should be continued at 22 °C. Seeds are collected at different developmental stages, prior to desiccation, typically from 8 days after pollination (daps) on.

2.2 Cereal Transformation for Endosperm ER and Endomembrane System Visualization

1. OsTIP3::PDIL1;1-GFP (ER lumen marker) [19].
2. OsTIP3::CherrySec61 (ER membrane marker) [10, 19].
3. OsTIP3::TiP3-GFP (tonoplast marker) [19].

2.2.1 Reporter Gene Constructs

2.2.2 Stable Maize Transformation

See Rademacher et al. [20] and information and notes therein.

1. Particle accelerator gun and accessories.
2. Temperature-controlled light incubator.
3. Vortexer.

Fig. 1 (continued) younger cells (*left*) contain a nucleus (n) and a few starch grains (s), while the older cells (*right*) are packed with starch grains (s) and zein bodies (*arrowheads*). *Cw* cell wall. (b–m) CLSM. (**b**) Maize endosperm. Transient expression of OsTIP3::PDIL1;1-GFP. *See* the fully developed ER network. (**c**) Maize endosperm. Immunolocalization of corn legumin-1 in a young endosperm cell (*arrow*). As counterstain, ER Tracker® green stains the zein bodies (pb). (**d**) Barley endosperm. ER Tracker® green and red perfectly co-localize and label a protein body (*arrow*). (**e**–**g**) Barley endosperm. (**e**) Neutral red, (**f**) Autofluorescence, (**g**) Merged. *See* that neutral red stains the protein body (*arrowhead*) within the storage vacuole (*arrow*). (**h**–**j**) Barley endosperm. (**h**) ER Tracker® red, (**i**) Autofluorescence, (**j**) Merged. *See* that ER Tracker® red stains the protein bodies (*arrows*). *Cw* cell wall, *s* starch. (**k**–**m**) Controls. Arabidopsis embryo. (**k**) Neutral red. (**l**) ER Tracker® green, (**m**) Merged. Note that in Arabidopsis embryos, neutral red stains the lumen of the storage vacuoles (*arrows*), while ER Tracker green® reveals the presence of a fine ER network (*arrowhead*). Bars 5 μm (**a**), 10 μm (**b**–**m**)

4. Microfuge.
5. Stock solution of plasmid DNA carrying the transgene of interest for study of the cereal endosperm ER and endomembrane system.
6. Gold particles (0.7–0.9 μm; Bio-Rad).
7. 100 μM spermidine.
8. 2.5 μm $CaCl_2$.
9. Ice cold 100% (v/v) ethanol.
10. Fine forceps and scalpel.
11. Petri dishes.
12. Culture pots and tubes.
13. Parafilm.
14. Sterile, double-distilled water.
15. 5% (w/v) sodium hypochlorite solution.
16. Cereal endosperm bombardment medium pH 5.8 (KOH): MS (Murashige and Skoog) salts 4.3 g/L (*see* **Note 1**), sucrose 30 g/L, gelrite 3 g/L.

2.2.3 Endosperm Transient Transformation

1. Confocal laser scanning microscope (CLSM).
2. Free software ImageJ.
3. Razor blades.
4. Forceps.
5. Reagent tubes (*see* **Note 2**).
6. Cover Glasses (High precision: 170 ± 5 μm).
7. Petroleum jelly.
8. DMSO.
9. 4 μM Neutral red (*see* **Note 3**).
10. ER Tracker®stock solution (*see* **Note 4**).

2.3 Immuno-localization of Endosperm ER and Endomembrane System Markers for CLSM

1. Vibratome.
2. Razor blades.
3. Embryo dishes.
4. Fine forceps.
5. Cyanoacryl glue (*see* **Note 5**).
6. 0.1 M Phosphate buffer (pH 7.4): 10.9 g/L Na_2HPO_4 (anhydrous), 3.2 g/L Na_2HPO_4.
7. Fixative: 4% paraformaldehyde in phosphate buffer 0.1 M pH 7.4 (*see* **Notes 6** and **7**).
8. PBT: phosphate buffer plus 0.25% Tween 20.

9. Microscopy glass slides.
10. Cover Glasses (High precision: 170 ± 5 μm).
11. Blocking solution: 5% BSA (Bovine serum albumin) in phosphate buffer, pH 7.4.

2.4 Electron Microscopy

1. Transmission electron microscope.
2. Ultramicrotome.
3. Fine forceps (*see* **Note 8**) and razor blades.
4. Diamond knife.
5. EM grids (*see* **Notes 9** and **10**).
6. 0.1 M cacodylate buffer, pH 7.4.
7. Fixative for immunolocalization: 4% paraformaldehyde plus 0.2% glutaraldehyde in cacodylate buffer, pH 7.4.
8. Fixative for ultrastructure: 2% paraformaldehyde plus 2.5% glutaraldehyde in cacodylate buffer, pH 7.4.
9. Secondary fixative (ultrastructure): 1% OsO4 plus 0.8% KCNFe in water (*see* **Note 11**).
10. 0.5% aqueous uranyl acetate.
11. Epoxy resin (*see* **Note 12**).
12. Beem capsules (size 00).

3 Methods

3.1 Cereal Transformation

3.1.1 Transient Transformation (Fig. 1b)

Coating of gold particles for particle bombardment

1. Mix 5 mg of sterile gold particles (mixture of 0.9 and 0.7 μm diameter) with 20 μg circular plasmid DNA.
2. Add sterile water to a final volume of 50 μl.
3. Add 50 μl of 0.1 M spermidine (*see* **Note 13**) and further vortex for 2 min.
4. Slowly add 50 μl of 2.5 M $CaCl_2$ and further vortex for 10 min.
5. Centrifuge.
6. Wash the gold pellet twice with ice cold 100% (v/v) ethanol.
7. Resuspend in 500 μl ice cold ethanol.
8. Store at −20 °C until further use.

3.2 Particle Bombardment of Young Endosperm Tissue

1. Collect immature ears (*see* **Note 14**) from growth chamber-grown cereals.
2. Remove the kernels from the ears and surface sterilize in 5% (v/v) NaClO for 20 min at room temperature (*see* **Note 15**).
3. Wash several times the kernels in sterile water.

4. Cut the kernels in thin sections (*see* **Note 16**) with a sharp razor blade and place the sections in the center of plates containing cereal endosperm bombarding medium.
5. Spot 50 μl of the prepared DNA-gold particle suspension in the core of a microcarrier.
6. Let the ethanol evaporate and assemble the gene gun according to the manufacturer's guidelines.
7. Use the appropriate rupture disk for bombardment (*see* **Notes 17** and **18**).
8. Reporter gene expression can be already detected 2 days after bombardment, depending on the experimental conditions.

3.3 Fluorescent Dyes for Endosperm ER and Endomembrane Visualization (Fig. 1d–j)

1. Collect immature ears from growth chamber-grown cereals (*see* **Note 19**).
2. Cut the kernels in thin sections (0.5–1 mm) with a razor blade.
3. Wash the sections with tap water (electrical conductivity: 280 μS/cm; pH 7.9) (*see* **Note 20**).
4. Transfer the sections to a new tube and soak them in the fluorescent dyes in the dark at room temperature.
5. Mount the sections in tap water (*see* **Notes 21** and **22**).
6. Immediately analyze the section by CLSM (*see* **Notes 23–25**).

3.4 Immunolocalization of Endosperm ER and Endomembrane System Markers for CLSM (Fig. 1c)

1. Harvest kernels at the appropriate developmental stage and cut in small pieces with a sharp razor blade, around 2 mm^3 (*see* **Notes 26** and **27**).
2. Fix the samples in 4% paraformaldehyde in phosphate buffer for 2 h at RT (*see* **Notes 28** and **29**).
3. Wash at least three times (10 min each) with phosphate buffer 0.1 M pH 7.4.
4. Glue the sample with cyanoacryl glue on the vibratome plate (*see* **Notes 30** and **31**).
5. Obtain vibratome sections and transfer them to a glass embryo dish (*see* **Notes 32** and **33**).
6. Dehydrate and rehydrate the sections through ethanol series (30%, 50%, 70%, 100%), 5′ steps.
7. Apply 2% cellulase in phosphate buffer 0.1 M pH 7.4 for 1 h at RT to digest the cell wall.
8. Remove the cellulase solution and add 0.5% Triton-100X in phosphate buffer 0.1 M pH 7.4 (*see* **Notes 34** and **35**).
9. Block the nonspecific binding sites with a solution of 5% BSA in phosphate buffer 0.1 M pH 7.4 for 10 min.

10. Incubate sections with the appropriate antibody diluted in phosphate buffer 0.1 M pH 7.4 for 2 h at RT (*see* **Notes 36** and **37**).
11. Wash three times (10 min each) in PBT 0.1 M pH 7.4.
12. Incubation sections with the secondary antibody diluted in phosphate buffer 0.1 M pH 7.4 for 1 h at RT in the dark (*see* **Notes 38** and **39**).
13. Wash three times (10 min each) in PB 0.1 M pH 7.4.
14. Mount and observe (*see* **Notes 40–42**).

3.5 Electron Microscopy

3.5.1 Ultrastructural Studies of Endosperm ER and Endomembrane System

Fixation and embedding: samples for fixation should not be bigger than 1 mm^3.

1. Immerse the tissue in a drop of fixative and cut small pieces (*see* **Notes 26** and **27**).
2. Fix the samples for 2 h at RT (*see* **Note 43**).
3. Wash the samples at least four times (10 min each) with cacodylate buffer 0.1 M pH 7.4 at 4 °C.
4. Post-fix the samples with 0.5% aqueous OsO4 and 0.8% KFeCN for 3 h at 4 °C.
5. Wash the samples several times (minimum five changes, 15 min each) with ddH_2O.
6. Incubate the samples with 0.5% aqueous uranyl acetate, 4 °C overnight.
7. Wash the samples at least four times (10 min each) with ddH_2O.
8. Dehydrate the samples in acetone series, keep the samples at 4 °C (10 min in 50% acetone, 10 min in 70% acetone (three times), 10 min in 90% acetone (three times), 10 min in 96% acetone (three times), 15 min in 100% acetone (three times).
9. Infiltrate the samples with epoxy resin. Incubate samples (overnight in 25% resin in 100% acetone at 4 °C, 3 h in 50% resin in 100% acetone, 3 h in 75% resin in 100% acetone).
10. Incubate overnight in pure resin at 4 °C.
11. Change to fresh resin and incubate for another 3 h.
12. Place the infiltrated tissue samples in beem capsules filled with resin. Polymerization of the resin takes 48 h at 65 °C (*see* **Notes 44** and **45**).
13. Sectioning: sections showing silver interferences (~90 nm) are collected on 200 mesh hexagonal grids. Sections can be directly observed by electron microscopy (*see* **Note 46**).

4 Notes

1. Can be purchased as ready-mixed powders from many suppliers (e.g., Duchefa, Sigma).
2. We prefer 2 ml Eppendorf tubes.
3. A 4 mM stock solution in distilled water can be aliquoted and kept for longer periods of time at −20 °C.
4. ER Tracker® is available in red, green, and blue. Follow manufacturer instructions to prepare the working solutions. Stock solutions can be stored for longer periods of time at −20 °C. We are using ER Tracker red and green depending on the experimental conditions, and we have not observed differences in the staining patterns of both (Fig. 1d).
5. Can be found in hardware stores, should be stored at 4 °C.
6. Cacodylate buffer 0.1 M, pH 7.4; 1×PBS, pH 7.4 are also suitable buffers.
7. A 10% stock solution can be aliquoted and kept at −20 °C.
8. Number 3–5 nonmagnetic forceps are recommended.
9. Gold or copper grids are suitable. To improve the stability of the sections under the electron beam, we recommend using grids coated with a formvar membrane.
10. Grids are available in different mesh and shapes. Grids with a high mesh number offer better support but less open area. We prefer 200 hexagonal mesh because they offer a good compromise between support and open area.
11. A stock solution of 4% OsO4 plus 3.2% KFeCN in water can be kept at 4 °C in a sealed glass vial for longer periods of time. Discard blackened solutions.
12. Epoxy resins facilitate the sectioning and are more stable under the electron beam. Spurr resin has been widely used for embedding; however, since one of its components has been retired from the market, equivalent options are available. Low viscosity resin kits can be purchased from many suppliers.
13. Drop the solution into the mixture under constant vortexing.
14. 10–14 daps for maize; 8–12 daps for barley.
15. Move to a sterile bench for the following steps.
16. 1 mm in thickness sections are optimal for bombardment.
17. Depending on the species and the developmental stage of the tissue, different rupture disks will be needed. Usual ranges are 600–1100 psi. An optimization of the protocol for specific needs is recommended.
18. Bombard each plate twice.

19. The optimal developmental stage depends on the experimental purposes. Seeds close to maturation have a higher content in starch grains that may difficult handling, labeling and imaging. For consistency between experiments, use seeds of the same age and cut tissue sections on the same area, we prefer cross sections on the medial axis of the seed.
20. Transfer the sections to a new specimen holder before washing them.
21. Sections can be also mounted on fresh fluorescent dye.
22. Use some petroleum jelly along the borders to avoid floating and to stabilize the cover glasses.
23. Neutral red and ER Tracker need short incubation times on cereal endosperm (10–15 min).
24. As the section is mounted in tap water for live cell imaging, the appropriate objective is a water objective.
25. It is important to use the laser settings as low as possible to avoid any damage to the sample and causing bleed-through if more fluorescent dyes will be used in parallel. High sensitivity detectors are recommended.
26. Use a piece of dental wax, put a drop of fixative on the wax sheet, and place the seed in it prior to cutting. The wax will prevent squeezing and the cut surface will be immediately in contact with the fixative improving its preservation.
27. Cut 2 mm thick slices from the endosperm and then cut them in pieces so that each piece of tissue includes the aleurone and pericarp. For consistency between experiments, we cut cross sections on the medial axis of the seed.
28. Work under a fume hood when using paraformaldehyde.
29. Alternatively overnight at 4 °C.
30. Avoid placing the tissue samples on the center of the plate; preferably place them close to the border of the plate. More than one sample can be glued together, with 120° separation in between.
31. For optimal results, glue the samples so that the pericarp faces the blade.
32. Optimally 30 μm, can be up to 70 μm for cereals.
33. Endosperm sections are very delicate due to the thin cell walls of endosperm cells. Using embryo dishes will increase the volume of reagents consumed but facilitates the handling of the sections.
34. The digestion of the cell walls and the disorganization of the plasma membrane induced by Triton-100X improve the penetration of the antibodies used for localization. However, these

treatments can induce many artifacts and destroy the tissue. Depending on the experimental purposes, these both steps can be shortened or even skipped.

35. At this point, sections can be difficult to see. Laying a black cardboard under the embryo dish and working with a binocular can ease the process of changing reagents.
36. Alternatively overnight at 4 °C.
37. The optimal dilution depends on the antibody used. Commonly, dilutions range between 1:100 and 1:500.
38. Cover the embryo dish with aluminium foil.
39. While any fluorophore labeled antibody is suitable for confocal microscopy, we prefer Alexa Fluor®-labeled antibodies because they are very bright and do not fade easily.
40. Mount in phosphate buffer or in phosphate buffer: glycerol 1:1 (v/v). Using a bit of petroleum jelly in each corner of the coverslip will help to fix the preparation and prevents the sample from squeezing.
41. The laser as well as the detector settings depends on the concentration of the epitope to detect and the fluorophore used.
42. The cereal endosperm matures centripetally, which means that the cells under the aleurone are much younger than the ones in the deeper layers of the starchy endosperm. For consistency between experiments, we like to work always with the same cell layers.
43. Alternatively, overnight at 4 °C.
44. A thin paper strip label can be embedded together with the sample for easy identification of the resulting blocks.
45. Put one drop of resin in the capsules before adding the tissue piece to avoid the formation of air bubbles at the block tip. It is not necessary to embed more than one piece of sample per capsule.
46. *See* **Note 42**.

Acknowledgments

The authors would like to thank the BOKU-VIBT imaging center for access and expertise.

References

1. Muntz K (1998) Deposition of storage proteins. Plant Mol Biol 38:77–99
2. Shewry PR, Halford NG (2002) Cereal seed storage proteins: structures, properties and role in grain utilization. J Exp Bot 53:947–958
3. Shewry PR, Napier JA, Tatham AS (1995) Seed storage proteins: structures and biosynthesis. Plant Cell 7:945–956
4. Galili G (2004) ER-derived compartments are formed by highly regulated processes and have

special functions in plants. Plant Physiol 136:3411–3413

5. Tosi P et al (2009) Trafficking of storage proteins in developing grain of wheat. J Exp Bot 60:979–991
6. Levanony H et al (1992) Evidence for a novel route of wheat storage proteins to vacuoles. J Cell Biol 119:1117–1128
7. Sabelli PA, Larkins BA (2009) The development of endosperm in grasses. Plant Physiol 149:14–26
8. Hoh B et al (1995) Protein storage vacuoles form de novo during pea cotyledon development. J Cell Sci 108:299–310
9. Wang Y et al (2010) OsRab5a regulates endomembrane organization and storage protein trafficking in rice endosperm cells. Plant J 64:812–824
10. Ibl V et al (2014) Fusion, rupture, and degeneration: the fate of in vivo-labelled PSVs in developing barley endosperm. J Exp Bot 65:3249–3261
11. Shy G et al (2001) Expression patterns of genes encoding endomembrane proteins support a reduced function of the Golgi in wheat endosperm during the onset of storage protein deposition. J Exp Bot 52:2387–2388
12. Vitale A, Hinz G (2005) Sorting of proteins to storage vacuoles: how many mechanisms? Trends Plant Sci 10:316–323
13. Saito Y et al (2012) Formation mechanism of the internal structure of type I protein bodies in rice endosperm: relationship between the localization of prolamin species and the expression of individual genes. Plant J 70:1043–1045
14. Shigemitsu T et al (2013) Accumulation of rice prolamin-GFP fusion proteins induces ER-derived protein bodies in transgenic rice calli. Plant Cell Rep 32:389–399
15. Wakasa Y, Takaiwa F (2013) The use of rice seeds to produce human pharmaceuticals for oral therapy. Biotechnol J 8:1133–1143
16. Woo YM et al (2001) Genomics analysis of genes expressed in maize endosperm identifies novel seed proteins and clarifies patterns of zein gene expression. Plant Cell 13:2297–2317
17. Arcalis E et al (2010) The changing fate of a secretory glycoprotein in developing maize endosperm. Plant Physiol 153:693–702
18. Arcalis E et al (2014) The dynamic behavior of storage organelles in developing cereal seeds and its impact on the production of recombinant proteins. Front Plant Sci 5:439
19. Onda Y, Kumamaru T, Kawagoe Y (2009) ER membrane-localized oxidoreductase Ero1 is required for disulfide bond formation in the rice endosperm. Proc Natl Acad Sci U S A 106:14156–14161
20. Rademacher T, Arcalis E, Stoger E (2009) Production and localization of recombinant pharmaceuticals in transgenic seeds. Methods Mol Biol 483:69–87

INDEX

A

Acceptor Photobleaching 140, 141, 145
Arabidopsis 2–4, 7–12, 15, 18, 19, 20, 24, 25, 29, 30, 67, 68, 76, 79, 88, 93, 94, 98, 99, 103, 104, 108, 117–122, 126, 140, 144, 147, 150, 156, 160, 162, 172, 182, 184, 186, 192, 193, 206, 210, 224–226, 231–238, 240–245, 247, 254
ATG8 240–247
Automated segmentation 47, 48, 57
Autophagy 239–248, 252

B

BY2 ..... 8, 35, 37, 38, 40

C

Ceramides 128, 134
Cereal endosperm 251–261
Chaperones 160, 187, 223
Chi-square analysis 24, 28, 30
Cisternae 1, 5, 17, 36, 43, 44, 46, 48, 55–57, 67, 76, 77, 83–93, 100
Co-immunoprecipitation 213
Concanamycin A 241
Confocal imaging 151, 241
Confocal microscopy 6, 12, 67, 208, 214, 216, 219, 243

D

3D EM 16, 19
Desmotubule 35, 41
Dithiothreitol 105, 223, 232
3D-SIM 35–35, 38, 41

E

Electron microscopy 15–20, 23, 24, 36, 253, 256, 258
  cereal endosperm 254
Embryo germination
  endoplasmic reticulum 67–74
  imaging chamber 67–73
  vacuole 79
Endomembrane system 18, 179, 251–261
Endoplasmic reticulum 1–13, 15–20, 23–31, 33–41, 43–56, 67–76, 100, 103, 119, 160, 168, 179, 205, 251, 252, 254, 255, 257, 259, 260
Endoplasmic reticulum stress
  stress arabidopsis 103, 231
  stress prolonged 30
  stress temporary 231–233
Enzyme assays 120, 122
Enzymes 2, 13, 17, 108, 112, 118, 122, 127, 128, 136, 148, 150, 151, 159, 160, 201, 206, 214, 220, 223, 241, 242
ERAD 209, 210, 217, 218, 220
ER-PM contact sites 24, 25, 27–30

F

FLIM 140, 145, 146, 147, 152, 154, 155, 161–164, 219
Fluorescence 1–13, 25, 33, 44, 47, 49, 53, 58–61, 65, 78, 93, 95, 139, 140, 141, 143–146, 148, 152–155, 161–164, 169, 170, 239–247, 254
Fluorescent dyes 79, 99, 170, 257, 260
Fluorescent organelle markers 172
  cereal endosperm 251–261
Fluorescent protein 2, 5, 24, 27, 47, 140, 141, 143, 208, 240, 242, 246
Free-flow electrophoresis 103–114, 125, 130
FRET 139–157, 161–164, 219
FRET-FLIM 140, 146, 147, 155, 161–164, 219

G

Gateway 4, 63, 140, 193, 194
  2in1 140
GC-FID, GC-MS 127, 129–132, 134
GFP-trap 161, 162
Glucosylceramides 126, 128, 134
Glycoprotein 206, 207, 209–212, 216–218, 220, 252
Golgi 15, 17, 18, 26, 75, 76, 104, 109, 167, 177, 187, 205–207, 209, 215, 219, 241, 252

Chris Hawes and Verena Kriechbaumer (eds.), *The Plant Endoplasmic Reticulum: Methods and Protocols*, Methods in Molecular Biology, vol. 1691, DOI 10.1007/978-1-4939-7389-7, © Springer Science+Business Media LLC 2018

Green fluorescent protein (GFP) 5, 6, 9, 11, 25, 26, 28, 35, 37–41, 57, 65, 77, 95, 96, 154, 155, 161, 163, 164, 169, 170, 214, 217, 219, 240, 243–246, 252, 254

H

High Performance Thin Layer Chromatography (HPTLC) 126, 128, 130–132, 134, 136

I

Immunofluorescence 2, 3, 4, 8, 10
Immuno-gold TEM 28
  N. benthamiana 24
Immunoprecipitation 161, 162, 188, 213

L

Labeling 1–13, 27, 28, 29, 30, 79, 136, 162, 163, 179, 181, 184, 244, 260
L-azetidine-2-carboxylic acid 223
LCB. *See* Long chain bases (LCB)
Liquid Chromatography-Mass Spectrometry (LC-MS) 106, 110, 127, 129, 130, 131, 132, 135
Live cell imaging 25–27, 34, 252, 254, 260
  cereal endosperm 254
Long chain bases (LCB) 130, 131, 133–134

M

Mating-based Split-Ubiquitin System (mbSUS) 192, 193, 194, 195, 196, 201
Membrane proteins 46, 61, 65, 79, 114, 191–202
Metabolon 159–165
Microsomal fraction 120, 121

N

NET3C 4, 9, 24, 25, 27, 30
Network analysis
  cisternae 46
  phase congruency 50, 51
  reticulon 56
  tubules morphology 48
Network flow 76, 77, 78, 95–98
Network movement 76, 77, 81–95
N-glycosylation 206–210, 212, 218, 219

O

Oligosaccharyltransferase 207
Optical Microscope eXperimental (OMX) 34, 38–39
Optical trap 167–171, 173–176

P

Persistency mapping 76, 77, 90–92, 95
Phase congruency 50, 51
Phospholipids 126, 127, 128, 131–135
Phytosterols 134, 135
Protein complex 27, 159, 206, 219
Protein folding 45, 206, 224, 231
Protein oligomerization 79, 179
Protein–protein interaction
  FLIM 140, 146, 161, 163–165, 219
  FRET 139, 140, 146, 161, 163–165, 219
Protein synthesis 117, 251
Proteomics 104, 106, 110, 112, 114
  arabidopsis 103
Pulse-chase 179, 180, 184

Q

qRT-PCR. *See* Quantitative RT-PCR (qRT-PCR)
Quality control 103, 206, 209–210
Quantitative RT-PCR (qRT-PCR) 224, 225, 228, 229

R

Ratiometric Bimolecular Fluorescence Complementation (rBiFC) 140–142, 143, 144, 152–153
Reticulon 56, 60, 160

S

SEC61 ..... 60, 144, 147, 192, 193
SER. *See* Sieve-element reticulum (SER)
Serial Block Face SEM 16
Sieve-element reticulum (SER) 35, 36, 39–40
Split ubiquitin 139, 191–202
  yeast 139, 191, 193–197, 198, 199, 200
Stable protein expression 2–4
SUB 90, 192, 193, 194

T

Transient protein expression 2, 24
Triacylglycerols 126
Tubules morphology 48, 56–58
Tunicamycin 219, 223, 224, 228, 229, 232
Tweezers 10, 167–185, 242
2in1 139–157

U

Ultracentrifugation 125, 130
Unfolded protein response 223–238

V

Vacuole 79, 187, 219, 239–248
VAP27 family 24, 27

Y

Yeast 2, 3, 24, 77, 146, 191, 193–200, 201, 202, 206, 209, 212, 220, 223, 224, 240, 241

Z

Zinc-iodide osmium tetroxide (ZIO) . 16, 17, 18, 19, 20, 36, 37, 39–40